ACTA TECHNICA

ACADEMIAE SCIENTIARUM HUNGARICAE

EDITOR-IN-CHIEF: P. MICHELBERGER

VOLUME 104
NUMBERS 1—3

CIVIL ENGINEERING — C/5

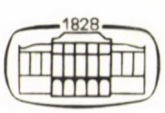

AKADÉMIAI KIADÓ, BUDAPEST 1991/92

ACTA TECHNICA

A JOURNAL OF THE HUNGARIAN ACADEMY OF SCIENCES

Acta Technica publishes original papers, preliminary reports and reviews in English, which contribute to the advancement of engineering sciences.
Acta Technica is published by

AKADÉMIAI KIADÓ
Publishing House of the Hungarian Academy of Sciences
H-1117 Budapest, Prielle K. u. 19—35

Subscription information

Orders should be addressed to

AKADÉMIAI KIADÓ
H-1519 Budapest, P.O. Box 245

Acta Technica is abstracted/indexed in Applied Mechanics Reviews, Current Contents–Engineering, Technology and Applied Sciences, GeoRef Information System, Science Abstracts.

CONTENTS

Acta Technica Acad.Sci.Hung., 104(1-3), pp. 3-38 (1991/92)

CONE SHELL CALCULATIONS

Computerizable method for calculation of complex shells of revolution

CSÁKÁNY, A.*, HEGEDÜS, I.**, KOLLÁR, L.P.***

(Received: 22 February 1990)

A practicable method widely used today, suited for manual calculation of rotationally symmetric structures, had been developed by

Dr. Gyula Márkus, deceased in 1989.

The present work, an earlier version of which had been read by Dr. Márkus himself, has been devoted to his memory.

Described in this work is the algorithm for general use in calculation of the stress acting upon structures subject to rotationally symmetric load, built together of shells of revolution and circular plates. The algorithm is based on the principle adopted in the displacement method of statically multiply indeterminate structures and thus it can be considered to be a variation of the most widely used finite elements method using large elements in the present case.

1. Introduction

Typical examples of complex rotation shell structure subject to rotationally symmetric load are underground or surface liquid tanks, gas tanks, silos, watertowers (Fig. 1).

The method of Márkus, analogous with the Cross moment distribution method, is used in general for manual calculation of complex rotation shells. This method requires that tables, diagrams and complicated formulae of a wide variety be used. On the basis of the same algorithm, computerization of the manual calculation is practically impossible.

For calculation of complex rotation shell structures, any process available for calculation of statically indeterminate structures (such as force method, displacement method,etc.) can be used. In our work, we show the application of the displacement method where the number of unknowns is

*Csákány, Anikó, H-1121 Budapest, Rácz Aladár u. 119, Hungary

**Hegedüs, István, H-2083 Solymár, Váci Mihály u. 10, Hungary

***Kollár, László, P., H-1122 Budapest, Karap u. 9, Hungary

Akadémiai Kiadó, Budapest

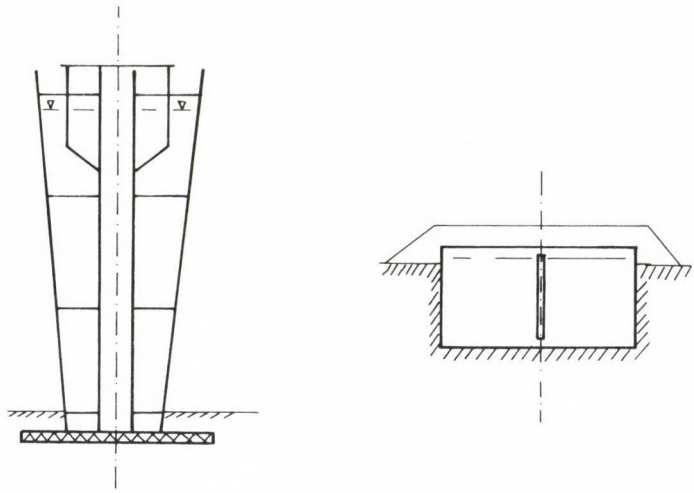

Fig. 1. Complex rotation shells

less in general. This displacement method can also be considered as a finite elements method where the finite elements are the structural elements like cone, cylinder, circular plate and annular elements themselves while the basic functions are the mathematically exact solutions of the different structural elements.

To write the condition equation system of the displacement method, it is necessary that the rigidity matrices and load vectors associated with the elements of the primary structure be determined. Discussed below is the calculation of cone shells of arbitrary apex angle that is, cone shells becoming a cylinder of vertical generatrix in the extreme case, permitting the calculation to be directly computerized. We also show how to take the vertical compressions of cone shells into consideration as this is not discussed in the literature /1, 2/.

2. Assumptions

To describe the cone shell, we adoped the assumptions of classic engineering shell theory in this work. That is, we assume that

- rotationally symmetric load is acting upon the rotationally symmetric structure,

- the structure is elastic and its material is homogeneous and isotropic,

- the thickness of the elements is invariable and small as compared with the other dimensions,

- the displacement of points on the middle surface is small as compared with the wall thickness of the elements,

- deformations resulting from stresses normal to the middle surface are negligible,

- points along the normal of the surface remain along the normal of the surface also after deformation (Kirchhoff-Love hypothesis).

The elements are connected to each other or to a fixed support (foundation) along so-called nodal lines, these lines being circular intersection lines of the middle surfaces of connected elements.

Displacements within the tangent plane of the surface are not neglected when the conditions of connection of the elements are written that is also changes in length of the cones and cylinders in the direction of the generatrix are taken into consideration.

Also, it is taken into consideration that displacement of the edges of the elements as compared with each other may be permitted or prevented by the construction of connections that is, the support may be roller-type or fixed against connection forces while hinged or clamp-type against moments.

Within the elements, two types of load distributed over the surface are taken into consideration, such as

- dead load (g), weight of unit shell or plate surface,

- liquid load, load applied to the surface at right angles by liquid of bulk density γ.

Acting upon the structure are horizontal ($\overline{P}_x$) or vertical ($\overline{P}_y$) forces uniformly distributed along the nodal lines that is along a circular line each as well as uniformly distributed moments ($\overline{M}$).

As a result of the loads, the following stresses arise in the structural elements:

- normal force in the direction of the generatrix or radius N_r,
- annular normal force N_ϕ,
- radial moments or moments acting in the direction of the generatrix M_r,
- annular moments M_ϕ,
- shear forces Q.

Indicated in Fig. 2 are stresses of positive sign.

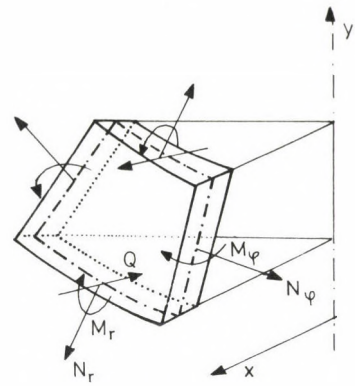

Fig. 2. Stresses of the shell element

3. Calculation method

The assumptions specified above permit the calculation of complex rotation shell structures to be traced back to the calculation of statically multiply indeterminate structures using a discrete model.

Primary structure is the structure obtained in such a way that the nodal lines of the structure investigated are prevented from being displaced.

Unknowns are the displacement components of the nodal lines, that is, the horizontal, and vertical shifts and angular displacements.

Let the co-ordinate system be plotted in such a way that axis y, pointing up, will coincide with the axis of symmetry while axis x will point outwards at right angles to this (Fig. 1), the origin being fixed at any arbitrary point along the axis of symmetry. Illustrated in Fig. 3 are positive displacements of a nodal line on the left of the axis of rotation of the structure.

The sign of loads along the nodal line (Fig. 3) is defined in a similar way, that is, load components resulting in positive work with the appropriate positive displacement components are considered positive. From among loads distributed over the surface of the elements, acting within the elements, the dead load is always positive. The liquid load will be positive if it forces the shell element outwards as compared with the axis of rotation. For bulk density γ of the liquid applying load to the structure, also negative sign can be assumed.

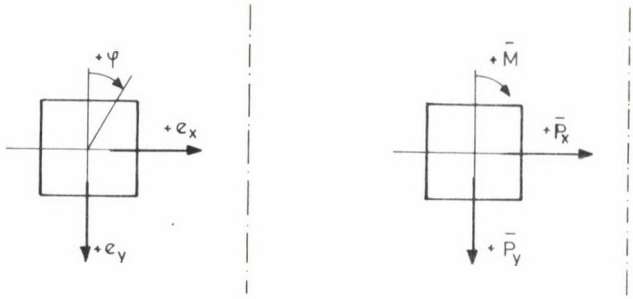

Fig. 3. Displacements and loads of a nodal line

In the calculation, first thing to do is to set up the condition equation system of displacement method

$$\underline{\underline{K}} \cdot \underline{u} = \underline{q} \ , \qquad (1)$$

where the elements of $\underline{u}$ are the displacement components of the nodal lines of the structure, $\underline{q}$ is the vector of loads reduced to the nodal lines of the primary structure while $\underline{\underline{K}}$ is the global rigidity matrix of the structure.

Equation system (1) describes the balance of external and internal forces and moments acting along nodal lines, each row being an equilibrium equation. With the sequence of elements in displacement vector $\underline{u}$ followed in writing of these equations, regularities are found in the coefficient matrix $\underline{\underline{K}}$ of the equation system, which can be used to simplify the equation system when written and, possibly, solved. A typical regularity is the block structure of the coefficient matrix.

The block of the coefficient matrix, usually of size 3x3, contains essentially the horizontal and vertical forces and moments (P_x^i, P_y^i, M^i) for unit periphery, arising along the i-th nodal line as a result of motion components $e_x^j = 1$, $e_y^j = 1$, $\phi^j = 1$ of unit size, inserted along the j-th nodal line.

Nonzero elements are contained by block (i, j) if the i-th and j-th nodal lines are interconnected by some shell or plate element of the structure. The block structure of coefficient matrix $\underline{\underline{K}}$ is determined by the structure of vector $\underline{u}$ of the displacements. This permits the blocks of the coefficient matrix to be superimposed from the blocks of the rigidity matrices of the elements.

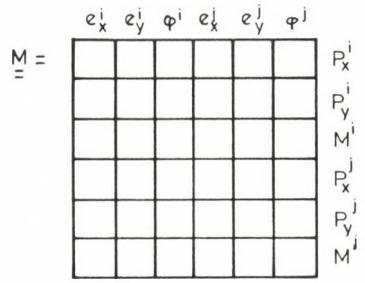

Fig. 4. A structural element's own rigidity matrix

The first column of rigidity matrix $\underline{\underline{M}}$ of size 6x6 of the structural element interconnecting the i-th and j-th nodal lines (Fig. 4) contains reactions P_x^i, P_y^i, M^i taking place on the kinematically definite primary structure associated with the element as a result of $e_x^i = 1$ inserted there along the i-th nodal line as well as reactions P_x^j, P_y^k, M^j taking place along the j-th nodal line. The second, third and the following columns contain reactions resulting from displacements $e_y^i = 1$, $\phi^i = 1$ and $e_x^j = 1$, $e_y^j = 1$, $\phi^j = 1$, respectively (Figs 4 and 5).

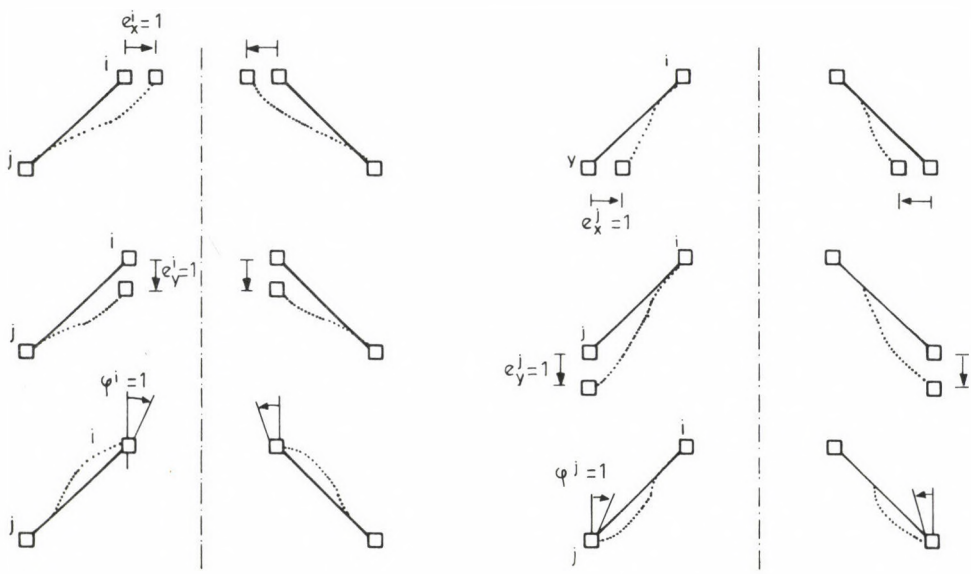

Fig. 5. Displacements of cone shell along nodal line

Note that the elements of rigidity matrix $\underline{\underline{M}}$ are quantities related to unit periphery and thus, because of the different edge radii, matrix $\underline{\underline{M}}$ is not symmetric, the ratio of symmetrically arranged elements being identical with the ratio of edge radii. As a result, 'global' rigidity matrix $\underline{\underline{K}}$ is not symmetric either but it can be made symmetric by multiplying its rows by appropriate numbers.

In the course of compilation, the appropriate blocks of the elementary rigidity matrices are added. It can be seen that diagonal block (i, i) of matrix $\underline{\underline{K}}$ will certainly contain nonzero element (at least in the principal diagonal). However, block (i, j) will contain nonzero element only if nodal lines i and j are interconnected by some shell or plate element.

With the displacement components corresponding to motions prevented by supports considered to be fixed unknowns (of zero value), an equation system is obtained where the number of equations exceeds the number of unknown motion components. The unknowns associated with 'excess' equations are the components of support reactions. The equilibrium equations relating to these components can be separated. Thus for unknown motion components, an equation system of reduced size, having a similarly square coefficient matrix, is obtained. Hence, after compilation, the appropriate rows and columns of the matrix shall be omitted to compress the matrix.

The load vector can be produced by reducing the loads to nodal lines.

On the basis of loads acting upon the elements, reactions along nodal lines are calculated on the primary structure. The elements of the load vector of the structural element interconnecting the i-th and j-th nodal lines are the opposite of the reactions transmitted from the element of the primary structure interconnecting nodal lines i and j to the nodal lines, P_x^i, P_y^i, M^i, P_x^j, P_y^j, M^j in due order.

The elements of load vector $\underline{q}$ of the entire structure shall be produced by adding the appropriate elements of six-element or three-element vectors t and loads $\overline{P}_x$, $\overline{P}_y$, $\overline{M}$ directly along the nodal lines.

The sign of the elements of the load vector shall be defined in compliance with the sign of the elements of the rigidity matrix. The horizontal or vertical load transmitted to the nodal line will be positive if it points inwards or downwards while the moment will be positive if it results in clockwise rotation when illustrated on the left of the axis of rotation in that part of the cross section that is if, with positive dual displacements, it results in positive work.

Hereinafter we deal with calculation of truncated conical shell elements in detail.

4. Rigidity matrix of one cone element

The rigidity matrix of the cone, denoted by $\underline{\underline{M}}$,, shall be produced, as follows:

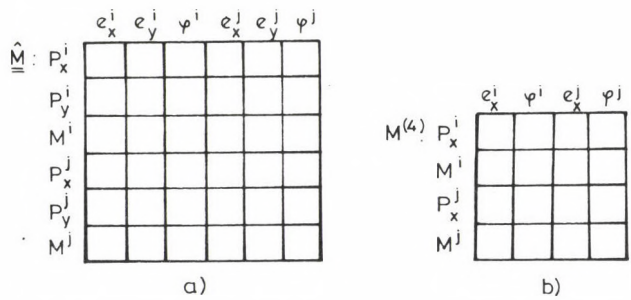

Fig. 6. Rigidity matrix of a truncated conical shell clamped at both edges

To be produced first is rigidity matrix $\hat{\underline{\underline{M}}}$ of the shell clamped at both edges (Fig. 6).

In doing so, a matrix $\underline{\underline{M}}^{(4)}$ containing 4x4 elements shall be filled first (Fig. 6) in which the horizontal edge forces and moments resulting from horizontal edge displacements and angular displacements are collected. These forces and moments are calculated, independently of the actual support conditions, for a structure where the vertical edge displacement can take place without any restriction (Fig. 7). The relationships used can be found in /1/.

Since the edge forces and moments according to the physical definition of the matrix elements are associated with other than exactly unit edge displacements (since the upper edge is not prevented from being displaced in vertical direction), the elements of matrix $\underline{\underline{M}}^{(4)}$ are not identical with the appropriate elements of the elementary rigidity matrix of the cone.

Matrix $\hat{\underline{\underline{M}}}$ enlarged by rows and columns corresponding to vertical edge displacement can then be produced on the basis of elements of $\underline{\underline{M}}^{(4)}$ already available and finally, matrix $\hat{\underline{\underline{M}}}$ shall be modified in accordance with the actual support conditions.

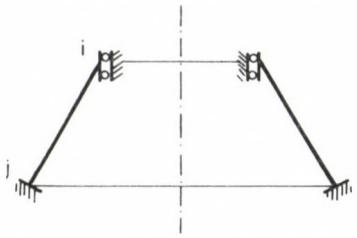

Fig. 7. Support permitting the upper edge to be displaced vertically

4.1 Rigidity matrix of a cone element clamped at both edges

4.1.1 Production of $\underline{\underline{M}}^{(4)}$

Let the following notation be introduced:

x_1 - radius of top edge,

x_2 - radius of bottom edge,

$$x_k = \frac{x_1 + x_2}{2} ,$$

x - radius parameter,

α_o - half summit angle of the cone,

ϑ - angular displacement of the shell surface,

Δr - change of horizontal radius of middle surface,

h - shell thickness,

E - modulus of elasticity,

μ - Poisson number,

$$K = \frac{E \cdot h^3}{12 \cdot (1 - \mu^2)} ,$$

$$\lambda = \sqrt[4]{\frac{E \cdot h \cdot tg^2 \alpha_o}{K}}$$ - so-called damping factor.

As a result of load, stresses defined according to Fig. 2 may arise on the shell.

With variables

$$U = x \cdot Q \quad \text{and} \quad \vartheta$$

introduced, the following inhomogeneous differential equations can be used to describe the states of the structure:

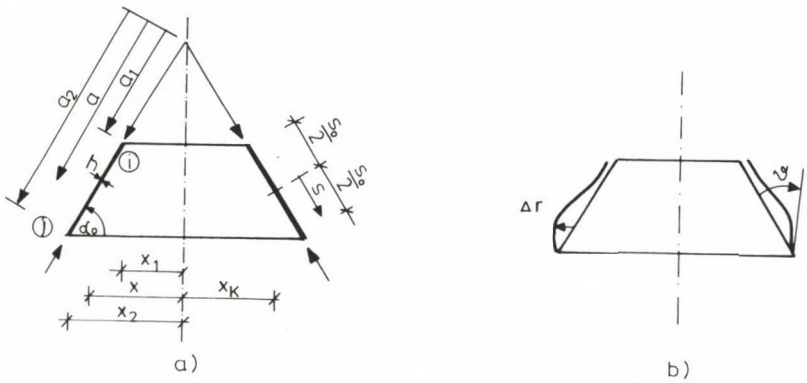

Fig. 8. Conical shell element

$$LL(\vartheta) + \lambda^4 \vartheta_{ms},$$

$$LL(U) + \lambda^{*4} U = Eh \cdot tg^2 \alpha_o \cdot \alpha(\vartheta_m), \tag{2}$$

where L is the Meissner operator,

$$L(...) = x \frac{d(...)}{dx^2} + \frac{d(...)}{dx} - \frac{1}{x}(...), \tag{3}$$

while ϑ_m indicates angular displacement on the structure supported in a way that deformations due to membrane forces can develop.

Bends on the shell supported in that way are assumed to be negligible as compared with the bending stresses resulting from boundary disturbances. That means that the membrane solution can be used as a particular solution of inhomogeneous equation (2). Thus the stresses and deformations of cone shells can be calculated by superposition of the membrane state and boundary disturbances. Since the action of membrane forces and the membrane deformations are known for the possible loads /1, 2/, it is enough to deal with the solution of homogeneous equations

$$LL(\vartheta) + \lambda^4 \vartheta = 0,$$

$$LL(U) + \lambda^4 U = 0 \tag{4}$$

describing the behaviour of a shell under load at the edges only.

These homogeneous fourth-order differential equations can be transformed into simultaneous Bessel-type differential equations /1/:

$$L(\vartheta) + i \lambda^2 \vartheta = 0$$

$$L(\vartheta) - i \lambda^2 \vartheta = 0 \tag{5a}$$

and

$$L(U) + i\ \lambda^2 U = 0$$
$$L(U) - i\ \lambda^2 U = 0 \qquad (5b)$$

with relationship $U = K \cdot L(\vartheta)$ (6)
existing between the unknowns.

Let variable

$$\alpha = 2\lambda\sqrt{x} \qquad (7)$$

and functions

$$G_9(\alpha) = \frac{2}{\alpha}\,\mathrm{bei}'(\alpha) - \mathrm{ber}(\alpha)\ ,$$
$$G_{10}(\alpha) = \frac{2}{\alpha}\,\mathrm{ber}'(\alpha) + \mathrm{bei}(\alpha)\ ,$$
$$G_{11}(\alpha) = \frac{2}{\alpha}\cdot\frac{2}{\pi}\cdot\mathrm{ker}'(\alpha) + \frac{2}{\pi}\cdot\mathrm{kei}(\alpha)\ , \qquad (8)$$
$$G_{12}(\alpha) = -\frac{2}{\alpha}\cdot\frac{2}{\pi}\cdot\mathrm{kei}'(\alpha) + \frac{2}{\pi}\cdot\mathrm{ker}(\alpha)$$

introduced by Hampe /1/ be used, where $\mathrm{ber}(\alpha)$, $\mathrm{bei}(\alpha)$, $\mathrm{ker}(\alpha)$, $\mathrm{kei}(\alpha)$ are zero-order Thomson functions obtained as a solution of differential equations (5) (for details see Appendix) while $(\ldots)'$ indicates differentiation with respect to α.

Functions of stresses and displacements of the shell /1/:

$$N_r = \frac{\mathrm{ctg}\,\alpha_o}{x}\left[\, C_1 . G_9(\alpha) + C_2 . G_{10}(\alpha) + C_3 . G_{11}(\alpha) + C_4 . G_{12}(\alpha)\,\right]\ , \qquad (9a)$$

$$N_\phi = \frac{\lambda\ \mathrm{ctg}\,\alpha_o}{x}\left[\, C_1 . G_9'(\alpha) + C_2 . G_{10}'(\alpha) + C_3 G_{11}'(\alpha) + C_4 . G_{12}'(\alpha)\,\right]\ , \qquad (9b)$$

$$M_r = \frac{1}{\lambda^2 x}\left\{ C_1\left[\lambda\sqrt{x}\, G_{10}'(\alpha) + \mu G_{10}(\alpha)\right] - C_2\left[\lambda\sqrt{x}\, G_9'(\alpha) + \mu G_9(\alpha)\right] + \right.$$
$$\left. + -C_3\left[\lambda\sqrt{x}\, G_{12}'(\alpha) + \mu G_{12}(\alpha)\right] - C_4\left[\lambda\sqrt{x}\, G_{11}'(\alpha) + \mu G_{11}(\alpha)\right]\right\}, \qquad (9c)$$

$$M_\phi = \frac{1}{\lambda^2 x}\left\{ C_1\left[\lambda\mu\sqrt{x}\, G_{10}'(\alpha) + G_{10}(\alpha)\right] - C_2\left[\lambda\mu\sqrt{x}\, G_9'(\alpha) + G_9(\alpha)\right] + \right.$$
$$\left. + C_3\left[\lambda\mu\sqrt{x}\, G_{12}'(\alpha) + G_{12}(\alpha)\right] - C_4\left[\lambda\mu\sqrt{x}\, G_{11}'(\alpha) + G_{11}(\alpha)\right]\right\}\ , \qquad (9d)$$

$$Q = \frac{1}{x}\left[C_1 G_9(\alpha) + C_2 G_{10}(\alpha) + C_3 G_{11}(\alpha) + C_4 G_{12}(\alpha) \right] , \tag{9e}$$

$$\vartheta = -\frac{1}{\lambda^2 K}\left[C_1 G_{10}(\alpha) - C_2 G_9(\cdot) + C_3 G_{12}(\alpha) - C_4 G_{11}(\alpha) \right] , \tag{9f}$$

$$\begin{aligned}\Delta r = \frac{\cos\alpha_0 . \operatorname{ctg}\alpha_0}{Eh}\Big\{ & C_1\left[\lambda\sqrt{x}\, G_9(\alpha) - \mu\, G_9(\alpha)\right] + \\ & + C_2\left[\lambda\sqrt{x}\, G_{10}'(\alpha) - \mu\, G_{10}(\alpha)\right] + C_3\left[\lambda\sqrt{x}\, G_{11}'(\alpha) - \mu G_{11}(\alpha)\right] + \\ & + C_4\left[\lambda\sqrt{x}\, G_{12}'(\alpha) - \mu G_{12}'(\alpha)\right]\Big\}\end{aligned} \tag{9g}$$

Here C_1, C_2 C_3 C_4 are integration constants.

Assume that the top edge of the conical shell investigated is connected to the i-th while the bottom edge to the j-th nodal line. Let the following vectors be introduced:

$$\underline{e} = \begin{bmatrix} \Delta r^i \\ \phi^i \\ \Delta r^j \\ \phi^j \end{bmatrix} , \quad \underline{x} = \begin{bmatrix} P_x^i \\ M^i \\ P_y^j \\ M^j \end{bmatrix} , \quad \underline{c} = \begin{bmatrix} C_1 \\ C_2 \\ C_3 \\ C_4 \end{bmatrix} . \tag{10}$$

On the basis of relationships (9), the reactions and edge displacements of the shell can be calculated, as follows:

$$\underline{x} = \underline{B} \cdot \underline{c} \tag{11}$$

$$\underline{e} = \underline{A} \cdot \underline{c} , \tag{12}$$

where, using notation

$$\alpha_i = 2\lambda\sqrt{x_i} ,$$

$$F_{m,n} = \frac{1}{\sin\alpha_0}\,\frac{1}{x_n}\, G_m(\alpha_n) , \qquad \begin{matrix} m = 9, 10, 11, 12 \\ n = 1, 2 \end{matrix}$$

$$H_{m,n} = \frac{1}{\lambda^2 x_n}\left[\lambda . \sqrt{x_n} G_m'(\alpha_n) + \mu . G_m(\alpha_n) \right] , \qquad \begin{matrix} m = 9, 10, 11, 12 \\ n = 1, 2 \end{matrix}$$

$$J_{m,n} = \frac{\cos\alpha_0}{Eh \sin\alpha_0}\left[\lambda\sqrt{x_n}\, G_m'(\alpha_n) - \mu G_m(\alpha_n)\right] , \qquad \begin{matrix} m = 9, 10, 11, 12 \\ n = 1, 2 \end{matrix}$$

and

$$K_{m,n} = \frac{1}{\lambda^2 K}\, G_m(\alpha_n) \qquad \begin{matrix} m = 9, 10, 11, 12 \\ n = 1, 2 \end{matrix}$$

matrix $\underline{A}$ and matrix $\underline{B}$ are:

$$\underline{A} = \begin{bmatrix} F_{9,1} & F_{10,1} & F_{11,1} & F_{12,1} \\ H_{10,1} & -H_{9,1} & H_{12,1} & -H_{11,1} \\ F_{9,2} & F_{10,2} & F_{11,2} & F_{12,2} \\ H_{10,2} & -H_{9,2} & H_{12,2} & -H_{11,2} \end{bmatrix}, \tag{13}$$

$$\underline{B} = \begin{bmatrix} J_{9,1} & J_{10,1} & J_{11,1} & J_{12,1} \\ -K_{10,1} & K_{9,1} & -K_{12,1} & K_{11,1} \\ J_{9,2} & J_{10,2} & J_{11,2} & J_{12,2} \\ -K_{10,2} & K_{9,2} & -K_{12,2} & K_{11,2} \end{bmatrix}. \tag{14}$$

With these matrices,

$$\underline{x} = \underline{B} \cdot \underline{A}^{-1} \cdot \underline{e} = \underline{M}^{(4)} \cdot \underline{e} , \tag{15}$$

that is matrix $M^{(4)}$ wanted can be obtained by means of the following formula:

$$M^{(4)} = \underline{B} \cdot \underline{A}^{-1} . \tag{16}$$

Thus,we have obtained rigidity matrix $\underline{M}^{(4)}$ of the shell element illustrated in Fig. 7. It is important to emphasize that this matrix is not the minor matrix of elementary rigidity matrix $\hat{\underline{M}}$ wanted, because also a vertical compression Δy belongs to displacement system $\underline{e}$ the magnitude of which is unknown for the time being.

4.1.2 Calculation of rigidity matrix $\hat{\underline{M}}$ by completion of $\underline{M}^{(4)}$

To complete matrix $\underline{M}^{(4)}$ with a second and fifth column and row we need the vertical compression resulting from load of direction y.

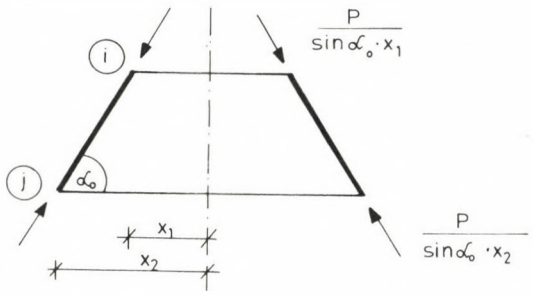

Fig. 9. Load system acting in the direction of the generatrix

To calculate this, let first the equilibrium force system according to Fig. 9 act upon the unsupported shell in the direction of the generatrix. As a result, a purely membrane type action of forces will develop. Associated with this action are edge displacements

$$\underline{e}_p = \begin{bmatrix} \Delta r^i \\ \phi^i \\ \Delta r^j \\ \phi^j \\ \Delta y_p \end{bmatrix} \text{ arise.} \tag{17}$$

Elements of vector $\underline{e}_p$ are as follows /2/:

$$\begin{aligned} \Delta r^i &= -\mu \frac{P}{2\pi Eh \sin\alpha_o}, \\ \phi^i &= -\frac{P \cos\alpha_o}{2\pi Eh\, x_1 \sin\alpha_o}, \\ \Delta r^j &= -\mu \frac{P}{2\pi Eh \sin\alpha_o}, \\ \phi^j &= -\frac{P \cos\alpha_o}{2\pi Eh\, x_2 \sin\alpha_o}; \end{aligned} \tag{18}$$

Δy_p is the relative vertical displacement of the upper and lower edge, consisting of two terms:

$$\Delta y_p = \Delta y' + \Delta y'' . \tag{19}$$

The first part results from compression in the direction of the generatrix. Normal force in the direction of the generatrix, resulting from system of vectors of vertical resultant P acting along the edges:

$$N_r = \frac{P}{2\pi x \sin \alpha_o} \quad . \tag{20}$$

The vertical component of compression in the direction of the generatrix resulting from this is given by expression

$$\Delta y' = \sin \alpha_o \int_{a_1}^{a_2} \frac{N_r}{Eh} \, da \tag{21}$$

using the notation of Fig. 8. Making use of equality

$$x = a \cos \alpha_o \, , \tag{22}$$

we obtain from expression (21) that

$$\Delta y' = \frac{\sin \alpha_o}{Eh} \int_{a_1}^{a_2} \frac{P}{2\pi a \sin \alpha_o \cos \alpha_o} \, da =$$

$$= \frac{P}{2\pi Eh \cos \alpha_o} (\ln a_2 - \ln a_1) \, . \tag{23}$$

In case of steep cylinder-like cones, formula (23) may result in numerical error while in case of cylinders, it becomes meaningless. Let therefore parameter 'a' be replaced by parameter 's' according to Fig. 8 that the algorithm for calculation of the cone and cylinder can be lumped. Thus, using relationships $x_k = \frac{1}{2}(x_1+x_2)$ and $x = x_K + s \cos \alpha_o$ and introducing variable

$$z = \frac{\cos \alpha_o \, s_o}{2 x_k} \, , \tag{24}$$

the following relationship can be obtained:

$$y' = \frac{P}{2\pi Eh \cos \alpha_o} \left[\ln (1+z) - \ln (1-z) \right] \, . \tag{25}$$

Since in case of cylinders, also this expression is meaningless, a further

transformation is necessary. With series

$$\ln(1+z) = z - \frac{z^2}{2} + \frac{z^3}{3} - \frac{z^4}{4} + \frac{z^5}{5} - \dots ,$$
$$\ln(1-z) = -\left(z + \frac{z^2}{2} - \frac{z^3}{3} + \frac{z^4}{4} - \frac{z^5}{5} + \dots \right) \tag{26}$$

of functions ln (1+z) and ln (1-z), the first part of the vertical compression is

$$\Delta y' = \frac{P}{2\pi Eh} \frac{s_o}{x_k} \left(1 + \frac{z^2}{3} + \frac{z^4}{5} + \dots \right) \tag{27}$$

according to (25).

With the first few terms of the power series taken into consideration, a formula applying to cones and cylinders alike, also numerically stable, will be obtained.

The second part of Δy_p is brought about as a result of deformation of the generatrix. As a result of the different displacement of the top and bottom edge, the second part of the vertical compression will be

$$\Delta y'' = (\Delta r^i - \Delta r^j) \operatorname{ctg} \alpha_o . \tag{28}$$

In the present case, $\Delta r^i = \Delta r^j$ according to (18). Therefore, $\Delta y'' = 0$, that is,

$$\Delta y_p = \Delta y' = \frac{P}{2\pi Eh} \frac{s_o}{x_k} \left(1 + \frac{z^2}{3} + \frac{z^4}{5} + \dots \right) . \tag{29}$$

Thus, all the elements of displacement system $\underline{e}_p$ according to (17) have been calculated.

Consider now system of forces

$$\underline{\hat{x}} = \underline{\underline{M}}^{(4)} \underline{\hat{e}} , \tag{30}$$

where the elements of $\underline{\hat{e}}$ are some of those of $\underline{e}_p$ according to (17):

$$\underline{\hat{e}} = \begin{bmatrix} \Delta r^i \\ \phi^i \\ \Delta r^j \\ \phi^j \end{bmatrix}$$

Vertical compression $\Delta\hat{y}$ associated with this system of forces is determined on the basis of Maxwell's interchangeability theorem. Accordingly, the contribution of the system of forces of equilibrium illustrated in Fig. 9 to displacements associated with force system $\underline{\hat{x}}$ complies with the contribution of system $\underline{\hat{x}}$ to displacement system $\underline{e}_p$. Hence, with the elementary works added,

$$\Delta\hat{y}\, P + \frac{2\pi x_1}{2\pi x_1} P \operatorname{ctg}\alpha_o \;\Delta r^i - \frac{2\pi x_2}{2\pi x_2} \operatorname{ctg}\alpha_o \;\Delta r^j = \tag{31}$$

$$= \left(\Delta r^i \hat{x}_1 + \phi^i \hat{x}_2\right) 2\pi x_1 + \left(\Delta r^j \hat{x}_3 + \phi^j \hat{x}_4\right) 2\pi x_2$$

where x_1 and x_2 are edge radii while $\hat{x}_1 \ldots, \hat{x}_4$ elements of forces system $\underline{\hat{x}}$.

As a resultant of the opposite of the equilibrium system according to Fig. 9 and force system $\underline{\hat{x}}$ according to (30), a load system can be produced, with which only vertical compression of a magnitude of

$$\Delta y = \Delta y_p - \Delta\hat{y}$$

is associated. Let parameter P of the equilibrium force system be selected so as to result in

$$\frac{P}{\sin\alpha_o} = 1 \,.$$

Then the elements of the second column of rigidity matrix $\underline{\hat{M}}$ can be obtained by dividing each element of the resultant force system by Δy, that is

$$\underline{m}_2 = \frac{1}{\Delta y} \begin{bmatrix} -\hat{x}_1 + \dfrac{\cos\alpha_o}{2\pi x_1} \\ \dfrac{\sin\alpha_o}{2\pi x_1} \\ -\hat{x}_2 \\ \hat{x}_3 - \dfrac{\cos\alpha_o}{2\pi x_2} \\ \dfrac{\sin\alpha_o}{2\pi x_2} \\ -\hat{x}_4 \end{bmatrix} \tag{32}$$

The opposite of fifth column $\underline{m}_2$:

$$\underline{m}_5 = -\underline{m}_2 . \tag{33}$$

The missing elements of the second and fifth column are obtained on the basis of the structural specialities of the elementary rigidity matrices:

$$\hat{m}_{2,1} = \hat{m}_{1,2} \qquad \hat{m}_{5,1} = \hat{m}_{1,5}\frac{x_1}{x_2}$$

$$\hat{m}_{2,3} = \hat{m}_{3,2} \qquad \hat{m}_{5,3} = \hat{m}_{3,5}\frac{x_1}{x_2}$$

$$\hat{m}_{2,4} = \hat{m}_{4,2}\frac{x_2}{x_1} \qquad \hat{m}_{5,4} = \hat{m}_{4,5}$$

$$\hat{m}_{2,6} = \hat{m}_{6,2}\frac{x_2}{x_1} \qquad \hat{m}_{5,6} = \hat{m}_{6,5}$$

The missing 4x4 elements of rigidity matrix $\hat{\underline{\underline{M}}}$ are the appropriate elements of matrix $\hat{\underline{\underline{M}}}^{(4)}$ obtained by modification of matrix $\underline{\underline{M}}^{(4)}$, the elements of the k-th column of matrix $\hat{\underline{\underline{M}}}^{(4)}$ being calculated by means of formula

$$\hat{\underline{m}}_k^{(4)} = \underline{m}_k^{(4)} + \frac{\hat{m}_{2,k}}{\hat{m}_{2,2}}\,\underline{m}_2^{(4)} . \tag{34}$$

Now rigidity matrix $\hat{\underline{\underline{M}}}$ of the truncated conical shell clamped at both edges is available.

4.2 Modification of rigidity matrix $\hat{\underline{\underline{M}}}$ in accordance with the real support conditions

Should the support permit some of the displacement components to develop at one of the edges of the shell element, it will be necessary that matrix $\hat{\underline{\underline{M}}}$ be modified accordingly.

Assume that free displacement of the edge in the direction of the support corresponding to the k-th column of $\hat{\underline{\underline{M}}}$ is possible. To produce matrix

$\hat{\underline{\underline{M}}}$ modified according to this assumption, let matrix

$$\underline{\underline{C}}_{(k)} = \underline{\underline{E}} - \frac{1}{\hat{m}_{k,k}} \underline{e}_{(k)} \hat{\underline{m}}_k^* \tag{35}$$

of size 6x6 be introduced, where $\underline{\underline{E}}$ is a sixth-order unit matrix, $\hat{m}_{k,k}$ are elements (k,k) of matrix $\hat{\underline{\underline{M}}}$, $\underline{e}_{(k)}$ is a six order unit vector the k-th element of which is 1 while $\hat{m}_k^*$ is the k-th row of matrix $\hat{\underline{\underline{M}}}$. Now matrix $\underline{\underline{M}}$ can be determined from relationship

$$\underline{\underline{M}} = \hat{\underline{\underline{M}}} \cdot \underline{\underline{C}}_{(k)} \cdot \tag{36}$$

If displacement of the edge is possible also in the direction of the support corresponding to the ℓ-th column in addition to the k-th column, then matrix $\underline{\underline{M}}$ shall be modified as required again.

5. Calculation of the elements of the load vector

The elements of the load vector of the shell element interconnection the i-th and j-th nodal lines are the opposite of the reactions transmitted from the shell element to the nodal lines. To produce the elements of the load vector, the force action of the membrane shell shall be taken as a starting point instead of solution of the inhomogeneous differential equation.

The elements of load vector $\underline{t}$ shall be produced, as follows:

a) Consider a shell supported in the direction of the generatrix at the bottom edge while free at the top one (Fig. 10). Assume that membrane force action develops as a result of these loads, with edge displacement system $\underline{e}_0$ and reaction system $\underline{x}_0$:

$$\underline{e}_0 = \begin{bmatrix} \Delta r^i \\ \Delta y^i \\ \phi^i \\ \Delta r^j \\ \Delta y^j \\ \phi^j \end{bmatrix}, \qquad \underline{x}_0 = \begin{bmatrix} 0 \\ 0 \\ 0 \\ P^j \\ P_j^x \\ 0^y \end{bmatrix}. \tag{37}$$

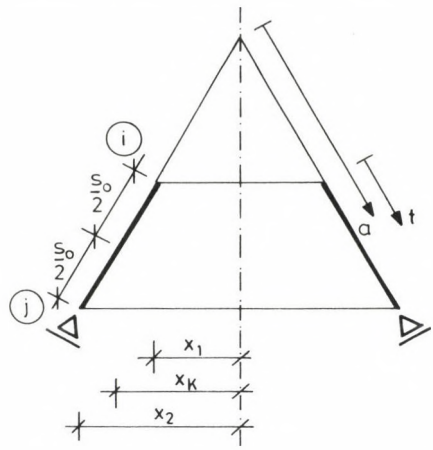

Fig. 10. Shell supported in accordance with membrane force action

Let the elements of $\underline{e}_o$ and $\underline{x}_o$ be produced. In doing so, the membrane stresses shall be determined first:

$$N_r = - \frac{G}{2 \pi x \sin \alpha_o} \tag{38}$$

$$N_\phi = - \frac{x}{\cos \alpha_o} p_z \operatorname{ctg} \alpha_o , \tag{39}$$

where G is the resultant of loads action upon the shell section above the point investigated and p_z is the component of normal direction of surface load.

The horizontal displacement is obtained by

$$\Delta r = \frac{x}{Eh} (N_\phi - \mu N_r) , \tag{40}$$

angular displacement by

$$\vartheta = \frac{\operatorname{ctg} \alpha_o}{Eh} \left[(N_r - N_\phi)(1 + \mu) + a \frac{d}{dt} (N_\phi - \mu N_r) \right] . \tag{41}$$

In the formula for ϑ, also the effect of compression in the direction of the generatrix has been taken into consideration. For calculation of (41), we need formulae

$$x = x_1 + t \cos \alpha_o , \tag{42}$$

$$\frac{dx}{dt} = \cos \alpha_o \tag{43}$$

In case of dead load,

$$G_p = g \pi t (x_1 + x) , \tag{44}$$

where g is the weight of shell element of unit surface.

$$N_{r,g} = - \frac{g}{2\sin \alpha_o} \frac{t(x+x_1)}{x} , \qquad N_{\phi,g} = - gx \frac{\cos \alpha_o}{\sin \alpha_o} . \tag{45}$$

$$\frac{dN_{r,g}}{dt} = - \frac{g}{2\sin \alpha_o} (1 + \frac{x_1^2}{x}) , \qquad \frac{dN_{\phi,g}}{dt} = - g \frac{\cos^2 \alpha_o}{\sin \alpha_o} \tag{46}$$

By means of these relationships, displacements Δr_g and ϑ_g can be obtained from formulae (40) and (41).

In case of liquid load, let the height of the liquid column above the top edge denoted by H, the height of the truncated cone by H_o while the length of the generatrix by s_o (Fig. 11). Now

$$H_o = s_o \sin \alpha_o . \tag{47}$$

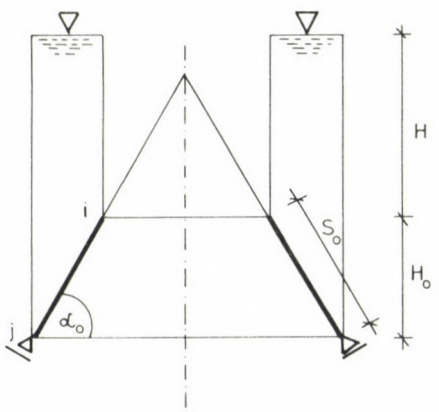

Fig. 11.

Let specific gravity γ of the liquid be positive if the shell is pressed outwards while negative if the shell is pressed inwards by the liquid. Now the formulae corresponding to (44)—(46) will be:

$$G_{\gamma} = \gamma\pi\left[H(x^2 - x_1^2) + \frac{H_0}{3}(2x^2 - x_1^2 - xx_1)\right], \tag{48}$$

$$\left.\begin{aligned} N_{r,\gamma} &= -\frac{\gamma}{2x\sin\alpha_0}\left[H(x^2 - x_1^2) + \frac{H_0}{3}(2x^2 - x_1^2 - xx_1)\right], \\ N_{\phi,\gamma} &= -\gamma(H + t\sin\alpha_0)\frac{x}{\sin\alpha_0}, \end{aligned}\right\} \tag{49}$$

$$\left.\begin{aligned} \frac{dN_{r,\gamma}}{dt} &= -\frac{\gamma\cos\alpha_0}{2\sin\alpha_0}\left[H\left(1 + \frac{x_1^2}{x^2}\right) + \frac{H_0}{3}\left(2 + \frac{x_1^2}{x^2}\right)\right], \\ \frac{dN_{\phi,\gamma}}{dt} &= -\frac{\gamma}{\sin\alpha_0}\left[H\cos\alpha_0 + x\sin\alpha_0 + t\sin\alpha_0\cos\alpha_0\right]. \end{aligned}\right\} \tag{50}$$

Shift Δr_{γ} and angular displacement ϑ_{γ} resulting from water pressure are obtained by substituting formulae (48—50) into relationships (40—41), respectively.

The stresses acting upon the structure can be obtained by adding the stresses resulting from the two different loads:

$$\begin{aligned} N_r &= N_{r,g} + N_{r,\gamma} \\ N_{\phi} &= N_{\phi,g} + N_{\phi,\gamma} \end{aligned} \tag{51}$$

Edge displacements are obtained as a result of the following additions:

$$\left.\begin{aligned} \Delta r^i &= \Delta r_g^i + \Delta r_\gamma^i \,, \\ \vartheta^i &= \vartheta_g^i + \vartheta_\gamma^i \,, \\ \Delta r^j &= \Delta r_g^j + \Delta r_\gamma^j \,, \\ \vartheta^j &= \vartheta_g^j + \vartheta_\gamma^j \,. \end{aligned}\right\} \qquad (52)$$

The principle of calculation of vertical compression $\Delta y_o = \Delta y^j - \Delta y^i$ agrees with what has been said in par 4.1.2 Δy_o can be calculated by means of relationship $\Delta y_o = \Delta y_o' + \Delta y_o''$ according to (19).

$\Delta y_o'$ resulting from compression in the direction of the generatrix can be determined by relationship

$$\Delta y_o' = \sin \alpha_o \int_o^{s_o} \frac{N_r - \mu N_\phi}{Eh} \, dt \,. \qquad (54)$$

Concerning variable s according to Fig. 8,

$$\Delta y_o' = \frac{\sin \alpha_o}{Eh} \int_{\frac{-s_o}{2}}^{\frac{s_o}{2}} (N_{r,g} + N_{r,\gamma} - \mu N_{\phi,g} - \mu N_{\phi,\lambda}) ds \,. \qquad (55)$$

The integration required here shall be performed for each term independently, one after the other. With variable z according to (24) introduced and the expensions in a series according to (26) used, the first term will be

$$I_1 = \frac{\sin \alpha_o}{Eh} \int_{-\frac{s_o}{2}}^{\frac{s_o}{2}} N_{r,g} ds = \qquad (56)$$

$$= - \frac{g}{Eh \cos \alpha_o} \left[x_k s_o - \frac{x_1^2 s_o}{x_k} \left(1 + \frac{z^2}{3} + \frac{z^4}{5} + \ldots\right) \right] \,.$$

This formula is numerically stable, it can be used also for steep cones and cylinders.

Similarly, the second term is

$$I_2 = \frac{\sin \alpha_0}{Eh} \int_{-\frac{s_0}{2}}^{\frac{s_0}{2}} N_{r,\gamma} ds = -\frac{\gamma}{2Eh} \left[\left(Hx_k - \frac{H_0}{3} x_1 - \frac{2H_0}{3} x_k \right) S_0 - \right. \tag{57}$$

$$\left. - x_1^2 \left(H + \frac{H_0}{3} \right) \frac{s_0}{x_k} \left(1 + \frac{z^2}{3} + \frac{z^4}{5} + \ldots \right) \right] .$$

The third and the fourth term can be calculated in a simpler way:

$$I_3 = \frac{\sin \alpha_0}{Eh} \int_{-\frac{s_0}{2}}^{\frac{s_0}{2}} (-\mu N_{\phi,g}) ds = \frac{\mu g \cos \alpha_0}{Eh} x_k s_0 , \tag{58}$$

$$I_4 = \frac{\sin \alpha_0}{Eh} \int_{-\frac{s_0}{2}}^{\frac{s_0}{2}} (-\mu N_{\phi,\gamma}) ds = \frac{\mu \gamma}{Eh} \left[Hx_k s_0 + \frac{x_k^2}{\cos \alpha_0} s_0 \sin \alpha_0 + \right. \tag{59}$$

$$\left. + \frac{\cos \alpha_0}{3} \frac{s_0^3}{8} \sin \alpha_0 - x_1 x_k \frac{\sin \alpha_0}{\cos \alpha} s_0 \right] .$$

Using relationships (56–59), the vertical compression according to (55) can be obtained by summation

$$\Delta y_0' = I_1 + I_2 + I_3 + I_4 . \tag{60}$$

The second part of Δy_0 can be obtained according to formula (8), taking the horizontal displacements according to (52), calculated earlier, into consideration. With the summation according to (19):

$$\Delta y_0 = \Delta y^j - \Delta y^i .$$

Considering that, because of support of the bottom edge in the direction of the generatrix, the magnitude of vertical shift of the bottom edge is

$$\Delta y^j = \Delta r^j \frac{\cos \alpha_o}{\sin \alpha_o} \tag{61}$$

the vertical shift of the top edge will be

$$\Delta y^i = \Delta r^j \frac{\cos \alpha_o}{\sin \alpha_o} - \Delta y_o \tag{62}$$

on the basis of relationships (53) and (61).

Now all the elements of vector $\underline{e}_o$ are available. To produce the elements of $\underline{x}_o$, consider resultant

$$G = G_g + G_\gamma \tag{63}$$

of the total load acting upon the shell. In the knowledge of this, components of the reaction taking place at the bottom edge will be

$$p_y^j = \frac{G}{2\pi x_2} \tag{64}$$

and

$$p_x^j = -\frac{G}{2\pi x_2} \frac{\sin\alpha}{\cos \alpha_o} . \tag{65}$$

The top edge of the membrane primary structure is unloaded. Thus vector $\underline{x}_o$ of the membrane reactions resulting from the load is:

$$\underline{x}_o = \begin{bmatrix} 0 \\ 0 \\ 0 \\ \frac{G}{2\pi x_2} \operatorname{tg} \alpha_o \\ -\frac{G}{2\pi x_2} \\ 0 \end{bmatrix} \tag{66}$$

b) The next step is to make the edge displacements equal to zero. For this purpose, it is necessary that the boundary vector system,

$$\underline{x} = - \underline{M}\, \underline{e}_0 \ , \tag{67}$$

resulting in edge displacements opposite to edge displacements $\underline{e}_0$ of the membrane primary structure, be actuated.

c) Vector $\underline{i}$ of loads reduced to the nodal lines is obtained by summation of the boundary vector system compensating for membrane displacements and the membrane reactions:

$$\underline{t} = \underline{x}_0 + \underline{x} \ . \tag{68}$$

In general, the support of the bottom edge is capable of taking up both horizontal and vertical force components that is the membrane reaction. In this case, load vector $\underline{t}$ of the shell element is obtained by means of formula (68).

Further calculations will be required if the bottom support is incapable of taking up membrane reactions. For details see Appendix F2.

6. Calculation of stresses within the elements

Vector $\underline{u}$ of displacements of the entire structure along nodal lines is available as a solution of equation system (1) of the displacement system. Below we show how to obtain the internal stresses of the conical shell by means of boundary displacements in $\underline{u}$.

a) Let vector

$$\underline{e}_0 = \begin{bmatrix} e_x^i \\ e_y^i \\ \phi^i \\ e_x^j \\ e_y^j \\ \phi^j \end{bmatrix} \tag{69}$$

set up of selected elements of vector $\underline{u}$ of displacements of the entire structure along nodal lines be denoted by $\underline{e}_0$, essentially the vector of displacements of the upper and lower edge of the shell element interconnecting the i-th and j-th nodal lines. Boundary force system

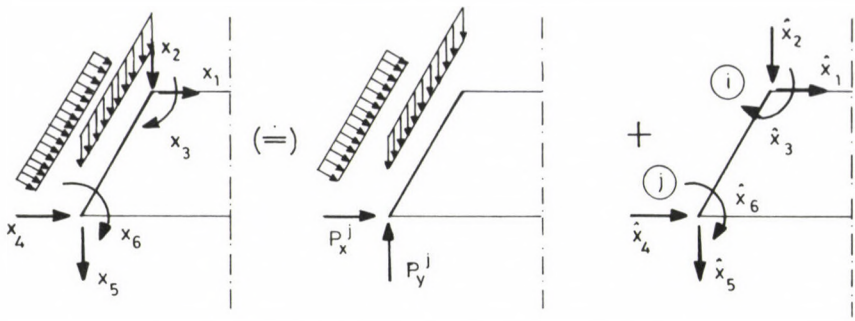

Fig. 12. Boundary force system of a shell element

$$\underline{x} = \underline{M}\,\underline{e} \tag{70}$$

belongs to this vector at the same place (Fig. 12).

b) Let this force system be decomposed into the sum of membrane force system $\underline{x}_o$ and boundary force system

$$\underline{\hat{x}} = \underline{x} - \underline{x}_o \ . \tag{71}$$

Now elements $\hat{x}_2$ and $\hat{x}_5$ of vector $\underline{\hat{x}}$ form a system of equilibrium. Let $\hat{x}_2$ and $\hat{x}_5$ be decomposed into components $\hat{P}^i$, $\hat{P}^j$ of generatrix direction and horizontal components $\hat{H}^i$, $\hat{H}^j$ (Fig. 13):

$$\left.\begin{aligned} \hat{P}^j &= \frac{\hat{x}_5}{\sin\ \alpha_o} \ , \qquad \hat{H}^j = \hat{x}_5 \ . \ \mathrm{tg}\ \alpha_o \ , \\ \hat{P}^i &= \frac{\hat{x}_2}{\sin\ \alpha_o} \ , \qquad \hat{H}^i = \hat{x}_2 \ . \ \mathrm{tg}\ \alpha_o \ . \end{aligned}\right\} \tag{72}$$

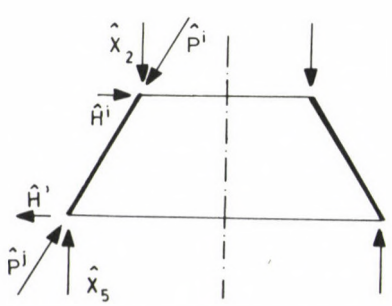

Fig. 13. Decomposition of horizontal force system

On the basis of the above decomposition, let all the boundary reactions taking place on the shell be decomposed into the sum of the following three force systems (Fig. 14):

- membrane force system $\underline{x}_o$,
- equilibrium force system $(\hat{P}^o \ . \ \hat{P}^j)$,
- force system $\underline{z} = \begin{bmatrix} \hat{x}_1 \\ \hat{x}_3 \\ \hat{x}_4 \\ \hat{x}_6 \end{bmatrix} + \begin{bmatrix} \hat{A}^i \\ 0 \\ \hat{A}^j \\ 0 \end{bmatrix}$.

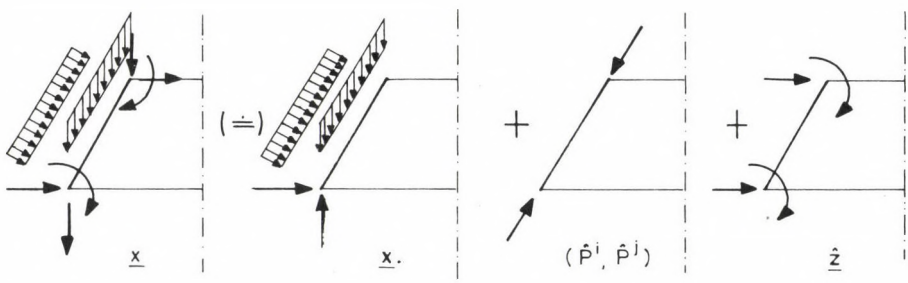

Fig. 14. Decomposition of the boundary reactions of a shell element into the sum of three force systems

c) The stresses associated with the three force systems shall be calculated separately for each system:

- membrane stresses N_r and N_ϕ associated with membrane reactions can be obtained by means of formulae (45, 49),
- N_r resulting from equilibrium vector system $(\hat{P}^i, \hat{P}^j)$ can be calculated on the basis of formula (20),
- on the basis of relationship (11), vector

$$\underline{c} = \underline{B}^{-1} \ . \ \underline{z}$$

of the integration constants is associated with force system $\hat{\underline{z}}$. With the elements of this vector substituted into formulae (9c, d, e), we obtain functions M_r, M_ϕ and Q.

As a sum of the three stress systems, all the stresses of the truncated conical shell have been obtained.

Appendix

F.1. Calculation of Thomson functions

Power series for determination of zero-order Thomson functions /9/ are as follows

$$\mathrm{ber}(x) = \sum_{k=0}^{\infty} \frac{(-1)^k\, x^{4k}}{2^{4k}\,[(2k)!]^2} = 1 - \frac{x^4}{2^4\ 2!^2} + \frac{x^8}{2^8\ 4!^2} - \frac{x^{12}}{2^{12}\ 6!^2} + \ldots \qquad (73a)$$

$$\mathrm{bei}(x) = \sum_{k=0}^{\infty} \frac{(-1)^k\, x^{4k+2}}{2^{4k+2}\,[(2k+1)!]^2} = \frac{x^2}{2^2\ 1!^2} - \frac{x^6}{2^6\ 3!^2} + \frac{x^{10}}{2^{10}\ 5!^2} - \ldots \qquad (73b)$$

$$\mathrm{ker}(x) = \frac{\pi}{4}\,\mathrm{bei}(x) - \ln\frac{\gamma x}{2}\,\mathrm{ber}(x) - \sum_{k=0}^{\infty}\left(\frac{-(1)^k\, x^{4k}}{2^{4k}\,[(2k)!]^2}\sum_{n=1}^{2k}\right)\frac{1}{n} =$$

$$= \frac{\pi}{4}\,\mathrm{bei}(x) - \ln\frac{\gamma x}{2}\,\mathrm{ber}(x) - \frac{x^4}{2^4\ 2!^2}\sum_{n=1}^{2}\frac{1}{n} + \frac{x^8}{2^8\ 4!^8}\sum_{n=1}^{4}\frac{1}{n} - \ldots \qquad (73c)$$

$$\mathrm{kei}(x) = -\frac{\pi}{4}\,\mathrm{ber}(x) - \ln\frac{\gamma x}{2}\,\mathrm{bei}(x) + \sum_{k=0}^{\infty}\left(\frac{(1)^k\, x^{4k+2}}{2^{4k+2}\,[(2k+1)!]^2}\sum_{n=1}^{2k+1}\frac{1}{n}\right) =$$

$$= -\frac{\pi}{4}\,\mathrm{ber}(x) - \ln\frac{\gamma x}{2}\,\mathrm{bei}(x) + \frac{x^2}{2^2\ 1!^2}\sum_{n=1}^{1}\frac{1}{n} - \frac{x^6}{2^6\ 3!^2}\sum_{n=1}^{3}\frac{1}{n} + \ldots \qquad (73d)$$

where $\ln\gamma = 0.577215$ is the so-called Eulerian constant.

Derivatives of these functions are:

$$\mathrm{ber}'(x) = \sum_{k=0}^{\infty} \frac{(-1)^k\ 4k\ x^{4k-1}}{2^{4k}\ [(2k)!]^2} = -\frac{x^3}{2^3\ 1!\ 2!} + \frac{x^7}{2^7\ 3!\ 4!} - \frac{x^{11}}{2^{11}\ 5!\ 6!} + \ldots \quad (74a)$$

$$\mathrm{bei}'(x) = \sum_{k=0}^{\infty} \frac{(-1)^k (4k+2)\ x^{4k+2}}{2^{4k+2}\ [(2k+1)!]^2} = \frac{x}{2^1\ 0!\ 1!} - \frac{x^5}{2^5\ 2!\ 3!} + \frac{x^9}{2^9\ 4!\ 5!} - \ldots \quad (74b)$$

$$\mathrm{ker}'(x) = -\frac{\pi}{4}\,\mathrm{ber}'(x) - \ln\frac{\gamma x}{2}\,\mathrm{ber}'(x) - \frac{1}{x}\,\mathrm{ber}(x) -$$

$$- \frac{x^3}{2^3\ 1!\ 2!} \sum_{n=1}^{2} \frac{1}{n} + \frac{\gamma x^7}{2^7\ 3!\ 4!} \sum_{n=1}^{4} \frac{1}{n} - \ldots \quad (74c)$$

$$\mathrm{kei}'(x) = -\frac{\pi}{4}\,\mathrm{ber}'(x) - \frac{1}{1}\ln\frac{\gamma x}{2}\,\mathrm{bei}'(x) - \frac{1}{3}\,\frac{1}{x}\,\mathrm{bei}(x) +$$

$$+ \frac{x}{2^1\ 0!\ 1!} \sum_{n=1} \frac{1}{n} - \frac{x^5}{2^5\ 2!\ 3!} \sum_{n=1} \frac{1}{n} + \ldots \quad (74d)$$

In case of high values of x, the convergence of these series is rather poor. In this case, the following asymptotic expressions shall reasonably be used /9/:

$$\mathrm{ber}(x) = \frac{e^{\alpha(x)}}{\sqrt{2\pi x}} \cos\beta(x)\ ,$$

$$\mathrm{bei}(x) = \frac{e^{\alpha(x)}}{\sqrt{2\pi x}} \sin\beta(x)\ ,$$

$$\mathrm{ker}(x) = \sqrt{\frac{\pi}{2x}}\, e^{\alpha(-x)} \cos\beta(-x)\ , \quad (75)$$

$$\mathrm{kei}(x) = \sqrt{\frac{\pi}{2x}}\, e^{\alpha(-x)} \sin\beta(-x)\ ,$$

where

$$\alpha(x) = \frac{x}{\sqrt{2}} + \frac{1}{8x\sqrt{2}} - \frac{25}{384x^3\sqrt{2}} - \frac{13}{128x^4} - \dots ,$$

$$\beta(x) = \frac{x}{\sqrt{2}} - \frac{\pi}{8} - \frac{1}{8x\sqrt{2}} - \frac{1}{16x^2} - \frac{25}{384x^3\sqrt{2}} - \dots . \tag{76}$$

Asymptotic expressions of the first derivatives are:

$$\begin{aligned}
\mathrm{ber}'(x) &= -\frac{1}{2x}\,\mathrm{ber}(x) + \alpha'(x)\,\mathrm{ber}(x) - \beta'(x)\,\mathrm{bei}(x) ,\\
\mathrm{bei}'(x) &= -\frac{1}{2x}\,\mathrm{bei}(x) + \alpha'(x)\,\mathrm{bei}(x) + \beta'(x)\,\mathrm{ber}(x) ,\\
\mathrm{ker}'(x) &= -\frac{1}{2x}\,\mathrm{ker}(x) - \alpha'(x)\,\mathrm{ker}(x) + \beta'(x)\,\mathrm{kei}(x) ,\\
\mathrm{kei}'(x) &= -\frac{1}{2x}\,\mathrm{kei}(x) - \alpha'(x)\,\mathrm{kei}(x) + \beta'(x)\,\mathrm{ker}(x) .
\end{aligned} \tag{77}$$

In case of high values of x, functions ber(x), bei(x)may assume very high absolute values while functions ker(x), kei(x) assume almost zero absolute values. In case of very low values of x,

$$\begin{aligned}
\lim_{x\to 0} \mathrm{ber}(x) &= 1 ,\\
\lim_{x\to 0} \mathrm{bei}(x) &= \lim_{x\to 0} \frac{x^2}{2} ,\\
\lim_{x\to 0} \mathrm{ker}(x) &= -\lim_{x\to 0} \ln\frac{\gamma x}{2} ,\\
\lim_{x\to 0} \mathrm{kei}(x) &= -\frac{\pi}{4} .
\end{aligned} \tag{78}$$

Since the coefficient matrix may include Thomson functional values associated with very high or very low values of x in the equation system written for determination of the integration constants present in the solution of the differential equation, the difference in the order of magnitude between the elements of the coefficient matrix may be significant. It is therefore necessary that the matrix be prevented from becoming ill conditioned and that the stability of the solution of the equation system be ensured.

In case of high values of x we proceed, as follows. Instead of the actual functional values, we use functional values multiplied by constants being here the values of a properly selected normalization function. In order to make higher values of very low values and lower values of very high values, a normalization function similar to the first factors in (75) that is an exponential normalization function shell be selected in such a way that the exponent will be the opposite of the first term of the appropriate expressions (76). Thus we use the following functions instead of the original ones:

$$\mathrm{ber}(x) \longrightarrow \mathrm{ber}(x)\, e^{\frac{x_2}{2}},$$

$$\mathrm{bei}(x) \longrightarrow \mathrm{bei}(x)\, e^{\frac{x_2}{2}},$$

$$\mathrm{ker}(x) \longrightarrow \mathrm{ker}(x)\, e^{\frac{x_1}{2}},$$

$$\mathrm{kei}(x) \longrightarrow \mathrm{kei}(x)\, e^{\frac{x_1}{2}}$$

where x_2 and x_1 are the (relative) co-ordinate of the external and internal edge of the shell, respectively. This normalization permits the values of functions bei(x) and ber(x) tending to $\pm\infty$ and the values of functions ker(x) and kei(x) tending to zero to be transformed so as to be treated in combination in case of high values of x. Another advantage of normalization is that in case of a considerable distance between the edges, the effect of normalization with respect to the one edge is not appreciable at the other one (and vice versa). The process is analogous with that used for investigation of so-called high bent cylindrical shells /2/.

This normalization results in change of the values of the wanted integration constants only, the function written in this way remains the solution of the differential equation.

F.2. Aid for calculation of the load vector of the shell element

If membrane reaction components according to (66) can not be transmitted to the bottom support, also the opposite of the calculated reaction components shall be applied to the structure.

a) Horizontally unsupported shell

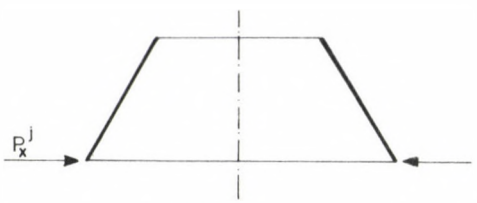

Fig. 15. Horizontal equilibrium vector system

Let the opposite of the horizontal reaction component of magnitude

$$P_x^j = \frac{G \operatorname{tg} \alpha_o}{2 \pi x_2}$$

at the bottom edge be applied to the unsupported shell (Fig. 15). If the edge is unsupported in direction x only, then boundary displacement system $\underline{e}_x^{(5)}$ resulting from boundary force $-P_x^j$ shall be calculated according to relationship

$$\underline{e}_x^{(5)} = \begin{bmatrix} \Delta r^i \\ \vartheta^i \\ \Delta r^j \\ \Delta y^j \\ \vartheta^j \end{bmatrix} = \left\{ \underline{\hat{M}}_x^{(5)} \right\}^{-1} \begin{bmatrix} 0 \\ 0 \\ -P_x^j \\ 0 \\ 0 \end{bmatrix} \tag{79}$$

Here matrix $\underline{\hat{M}}^{(5)}$ is obtained by omitting the second row and column, resulting in singularity, of rigidity matrix $\underline{\hat{M}}$ of size 6x6 of the support fixed at both ends /see (33)/. If the bottom edge is unsupported also in direction y, then vector $\underline{e}$ of the boundary displacements will be obtained by means of the following relationship:

$$\underline{e}_x^{(5)} = \begin{bmatrix} \Delta r^i \\ \vartheta^i \\ \Delta r^j \\ \Delta y^j \\ \vartheta^j \end{bmatrix} = \left\{ \underline{\hat{M}}_y^{(5)} \right\}^{-1} \begin{bmatrix} 0 \\ 0 \\ 0 \\ -P_x^j \\ 0 \end{bmatrix} \tag{80}$$

Here matrix $\underline{\hat{M}}_y^{(5)}$ can be obtained by omitting the fifth row and column of matrix $\underline{\hat{M}}$.

Let vector $\underline{e}_x^{(5)}$ be completed with the missing edge shift of zero value and direction y to be inserted as a second or fifth element in the appropriate place so that the vector will be a six-element vector. Let this six-element vector be called $\underline{e}_x$.

Boundary displacements $\underline{e}_x$ shall be eliminated according to what has been said in par 5. For this purpose, it is necessary that vector system

$$\underline{x}_x = \underline{M} \cdot \underline{e}_x \tag{81}$$

be actuated. Then vector $\underline{t}$ of loads reduced to the nodal lines can be obtained by summation of the vector systems according to (66, 67) and (81):

$$\underline{t} = \underline{x}_0 + \underline{x} + \underline{x}_x \ . \tag{82}$$

b) Shell unsupported in direction y

The lower edge is incapable of taking up vertical forces. Thus the upper edge must be supported in direction y. Hence, let the opposite of the vertical component of magnitude

$$P_y^j = - \frac{G}{2\pi x_2}$$

of the membrane reaction be actuated on the structure according to Fig. 16a.

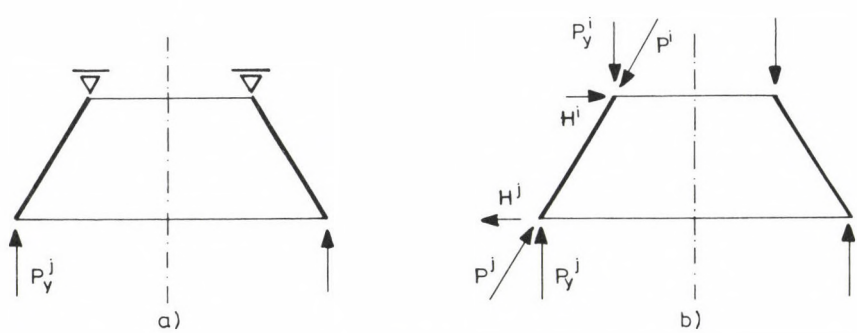

Fig. 16. Vertical component of membrane reaction

Let of rce $-P_y^j$ decomposed into component P^j of generatrix direction and horizontal component H^j (Fig. 16b):

$$P^j = -\frac{P_y^j}{\sin \alpha_o}, \qquad H^j = -P_y^j \operatorname{tg} \alpha_o . \tag{83}$$

Appropriate components P^i, H^j of reaction P_y^i taking place at the upper edge:

$$P^k = -\frac{P_y^j}{\sin \alpha_o}\frac{x_2}{x_1}, \qquad H^j = -P_y^j \operatorname{tg} \alpha_o \frac{x_2}{x_1} . \tag{84}$$

Boundary displacements $\underline{e}_H$ resulting from horizontal components H^i, H^j are calculated in a way similar to (80):

$$\underline{e}_H = \begin{bmatrix} \Delta r_H^i \\ \vartheta_H^i \\ \Delta r_H^j \\ \Delta y_H^j \\ \vartheta_H^j \end{bmatrix} = \left\{ \underline{\hat{M}}_y^{(5)} \right\}^{-1} \begin{bmatrix} H^i \\ 0 \\ 0 \\ H^j \\ 0 \end{bmatrix} \tag{85}$$

The elements of displacement system $\underline{e}_P$,

$$\underline{e}_P = \begin{bmatrix} \Delta r_P^i \\ \vartheta_P^i \\ \Delta r_P^j \\ \Delta y_P^j \\ \vartheta_P^j \end{bmatrix} \tag{86}$$

resulting from the action of equilibrium vector system (P^i, P^j) in the direction of the generatrix are calculated by means of relationships (18) and (29) on the basis of what has been said in par 4.

Hence, we have boundary displacement system $\underline{e}_y^{(5)}$ resulting from boundary force - P_y^j compensating for the vertical component of the membrane reaction:

$$\underline{e}_y^{(5)} = \underline{e}_H + \underline{e}_P \ . \tag{87}$$

Let five-order vector $\underline{e}_y^{(5)}$ be completed with zero boundary displacement y^j, inserted as a fifth element, so as to be a six-element vector.

To eliminate displacement system $\underline{e}_y$, vector system

$$\underline{x}_y = \underline{M} \cdot \underline{e}_y \ . \tag{88}$$

must be actuated similarly to the case according to (67). Load vector $\underline{q}$ of the shell element can be calculated by summation of the vector systems according to (66, 67) and (88):

$$\underline{q} = \underline{x}_0 + \underline{x} + \underline{x}_y \ . \tag{89}$$

Now the elements of the load vector - in case of optional conditions of support - are available.

REFERENCES

1. Hampe, E.: Statik rotationssymmetrischer Flächentragwerke 2, 3, 4. VEB Verlag für Bauwesen, Berlin, 1964
2. Márkus, Gy.: Theory and calculation of rotationally symmetric structure (in Hungarian). Műszaki Könyvkiadó, Budapest, 1964
3. Bölcskei, E. - Orosz, Á.: Shells (in Hungarian). Tankönyvkiadó, Budapest, 1978
4. Popper, Gy.: Numerical methods for use by engineers (in Hungarian). Műszaki Könyvkiadó, Budapest, 1975
5. Szabó, J. - Roller, B.: Theory and calculation of bar structures (in Hungarian). Műszaki Könyvkiadó, Budapest, 1971
6. Timoshenko, S. - Wolnowsky-Krieger, S.: Theory of plates and shells (in Hungarian). Műszaki Könyvkiadó, Budapest, 1966
7. Márkus, Gy.: Calculation of round storage basins of flat top and bottom plate using the method of moment distribution (in Hungarian). Vízügyi Közlemények, No. 2, Budapest, 1953
8. Rózsa, P.: Linear algebra and its applications. Műszaki Könyvkiadó, Budapest, 1974
9. Rijik-Grandstein: Tabele de integrale (in Rumanian). Editura Tehnica, Bucureşti, 1960

Acta Technica Acad.Sci.Hung., 104(1-3), pp. 39-62 (1991/92)

STRENGTH CALCULATION OF THE THIN-WALLED BOXGIRDER

DESEÖ, Z.*

(Received: 14 August 1990)

For the strength calculation of the thin-walled boxgirder with complicated cross-section (ships, floating cranes) the finite element method uses equations with a large number of unknowns. This paper describes a method for the strength calculation of the midpart of the girder (where the stresses are the greatest) which uses only a small number of unknowns.

Introduction

The paper describes an alternative method for the calculation of the bending and torsion of box girders. The results of the examined examples show a significant deviation from the results of the classical torsion theory. Its reason is that the classical theory assumes that the form of the cross section remains undeformed, though it in fact does not. For closed thin-walled tubes, the results of the classical torsion theory and the undeformability of the cross section are ab initio incompatible.

The cross section is approximated by a number of flat plates with constant thicknesses which are joined to each other at their edges.

Two different coordinate systems are used: global coordinates for box-girders X, Y, Z, and local coordinates x, y for the plates, see Fig. 1.

1. External forces

External forces (a distributed load) are applied in the planes of the plates, at their edges, see Fig. 1a and 1b (bending and torsion). The

*Deseö, Zoltán, H-1141 Budapest, Tarnóc u. 15, Hungary

Akadémiai Kiadó, Budapest

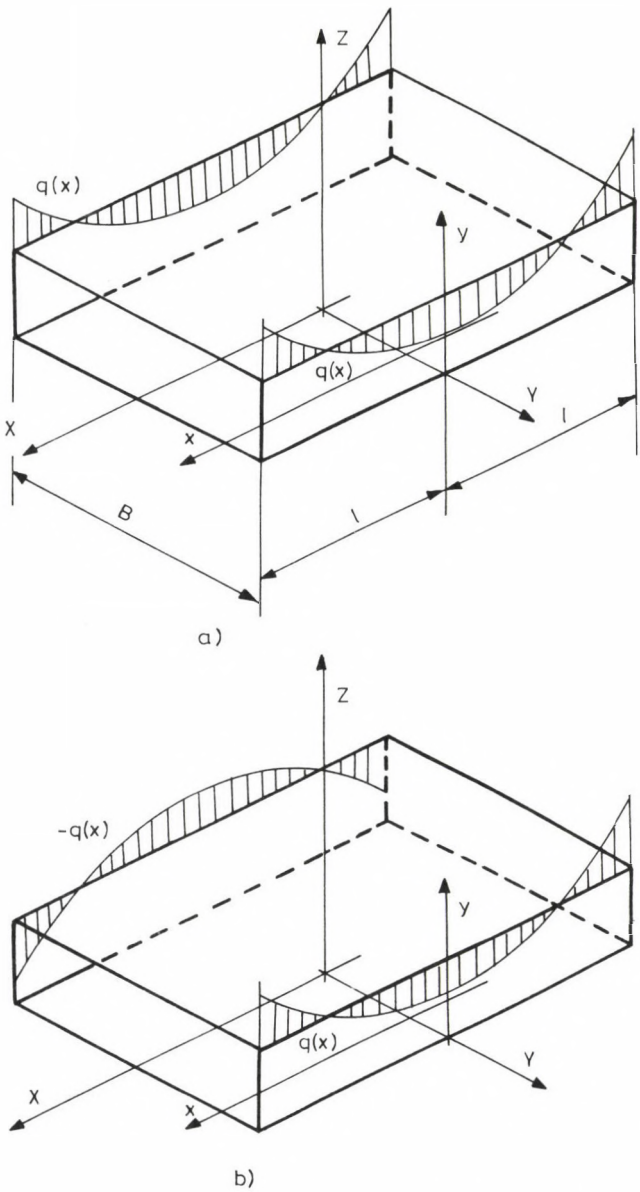

Fig. 1a. Distributed external load for the bending

Fig. 1b. Distributed external load for the torsion

bending moment caused by the external loads (in plates 1 and 2) in the vicinity of the origo x=0, may be written as follows:

$$M(x) = M_0 + N_0 x + (q_0/2)x^2 , \qquad (1)$$

where

$M_0 = \int_{-1}^{0}\int q(x)dx\,dx$ the bending moment at x=0

$N_0 = \int_{-1}^{0} q(x)dx$ the shear force at x=0

q_0 the load at x=0 .

Function M(x) is a quadratic Taylor's polynomial. The results are satisfactory, of course, only for section x=0. However, origo x=0 can be always chosen at the examined section.

2. Theoretical ground of the calculation

The stresses are expressed by Airy's stress function F(x,y). The boundary conditions for the plates are expressed by the external forces, and we can couple the plates by comparing the common edges.

Stress function F(x,y) satisfies the differential equation:

$$\frac{\partial^4 F}{\partial x^4} + 2\frac{\partial^4 F}{\partial x^2\,\partial y^2} + \frac{\partial^4 F}{\partial y^4} = 0 ,$$

or its abbreviated form $\Delta\Delta F=0$.

The stresses derived from F(x,y) are:

$$\sigma_x = \frac{\partial^2 F}{\partial y^2} \qquad \sigma_y = \frac{\partial^2 F}{\partial x^2} \qquad \tau_{xy} = -\frac{\partial^2 F}{\partial x\,\partial y} .$$

The stress function can be expressed by the polynomial as follows:

$$F(x,y) = \alpha_{00} + \alpha_{10}\,y + \alpha_{20}\,y^2 + \alpha_{30}\,y^3 + \alpha_{40}\,y^4 + \alpha_{50}\,y^5 +$$
$$+ (\alpha_{01} + \alpha_{11}\,y + \alpha_{21}\,y^2 + \alpha_{31}\,y^3)x +$$
$$+ (\alpha_{02} + \alpha_{12}\,y + \alpha_{22}\,y^2 + \alpha_{32}\,y^3)x^2 - \tag{2}$$
$$- (1/3\,\alpha_{22} + \alpha_{40} + \alpha_{32}\,y + 5\,\alpha_{50}\,y)x^4 .$$

The stresses corresponding to (2) are:

$$\sigma_x = 2\,\alpha_{20} + 6\,\alpha_{30}y + 12\,\alpha_{40}y^2 + 20\,\alpha_{50}y^3 +$$
$$+ (2\,\alpha_{21} + 6\,\alpha_{31}y)x + (2\,\alpha_{22} + 6\,\alpha_{32}y)x^2 , \tag{3}$$

$$\sigma_y = 2\,\alpha_{02} + 2\,\alpha_{12}y + 2\,\alpha_{22}y^2 + 2\,\alpha_{32}y^3 -$$
$$- (4\,\alpha_{22} + 12\,\alpha_{40} + 12\,\alpha_{30}y + 60\,\alpha_{50}y)x^2 , \tag{4}$$

$$\tau_{xy} = -(\alpha_{11} + 2\,\alpha_{21}y + 3\,\alpha_{31}y^2) - (2\,\alpha_{12} + 4\,\alpha_{22}y +$$
$$+ 6\,\alpha_{32}y^2)x + 4(\alpha_{32} + 5\,\alpha_{50})x^3 . \tag{5}$$

3. Conditional equations

3.1 The equilibrium condition of the individual plate

Figure 2 shows the equilibrium of an element of the plate. Equilibrium of the moment is:

$$2bs_s\tau(b)dx + \frac{dM}{dx}dx + Ndx = 0 . \tag{6}$$

Equilibrium of the shear forces is:

$$t(\sigma_y(b) - \sigma_y(-b))dx + \frac{dN}{dx}dx = 0 . \tag{7}$$

Substituting (7) in (6) we obtain

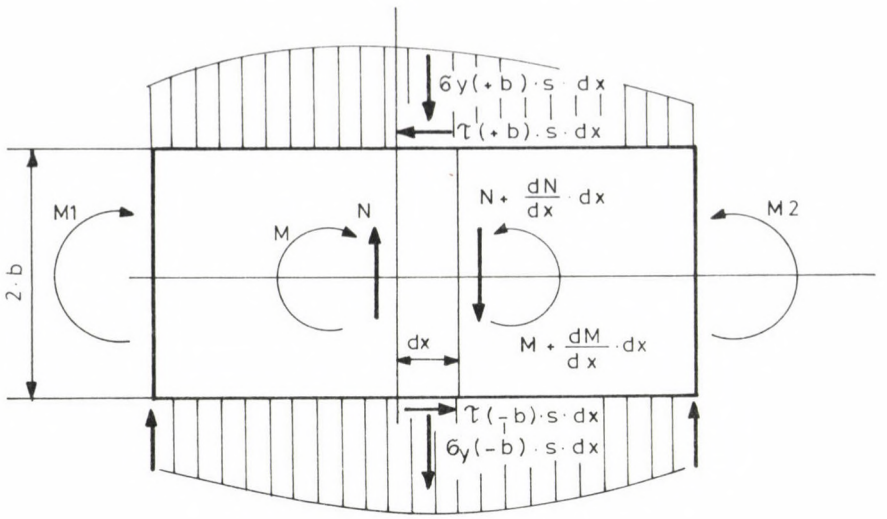

Fig. 2. The equilibrium of the element

$$\int_{-1}^{0} {}_s\tau(b)dx + \left(\frac{1}{2hs}\right)M - \left(\frac{1}{2bs}\right)\left(\mu(+b) - \mu(-b)\right) = 0 \tag{8}$$

where ${}_s\tau(b)$ is the symmetrical component of shear stress at y=b.

$$M = \int_{-b}^{+b} \sigma_x y dy = 4b^3 s\,\alpha_{30} + 8b^5 s\,\alpha_{50} + 4b^3 s\,\alpha_{31}x + 4b^3 s\,\alpha_{32}x^2 , \tag{9}$$

$$\mu(\pm b) = s\int_{-1}^{0}\int^{x} \sigma_y(\pm b)dx\,dx = F(x,\pm b) \tag{10}$$

s is the thickness of the plate.

3.2 Boundary conditions

Figure 3 shows the cross section of the three coupled plates. The conditions are in the common edge:

$$t_1 + t_2 + t_3 = 0 , \tag{11}$$

$$\varepsilon_{x1} = \varepsilon_{x2} = \varepsilon_{x3} , \tag{12}$$

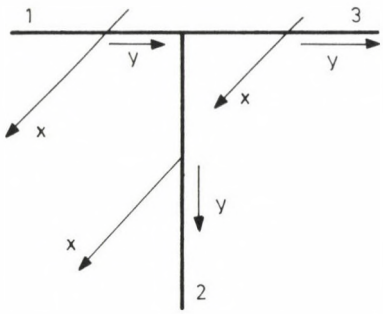

Fig. 3. Cross-section of the three coupled plates

$$s_1 \sigma_{y1} - s_3 \sigma_{y3} = q(x) , \tag{13}$$

$$s_2 \sigma_{y2} = q_1(x) , \tag{14}$$

$$v_1'' = v_3'' \tag{15}$$

where

t is the shear flow,

ε_x is the strain in x direction,

q(x) is the external load,

s is the thickness,

v is the displacement in y direction, due to the normal stress.

Considering that $\sigma_y \ll \sigma_x$, we may write instead of (12):

$$\sigma_{x1} = \sigma_{x2} = \sigma_{x3} . \tag{12a}$$

Moreover

$$v'' = \frac{1}{E}\left[\frac{\partial \sigma_x}{\partial y} + (2 + \nu)\frac{\partial \sigma_y}{\partial y}\right] \tag{16}$$

where ν is the Poisson's ratio.

Substituting (3) and (4) into (16), we find:

$$v'' = 2n\alpha_{12} + 6\alpha_{30} + (4\alpha_{22} + 24\alpha_{40})y +$$

$$+ (6\alpha_{32} + 60\alpha_{50})y^2 + 6\alpha_{31}x +$$

$$+ (6\alpha_{32} - n(12\alpha_{32} + 60\alpha_{50}))x^2 \qquad \text{where } n = 2 + \nu .$$

3.3 Equation for the calculation of coefficients α_{ik}

By substituting F(x,y) into equilibrium and boundary conditions, and by comparing the terms involving x and y with identical exponents, we obtain the equations for coefficients α_{ik} separated:

for α_{11} α_{21} α_{31} ,
for α_{12} α_{22} α_{32} α_{40} α_{50} ,
for α_{10} α_{20} α_{30} .

Eliminating coefficients α_{ik} from the equations, we find for α_{11} α_{21} α_{31};

$$\underline{A}\ {}_1\underline{I} = {}_1\underline{m} \ . \tag{17}$$

For coefficients α_{12} α_{22} α_{32} α_{40} α_{50}

$$\underline{A}\ {}_2\underline{I} = {}_2\underline{m} \ . \tag{18}$$

For coefficients α_{10} α_{20} α_{30}

$$\underline{A}\ {}_o\underline{I} = {}_o\underline{m} + \underline{a} \ . \tag{19}$$

Matrix $\underline{A}$ is identical in the in eqs (17), (18), (19)

$$\underline{A} = \begin{bmatrix} -4/s & -2/s & -B & 0 & 0 & 0 & 3/(Bs) & -3/(Bs) \\ -2/s & -4/s & 0 & B & 0 & 0 & 3/(Bs) & -3/(Bs) \\ 0 & 0 & -1 & 1 & B & 0 & 0 & 0 \\ 0 & 0 & -1 & 1 & 0 & B & 0 & 0 \end{bmatrix} , \tag{20}$$

$$ {}_1\underline{I} = \begin{bmatrix} {}_0t(b) \\ {}_0t(-b) \\ {}_1\sigma x(b) \\ {}_1\sigma x(-b) \\ {}_1v''(b) \\ {}_1v''(-b) \\ {}_1\mu(b) \\ {}_1\mu(-b) \end{bmatrix} , \quad {}_o\underline{I} = \begin{bmatrix} {}_{-1}t(b) \\ {}_{-1}t(-b) \\ {}_o\sigma x(-b) \\ {}_o\sigma x(-b) \\ {}_ov''(b) \\ {}_ov''(-b) \\ {}_o\mu(b) \\ {}_o\mu(-b) \end{bmatrix} , \quad {}_2\underline{I} = \begin{bmatrix} {}_1t(b) \\ {}_1t(-b) \\ {}_2\sigma x(b) \\ {}_2\sigma x(-b) \\ {}_2v''(b) \\ {}_2v''(-b) \\ {}_2\mu(b) \\ {}_2\mu(-b) \end{bmatrix} , \tag{21}$$

$$ {}_1\underline{m} = 6\begin{bmatrix} N_o \\ N_o \\ 0 \\ 0 \end{bmatrix}, \qquad {}_o\underline{m} = 6\begin{bmatrix} M_o \\ M_o \\ 0 \\ 0 \end{bmatrix}, \qquad {}_2\underline{m} = 6\begin{bmatrix} q_o \\ q_o \\ 0 \\ 0 \end{bmatrix}, \tag{22} $$

$$ \underline{a} = \begin{bmatrix} 0 & B & B \\ 0 & -B & B \\ -n & 6 & 5p \\ -n & 6 & 5p \end{bmatrix} \cdot \begin{bmatrix} \alpha_{12} \\ b\alpha_{40} \\ b^2\alpha_{50} \end{bmatrix} \tag{23} $$

where $B = 2b$,
$n = \nu + 2$,
$p = 3\nu + 2$.

We obtain the values of the shear flows from Eq. (17), and the values of the normal stresses, the v" and the μ in the nodes from Eqs (18), (19). We can express the values of coefficient α_{ik} by the boundary values deriving from Eqs (17), (18), (19) as follows:

$$ \alpha_{11} = -b\,\frac{{}_1\sigma x(b) - {}_1\sigma x(-b)}{4} - \frac{{}_o t(b) + {}_o t(-b)}{2s}, $$

$$ \alpha_{21} = -b\,\frac{{}_1\sigma x(b) - {}_1\sigma x(-b)}{4} \qquad \alpha_{31} = -b\,\frac{{}_1\sigma x(b) - {}_1\sigma x(-b)}{4}, $$

$$ \alpha_{12} = -b\,\frac{{}_2\sigma x(b) + {}_2\sigma x(-b)}{4} - \frac{{}_1 t(b) + {}_1 t(-b)}{4} \tag{24} $$

$$ \alpha_{40} = \frac{{}_2\sigma x(b) + {}_2\sigma x(-b)}{12} \qquad \alpha_{50} = \frac{-{}_2\sigma x(b) + {}_2\sigma x(-b)}{60b}, $$

$$ \alpha_{20} = \frac{{}_o\sigma x(b) + {}_o\sigma x(-b)}{12} - 6b^2\alpha_{40}, $$

$$ \alpha_{30} = \frac{{}_o\sigma x(b) - {}_o\sigma x(-b)}{12b} - \frac{10}{3}b^2\alpha_{50}. $$

Finally, we can write down the stresses for $x = 0$:

$$ \sigma^x = 2\alpha_{20} + 6\alpha_{30}y + 12\alpha_{50}y^2 + 20\alpha_{50}y^3, \tag{25} $$

$$ \tau = t/s = -\alpha_{11} - 2\alpha_{21}y - 3\alpha_{31}y^2. \tag{26} $$

If a panel has different thicknesses, or it is stiffened by longitudinal flanges, which subdivide the panel into plates, see Fig. 4, we can write matrix $\underline{A}$ and vector $\underline{I}$ from Eqs (17), (18), (19) in partitioned form:

$$\underline{A} = (\underline{A}_1, \ \underline{B}) \ , \qquad {}_i\underline{I} = \begin{bmatrix} {}_i\underline{I}_1 \\ {}_i\underline{I}_2 \end{bmatrix}$$

So can be written Eqs (17), (18), (19) in the form as follows:

$$\underline{A}_1 \ {}_1\underline{I}_1 + \underline{B} \ {}_1\underline{I}_2 = {}_1\underline{m} \ ,$$

$$\underline{A}_1 \ {}_o\underline{I}_1 + \underline{B} \ {}_o\underline{I}_2 = {}_o\underline{m} + \underline{a} \ ,$$

$$\underline{A}_1 \ {}_2\underline{I}_1 + \underline{B} \ {}_2\underline{I}_2 = {}_2\underline{m} \ .$$

By premultiplying with B, we find

$$\underline{B}^{-1} \ \underline{A}_1 \ {}_1\underline{I}_1 + {}_1\underline{I}_2 = \underline{B}^{-1} \ {}_1\underline{m} \ , \tag{27}$$

$$\underline{B}^{-1} \ \underline{A}_1 \ {}_o\underline{I}_1 + {}_o\underline{I}_2 = \underline{B}^{-1} \ {}_o\underline{m} + \underline{B}^{-1} \ \underline{a} \ , \tag{28}$$

$$\underline{B}^{-1} \ \underline{A}_1 \ {}_2\underline{I}_1 + {}_2\underline{I}_2 = \underline{B}^{-1} \ {}_2\underline{m} \ ; \tag{29}$$

now we can express from Eqs (27), (28), (29) the $\underline{I}_2$

$${}_i\underline{I}_2 = \underline{C} \ {}_i\underline{I}_1 + \underline{B}^{-1} \ {}_i\underline{m} \ \ (+\underline{B}^{-1} \ \underline{a}) \ , \tag{30}$$

where $\underline{C} = \underline{B}^{-1} \ \underline{A}$.

$$\underline{I}_2 = \begin{bmatrix} t \\ \sigma x \\ v'' \\ \chi \end{bmatrix}_{(-b)} \ , \qquad \underline{I}_1 = \begin{bmatrix} t \\ \sigma x \\ v'' \\ \chi \end{bmatrix}_{(+b)} \ ,$$

$$\underline{C} = \begin{bmatrix} 1 & Bs+f & -Bs/2 & 0 \\ 0 & 1 & -B & 0 \\ 0 & 0 & 1 & 0 \\ -B & -Bs/2-Bf & Bs/6 & 1 \end{bmatrix},$$

$$\underline{B} = \begin{bmatrix} s/2 & -s/2 & Bs/2 & 0 \\ 0 & 0 & 1 & 0 \\ 0 & 0 & -1/B & 1/B \\ -Bs/3 & Bs/6 & -Bs/6 & 0 \end{bmatrix}$$

where f is the cross-sectional area of the flange on the fore node of the field.

By Eq. (30) we can immediately express the boundary values of edge 2 from the boundary values of edge 1, see Fig. 4. So we can avoid the increase in the number of unknowns.

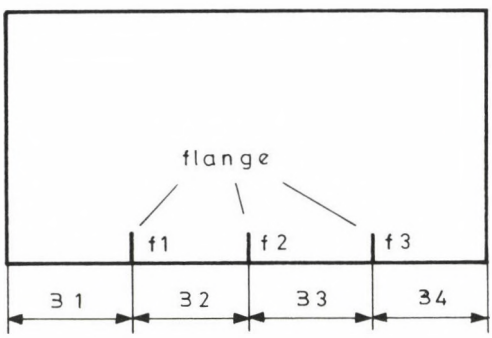

Fig. 4. f_i-area of the cross-section of flange i

4. Numerical examples

The classical theory assumes that the shape of the cross-section doesn't become deformed, that is the cross-section is absolute rigid in its own plane. This method cannot regard the rigidity of the cross-structure, so the values and the flow of the calculated stresses depend from the input of the external load. The role of the cross-stiffness to transmit the load applied to one plate, to the neighbouring plates. Thus by an appropriate input of the external loads we can ensure the undeformity. To find the

necessary input external forces, we prescribe the relative displacements of properly chosen nodals relating to a given basic nodal (edge), and instead of the prescribed displacements, internal forces μ can be regarded as unknown output external loads. To ensure the equilibrium of the output external loads, we can complete the equations by three equilibrium equations. (Forces in direction Y and Z, and moment.)

To illustrate the application of the foregoing analysis, we determine the normal stress and the shearflow distribution, and the deformation for three cross sections. The cross sections and theirs loading are illustrated in Figs 5, 6. The cross sections are of one axis of symmetry. For the preparation of input data only one half of the cross sections considered. For the nodals of symmetry we must prescribe the conditions as follows:

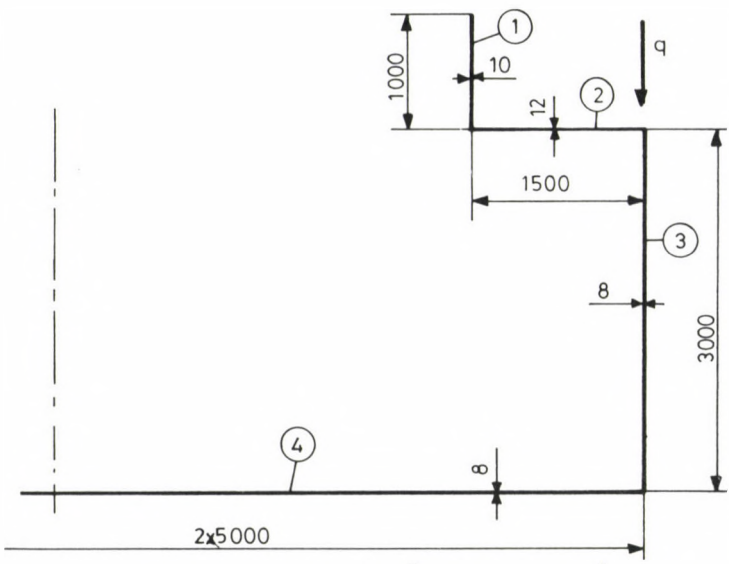

Fig. 5. Cross-section 1 (for bending: $M_o = 2.10^7$ daNcm; $N_o = 16.10^4$ daN; $q_o = -50$ daN/cm; for torsion: $M_o = 1.10^7$ daNcm; $N_o = 8.10^4$ daN; $q = 0$)

$$\text{bending} \qquad t = v'' = 0 \,,$$
$$\text{torsion} \qquad \sigma_x = \mu = 0 \,.$$

If there is plate in axis of symmetry, we must take for this plate half thickness, and from condition given above, we must prescribe only

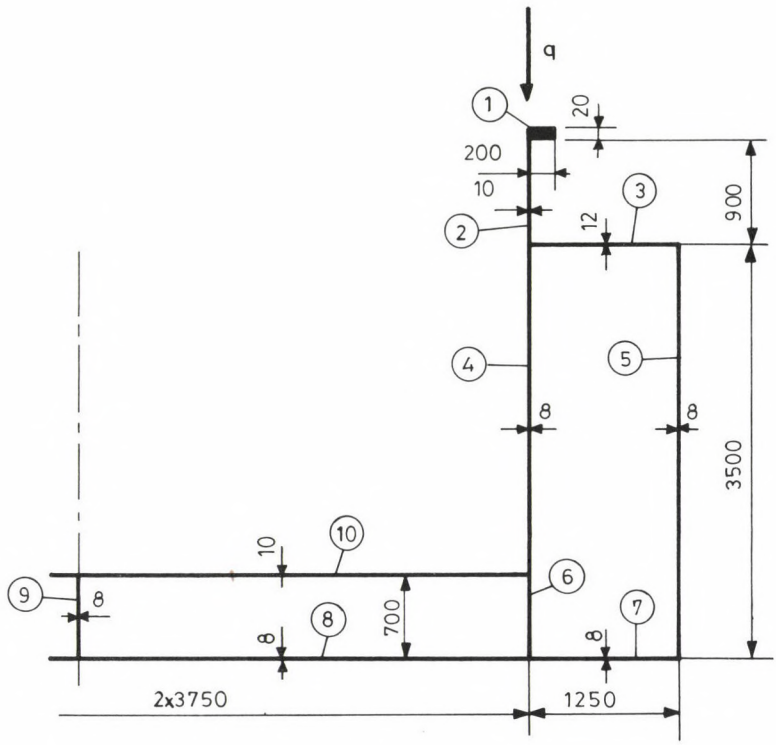

Fig. 6. Cross-section 2

bending $v'' = 0$,

torsion this plate hasn't any role, and it can be neglected.

The results are illustrated in Figs 7-14. The arrows show the output external loads, which must be added to the input external load, to ensure the undeformability of the cross section. The numerical results see in the appendix.

Figures 7 and 10 show the bending and torsion for cross section 1, without rigidity, and with full rigid construction. Ensured the full-rigidity of the cross section we find for the open tube, that the results are identical with the results of the classical theory.

Figures 11-14 show the results of the bending and torsion of cross section 2. Figures 11 and 13 show the results derived without the cross-rigidity for the bending and torsion. Figures 12 and 14 show the results for the fully rigid cross section.

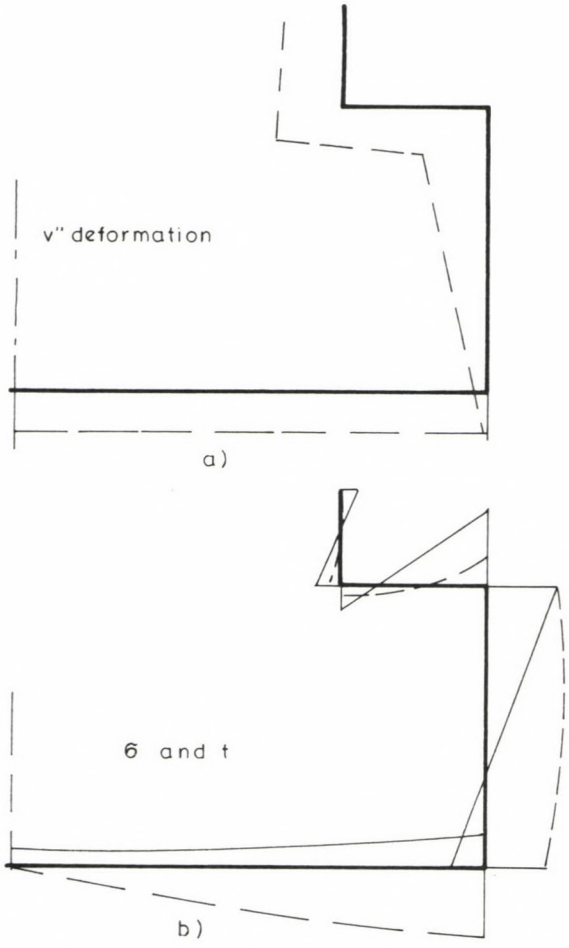

Fig. 7. Bending of cross section 1 (—— : normal stress, 1 cm ≙ 500 daN/cm^2; --- t: shear flow, 1 cm ≙ 500 daN/cm)

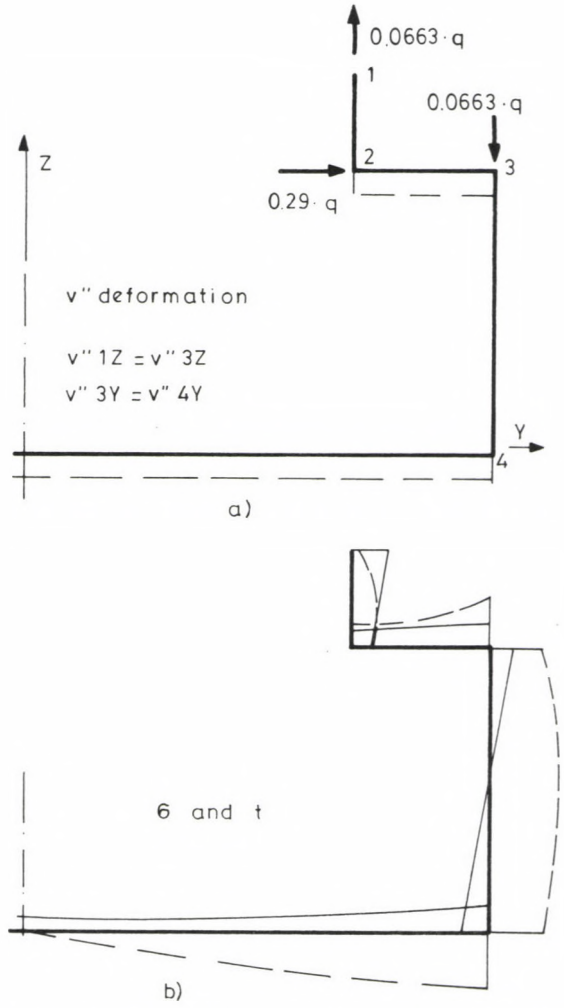

Fig. 8. Bending of cross section 1 (—— : normal stress, 1 cm ≙ daN/cm^2; --- t: shear flow, 1 cm ≙ 500 daN/cm)

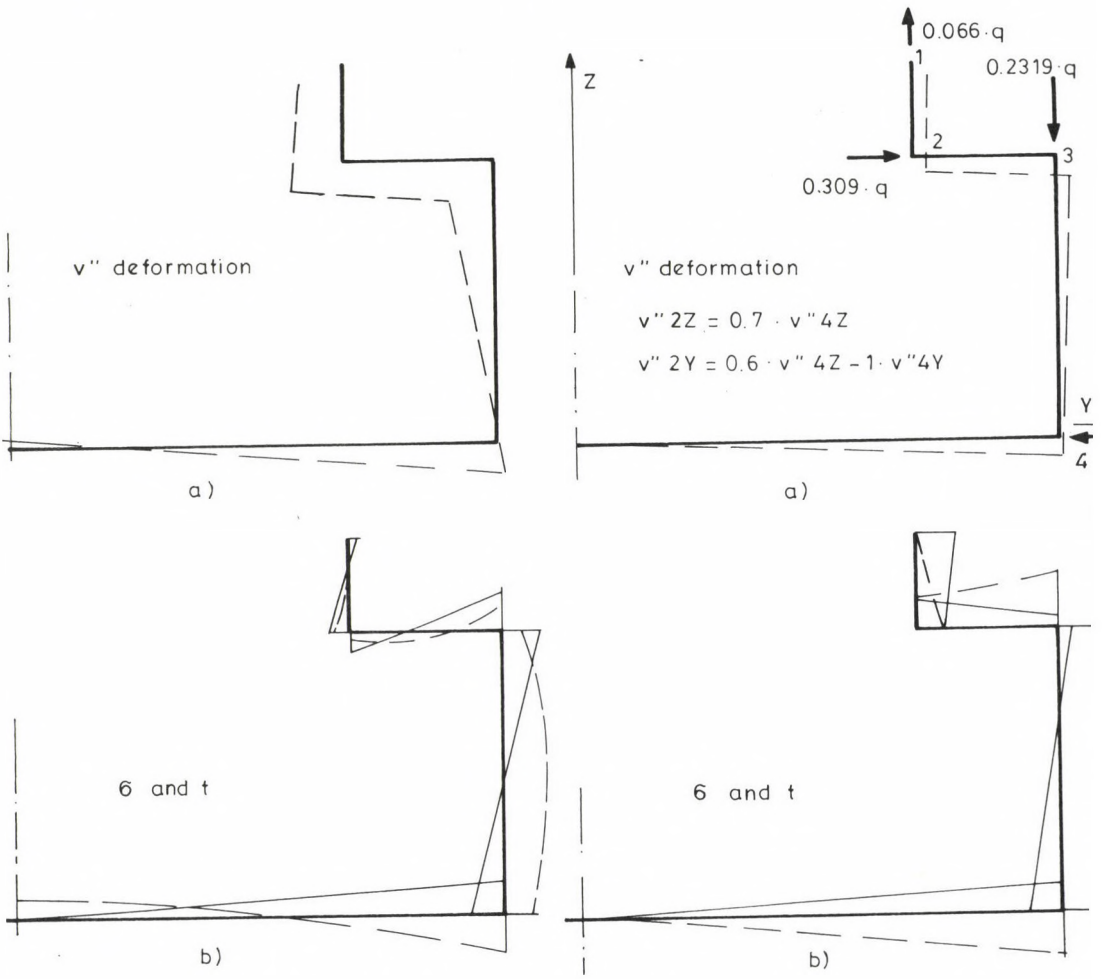

Fig. 9. Torsion of cross-section 1 (— ∂: normal stress, 1 cm ≙ 400 daN/cm^2; (--- t: shear flow, 1 cm ≙ 400 daN/cm)

Fig. 10. (— ∂: normal stress, 1 cm ≙ 200 daN/cm^2; --- t: shear flow, 1 cm ≙ 200 daN/cm)

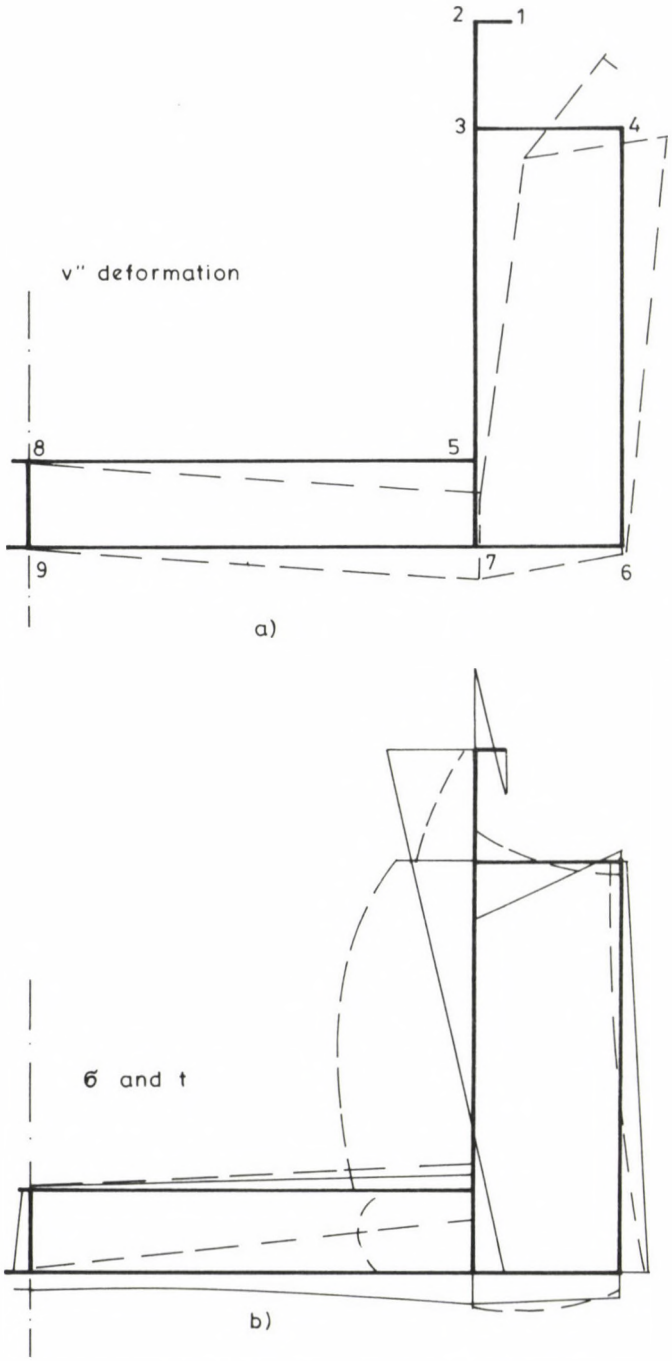

Fig. 11. Bending of cross-section 2
(— ∂ : normal stress, 1 cm ≙ 250 daN/cm²; --- t: shear flow, 1 cm ≙ 250 daN/cm)

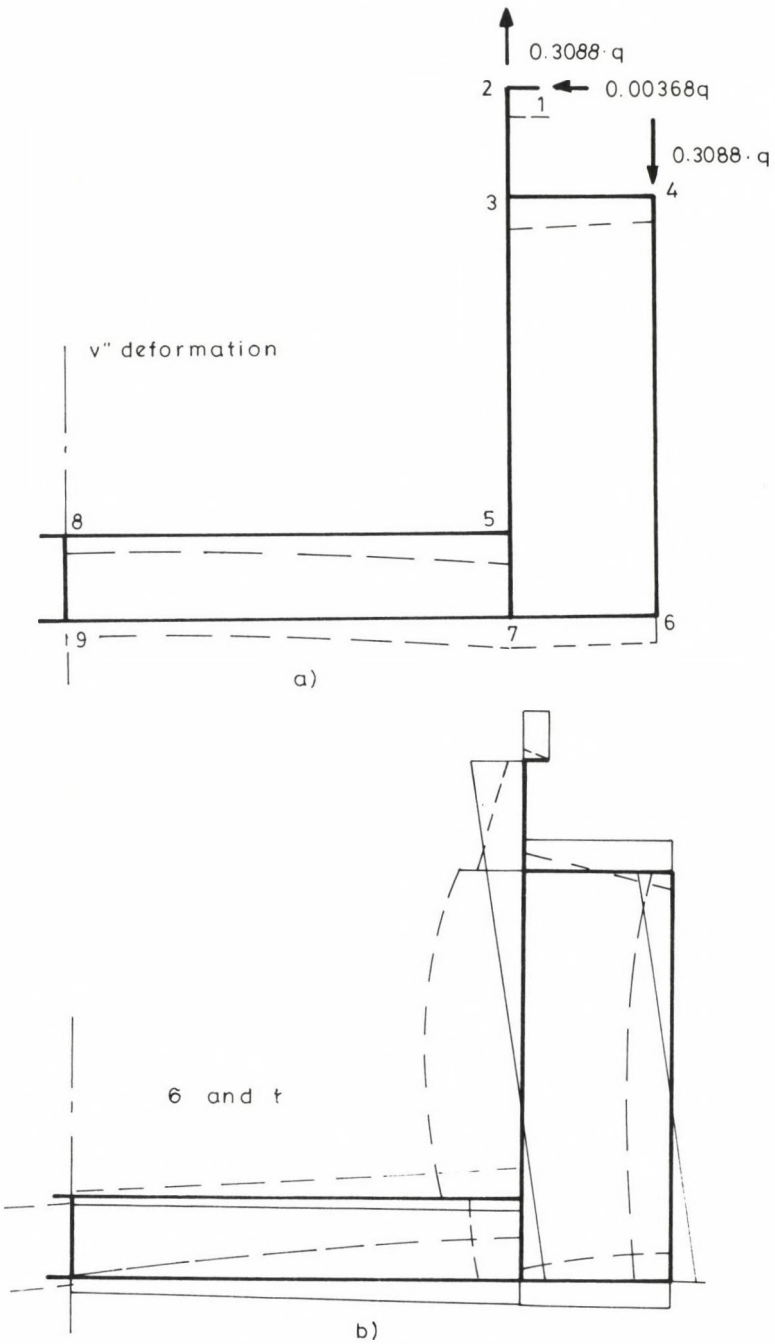

Fig. 12. Bending of cross-section 2
(—— ∂: normal stress, 1 cm ÷ 250 daN/cm^2; --- t: shear flow, 1 cm ÷ 250 daN/cm)

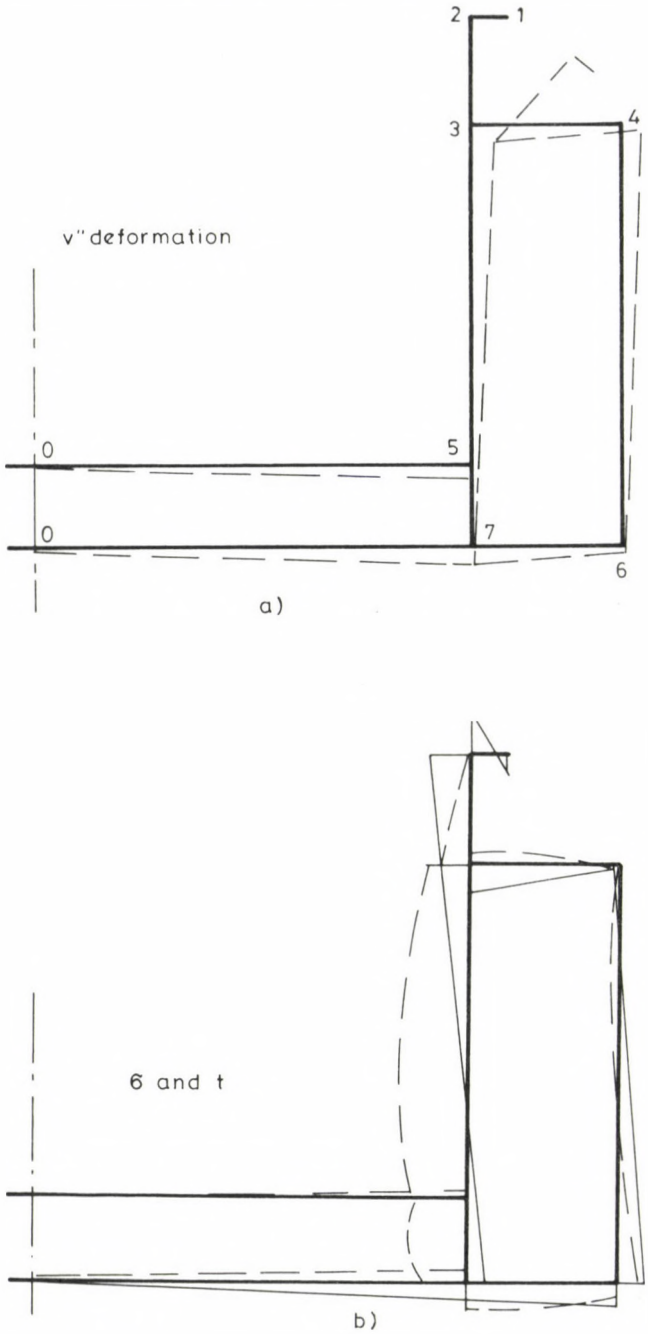

Fig. 13. Torsion of cross-section 2
(— ∂: normal stress, 1 cm ≙ 250 daN/cm^2; --- t: shear flow, 1 cm ≙ 250 daN/cm)

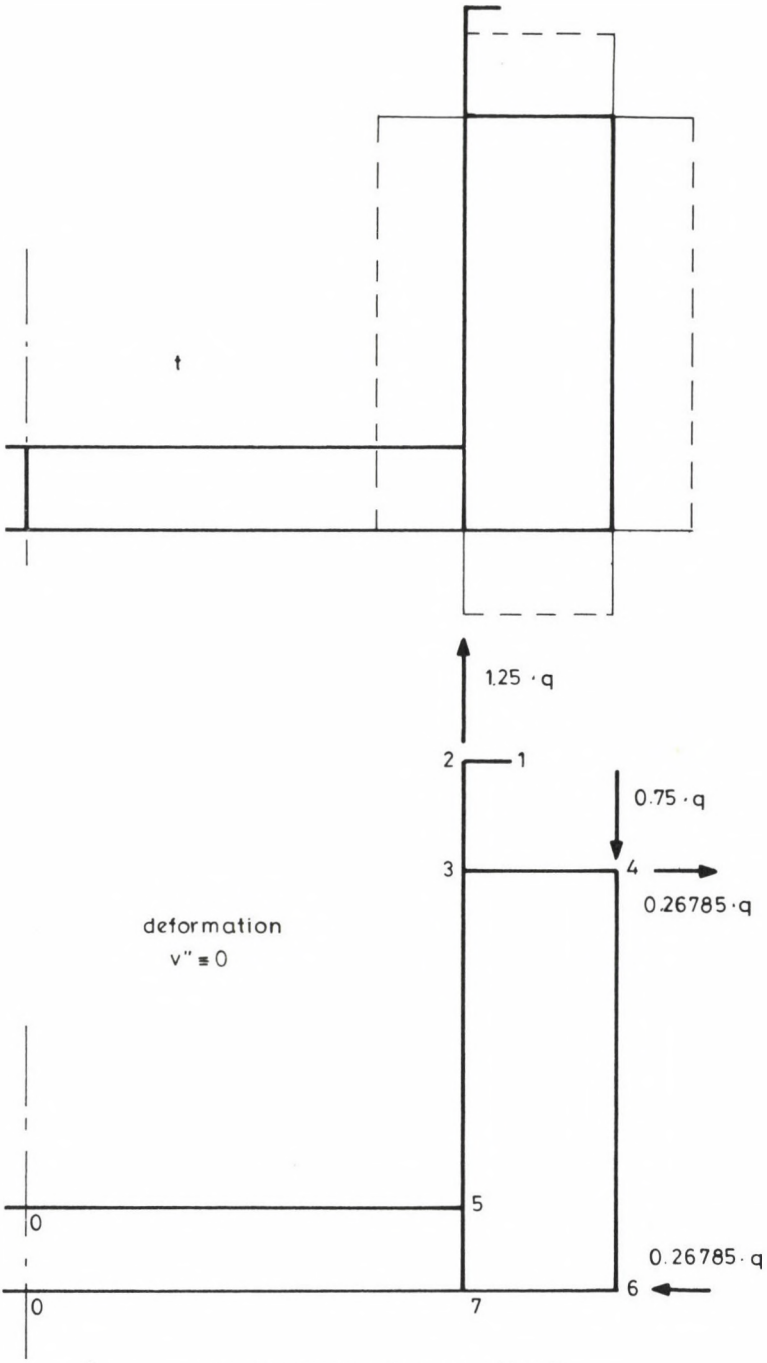

Fig. 14. Torsion of cross-section 2
($\vartheta \equiv 0$; --- t: shear flow, 1 cm ≙ daN/cm)

Appendix

Bending for cross-section without cross-rigidity to Figure 11

No.	t_1	t_2	σ_1	σ_2	Ev''_1	Ev''_2
1-2	0	-25	167	-335	2.510e + 001	2.510e + 001
2-3	-25	-218	-335	-226	-1.294e + 000	-1.313e + 000
3-4	89	-41	-226	12	-1.894e + 000	-1.904e + 000
3-5	-307	-486	-226	37	-1.313e + 000	-1.333e + 000
4-6	-41	72	12	90	-2.274e - 001	-2.142e - 001
5-7	-398	-371	37	106	-1.333e + 000	-1.330e + 000
6-7	72	145	90	106	-3.417e - 002	-2.563e - 002
7-9	-227	-8	106	71	-2.563e - 002	0.000e + 000
9-8	-8	5	71	26	6.464e - 001	6.495e - 001
8-5	5	88	26	37	0.000e + 000	7.724e - 003

No.	M_1	M_2	N_1	N_2	q_1	q_2
1	0.000e + 000	0.000e + 000	0.000e + 000	0.000e + 000	0.000e + 000	0.000e + 000
2	0.000e + 000	-1.849e + 007	0.000e + 000	-1.486e + 005	0.000e + 000	4.645e + 001
3	0.000e + 000	0.000e + 000	0.000e + 000	0.000e + 000	0.000e + 000	0.000e + 000
4	-1.849e + 007	-3.246e + 006	-1.486e + 005	-2.708e + 004	4.645e + 001	8.463e + 000
5	0.000e + 000	0.000e + 000	0.000e + 000	0.000e + 000	0.000e + 000	0.000e + 000
6	-3.246e + 006	0.000e + 000	-2.708e + 004	0.000e + 000	8.463e + 000	0.000e + 000
7	0.000e + 000	-1.664e + 006	0.000e + 000	-1.353e + 004	0.000e + 000	4.227e + 000
8	-1.664e + 006	2.984e + 006	-1.353e + 004	3.042e + 004	4.227e + 000	-9.505e + 000
9	0.000e + 000	0.000e + 000	0.000e + 000	0.000e + 000	0.000e + 000	0.000e + 000
10	2.177e + 006	0.000e + 000	1.749e + 004	0.000e + 000	-5.467e + 000	0.000e + 000

Coefficient of the polynomial for the normal stresses

No.	a_0	a_1	a_2	a_3
1	-8.3668e + 001	2.5101e + 001	-1.9315e - 004	1.9315e - 005
2	-2.7877e + 002	-1.2117e + 000	-6.7030e - 004	-7.5791e - 007
3	-1.0566e + 002	-1.8947e + 000	-2.7154e - 004	-1.5810e - 006
4	-8.9397e + 001	-9.2254e - 001	-2.4966e - 004	-7.5791e - 007
5	4.7161e + 001	-2.1665e - 001	1.2636e - 004	-1.9327e - 007
6	7.1226e + 001	-9.8372e - 001	1.4824e - 004	-7.5791e - 007
7	9.7035e + 001	-1.2712e - 001	2.2782e - 004	-6.5052e - 022
8	8.0523e + 001	9.2468e - 002	2.2782e - 004	9.6374e - 023
9	4.8326e + 001	6.4729e - 001	1.4824e - 004	7.5791e - 007
10	2.8969e + 001	-2.9667e - 002	6.8661e - 005	1.8070e - 022

E is the Young's modulus

Coefficient of the polynomial for the shear stresses

No.	a_0	a_1	a_2
1	3.0905e + 000	6.1809e - 001	-9.2714e - 002
2	-1.2861e + 002	2.1450e + 000	3.6380e - 003
3	-9.8812e + 000	8.6894e - 001	7.5888e - 003
4	-5.6647e + 002	7.9891e - 001	3.6380e - 003
5	-9.4700e + 000	-4.0434e - 001	9.2768e - 004
6	-4.8506e + 002	-4.7437e - 001	3.6380e - 003
7	1.3526e + 002	-7.2903e - 001	3.9968e - 018
8	-1.4648e + 002	-7.2903e - 001	-7.4015e - 019
9	1.4855e + 000	-4.7437e - 001	-3.6380e - 003
10	4.6649e + 001	-2.1972e - 001	1.4803e - 019

Bending for rigid cross section to Figure 12

No.	T_1	T_2	σ_1	σ_2	Ev''_1	Ev''_2
1-2	0	-59	-200	-200	-2.154e - 002	-2.430e - 002
2-3	-59	-172	-200	-127	-8.869e - 001	-8.975e - 001
3-4	77	-77	-127	-129	2.430e - 002	1.223e - 002
3-5	-249	-325	-127	48	-8.975e - 001	-9.065e - 001
4-6	-77	-125	-129	107	-7.932e - 001	-7.988e - 001
5-7	-189	-160	48	100	-9.065e - 001	-9.031e - 001
6-7	-125	-56	107	100	-3.240e - 002	-2.430e - 002
7-9	-215	-8	100	67	-2.430e - 002	0.000e + 000
9-8	-8	6	67	31	5.149e - 001	5.183e - 001
8-5	6	137	31	48	0.000e + 000	1.220e - 002

No.	M_1	M_2	N_1	N_2	q_1	q_2
1	0.000e + 000	7.988e + 004	0.000e + 000	5.8920 + 002	0.000e + 000	-1.841e - 001
2	5.756e + 006	-1.282e + 007	4.942e + 004	-9.991e + 004	-1.544e + 001	3.122e + 001
3	0.000e + 000	0.000e + 000	0.000e + 000	0.000e + 000	0.000e + 000	0.000e + 000
4	-1.282e + 007	-1.714e + 006	-9.991e + 004	-1.232e + 004	3.122e + 001	3.849e + 000
5	-5.756e + 006	0.000e + 000	-4.942e + 004	0.000e + 000	1.544e + 001	0.000e + 000
6	-1.714e + 006	0.000e + 000	-1.232e + 004	0.000e + 000	3.849e + 000	0.000e + 000
7	0.000e + 000	9.029e + 005	0.000e + 000	1.128e + 004	0.000e + 000	-3.524e + 000
8	9.029e + 005	5.294e + 006	1.128e + 004	5.318e + 004	-3.524e + 000	-1.662e + 001
9	0.000e + 000	0.000e + 000	0.000e + 000	0.000e + 000	0.000e + 000	0.000e + 000
10	2.610e + 006	0.000e + 000	2.681e + 004	0.000e + 000	-8.380e + 000	0.000e + 000

E is the Young's modulus

Coefficient of the polynomial for the normal stresses

No.	a_0	a_1	a_2	a_3
1	-1.9964e + 002	-1.2332e - 002	-4.6034e - 004	-1.0029e - 019
2	-1.6244e + 002	-8.0628e - 001	-3.9117e - 004	-5.1238e - 007
3	-1.2679e + 002	1.8263e - 002	-3.2200e - 004	-1.0119e - 021
4	-3.7460e + 001	-6.1389e - 001	-1.0680e - 004	-5.1238e - 007
5	-9.6368e - 000	-6.5818e - 001	-5.2995e - 005	-5.1238e - 007
6	7.3741e + 001	-7.4627e - 001	1.6220e - 004	-5.1238e - 007
7	1.0253e + 002	5.2690e - 002	2.1600e - 004	1.4456e - 022
8	7.5940e + 001	8.8252e - 002	2.1600e - 004	2.1684e - 022
9	4.8700e + 001	5.1615e - 001	1.6220e - 004	5.1238e - 007
10	3.5494e + 001	-4.5297e - 002	1.0840e - 004	1.9275e - 022

Coefficient of the polynomial for the shear stresses

No.	a_0	a_1	a_2
1	-1.4731e + 001	1.4731e + 000	9.5479e - 016
2	-1.2023e + 002	1.2517e + 000	2.4594e - 003
3	-1.3332e - 013	1.0304e + 000	5.3291e - 013
4	-4.0712e + 002	3.4175e - 001	2.4594e - 003
5	-2.0160e + 002	1.6959e - 001	2.4594e - 003
6	-2.2092e + 002	-5.1906e - 001	2.4594e - 003
7	-1.1275e + 002	-6.9122e - 001	4.4409e - 019
8	-1.3969e + 002	-6.9122e - 001	-1.3323e - 018
9	1.0043e + 000	-5.1906e - 001	-2.4594e - 003
10	7.1506e + 001	-3.4690e - 001	7.4015e - 020

Torsion for cross-section without cross rigidity to Fig. 13

No.	t_1	t_2	σ_1	σ_2	Ev''_1	Ev''_2
1-2	0	-13	78	-157	1.175e + 001	1.175e + 001
2-3	-13	-109	-157	-112	-4.918e - 001	-4.918e - 001
3-4	46	-25	-112	-6	-8.487e - 001	-8.4873 - 001
4-5	-156	-234	-112	25	-4.918e - 001	-4.918e - 001
4-6	-25	57	-6	80	-2.455e - 001	-2.455e - 001
5-7	-208	-109	25	60	-4.918e - 001	-4.918e - 001
6-7	57	113	80	60	1.592e - 001	1.592e - 001
7-0	-77	-5	60	0	1.592e - 001	1.592e - 001
0-5	-13	25	0	25	-6.744e - 002	-6.744e - 002

E is the Young's modulus

No.	M_1	M_2	N_1	N_2	q_1	q_2
1	0.000e + 000	0.000e + 000	0.000e + 000	0.000e + 000	0.000e + 000	0.000e + 000
2	0.000e + 000	-9.284e + 006	0.000e + 000	-7.427e + 004	0.000e + 000	0.000e + 000
3	0.000e + 000	0.000e + 000	0.000e + 000	0.000e + 000	0.000e + 000	0.000e + 000
4	-9.284e + 006	-1.751e + 006	-7.427e + 004	-1.401e + 004	0.000e + 000	0.000e + 000
5	0.000e + 000	0.000e + 000	0.000e + 000	0.000e + 000	0.000e + 000	0.000e + 000
6	-1.751e + 006	0.000e + 000	-1.401e + 004	0.000e + 000	0.000e + 000	0.000e + 000
7	0.000e + 000	-1.348e + 006	0.000e + 000	-1.079e + 004	0.000e + 000	0.000e + 000
8	-1.348e + 006	0.000e + 000	-1.079e + 004	0.000e + 000	0.000e + 000	0.000e + 000
9	0.000e + 000	0.000e + 000	0.000e + 000	0.000e + 000	0.000e + 000	0.000e + 000

Coefficient of the polynomial for the normal stresses

No.	a_0	a_1	a_2	a_3
1	-3.9168e + 001	1.1750e + 001	0.0000e + 000	0.0000e + 000
2	-1.3454e + 002	-4.9178e - 001	0.0000e + 000	0.0000e + 000
3	-5.9363e + 001	-8.4875e - 001	0.0000e + 000	0.0000e + 000
4	-4.3560e + 001	-4.9178e - 001	0.0000e + 000	0.0000e + 000
5	3.6652e + 001	-2.4553e - 001	0.0000e + 000	0.0000e + 000
6	4.2502e + 001	-4.9178e - 001	0.0000e + 000	0.0000e + 000
7	6.9667e + 001	1.5924e - 001	0.0000e + 000	0.0000e + 000
8	2.9857e + 001	1.5924e - 001	0.0000e + 000	0.0000e + 000
9	1.2645e + 001	-6.7440e - 002	0.0000e + 000	0.0000e + 000

Coefficients of the polynomial for the shear stresses

No.	a_0	a_1	a_2
1	1.5667e + 000	3.1334e - 001	-4.7001e - 002
2	-6.4952e + 001	1.0763e + 000	1.9671e - 003
3	-4.4206e + 000	4.7490e - 001	3.3950e - 003
4	-2.8188e + 002	3.4848e - 001	1.9671e - 003
5	-1.0026e + 001	-2.9321e - 001	9.8213e - 004
6	-2.5101e + 002	-3.4002e - 001	1.9671e - 003
7	1.0869e + 002	-5.5734e - 001	-6.3696e - 004
8	-2.8488e + 001	-2.3886e - 001	-6.3696e - 004
9	-3.1612e + 000	-1.0116e - 001	2.6976e - 004

Torsion for rigid cross section to Fig. 14

No.	t_1	t_2	σ_1	σ_2	Ev''_1	Ev''_2
1-2	0	0	0	0	6.147e - 010	6.147e - 010
2-3	0	0	0	0	2.099e - 014	-1.821e - 015
3-4	-343	-343	0	0	-6.147e - 010	-6.147e - 010
3-5	343	343	0	0	-1.821e - 015	-1.821e - 015
4-6	-343	-343	0	0	-1.438e - 015	-1.487e - 015
5-7	343	343	0	0	-1.821e - 015	-1.115e - 015
6-7	-343	-343	0	0	6.147e - 010	6.147e - 010
7-0	0	0	0	0	6.147e - 010	6.147e - 010
0-5	-0	0	0	0	-6.147e - 010	-6.147e - 010

No.	M_1	M_2	N_1	N_2	q_1	q_2
1	0.000e + 000	-9.549e - 005	0.000e + 000	-7.6393 - 007	0.000e + 000	0.000e + 000
2	2.500e + 007	1.500e + 007	2.000e + 005	1.200e + 005	0.000e + 000	0.000e + 000
3	0.000e + 000	5.357e + 006	0.000e + 000	4.286e + 004	0.000e + 000	0.000e + 000
4	1.500e + 007	3.000e + 006	1.200e + 005	2.400e + 004	0.000e + 000	0.000e + 000
5	-1.500e + 007	0.000e + 000	-1.200e + 005	0.000e + 000	0.000e + 000	0.000e + 000
6	3.000e + 006	0.000e + 000	2.400e + 004	0.000e + 000	0.000e + 000	0.000e + 000
7	-5.357e + 006	1.125e - 001	-4.286e + 004	8.998e - 004	0.000e + 000	0.000e + 000
8	1.125e - 001	0.000e + 000	8.998e - 004	0.000e + 000	0.000e + 000	0.000e + 000
9	0.000e + 000	0.000e + 000	0.000e + 000	0.000e + 000	0.000e + 000	0.000e + 000

Coefficient of the polynomial for the normal stresses

No.	a_0	a_1	a_2	a_3
1	2.3667e - 007	6.1523e - 010	0.0000e + 000	0.0000e + 000
2	2.3052e - 007	6.0099e - 015	0.0000e + 000	0.0000e + 000
3	2.68943 - 007	-6.1471e - 010	0.0000e + 000	0.0000e + 000
4	2.3052e - 007	-9.1324e - 016	0.0000e + 000	0.0000e + 000
5	3.0736e - 007	-8.8998e - 016	0.0000e + 000	0.0000e + 000
6	2.3052e - 007	-1.0795e - 015	0.0000e + 000	0.0000e + 000
7	2.6894e - 007	6-1471e - 010	0.0000e + 000	0.0000e + 000
8	1.1526e - 007	6.1471e - 010	0.0000e + 000	0.0000e + 000
9	1.1526e - 007	-6.1471e - 010	0.0000e + 000	0.0000e + 000

E is the Young's modulus

Coefficient of the polynomial for the shear stresses

No.	a_0	a_1	a_2
1	1.9179e - 008	-1.8934e - 009	-2.4606e - 012
2	1.5872e - 007	-1.8441e - 009	-7.2180e - 017
3	-2.8571e + 002	-2.1515e - 009	2.4589e - 012
4	4.2857e + 002	-1.8441e - 009	5.9061e - 018
5	-4.2857e + 002	-2.4588e - 009	1.0989e - 018
6	4.2857e + 002	-1.8441e - 009	3.6156e - 019
7	-4.2857e + 002	-2.1515e - 009	-2.4588e - 012
8	3.0380e - 006	-9.2207e - 010	-2.4588e - 012
9	-2.8815e - 008	-9.2207e - 010	2.4588e - 012

REFERENCES

1. Wlassow: Allgemeine Shcalentheorie und ihre Anwendung in der Technik. Akademie-Verlag. Berlin 1958

2. Wlassow: Dünnwandige elastische Stäbe. VEB Verlag für Bauwesen. Berlin 1964

3. Schnadel: Die Spannungsverteilung in den Flanschen dünnwandiger Kastenträger. Jahrbuch der Schiffbautechnischen Gesellschaft B. 27. 1926

4. Schade: Thin-walled box girder-theory and experiment. Schiff und Hafen 1965 H.1

5. Deseö: Die mittragende Breite der Schiffsdecken. Schiff und Hafen H10/1976, H5/1978

6. Deseö: Zur Berechnung von auf Biegung und Torsion beanspruchten dünnwandigen Trägern nach der Scheibentheorie. Der Stahlbau 1972/9

7. Deseö: Biegung und Torsion der Schiffe. Schiffbauforschung 22 4/1983. Rostock

Acta Technica Acad.Sci.Hung., 104(1-3), pp. 63-76 (1991/92)

BUCKLING OF A CORD UNDER TENSION

DOMOKOS, G.*

(Received: 11 July 1989)

It is shown that a cord may buckle under pure tension if its shear stiffness is smaller than its tensile stiffness. The investigation is based on the matrix differential equation derived in /4/ describing the large deflections of one-dimensional elastic continua. If the bending stiffness is zero, but there are finite shear and tensile stiffnesses, the solutions of the mentioned differential equation will not depend uniquely on the initial conditions, i.e. there exist multiple equilibrium positions and the bifurcation belongs to the standard cusp catastrophe type. Small bending stiffness is introduced as an imperfection parameter in the cusp catastrophe.

1. Introduction

In the theory of elasticity, if strains are assumed to be small, then an infinitesimal square will be transformed by pure shear into a rhombus, and this transformation preserves both the area and the side length. The theory of small strains will be capable of describing geometrically non-linear problems if the displacements of the structure are due to bending only. However, if the geometric non-linearity is due to shear (and/or axial) deformations, then the theory of small strains can not be applied.

If the strain is significant, then one of the previous statements about shear deformation (preservation of side length and preservation of area) shall be abandoned. By describing the effect of shear force on the critical load of a compressed cantilever, Timoshenko /1/ implicity suggests to abandon the last one. His point of view is illustrated in Fig. 1.

According to this theory, a cantilever with infinite bending stiffness and finite shear stiffness can buckle due to a compressive force, since shear deformations of the bar imply a change in the potential energy

*Domokos, Gábor, H-1056 Budapest, Váci u. 44, Hungary

Akadémiai Kiadó, Budapest

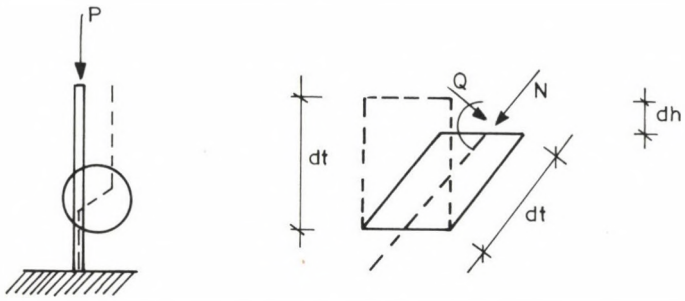

Fig. 1. Cantilever and line element described by Timoshenko

(Pdh) of load P. The arch length does not change under shear deformations. The main aim of this theory is not to comply with the mathematical theory of large strains, but to provide a continuous bar model capable of describing the behaviour of a wiede range of structures under shear.

By describing the in-plane deformation of a bar coss section due to shearing, Love /2/ displays a different point of view. In his opinion, the area of the cross section is preserved, but the side lengths change. It seems to be worth investigating what is the consequence of this viewpoint in the elementary bar theory, i.e. to require the invariance of area in case of shear deformations of a planar line element between two rigid cross sections. This paper a contribution to the solution of this problem. The deformation of a line element is illustrated in Fig. 2.

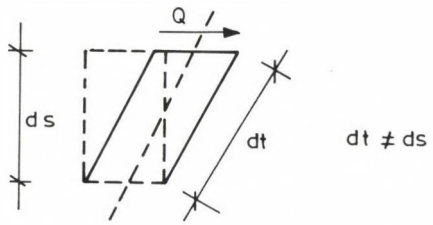

Fig. 2. Line element corresponding to the theory of Love

Let us compare the behaviour of the compressed cantilever consisting of the above type of line elements with the previously described one (Fig. 1). In this case, the arch length would change under shear deformation, but shear deformation does not imply change in the potential energy, i.e. the cantilever will not buckle under compressive force. To illustrate the

mechanical behaviour of a line element illustrated in Fig. 2 a finite mechanical model is presented in Fig. 3. The vertical spring in Fig. 3a can be associated with the tensile stiffness, the horizontal springs with the shear stiffness of the bar.

Figure 3a illustrates the trivial state of equilibrium of the model under pure tension (P). Figure 3b demonstrates that (under certain conditions for the ratio of the stiffnesses to be discussed later) non-trivial equilibrium positions are existing (the symmetric pair of Fig. 3b is not illustrated). In the forthcoming figures, this type of line element is symbolized by the contours of the finite model, i.e. by "T".

The differential equation system describing arbitrarily large deflections of one-dimensional elastic continua subjected to distributed, conservative loads, based on the usual assumptions of elementary strength of materials, was first derived by Clebsch in 1862 /3/. During the recent 127 years, several authors have dealt with the problem and generalized the equation system of Clebsch in many respects. The author of the present paper derived this equation system in /4/ based on the investigations of Gáspár /7/, as an explicit, second order matrix equation, allowing bars with large initial curvature and arbitrary initial state of stress to be analyzed. Numerical application of this equation to the analysis of guyed masts can be found in /5/. It is remarkable that the equations of Clebsch

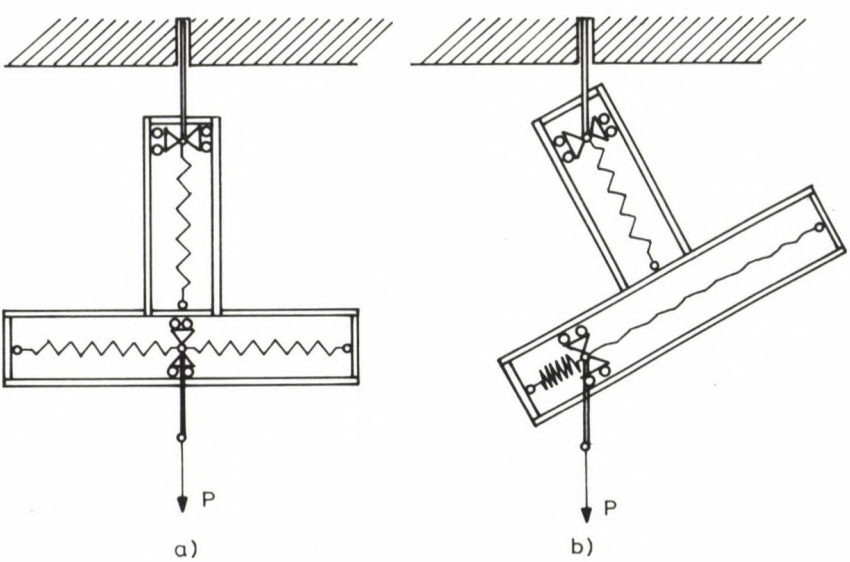

Fig. 3. Finite model for the line element in Fig. 2

(and therefore the equation in /4/) are consistent with the large shear strain theory of Love /2/, therefore the effect of shearing in this interpretation on the stability of line continua can be studied by the differential equation in /4/.

If the stiffness parameters of the bar are non-zero, then the Uniqueness Theorem of Peano (see /8/) can be applied to this differential equation. This Theorem states that the solutions are uniquely determined by the Cauchy-type initial conditions. Based on this Theorem, the author introduced in /6/ the global description of the equilibrium path in finite dimensional space.

The present paper is devoted to the case when the bending stiffness is zero.

2. The differential equation

The matrix differential equation presented in /4/ is defined for planar bars in the co-ordinate systems illustrated in Fig. 4.

The system (xy) is global, the system $(\overline{xy})$ is the local one, attached to each cross section. If the cross section is orthogonal to the bar axis, then $\alpha = \beta$, but in general the tangent of the bar axis and the normal of the cross section do not coincide. The unstressed (original) arch length is denoted by s, the arch length of the deformed bar by S. The differential operator $\frac{d}{ds}$ is denoted by $(\ )'$ (dot).

The differential equation can be derived from the equation expressing the static equilibrium of line element ds illustrated in Fig. 5.

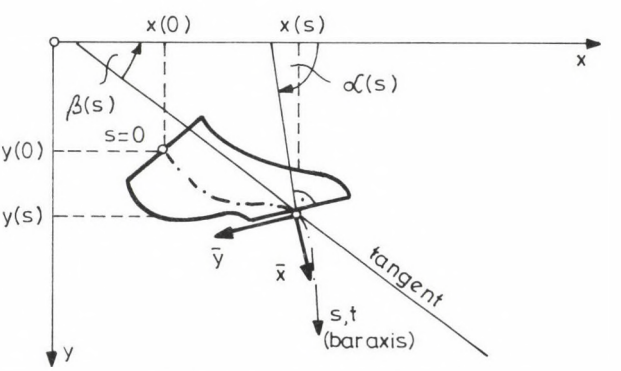

Fig. 4. The co-ordinate systems

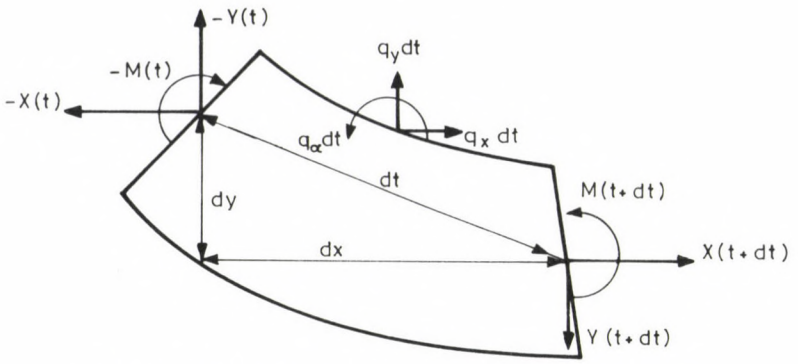

Fig. 5. The line element, the loads and the internal forces

By introducing vector D(s) of the internal forces, vector q(s) of the load intensities and the transfer matrix B(s):

$$D(s) = \begin{bmatrix} X(s) \\ Y(s) \\ M(s) \end{bmatrix}, \quad q(s) = \begin{bmatrix} q_x(s) \\ q_y(s) \\ q_\alpha(s) \end{bmatrix}, \quad B(s) = \begin{bmatrix} 1 & 0 & 0 \\ 0 & 1 & 0 \\ -y(s) & x(s) & 1 \end{bmatrix}$$

the condition of static equilibrium can be formulated as

$$\dot{D} = \dot{B}D - q \ . \tag{1}$$

The deformed shape of the bar will be described by vector z(s):

$$z(s) = \begin{bmatrix} x(s) \\ y(s) \\ \alpha(s) \end{bmatrix},$$

The co-ordinates of z(s) are defined in Fig. 4. The co-ordinates of derivative $\dot{z}(s)$ are the strains. The initial deformation (the deformation where the stresses are zero) of the bar is given by a vector $\dot{z}_0(s)$ (not describing the rigid-body position of the bar). In case of an originally straight bar with cross sections perpendicular to the bar axis we have

$$\dot{z}_0(s) = \begin{bmatrix} b \\ a \\ 0 \end{bmatrix}$$

where

$$a = \sin(\alpha(s)), \qquad b = \cos(\alpha(s)) \ .$$

This paper treats the above case only since the initial curvature of a cord without bending stiffness does not imply strains, i.e. does not affect the solution curve. A more detailed explanation of $\dot{z}_0$ can be found in /6/.

By introducing the flexibility matrix of line element F(s) expressed in the (xy) global system, Hooke's Law can be formulated as

$$(\dot{z} - \dot{z}_0) = FD \ . \tag{2}$$

The connection between the global and the local system is expressed by the common rotation matrix T(s):

$$T(s) = \begin{bmatrix} b & a & 0 \\ -a & b & 0 \\ 0 & 0 & 1 \end{bmatrix} .$$

The well-known definition of the flexibility matrix in the local $(\bar{x}\bar{y})$ system is denoted by $\bar{F}$ and it is assumed to be diagonal and constant (not depending on s):

$$\bar{F} = <\frac{1}{T} \frac{1}{S} \frac{1}{B}>,$$

T, S, B denoting tensile, shear and bending stiffness, respectively.

On the basis of the transformation rules for tensor representations F is expressed as

$$F = T^{-1}\bar{F}T = \begin{bmatrix} u & v & 0 \\ v & w & 0 \\ 0 & 0 & \frac{1}{B} \end{bmatrix} \tag{3}$$

where

$$u = \frac{1}{T}b^2 + \frac{1}{S}a^2 ,$$

$$v = ab\left(\frac{1}{T} - \frac{1}{S}\right) ,$$

$$w = \frac{1}{T}a^2 + \frac{1}{S}b^2 .$$

Substitution of the material law (2) into the static equilibrium equation (1) yields the differential equation of the elastic bar:

$$\dot{z} = (F\dot{B} + \dot{F})D + \dot{z}_0 - F_q . \tag{4}$$

The initial condition expresses that strain vector $\dot{z}$ at initial point $s = 0$ is a function of the concentrated end-loads.

Equation (4) is equivalent to the following system of scalar equations:

$$1. \qquad \ddot{x} = f_1(\dot{x},\dot{y},x,y,\frac{1}{T},\frac{1}{S},\alpha) ,$$

$$2. \qquad \ddot{y} = f_2(\dot{x},\dot{y},x,y,\frac{1}{T},\frac{1}{S},\alpha 9 , \tag{5}$$

$$3. \qquad \ddot{\alpha} = \frac{1}{B}(X\dot{y} - Y\dot{x}) .$$

The exact form of functions f_1 and f_2 can be derived from (4) and (3), respectively, but it does not affect our further investigations.

3. Cord with zero bending stiffness

In case of zero bending stiffness $B = 0$, equations (5)/1 and /2 do not change, but in order to avoid infinite changes of curvature, Eq. (5)/3 is transformed into the condition

$$X\dot{y} - Y\dot{x} = 0 \ , \tag{6}$$

i.e. the third scalar differential equation turned into an algebraic one. The unknown vector describing the deformed shape of the bar has now only two co-ordinates (x,y), but the differential equation system formed by (5/1) and (5/2) has an additional parameter α which has to be determined from condition (6).(Note that if $\frac{1}{T} = \frac{1}{S} = 0$, then (6) will express vanishing of the shear force.) The number of independent scalar initial conditions is reduced from the original 6 ($\dot{x}(0),\dot{y}(0),\dot{\alpha}(0),x(0),y(0)\alpha(0)$) to 4 ($\dot{x}(0),\dot{y}(0),x(0),y(0)$). The Uniquness Theorem will hold if by fixing the just mentioned 4 initial values, the solution curve of the differential equation is uniquely identified. This will be the case only if condition (6) yields an unique value for parameter α, else the theorem can not be applied. Therefore the possible number of solutions of (6) will be investigated now.

By using the material law (2) assuming that $\frac{1}{T} \neq 0$, $\frac{1}{S} \neq 0$, forces X and Y can be expressed as functions of strains $\dot{x}$ and $\dot{y}$. Substitution of these expressions into (6) yields

$$v(\dot{x}^2 - \dot{y}^2) + \dot{x}\dot{y}\ (w - u) + \dot{y}(va - wb) + \dot{x}(ua - vb) = 0 \ . \tag{7}$$

In order to simplify the above equation, variables $\dot{t}$ and β defined in Fig. 4 will be introduced. The old variables can be expressed with the new ones:

$$\begin{aligned} \dot{x} &= \dot{t}\cos(\beta) \ , \\ \dot{y} &= \dot{t}\sin(\beta) \ . \end{aligned} \tag{8}$$

Substitution of (8) into (7) yields

$$\dot{t}\sin(\alpha - \beta)\left[\dot{t}\left(\frac{1}{T} - \frac{1}{S}\right)\cos(\alpha - \beta) + \frac{1}{S}\right] = 0 \ . \tag{9}$$

By excluding the degenerate case $\dot{t} = 0$, condition (9) can be satisfied either by

$$\sin(\alpha - \beta) = 0 \tag{10}$$

or by

$$\cos(\alpha - \beta) = \frac{\frac{1}{S}}{\dot{t}\left(\frac{1}{S} - \frac{1}{T}\right)} \tag{11}$$

The solution of (10) is

$$\alpha = \beta \pm k\pi \qquad (k=0,2,4,\ldots) \tag{12}$$

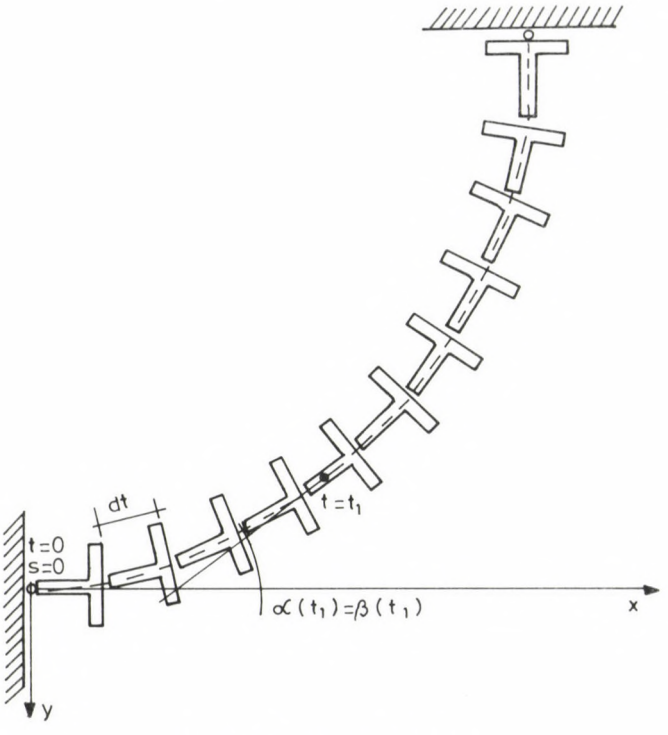

Fig. 6. The trivial solution

(The odd values (1,3,5,...) of k have been omitted, because we restrict ourselves to cords under tension with positive axial strain.) Equation (12) defines the trivial solution, when the line elements ds are always tangent to the curve in the (xy) plane. This solution is illustrated in Fig. 6.

Equation (11) can be solved only if

$$\frac{\frac{1}{S}}{\dot{t}\left(\frac{1}{S} - \frac{1}{T}\right)} \leq 1 .$$

Since only the cord under tension with positive axial strain is investigated, the negative values for $\cos(\alpha - \beta)$ and for $\dot{t}$ can be excluded to yields

$$\frac{S}{T} \leq -\frac{1}{\dot{t}} \qquad (13)$$

or by expressing $\dot{t}$

$$\dot{t} \geq \frac{T}{T - S} \qquad (S < T) \ . \tag{14}$$

If condition (14) is satisfied, then, in addition to the already investigated trivial solution (12), a new solution will appear. From (14) we learn that this can not happen in the case of tension and positive axial strain, if $S > T$. This new solution will coincide with the trivial one if

$$\dot{t} = \dot{t}_{cr} = \frac{T}{T - S} \qquad (S < T) \tag{15}$$

Since in case of the trivial solution $\alpha = \beta$, $\dot{t}_{triv} = 1 + N/T$, (N denotes the normal force). Substituting this expressioninto (15), the critical normal force N_{cr} corresponding to $\dot{t}_{triv}$ is found to be

$$N_{cr} = \frac{TS}{T - S} \qquad (S < T) \tag{16}$$

with

$$\lim_{T \to \infty} N_{cr} = S \ . \tag{17}$$

If $\dot{t} > \dot{t}_{cr}$ then the new solution bifurcates, and two secondary solutions emerge at the sides of the trivial one. This could be illustrated in a two-dimensional diagram (Fig. 7):

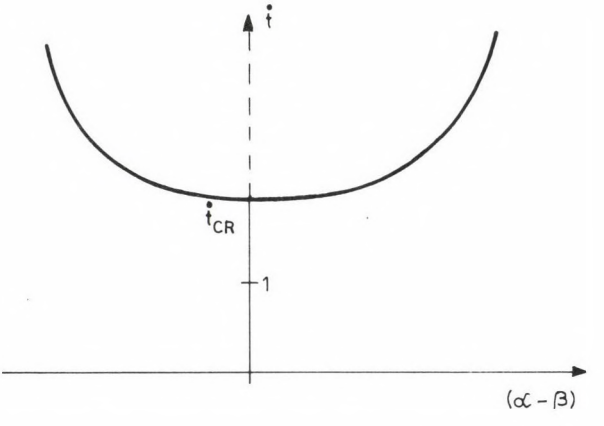

Fig. 7. The equilibrium positions of the line element

Since the unique solution for $\dot{t} < \dot{t}_{cr}$ is the well-known trivial solution, this equilibrium position is stable. On the basis of the elementary catastrophe theory, the trivial solution loses its stability at the critical point and the secondary solutions are stable. (We have a standard cusp catastrophe.) The bifurcation parameter is in our case not the load, but the deformation of the arch length, therefore both states of equilibrium (trivial and buckled) can be illustrated on the same structure with constant loading.

The structure investigated is a cord under constant dead load, fixed by hinges at both ends, with horizontal tangent at the left end (Fig. 8). Since the axial strain is minimum in case of a horizontal tangent of the cord, the dead load can be chosen in such a way that at the left end (Fig. 8) the trivial equilibrium is still stable ($\dot{t} < \dot{t}_{cr}$) but at a certain point, $\dot{t}$ reaches the critical value, and all additional line elements (or cross sections) may buckle. In Fig. 8 the buckled state of equilibrium is illustrated for these line elements.

Note that in case of a cord with only end loads, the normal force and strain of the arch length are constant. In this case, the cord is straight. Either the trivial state of equilibrium is stable for all line elements, or, by increasing the end load, the trivial state of equilibrium becomes unstable for all line elements simultaneously, i.e. the bifurcation parameter is now the load parameter.

4. The effect of bending stiffness

Real cords have a small bending stiffness. In this case, the solution of (4) remains unique, i.e. no bifurcation or buckling is possible in the sense of the previous section. (Naturally, the "traditional", global type of buckling, i.e. buckling due to increasing external load is not excluded at all. E.g. the just described straight cord can buckle in the "traditional" way even in the case of non-zero bending stiffness.) All the same, from the catastrophe theory we learn that the observed phenomena are typically structurally stable, i.e. the small change of a parameter can not result in the abrupt change of the solution curve. In our case the "observed phenomenon" is a boundary value problem. We are looking for solutions of the equation system (5) for very small values of bending stiffness B in the vicinity of the solutions for B = 0 investigated in the

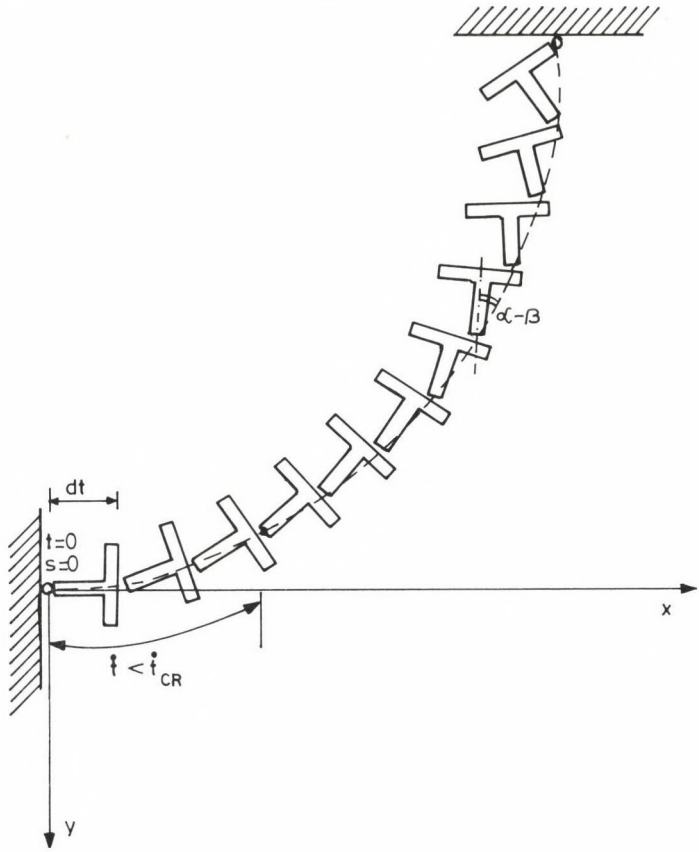

Fig. 8. The non-trivial solution

previous section. Variables corresponding to the solution with zero bending stiffness will have index 0, variables in the solution for small $B = \varepsilon < 1$) bending stiffness index ε. Our aim is to verify whether these latter solutions (selected from the infinitely many possible ones) have the structure predicted by the elementary catastrophe theory or not. The "vicinity" of a point will be selected on condition that the initial condition satisfy

$$\ddot{\alpha}_0(0) = \ddot{\alpha}_\varepsilon(0) ,$$

$$\dot{\alpha}_0(0) = \dot{\alpha}_\varepsilon(0) ,$$

$$\dot{x}_0(0) = \dot{x}_\varepsilon(0) \ ,$$

$$\dot{y}_0(0) = \dot{y}_\varepsilon(0) \ , \tag{18}$$

$$x_0(0) = x_\varepsilon(0) \ ,$$

$$y_0(0) = y_\varepsilon(0) \ .$$

Condition (18) implies on the basis of (5)/3 that

$$(X(0)\dot{y}_\varepsilon(0) - Y(0)\dot{x}_\varepsilon(0)) = \varepsilon\,\ddot{\alpha}_0(0) \ . \tag{19}$$

The solutions of this equation are illustrated in Fig. 9a. It can be realized that this solutions display exactly the structure predicted by

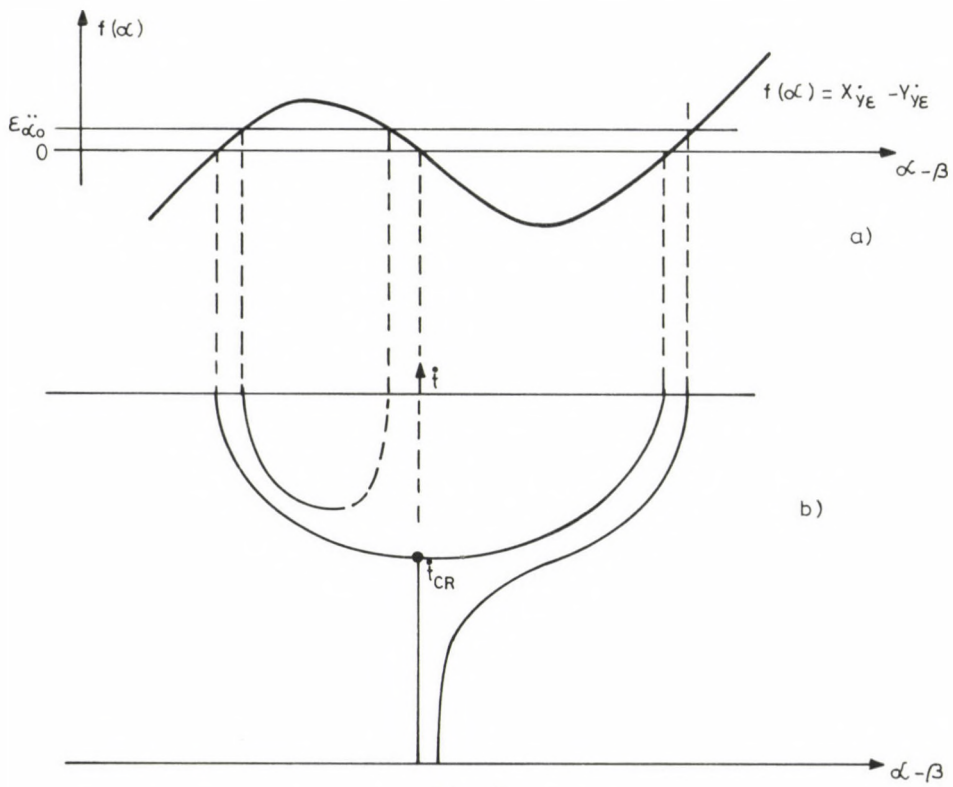

Fig. 9.
a) Solutions for a small bending stiffness,
b) Imperfection due to a small bending stiffness

the elementary catastrophe theory for the unfolding of the standard cusp catastrophe /9/.

According to this, the (sufficiently) small bending stiffness can be regarded as an imperfection parameter necessary to the unfolding of the cusp catastrophe point just mentioned. In mechanics, this can be easily interpreted, since in the case of non-zero bending stiffness, the internal force vector of the cord is not exactly tangent to the cord, i.e. $\alpha - \beta \neq 0$. The solution curve for this case is illustrated in Fig. 9b.

5. Summary

A new type of buckling has been introduced in this paper. It proved to be - like the classic Euler problem of compressed members - a stable-symmetric bifurcation. The main difference between the two types of buckling is that in our case it is not the entire beam (cord), but the individual line elements (cross sections) that buckle(s). Mathematically, this means that in the classic case the boundary value problem has a bifurcation point while in our case, the initial value problem shows a point of bifurcation (the Uniquness Theorem can not be applied). This type of buckling is not displayed by common structures, all the same a discrete model has been demonstrated for mechanical evidence.

REFERENCES

1. Timoshenko, S.P.—Gere, J.M.: Theory of elastic stability, 2. ed. McGraw-Hill, New York 1961
2. Love, A.E.H.: Treatease on the mathematical theory of elasticity, 4. ed. Dover Publ., New York 1944
3. Clebsch, A.: Elastizität. Teubner, Leipzig 1862
4. Domokos, G.: Large deflections of elastic bars subject to arbitrary, distributed loads. Newsletter of the Technical University of Budapest, Vol. VI, No. 2, pp. 6-11., 1988
5. Domokos, G.: Postkritisches Verhalten von abgespannten Masten. ZAMM Bd. 69 (1989), No. 5, T373-T376
6. Domokos, G.: Large deflections of guyed masts (in Hungarian). Candidate's Thesis, Budapest 1989
7. Gáspár, Zs.: Large deflection analysis of bar structures. Acta Techn. Hung. Vol. 87 (1978), 49-58.
8. Bieberbach, L.: Differentialgleichungen. Springer, Berlin 1923
9. Gáspár, Zs.: Critical imperfection territory. J. Struct. Mech., Vol. 11 (1983), No. 3, 297-325

Acta Technica Acad.Sci.Hung., 104(1-3), pp. 77-93 (1991/92)

DISCRETE FOURIER INTEGRALS AS SINGULARITY-BEARING SOLUTIONS OF PARTIAL DIFFERENCE EQUATIONS

HEGEDŰS, I.*

(Received: 10 May 1990)

Discrete Fourier integrals are analogues of common Fourier integrals in case of functions with discrete variables. They can be produced and used analogously to common Fourier integrals of functions with continuous variables. The paper introduces these integrals and presents a method for producing discrete Fourier integrals which are singularity-bearing solutions of partial linear difference equations of constant coefficients. Also discrete Fourier integrals of some singularity-bearing solutions of second and fourth order partial difference equations of important applications in the analysis of lattice structures are presented.

1. Fourier series and Fourier integral of functions with integer variables

Let $f(j)$ a periodic function of integer variable j with a period $2n$. The values of $f(j)$ are determined for any $-\infty \leq j \leq \infty$ values by taking a series of $2n$ independent values

$$f(-n),\ f(-n+1),\ \ldots,\ f(j),\ \ldots,\ f(n-1),\ f(n),$$

and applying the equation

$$f(j-n) = f(j+n). \tag{1}$$

Eqn.1 defines the $2n$ periodicity.

An alternative way of defining $f(j)$ is using a composition of formerly defined $2n$ linearly independent sets of values

$$\phi_k(j),\ j,k = 1,\ 2,\ \ldots,\ 2n$$

as follows:

$$f(j) = c_1\phi_1(j) + \ldots + c_k\phi_k(j) + \ldots + c_{2n}\phi_{2n}(j), \tag{2}$$

* István HEGEDŰS, H-2083 Solymár, Váci Mihály u. 10., Hungary

Akadémiai Kiadó, Budapest

and extending the interpretation of Eqn.2. by Eqn.1.

Linear independence of sets $\phi_k(j)$ means that their Casorati determinant must not equal to zero (Spiegel 1970):

$$\det [d_{kj}] = \det [\phi_k(j)] \neq 0. \tag{3}$$

Component sets ϕ_k can easily be found as trigonometric functions of integer variables (Korn- Korn 1968, Bleich- Melan 1927). Values produced by introducing elements of a $2n$ successive sequence of integers j into trigonometric expressions

$$\cos\frac{k\pi j}{n},\ k = 0,\ 1,\ \ldots,\ n, \text{ and } \sin\frac{k\pi j}{n},\ k = 1,\ 2,\ \ldots,\ n-1$$

form linear independent sets which are orthogonal and normed in the sense as follows:

$$\sum_{j=1}^{2n} \cos\frac{k\pi j}{n} \cos\frac{l\pi j}{n} = \begin{cases} 2n \text{ if } k = l = 0 \text{ or } n \\ n \text{ if } k = l \neq 0 \text{ or } n; \\ 0 \text{ else} \end{cases} \tag{3.a}$$

$$\sum_{j=1}^{2n} \sin\frac{k\pi j}{n} \sin\frac{l\pi j}{n} = \begin{cases} n \text{ if } k = l \neq 0 \text{ or } n \\ 0 \text{ else} \end{cases}; \tag{3.b}$$

$$\sum_{j=1}^{2n} \cos\frac{k\pi j}{n} \sin\frac{l\pi j}{n} = 0. \tag{3.c}$$

These relations are discrete analogues of the orthogonality relations of sines, and cosines used in Fourier expansions.

Linear independence of sets

$$\cos\frac{k\pi j}{n},\ k = 0,\ 1,\ \ldots,\ n, \text{ and } \sin\frac{k\pi j}{n},\ k = 1,\ 2,\ \ldots,\ n-1$$

permits us to express an arbitrary periodic function $f(j)$ with $2n$ period in a form which can be assumed as the discrete Fourier expansion of $f(j)$:

$$f(j) = \frac{a_0}{2} + a_1 \cos\frac{1\pi j}{n} + a_2 \cos\frac{2\pi j}{n} + \ldots + \frac{a_n}{2} \cos\frac{n\pi j}{n} +$$

$$+ b_1 \sin\frac{1\pi j}{n} + b_2 \sin\frac{2\pi j}{n} + \ldots + b_{n-1} \sin\frac{(n-1)\pi j}{n}. \tag{4}$$

Coefficients a_k, and b_k in Eqn.4 can also be expressed analogously to those of Fourier expansions using orthogonality

relations 3.a-c :

$$a_k = \frac{1}{n} \sum_{j=1}^{2n} f(j) \cos\frac{k\pi j}{n} \quad , \; k = 0, 1, \ldots, n; \tag{5.a}$$

$$b_k = \frac{1}{n} \sum_{j=1}^{2n} f(j) \sin\frac{k\pi j}{n} \quad , \; k = 1, 2, \ldots, n-1. \tag{5.b}$$

By introducing Eqs.5.a, and 5.b into Eqn.4, it can also be written in an alternative form

$$f(j) = \frac{1}{\pi} \sum_{k=1}^{n} \sum_{l=1}^{2n} f(l) \cos \frac{k\pi(j-l)}{n} \frac{\pi}{n} . \tag{6}$$

This expression is the base of deriving discrete Fourier integrals of not periodic functions of integer variable j in a way as follows.

Let period $2n$ be increased in a way that elements inside its original length $2n_0$ keep their original places, and values, while at the extended regions of the period let $f(j)=0$. In this case Eqn.6 changes only in the upper limit of the second summa, because zeros in the extended region need not be summed.

$$f(j) = \frac{1}{\pi} \sum_{k=1}^{n} \sum_{l=1}^{2n_0} f(l) \cos \frac{k\pi(j-l)}{n} \frac{\pi}{n} . \tag{7}$$

Tending to the infinity with n, the summation by k in Eqn.7 can be replaced for an integration by the variable

$$\alpha = \frac{k\,\pi}{n}$$

as follows:

$$f(j) = \lim_{n \to \infty} \frac{1}{\pi} \sum_{k=1}^{n} \sum_{l=1}^{2n_0} f(l) \cos \frac{k\pi(j-l)}{n} \frac{\pi}{n} =$$

$$= \frac{1}{\pi} \int_{\alpha=0}^{\pi} \sum_{l=1}^{2n_0} f(l) \cos (j-l)\alpha \, d\alpha =$$

$$= \frac{1}{\pi} \sum_{l=1}^{2n_0} \int_{\alpha=0}^{\pi} f(l) \cos (j-l)\alpha \, d\alpha . \tag{8}$$

Expression (8) is called the discrete Fourier integral of function $f(j)$. It is the analogue of common Fourier integrals of functions with continuous variables (Korn- Korn 1968).

The result of the derivation can easily be checked by

performing the integration in Eqn.(8) as follows:

$$f(j) = \frac{1}{\pi} \sum_{l=1}^{2n_0} f(l) \frac{\sin(j-l)\pi}{j-l} = \sum_{l=1}^{2n_0} f(l)\, \delta_{jl} \equiv f(j).$$

A basic difference between common Fourier integrals and discrete Fourier integrals is that Eqn.8 only contains integration on the interval $0 \le \alpha \le \pi$ and not on $0 \le \alpha \le \infty$. This difference can make easier the evaluation of discrete Fourier integrals using numeric integration.

2. Singularity- bearing solutions of difference equations

Let $p(j_0;j)$ a function which takes zero values at $j \neq j_0$, while $p(j_0;j_0) = 1$. This function can be physically interpreted as that of a single unit load acting at the point $j = j_0$. Its discrete Fourier integral produced by Eqn.8. is also a single term

$$p(j_0;j) = \frac{1}{\pi} \int_{\alpha=0}^{\pi} \cos\,[(j-j_0)\alpha]\, d\alpha\ , \tag{9}$$

because the summation by l only extends to $l = j_0$. Eqn.9. shall be used in the subsequent sections for deriving singularity-bearing solutions of partial difference equations.

Let $F(i,j)$ a function of integer variables i, and j, and let $\mathcal{D}$ a linear partial difference operator of constant coefficients which can be expressed as an algebraic expression of elementary shifting operators E_1, and E_2 or as a polynomial of first order central difference and average operators δ_1, δ_2, and μ_1, μ_2, in variables i, and j, respectively.

Function F is called a singularity-bearing solution of the homogeneous difference equation

$$\mathcal{D}\,[F(i,j)] = 0 \tag{10}$$

if it meets Eqn.10 at each points $\{i,j\}$ inside the domain of interpretation, excepting $i = i_0$, $j = j_0$, where the right side of the equation takes 1 instead of 0. Thus, this solution meets the equation

$$\mathcal{D}\,[F(i,j)] = p(i_0,j_0;i,j), \tag{11}$$

instead of Eqn.10 , where

$$p(i_0,j_0;i,j) = p(i_0;i)\ p(j_0;j).$$

Though singularity at the point (i_0,j_0) does not emerge with infinitely large absolute values, it is a discrete analogue of those of singular solutions of partial differential equations.

Solutions of this kind may have a great practical importance in the static and dynamic analysis of large lattices with regular networks.

In the subsequent sections singular solutions of different partial difference equations are dealt with.

In most practical cases difference operator $\mathcal{D}$ has a specific built-up, namely, it is a self-adjoint difference operator. (Rózsa 1971., Kollár-Hegedűs 1985.) That means, it is invariant against the changes in sign of difference operators δ_1 or δ_2. This property of $\mathcal{D}$ will also be assumed here, $\mathcal{D}$ is a self adjoint partial difference operator of constant coefficients and of the order $2N$.

2.1 Direct algebraic solution for limited domain of interpretation

Correct setting of a problem of producing solutions for Eqn.11 needs a definition for the domain of interpretation and also needs properly stated boundary conditions.

If the problem concerns a domain of interpretation limited e.g. by the condition that values of $F(i,j)$ can only differ from zero if

$$m_0 + 1 \le i \le m_0 + m, \quad \text{and} \quad n_0 + 1 \le j \le n_0 + n,$$

then Eqn.11 can be replaced for a set of linear algebraic equations of $m*n$ unknowns. Denoting the vector of the unknown values of $F(i,j)$ by $\mathbf{f}$, and that of values of $p(i_0,j_0;i,j)$ by $\mathbf{p}$, algebraic solution formally needs inverting the vectorial equation

$$\mathbf{Af} = \mathbf{p}, \tag{12.a}$$

as

$$\mathbf{f} = \mathbf{A}^{-1}\mathbf{p}. \tag{12.b}$$

Mathematical determinacy of the problem appears in the regularity of **A** and self adjointness of operator $\mathcal{D}$ does so in the symmetry of **A**.

Since elements of **p** are zeros, excepting a single 1, Eqn.12.b yields a column vector of $\mathbf{A}^{-1}$ for **f**, that is, $\mathbf{A}^{-1}$ can be considered as consisted of column vectors **f** of singularity-bearing solutions associated with different functions $p(i_0, j_0; i, j)$. This property of inverse matrix $\mathbf{A}^{-1}$ is analogous to that of the Green functions of boundary value problems of ordinary and partial differential equations of self-adjoint differential operator; actually, $\mathbf{A}^{-1}$ works as the discrete analogue of a Green function (Frank-Mises 1927, Rózsa 1971).

Boundary conditions of other kind for $F(i,j)$ can also be taken into account in coefficient matrix **A**.

3. Solution for not limited domain of interpretation

Direct algebraic solution of Eqn.11 fails if the domain of interpretation is not limited. However, discrete Fourier integrals can be used to produce solutions of Eqn.11. also in this case.

Missing boundary conditions are replaced as a rule by symmetry conditions and requirements that higher differences of $F(i,j)$ have to show a decaying character at large absolute values of $i - i_0$, and $j - j_0$.

First, discrete field solutions of Eqn.10 are analytically produced for $-\infty \le i \le \infty$ and $-\infty \le j \le \infty$. For the sake of simplicity $i_0 = j_0 = 0$ is assumed.

Self adjointness of difference operator $\mathcal{D}$ permits us to assume discrete field solutions as products of $2n$ periodic functions of either variable and properly chosen algebraic functions of the other one, e.g. in the form as follows:

$$F(i,j)_k^0 = [Y_k] \left\{ \begin{matrix} \cos \\ \sin \end{matrix} \right\} \left(\frac{ik\pi}{n} \right), \qquad (13)$$

where $n > 1$ and $0 \le k \le n$ are integers and Y_k only depends on discrete variable j.

Introducing expression (13) into Eqn.10, an ordinary dif-

ference equation can be derived for Y_k as

$$\mathcal{D}_k [Y_k(j)] = 0. \tag{14}$$

According to the self adjointness of partial difference operator $\mathcal{D}$, also difference operator $\mathcal{D}_k$ is self adjoint and solutions of common linear difference equation Eqn.14 can be assumed by pairs in the form

$$Y_k = j^m \begin{Bmatrix} z_k^j \\ z_k^{-j} \end{Bmatrix}, \tag{15}$$

where z_k is a real or complex number and m is a not negative integer. Assuming first that $m = 0$ and introducing expression (15) into Eqn.14, an algebraic equation of real coefficients can be derived for z_k. The order of this equation is the same as that of difference operator $\mathcal{D}_k$ and the self adjointness guarantees that its roots are reciprocals by pairs.

If the roots are complex numbers, they are conjoint by pairs, that is, powers of complex numbers z_k and $\bar{z}_k$ can be replaced by products of real powers and trigonometric functions of j in expression (15).

If the algebraic equation has multiple roots

$$z_{k(1)} = z_{k(2)} = \cdots = z_{k(m+1)},$$

then functions

$$z_{k(1)}^j, \quad j z_{k(1)}^j, \quad j^2 z_{k(1)}^j, \quad \cdots, \quad j^m z_{k(1)}^j$$

are linearly independent solutions of Eqn.14, thus, 2N, the total number of independent solutions of Eqn.14 is the same in all cases as the order of $\mathcal{D}_k$.

Let $Y_{k(1)}, \cdots, Y_{k(\nu)}, \cdots, Y_{k(N)}$ linearly independent solutions of Eqn.14 with

$$\text{abs}(z_{k(\nu)}) \leq 1.$$

A general $2n$ periodic discrete field solution with decaying character in positive j direction can be set in the form as follows:

$$F(i,j)^0 = \sum_{k=1}^{n} a_k \left\{ \sum_{\nu=1}^{N} \beta_{k\nu} Y_{k(\nu)} \right\} \cos \frac{k\pi i}{n} + b_k \left\{ \sum_{\nu=1}^{N} \hat{\beta}_{k\nu} Y_{k(\nu)} \right\} \sin \frac{k\pi i}{n}, \tag{16}$$

where a_k, b_k, $\beta_{k\nu}$, and $\hat{\beta}_{k\nu}$ are arbitrary numbers.

Let this solution of Eqn.10 be modified in a way as follows.

$$F(i,j) = \sum_{k=1}^{n} a_k \left\{ \sum_{\nu=1}^{N} \beta_{k\nu} Y_{k(\nu)}[\mathrm{abs}(j)] \right\} \cos \frac{k\pi i}{n} +$$

$$+ b_k \left\{ \sum_{\nu=1}^{N} \hat{\beta}_{k\nu} Y_{k(\nu)}[\mathrm{abs}(j)] \right\} \sin \frac{k\pi i}{n}. \qquad (17)$$

Expression (17) is an even function of j and automatically meets Eqn.10 at $\mathrm{abs}(j) \geq N$. However, at values $\mathrm{abs}(j) < N$ the discontinuity in the differences of $\mathrm{abs}(j)$ yields a discontinuity also in $\mathcal{D}[F(i,j)]$.

Coefficients $\beta_{k\nu}$, and $\hat{\beta}_{k\nu}$ can be chosen in a way that Eqn.10 also becomes met at $0 < \mathrm{abs}(j) < N$ and expressions in the braces { } take 1 values at $j = 0$. By so doing, the discontinuity in $\mathcal{D}[F(i,j)]$ reduces to the line $j = 0$:

$$\mathcal{D}[F(i,j)] = p(0;j) \left\{ \sum_{k=1}^{n} a_k \cos \frac{k\pi i}{n} + b_k \sin \frac{k\pi i}{n} \right\}. \qquad (18)$$

At this point the connection with discrete Fourier integrals becomes obvious: tending with n to the infinity, Eqn.17 , and Eqn.18 can be replaced for a discrete Fourier integral. The integral of F takes the form as follows:

$$F(i,j) = \frac{1}{\pi} \int_{\alpha=0}^{\pi} A(\alpha) \left\{ \sum_{\nu=1}^{N} \beta_\nu(\alpha)\, Y[\alpha, \mathrm{abs}(j)]_\nu \right\} \cos(\alpha i)\, d\alpha, \qquad (19)$$

where $A(\alpha)$, $\beta_\nu(\alpha)$, and $Y[\alpha,\mathrm{abs}(j)]_\nu$ are properly chosen functions. Interchangeability of difference and integral operations permits us to apply $\mathcal{D}$ upon Eqn.19 and to express the discrete Fourier integral of $\mathcal{D}[F(i,j)]$ in a similar form:

$$\mathcal{D}[F(i,j)] = \frac{1}{\pi} \int_{\alpha=0}^{\pi} A(\alpha) \left\{ \sum_{\nu=1}^{N} \gamma_\nu(\alpha)\, \mathcal{D}_\nu \{ Y[\alpha,\mathrm{abs}(j)]_\nu \} \right\} \cos(\alpha i)\, d\alpha, \qquad (20)$$

where functions $\gamma_\nu(\alpha)$, and difference operators $\mathcal{D}_\nu$ are determined by functions $\beta_\nu(\alpha)$ and by difference operator $\mathcal{D}$.

Functions $Y[\alpha,\mathrm{abs}(j)]_\nu$ have to be assumed in a form analogous to Eqn.15:

$$Y\,[\alpha,\mathrm{abs(j)}]_\nu = \mathrm{abs}(j^m)\; z_{k(\nu)}(\alpha)^{\mathrm{abs(j)}}.$$

Functions $z(\alpha)_{k(\nu)}$ can be determined from the condition that the integrand of Eqn.20 must vanish independently of $A(\alpha)$, and

$\gamma_\nu(\alpha)$ for any values of j when $\text{abs}(j) \geq N$ holds. For obtaining singular solutions of decaying character at large values of $\text{abs}(j)$, $\text{abs}[z_{k(\nu)}(\alpha)] \leq 1$ also must hold.

For values $0 < \text{abs}(j) < N$, the integrand of $\mathcal{D}[F(i,j)]$ must also vanish independently of $A(\alpha)$. Using this condition, functions $\gamma_\nu(\alpha)$ can be determined. Then, connections between $\beta_\nu(\alpha)$, and $\gamma_\nu(\alpha)$ makes possible to determine functions $\beta_\nu(\alpha)$.

Finally, $A(\alpha)$ can be determined from the condition that Eqn. 11 must hold, thus, the discrete Fourier integral of $\mathcal{D}[F(i,j)]$ has to take the form of that of $p(0,0;i,j)$:

$$\mathcal{D}[F(i,j)] = \frac{1}{\pi} \int_{\alpha=0}^{\pi} p(0;j) \cos(i\alpha)\, d\alpha. \tag{21}$$

This condition can always be met, hence, a singularity-bearing solution can always be produced.

It may easily happen that the outlined procedure obtains a divergent discrete Fourier integral of $F(i,j)$. Nevertheless, functions derived from the solution which have physical meanings, and applications are, as a rule, convergent integrals.

3.1 **Discrete harmonic singularity-bearing function (square network)**

As the first example of application, let the singularity--bearing solution $F(0,0;i,j)$ of the discrete harmonic difference equation

$$(\delta_1^2 + \delta_2^2)F = 0,$$

thus, the solution $F(i,j) = F(0,0;i,j)$ of the equation

$$(\delta_1^2 + \delta_2^2)F = p\ (0,0;i,j) \tag{22}$$

be analyzed. Values of function $F(i,j)$ can be physically interpreted as small deflections of an infinitely large net consists of two sets of uniformly stressed chords normal to each other and loaded perpendicularly to the plane of the net at the net point $i_0 = j_0 = 0$ by a unit force (Bleich-Melan 1927).

Difference operator $\mathcal{D}$ of Eqn.22 is a second order operator, thus, $N = 1$ and the singular solution can be assumed in the simple form

$$F = \lim_{n\to\infty} \sum_{k=1}^{n} A_k \, z_k^{abs(j)} \cos \frac{ik\pi}{n} =$$

$$= \frac{1}{\pi} \int_{\alpha=0}^{\pi} A(\alpha) \, z(\alpha)^{abs(j)} \cos(\alpha i) \, d\alpha. \qquad (23)$$

Introducing expression (23) into Eqn.22 yields the expression as follows:

$$\mathcal{D}[F] = \frac{1}{\pi} \int_{\alpha=0}^{\pi} A(\alpha) \, z(\alpha)^{abs(j)} \left\{ z(\alpha) + \frac{1}{z(\alpha)} + 2\cos(\alpha) - 4 \right\} \cos(\alpha i) \, d\alpha. \qquad (24)$$

For vanishing $\mathcal{D}[F]$ at $abs(j) > 0$, equation

$$z(\alpha) + \frac{1}{z(\alpha)} + 2\cos(\alpha) - 4 = 0$$

must hold. Hence,

$$z(\alpha) = [2 - \cos(\alpha)] - \sqrt{[2 - \cos(\alpha)]^2 - 1} =$$

$$= 1 + 2\sin^2(\tfrac{\alpha}{2}) - \sqrt{[1 + 2\sin^2(\tfrac{\alpha}{2})]^2 - 1} \, . \qquad (25)$$

Introducing expression (25), and $j = 0$ into expression (24) and taking Eqn.21 into account, the following condition can be stated:

$$\frac{1}{\pi} \int_{\alpha=0}^{\pi} A(\alpha)(-2)\sqrt{[1 + 2\sin^2(\tfrac{\alpha}{2})]^2 - 1} \cos(\alpha i) \, d\alpha = \frac{1}{\pi} \int_{\alpha=0}^{\pi} \cos(\alpha i) \, d\alpha.$$

Hence,

$$A(\alpha) = \frac{-1}{2\sqrt{[1 + 2\sin^2(\tfrac{\alpha}{2})]^2 - 1}} \qquad (26)$$

and the discrete Fourier integral of the singularity-bearing solution is obtained as

$$F = -\int_{\alpha=0}^{\pi} \frac{\left[1 + 2\sin^2(\tfrac{\alpha}{2}) - \sqrt{[1 + 2\sin^2(\tfrac{\alpha}{2})]^2 - 1} \right]^{abs(j)}}{2\pi\sqrt{[1 + 2\sin^2(\tfrac{\alpha}{2})]^2 - 1}} \cos(\alpha i) \, d\alpha. \qquad (27)$$

This integral cannot be directly evaluated because it yields infinitely large values for any finite pairs of i, and j. However,

discrete Fourier integral of function

$$\tilde{F}(i,j) = F(i,j) - F(0,0), \tag{28}$$

which bears the same singularity as $F(i,j)$ bears, can be easily produced as

$$\tilde{F} = -\int_{\alpha=0}^{\pi} \frac{\left[1 + 2\sin^2(\frac{\alpha}{2}) - \sqrt{[1 + 2\sin^2(\frac{\alpha}{2})]^2 - 1}\right]^{abs(j)} \cos\alpha - 1}{2\pi\sqrt{[1 + 2\sin^2(\frac{\alpha}{2})]^2 - 1}} d\alpha, \tag{29}$$

and this integral can be evaluated for any not too large pairs of i, and j by using numerical integration. Values of Table 1. have been computed on IBM personal computer by using a standard routine for numerical integration of a mathematical subprogram. The results precisely show the mathematical symmetry of $\tilde{F}$ despite of the formal unsymmetry of variables i, and j in the discrete Fourier integral. The values have also been numerically checked by a comparison with the analogue results obtained by a direct algebraic solution of Eqn.22 with zero-value boundary conditions at the lines $abs(i) = C$, $abs(j) = C$, with C = 10, 20, 50, and 100. The first two sets of results gave poor agreements at large values of i and j, the others have shown excellent agreements.

Table 1

j \ i	0	1	2	3	4	5	6	7	8
0	.0000	.2500	.3634	.4303	.4770	.5129	.5421	.5668	.5881
1	.2500	.3183	.3866	.4404	.4822	.5162	.5444	.5684	.5893
2	.3634	.3866	.4244	.4622	.4960	.5253	.5508	.5732	.5930
3	.4303	.4484	.4622	.4880	.5139	.5382	.5604	.5805	.5987
4	.4770	.4822	.4960	.5139	.5355	.5532	.5720	.5896	.6062
5	.5129	.5162	.5253	.5382	.5532	.5689	.5847	.6000	.6146
6	.5421	.5444	.5508	.5604	.5720	.5847	.5978	.6110	.6239
7	.5668	.5684	.5732	.5805	.5896	.6000	.6110	.6223	.6337
8	.5881	.5893	.5930	.5987	.6062	.6146	.6239	.6337	.6436

Eqn.20 is a discrete analogue of the differential equation of a singular harmonic function, the function of a surface of revolution having a logarithmic meridian.

3.2 Discrete harmonic singularity-bearing function (triangular network)

As another example, singularity-bearing solution $F(i,j) = F(0,0;i,j)$ of the difference equation

$$c_M\{E_2[E_1^{+0.5} + E_1^{-0.5}] + E_2^{-1}[E_1^{+0.5} + E_1^{-0.5}] + E_1 + E_1^{-1} - 6\}F(i,j) = p(0,0,i,j) \qquad (30)$$

is shown, where symbols E_1, and E_2 stand for elementary shifting operations in the directions of i, and j, respectively. The points of interpretation of $F(i,j)$ are at the integer values values of i when j is an even number and at the bisecting points when j is odd. These points form a system of nodes of a regular triangular mesh. Eqn.30 multiplied by 2/3 again is a discrete analogue of the differential equation of a singular harmonic function.

Using the assumption shown in Eqn.22 and following the procedure shown in connection of Eqs.22-25, a divergent discrete Fourier integral can be obtained as follows:

$$F = -\int_{\alpha=0}^{\pi} \frac{\left\{\frac{3-\cos\alpha}{2\cos\frac{\alpha}{2}} - \sqrt{\left[\frac{3-\cos\alpha}{2\cos\frac{\alpha}{2}}\right]^2 - 1} - 1\right\}^{abs(j)}}{2\pi\sqrt{7 - 8\cos\alpha + \cos^2\alpha}} \cos(i\alpha)\, d\alpha. \qquad (31)$$

The transformation of F to $\tilde{F}$ used in Eqn.28 again yields a discrete Fourier integral which can be evaluated by numeric integration:

$$\tilde{F} = -\int_{\alpha=0}^{\pi} \frac{\left\{\frac{3-\cos\alpha}{2\cos\frac{\alpha}{2}} - \sqrt{\left[\frac{3-\cos\alpha}{2\cos\frac{\alpha}{2}}\right]^2 - 1} - 1\right\}^{abs(j)} \cos(i\alpha) - 1}{2\pi\sqrt{7 - 8\cos\alpha + \cos^2\alpha}} d\alpha. \qquad (32)$$

Values of Table 2 have been calculated using the same subprogram for evaluating integral (32) as used in the case of Table 1 for integral (29). The results clearly show the hexagonal cyclic symmetry of function $\tilde{F}$.

Table 2

j \ i	0	0.5	1	1.5	2	2.5	3	3.5	4	4.5	5	5.5	6	6.5
0	.0000		.1667		.2381		.2681		.2946		.3151		.3318	
1		.1667		.2180		.2566		.2850		.3071		.3250		.3400
2	.2180		.2307		.2566		.2814		.3025		.3203		.3355	
3		.2566		.2681		.2850		.3025		.3186		.3331		.3460
4	.2814		.2850		.2946		.3071		.3203		.3331		.3451	
5		.3025		.3071		.3151		.3250		.3355		.3460		.3561
6	.3186		.3203		.3250		.3318		.3400		.3486		.3576	
7		.3331		.3355		.3400		.3460		.3530		.3604		.3680

Function $\tilde{F}$ also has a direct physical interpretation. It can be assumed as the function of small deflections of an infinitely large triangular net consists of three sets of uniformly stressed chords and loaded perpendicularly to the plane of the net at the net point $i_0 = j_0 = 0$ by a unit force, provided the origin of the co-ordinate system is fixed at the same net point. This singularity-bearing function is another discrete analogue of the singularity-bearing function of the surface of revolution with logarithmic meridian.

3.3 **Singular solutions for grillages of regular network**

Discrete Fourier integrals can also be used in the analysis of large plane frames with rigid joints.

The difference equation of the rotation of joints of a square grillage of bars with equal bending stiffnesses is

$$M(i,j) = s\,\{[12 + \delta_1^2 + \delta_2^2]\,\phi(i,j)\}, \qquad (33)$$

where M, and ϕ stand for the function of nodal moments and of the rotations, respectively and s is a constant multiplier which represents the resistance against rotation of one consisting bar.

Singularity-bearing solution $\phi(i_0, j_0; i, j)$ of the difference equation

$$[12 + \delta_1^2 + \delta_2^2]\,\phi(i_0, j_0; i, j) = p(i_0, j_0; i, j) \qquad (34)$$

can be interpreted as the function of rotations of the joints caused by a single moment of the size s acting at the joint (i_0, j_0). The discrete Fourier integral of this function can be obtained in the same way as in Sec. 3.1. by assuming it in the form

$$\phi(0,0;i,j) = \frac{1}{\pi} \int_{\alpha=0}^{\pi} A(\alpha)\, z(\alpha)^{abs(j)}\, (-1)^{i+abs(j)}\, \cos(\alpha i)\, d\alpha. \qquad (35)$$

The outlined procedure yields the discrete Fourier integral as follows:

$$\phi(0,0;i,j) = \int_{\alpha=0}^{\pi} \frac{\left[\cos(\alpha) - 4 + \sqrt{\cos^2(\alpha) - 8\cos(\alpha) + 1}\right]^{abs(j)}}{4\pi\sqrt{\cos^2(\alpha) - 8\cos(\alpha) + 15}} \cos(\alpha i)\, d\alpha. \qquad (36)$$

This integral is convergent for any discrete values of i, and j. Values obtained by a numeric integration of Eqn.36 can be easily checked by using a Hardy-Cross relaxation of moments for a sufficiently large frame of square network and of bars with equal bending stiffness.

An analogous solution for the difference equation

$$[12 + E_1 + E_1^{-1} + 2\mu_1(E_2 + E_2^{-1})]\, \phi(i_0, j_0; i, j) = p(i_0, j_0; i, j) \qquad (37)$$

of grillages having regular triangular network yields a discrete Fourier integral as follows:

$$\phi(0,0;i,j) = \int_{\alpha=0}^{\pi} \frac{\left\{\sqrt{\left[\frac{6 + \cos(\alpha)}{2\cos(\alpha/2)}\right]^2 - 1} - \frac{6 + \cos(\alpha)}{2\cos(\alpha/2)}\right\}^{abs(j)}}{3\pi\sqrt{\cos^2(\alpha) - 10\cos(\alpha) + 15}} \cos(\alpha i)\, d\alpha \qquad (38)$$

This integral is also convergent and the values produced at the points of interpretation show the same cyclic symmetry as the values in Table 2.

3.4 Discrete biharmonic singularity-bearing solution (square network)

As the last example, let the discrete Fourier integral of the singularity-bearing solution $F(i,j) = F(0,0;i,j)$ of the difference

equation

$$(\delta_1^2 + \delta_2^2)^2 F = (\delta_1^4 + 2\delta_1^2\delta_2^2 + \delta_2^4) F = p\ (0,0;i,j) \qquad (39)$$

be analyzed.

The discrete Fourier integral of F can be assumed in the form as follows:

$$F = \frac{1}{\pi} \int_{\alpha=0}^{\pi} A(\alpha) \left[1 + \beta(\alpha)\ \mathrm{abs}(j) \right] z(\alpha)^{\mathrm{abs}(j)} \cos(\alpha i)\ d\alpha. \qquad (40)$$

Function $z(\alpha)$ is the same as in the first example,

$$z(\alpha) = 1 + 2\sin^2(\tfrac{\alpha}{2}) - \sqrt{[1 + 2\sin^2(\tfrac{\alpha}{2})]^2 - 1}\ ,$$

functions $\beta(\alpha)$, and $A(\alpha)$ can be determined using the procedure outlined in Section 3.1.

$$\beta(\alpha) = \frac{1 - z(\alpha)^2}{1 - z(\alpha)^2} = \frac{\sqrt{[1 + 2\sin^2(\frac{\alpha}{2})]^2 - 1}}{1 + 2\sin^2(\frac{\alpha}{2})}\ , \qquad (41)$$

and

$$A(\alpha) = \{\ 2(1+2\beta)z^2 - 8[2-\cos\alpha](1+\beta)z + 14 - 8\cos\alpha + 4[1-\cos\alpha]^2\}^{-1}. \qquad (42)$$

Introduction of the above functions into Eqn.40 yields a discrete Fourier integral which is divergent for any (integer) values of i, and j. However, discrete Fourier integrals of its differences having real physical interpretations are convergent. For instance, second partial difference

$$F_1(i,j) = F(i-1,j) - 2F(i,j) + F(i+1,j) =$$

$$= -\frac{2}{\pi} \int_{\alpha=0}^{\pi} A(\alpha) \left[1 + \beta(\alpha)\ \mathrm{abs}(j)\right] z(\alpha)^{\mathrm{abs}(j)} [1 - \cos\alpha] \cos(\alpha i)\ d\alpha$$

is convergent.

In Table 3 values of

$$\tilde{F}_1(i,j) = F_1(i,j) - F_1(0,0)$$

are given. These values have been directly computed by a numerical

integration of the discrete Fourier integral

$$\frac{2}{\pi}\int_{\alpha=0}^{\pi} A(\alpha)\left[1+\beta(\alpha)\,\mathrm{abs}(j)\right] z(\alpha)^{\mathrm{abs}(j)} [1-\cos\alpha][1-\cos(\alpha i)]\,d\alpha.$$

Table 3

j \ i	0	1	2	3	4	5	6	7	8
0	.0000	.1704	.2268	.2577	.2798	.2972	.3115	.3236	.3342
1	.0796	.1592	.2162	.2521	.2768	.2953	.3102	.3227	.3335
2	.1366	.1704	.2122	.2460	.2716	.2914	.3072	.3205	.3318
3	.1725	.1883	.2162	.2440	.2679	.2877	.3040	.3177	.3294
4	.1972	.2056	.2243	.2460	.2668	.2852	.3012	.3149	.3269
5	.2157	.2209	.2339	.2505	.2679	.2845	.2995	.3128	.3247
6	.2307	.2342	.2435	.2564	.2708	.2852	.2988	.3116	.3231
7	.2432	.2457	.2527	.2628	.2747	.2872	.2995	.3113	.3221
8	.2539	.2558	.2613	.2694	.2792	.2899	.3009	.3116	.3218

It can be checked that values of $\tilde{F}_1(i,j)$ meet the difference equation

$$(\delta_1^4 + 2\delta_1^2\delta_2^2 + \delta_2^4)\,\tilde{F}_1 = p\,(-1,0;i,j) - 2\,p\,(0,0;i,j) + p\,(1,0;i,j).$$

4. Conclusions

Examples (like discrete harmonic and biharmonic functions) in Chapter 3 show that discrete Fourier integrals can be used for constructing singularity-bearing analytical solutions of partial linear difference equations. That means, the analogy between analytical solutions of partial linear differential and difference equations can be extended to their singular solutions as well.

This perception may have a great practical importance, because the analogy permits us to apply in the analysis of lattice structures the discrete analogues of efficient methods based on the use of singular solutions of partial differential equations.

REFERENCES

1. Bleich, F.- Melan, E.: Die gewöhnlichen und partiellen Differenzengleichungen der Baustatik. Berlin, Verlag Julius Springer, 1927

2. Frank, Ph.- Mises, R. v.: Die Differential- und Integralgleichungen der Mechanik und Physik. Braunschweig, Dover-Vieweg, 2. Auflage, 1961
3. Korn, G.A.- Korn, T.M.: Mathematical Handbook for Scentists and Engineers. New York, McGraw-Hill, 1968
4. Spiegel, M.R.: Calculus of Finite Differences and Difference Equations. New York etc. McGraw-Hill, 1970
5. Rózsa Pál: Lineáris algebra és alkalmazásai. Budapest, Műszaki Könyvkiadó, 1971
6. Kollár, L.- Hegedűs, I.: Analysis and Design of Space Frames by the Continuum Method. Budapest, Akadémiai Kiadó-Elsevier Science Publishers, 1985

Acta Technica Acad.Sci.Hung., 104(1-3), pp. 95-123 (1991/92)

STRESS CHANGES IN SOIL AFTER PILE PENETRATION

IMRE, E.*

(Received: 15 August 1989)

State of stress in soil after the penetration of a pile well above the tip was described by a joined model consisting of a one-dimensional coupled consolidation part-model, a phenomenological-type relaxation part-model and a self-weight part-model which were connected by the principle of superposition.

The consolidation part-model deviates from its antecedents in the fact that kinematic type (constant radial displacement) boundary condition was applied to the shaft-soil interface instead of the static type one (constant radial total stress) which is used in the existing theories. Relaxation was described at the shaft-soil interface only.

Experiences - which are in contradiction with the results of the existing theories - were explained with the help of the results from the joined model suggested herein.

NOTATIONS

A $\dfrac{1}{m}$

B $\dfrac{2r}{3(r_1^2 - r_o^2)m}$

C $\dfrac{K}{m}$

c_v coefficient of consolidation

D deviatoric stress

D $-\dfrac{K}{m}\ \dfrac{2r}{3(r_1^2 - r_o^2)}$

E $3 - \dfrac{K}{m}$

F $\dfrac{K}{m}\ \dfrac{2r}{3(r_1^2 - r_o^2)}$

*Imre, Emőke, H-1024 Budapest, Káplár u. 4, Hungary

Akadémiai Kiadó, Budapest

f_s local side friction of cone penetrometer

f_{su} local side friction at the end of penetration

G shear modulus of soil

I_P plasticity index

k permeability

K bulk modulus, $2G(1 + \nu)/1 - 2\nu)$

K_0 coefficient at rest

m $2G\ (1-\nu)/(1-2\nu)$

q flux (water volume/area/time)

q_c cone resistance of cone penetrometer

q_{cu} cone resistance at the end of penetration

r radial distance

r_0 radius of pile

r_1 radius of the outer boundary of the domain

t time, elapsed time from the end of penetration

t_0^* parameter for an empirical relaxation model

t^* elapsed time from the beginning of relaxation

T time factor, $c_v t/r_o^2$

u $\Delta u + u_0$, pore water pressure

u_0 $z\gamma_v$

Δu excess pore water pressure

v radial displacement

v_0 boundary condition at r_0

w vertical displacement

z vertical distance

γ_t unit weight of the saturated soil

γ_t $\gamma_t - \gamma_v$

γ_v unit weight of water

ε_{ij} strain tensor

ε volumetric strain

ν Poisson ratio in terms of effective stress

$\sigma_{ij}, \sigma'_{ij}$ total and effective stress tensors

σ, σ' first invariant of the total and effective stresses

SUPERSCRIPTS

c total solution of the consolidation part-model

r relaxation part-model

s steady-state component of the consolidation part-model

t transient component of the consolidation part-model

w self-weight part-model

' effective stress component

- normalized by $\Delta u(o,r_0)$

SUBSCRIPTS

m mean normal

m_0 mean normal prior to penetration

r radial normal

vo vertical normal prior to penetration

z vertical normal

ϕ circumferential normal

1. Introduction

Displacement piles and penetrometers are placed in the ground by driving, jacking or vibration. Their placement causes changes in the total stress state, induces some excess pore water pressure and results in various rheological processes in the soil afterwards, such as consolidation, creep, relaxation and thixotropy (see Appendix 1).

Theoretical models describing penetration effects are applicable for the evaluation of rheological type cone penetrometer tests (see Appendix 1) and for the modelling of the bearing capacity of the displacement piles.

Existing theories can not be verified by the experimental results available. Consolidation theories apply the assumption that the radial total stress is constant at the shaft-soil interface (coupled theories use this assumption as a boundary condition, uncoupled theories consider that the total stress state of the whole displacement domain is constant). However, data measured by the piezo-lateral stress cell in Boston Blue Clay show that the radial total stress decreases by 73% of its initial value after penetration (Baligh et al., 1985; Fig. 1).

This contradiction was resolved by applying kinematic type (constant

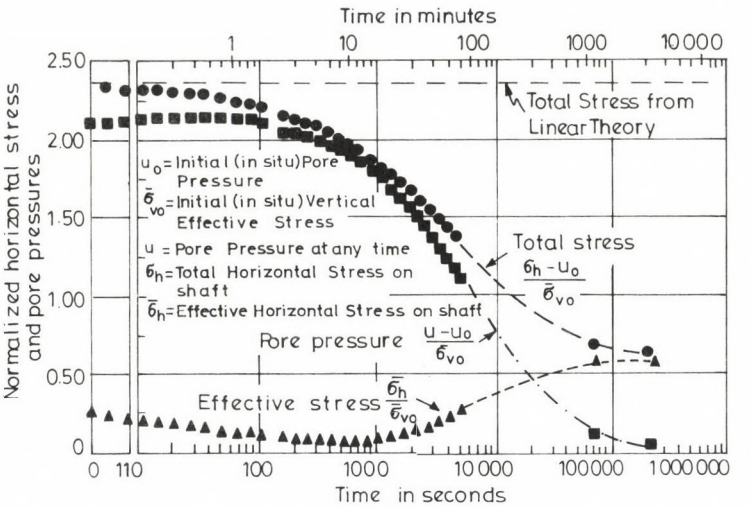

Fig. 1. Stress changes after penetration measured by the piezo-lateral stress cell in Boston Blue Clay (Baligh et al., 1985)

radial displacement) boundary condition at the shaft-soil interface and, furthermore, by modelling the relaxation at the same boundary.

A joined model was elaborated consisting of a self-weight part-model, a one-dimensional coupled consolidation part-model and a phenomenological-type relaxation part-model connected by the principle of superposition.

The objective of this paper is to present the mathematical description of the joined model and, to show the results which well agree with the experiences. The results presented in earlier papers are recapitulated, expanded and discussed (Imre, 1990a, 1990b).

2. The joined model

Assumptions and equations describing the self-weight, consolidation and the relaxation part-models are presented in this section.

2.1 The self-weight part-model

The self-weight part-model comprises the stress and strain states valid prior to penetration which was described by using the following assumptions.

(1) The soil is linearly elastic, isotropic, homogeneous, saturated.

(2) Linear strain state holds in horizontal direction.

(3) The surface of the half-space is unloaded (the excess pore water pressure is zero), the phreatic line is situated on the surface.

The following equations were written for the self-weight stress state (see Appendix 2):

$$\sigma_z^w(z) = \sigma_z'^w(z) + u_0(z) = \gamma_t' z + \gamma_v z , \qquad (1)$$

$$\sigma_r^w(z) = \sigma_r'^w(z) + u_0(z) = \frac{\nu}{1-\nu} \sigma_z'^w(z) + \gamma_v z = K_0 \gamma_t' z + \gamma_v z . \qquad (2)$$

2.2 The consolidation part-model

The consolidation part-model comprises the stress and strain states of the weightless soil after penetration which change during the pore water pressure dissipation.

2.2.1 Assumptions

(4) Soil is saturated.

(5) Water and soil grains are incompressible.

(6) The Darcy's law holds.

(7) Soil is linearly elastic, isotropic, homogeneous and weightless.

(8) The pore water pressure is not influenced by the total stress variation during consolidation.

(9) Plane strain condition is assumed in vertical direction. Stream lines are radial. The stress and strain states possess axial symmetry. The radial, vertical and circumferential directions are the principal ones. The displacements are small.

(10) The radial displacement of the soil at the pile-soil interface is constant.[1]

(11) The radial displacement is negligible at a radial distance of r_1.

(12) The pile material is impermeable (no water flow takes place through this boundary).

(13) The pore water pressure is negligible at a radial distance of r_1.

Assumptions (4)-(9) are generally applied in coupled theories.

---

[1] This assumption is reasonable if the pile displacement has no radial component after penetration originated either from elastic deformation or from rigid body motion. This condition holds if the pile is infinitely rigid and if both the pile shaft and the pile load are vertical.

2.2.2 The mathematical model

The axisymmetrical one-dimensional coupled consolidation can be described by the following system of differential equations (see Appendix 3):

$$m\left(\frac{\partial^2 v}{\partial r^2} + \frac{1}{r}\frac{\partial v}{\partial r} - \frac{1}{r^2}v\right) = \frac{\partial u}{\partial r} \quad ; \tag{3}$$

$$\frac{\partial^2 v}{\partial r \partial t} + \frac{1}{r}\frac{\partial v}{\partial t} - c_v\left(\frac{\partial^3 v}{\partial r^3} + \frac{2}{r}\frac{\partial^2 v}{\partial r^2} - \frac{1}{r^2}\frac{\partial v}{\partial r} + \frac{1}{r^3}v\right) = 0 \ . \tag{4}$$

According to assumptions (10)-(13), the boundary conditions can be written as follows:

$$v(t,r_0) = v_0 \ , \tag{5}$$

$$v(t,r_1) = 0 \ , \tag{6}$$

$$\frac{\partial u(t,r_0)}{\partial r} = m\frac{\partial^2 v(t,r_0)}{\partial r^2} + \frac{1}{r_0}\frac{\partial v(t,r_0)}{\partial r} - \frac{1}{r_0^2}v(t,r_0) = 0 \ , \tag{7}$$

$$u(t,r_1) = 0 \ . \tag{8}$$

2.2.3 Solution of the consolidation part-model

Solution of the coupled consolidation part-model consists of a steady-state part and a transient part. In terms of stress tensors:

$$\sigma_{ij}^{c}(t,r) = \sigma_{ij}^{s}(r) + \sigma_{ij}^{t}(t,r) \ , \tag{9a}$$

$$\sigma'^{c}_{ij}(t,r) = \sigma^{s}_{ij}(r) + \sigma'^{t}_{ij}(t,r) \ . \tag{9b}$$

The steady-state part of the consolidation part-model is the total solution of the homogeneous part of Eq. (3) with non-homogeneous boundary conditions (5), and boundary condition (6). Its solutions in terms of the total and effective stresses are equal, since excess pore water pressure $u^s(t,r)$ is zero. The analytical solution for infinite domain ($r_1 = \infty$) is the following (Baguelin et al., 1978):

$$\sigma_r^s(r) = \sigma'^{s}_{r}(r) = 2G\frac{v_0 r_0}{r^2} \quad ; \quad \sigma_\phi^s(r) = \sigma_\phi'^{s}(r) = -2G\frac{v_0 r_0}{r^2} \ . \tag{10a,b}$$

If function $u(t,r)$ is assumed to be known, the transient part of the consolidation part-model can be considered as the set of particular solutions of non-homogeneous Eq. (3) with the homogeneous forms of (5), and (6)–(7) (each solution is associated with a possible time value). Function $u(t,r)$ being unknown, these particular solutions can be determined by solving Eq. (4) with the homogeneous forms of (5), and (6)-(7). Then first order differential Eq. (3) for unknown function $u(t,r)$ can be solved by integration using (6) and (8).

Equation (4) was solved by the use of a finite difference implicite scheme with the homogeneous forms of (5), and (6)-(7).[2]

The total stress and strain variables are not prescribed at the outer boundary. The first invariant of total stress tensor ($\overline{\sigma}^t$) was found positive, the first invariant of strain tensor ($\overline{\varepsilon}^t$) was found negative at $r_1 (r_1 < \infty, t < \infty)$, with the use of some explicite expressions given in Appendix 3.

Assuming that $u(\infty,r) = 0$ holds, it can be stated that the solution of the transient part is zero for every stress and strain component with infinite time. This follows from the fact, that the non-homogeneous Eq. (3) is reduced to its homogeneous part, and its solution with homogeneous boundary conditions (5) and (6) is identically equal to zero.

2.3 The relaxation part-model

According to the definition given in Appendix 1, relaxation takes place on the boundary if kinematic type boundary condition is prescribed.

Let us consider the displacement domain of the joined model, which comprises a hollow soil cylinder with inner radius r_0 and outer radius r_1 cut by two horizontal planes situated at some arbitrary depths z_1, z_2 along the length of the pile. Both the consolidation and self-weight part-models yields kinematic condition for the cylindrical boundaries. At the horizontal boundaries, the consolidation part-model entails kinematic condition, the self-weight part-model static condition. Because of this difference, relaxation was taken into account at the shaft-soil interface only.[3]

---

[2] Analytical solution to infinite domain ($r_1 = \infty$) was given. However, no proper complementary condition was found (due to the infinite nature of the domain), and initial condition could not be taken into account.

[3] If the relaxation part-model is extended into the inside of the body, the extended stress field is statically admissible in the case of weightless soil only (Imre, 1991).

Not too many experiences are available regarding the measurement of relaxation around piles. Due to this fact, the relaxation part-model was constructed on the basis of laboratory test results. The 'immediate relaxation'[4] and the case of 'partial unloading' were disregarded, and the phenomenological equation of the 'time-dependent relaxation' was used in a modified form (see Appendix 1).

On the basis of the considerations mentioned above the following assumption was made.

(14) Relaxation at the shaft-soil interface can be written in terms of radial total stress decrease as follows:

$$\Delta\sigma_r^r(t^*,r_0) = s\ \sigma_r(t_0^*,r_0)\ \log(t^*/t_0^*)\ ,\quad t^* \geq t_0^* \tag{11}$$

Equation (11) is valid for a time period of a few weeks.

2.4 Assumptions made to join the part-models

(15) Consolidation begins at the end of the penetration process, and the previous stress history can be neglected. The relationship between the initial time of consolidation and relaxation:

$$t^* = t + t_0^* \ . \tag{12}$$

(16) The consolidation, self-weight and relaxation part-models can simply be superimposed.

For radial stresses on the shaft:

$$\sigma_r(t,r_0,z) = \sigma_r^t(t,r_0) + \sigma_r^s(r_0) - \Delta\sigma_r^r(t + t_0^*,r_0) + \sigma_r^w(z) \ . \tag{13}$$

For any other case:

$$\sigma_{ij}(t,r,z) = \sigma_{ij}^s(r) + \sigma_{ij}^t(t,r) + \sigma_{ij}^w(z)\ , \tag{14}$$

$$\sigma'_{ij}(t,r,z) = \sigma_{ij}^s(r) + \sigma'^t_{ij}(t,r) + \sigma'^w_{ij}(z)\ , \tag{15}$$

$$\varepsilon_{ij}(t,r,z) = \varepsilon_{ij}^s(r) + \varepsilon_{ij}^t(t,r) + \varepsilon_{ij}^w(z)\ , \tag{16}$$

---

*No describing model is available for the immediate relaxation.

3. Initial condition and final state

The initial condition for every stress and strain component can be expressed by Eqs (14)-(16) if variable t is set to zero (since according to Eq. (11), value of the term $\Delta\sigma_r^r(t+t_0^*,r_0)$ is zero at t=0).

As the final value of the transient component is zero, the final state was written as follows by using Eqs (14)-(16):

$$\sigma_{ij}(\infty,r,z) = \sigma_{ij}^{S}(r) + \sigma_{ij}^{W}(z) , \tag{17}$$

$$\sigma'_{ij}(\infty,r,z) = \sigma_{ij}^{S}(r) + \sigma'^{W}_{ij}(z) , \tag{18}$$

$$\varepsilon_{ij}(\infty,r,z) = \varepsilon_{ij}^{S}(r) + \sigma_{ij}^{W}(z) . \tag{19}$$

No precise solution to the whole initial condition is available.[5] A set of initial conditions was constructed by using the following quantities in the function of K_0 (see Appendix 4): (i) the initial radial effective stress measured by the piezo-lateral stress cell at the shaft-soil interface (Baligh et al., 1985; Fig. 1); (ii) the initial transient stress and strain states calculated with the use of excess pore water pressure results obtained by the strain path method (Baligh, 1986, p. 494; Fig. 4).

The calculated initial and final stress states are shown in Fig. 2 as a function of K_0. According to the results, in the case of K_0=1, the initial radial and circumferential stresses were about equal and the first principal stress was vertical at the shaft-soil interface in accordance with the strain path prediction (Baligh, 1986). In the case of $K_0 \leq 0.9$, the initial circumferential stress was negative in the vicinity of the pile. This result indicates that if small variation in the initial condition is made, the joined model may result in hydraulic fracturing around the pile. This result supports the hypothesis that hydraulic fracturing can be caused by penetration in soft clay (Massarch and Broms, 1977).

---

[5] Solutions of penetration theories (cavity expansion theories (Baguelin et al., 1978), strain path method (Baligh, 1985)) may serve as initial condition. According to some comparative studies, penetration is advisable to be simulated by the strain path method (Baligh, 1986). However, published results of the strain path method have some limitations: (i) they concern the pore water pressure distribution for small permeability soils (i.e. undrained penetration) only, (ii) no information on the initial total stress is available.

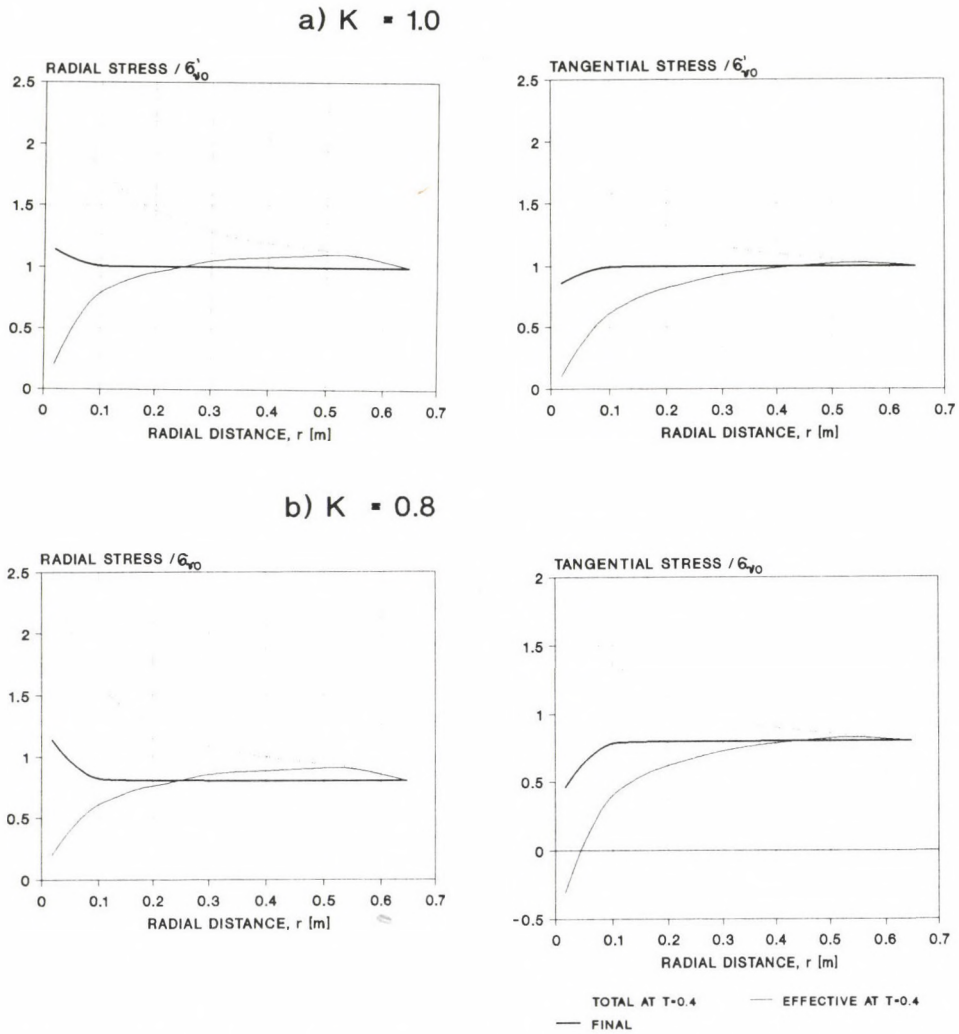

Fig. 2. Initial (T=0.4) and final (T=∞) state for the coupled consolidation part-model in the case of two different values of K_0

4. Results

The results of the joined model are compared to the results of the consolidation theories available. The axisymmetrical, one-dimensional, uncoupled theory represents the solution of every known theory, if consolidation is considered well above the tip.[6]

Spatial distribution of the pore water pressure and the volumetric strain increment:

Time variation of the pore water pressure showed steadily decreasing tendency at every point (Fig. 3). Solution of the uncoupled theory can be characterized by a monotonous decrease in the vicinity of the pile, and a temporary increase at a greater distance (Fig. 4).

The transient volumetric strain showed compression in the vicinity of the shaft, and swelling at greater distances during dissipation in a way that the volume of the domain remained constant (Fig. 5).

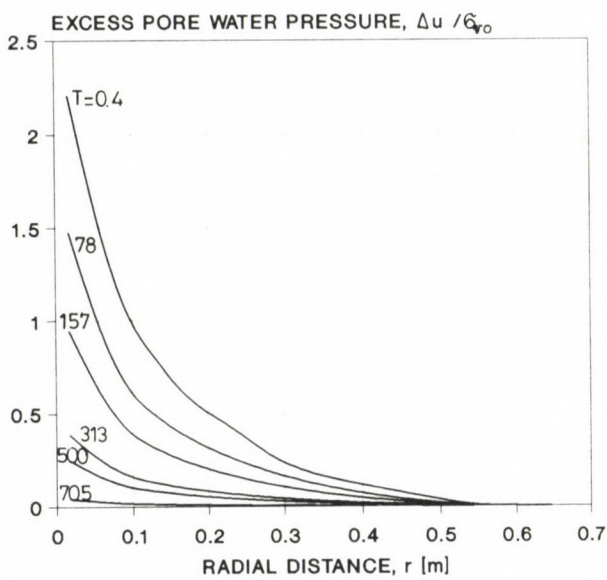

Fig. 3. Pore water pressure function determined with the coupled consolidation part-model

[6](i) one-dimensional, axisymmetrical coupled theory is reduced to the uncoupled case if constant radial total stress boundary condition at the shaft-soil interface is applied (Sills, 1975); (ii) solutions of the one- and two-dimensional uncoupled theories do not differe significantly (Levadoux - Baligh, 1986).

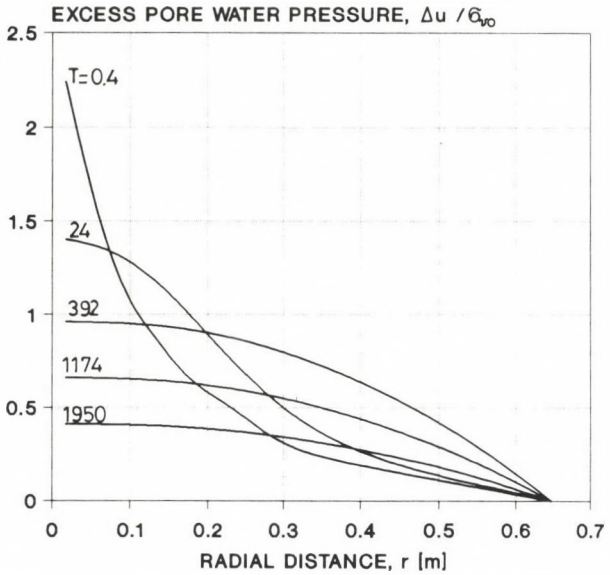

Fig. 4. Pore water pressure function determined with uncoupled theory of Soderberg (1962) under the same initial condition as in the case of Fig. 3

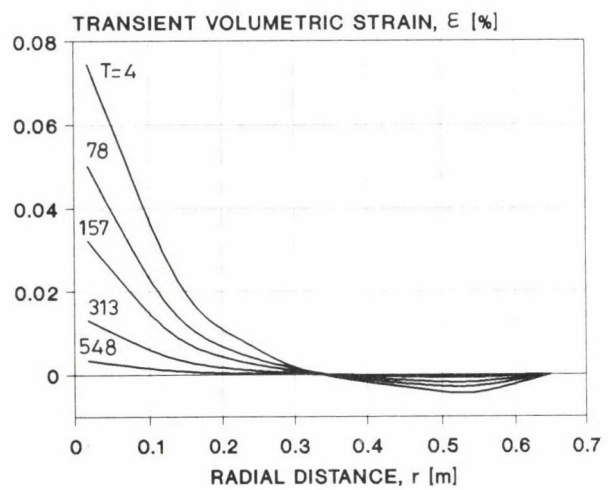

Fig. 5. Transient volumetric strain function determined with the coupled consolidation part-model

Solution of the uncoupled theory can be characterized by temporary swelling at greater distances, and by compression otherwise. (This follows from the pore water pressure solution since the total stress state is constant.)

Radial stresses at the shaft-soil interface for small permeability soils:

Time variation of the radial normal stress functions at the shaft-soil interface was determined by the joined model in a special case. Initial condition was determined according to Section 3. The radius of the standard CPT was substituted for r_0. The coefficient of relaxation (s) was 0.06 and the coefficient of consolidation (c_v) was 5.1 . 10^{-6} m^2/s (in this case, the time factor was equal to the elapsed time in minutes). Results are shown in Figs 6, 7 and 8.

The dissipation curve showed a lower rate of stress decrease in the initial period, and showed a higher rate afterwards resulting in lower dissipation time t_{90} than the solution of the uncoupled theory by about one order (Fig. 6).

The joined model resulted in a radial total stress decrease of 73% in terms of its initial value until the end of the dissipation; 20% was originated from relaxation, 53% was originated from consolidation.

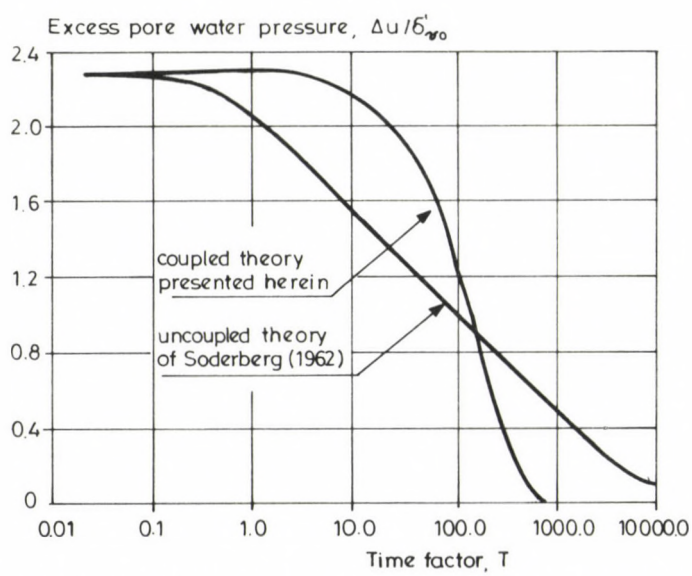

Fig. 6. Dissipation curve determined with the coupled consolidation part-model and theory of Soderberg (1962) (from Imre, 1989)

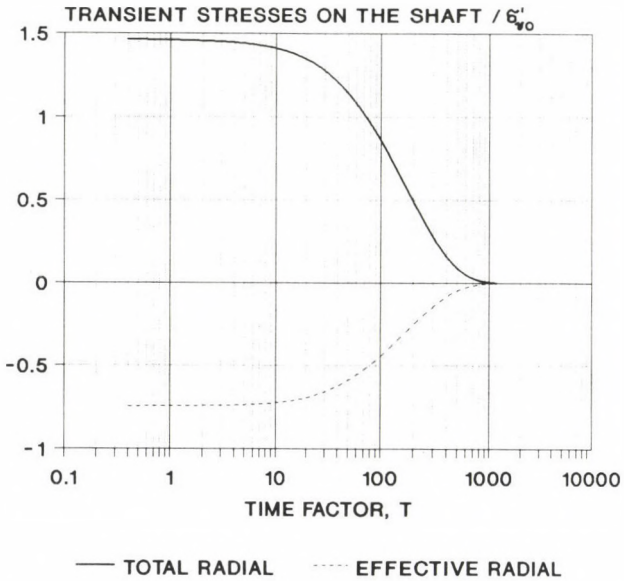

Fig. 7. The transient component of the radial stresses valid for the pile-soil interface determined by the coupled consolidation part-model

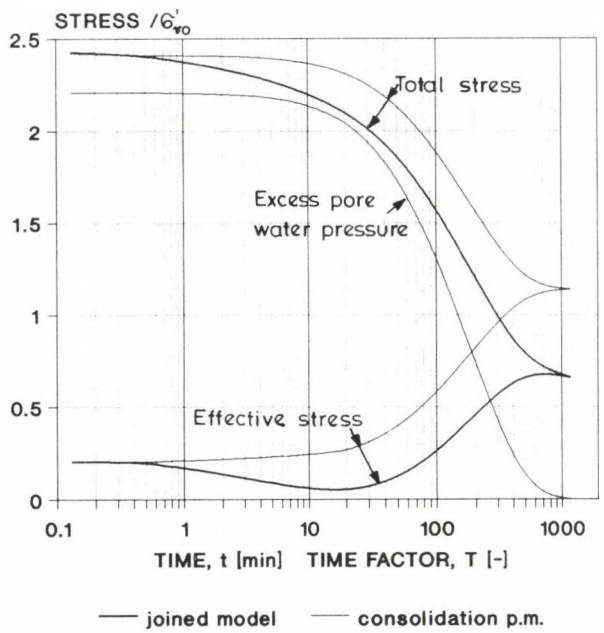

Fig. 8. Radial stresses acting on the pile-soil interface determined by the joined model

Time variation of the radial effective stress at the shaft-soil interface showed a decreasing tendency in the initial period of dissipation, while an increasing tendency up to the moment when the pore water pressure became negligible, and a monotonous decrease afterwards. In increase of 39%[7] was caused by consolidation and a decrease of 20% was caused by relaxation until the end of dissipation (Figs 7, 8).

Radial stresses at the shaft-soil interface for various soils:

Time variation of the radial total and effective stresses acting on the shaft-soil interface was calculated by the use of the joined model for various soils. In the lack of proper data, initial condition shown in Section 3 was applied in every case. It was assumed that the constant initial condition did not impose a qualitative effect on the solution of the joined model.[8] The radius of the standard CPT was substituted for r_0.

There are some stochastic relationships between soil type and permeability (which determine the order of the coefficient of consolidation) and, between plasticity index and coefficient of relaxation (Figs 9, 10). On the basis of these relationships, ranges (10^{-1}-10^{-10} m^2/s); (0.0-10^{-1}) were used in the frame work of a parametric analysis for the coefficient of consolidation and coefficient of relaxation, respectively.

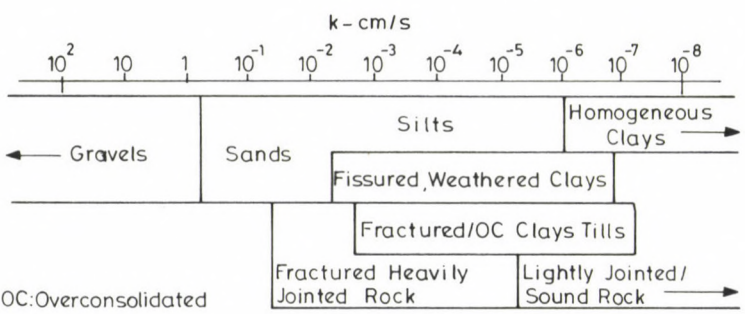

Fig. 9. Approximate range of permeability (k) in soil and rock (from Milligan, 1975)

---

[7] The initial value of the radial effective stress was about 8% only, its initial transient component was of -39% and its time-independent part was of 47% in terms of the initial radial total stress at the shaft-soil interface.

[8] Any change in the initial condition can be roughly simulated by changing the normalization unit for the pore water pressure ($u(0,r_0)$) and the time-independent part (sum of the steady-state and the self-weight parts) of the solution. As a result, the solutions (and also their first time derivatives) to both the consolidation and the relaxation part-models change linearly (see App. 3, Eq. (11)), consequently the time variation tendencies of the solution of the joined model may not change.

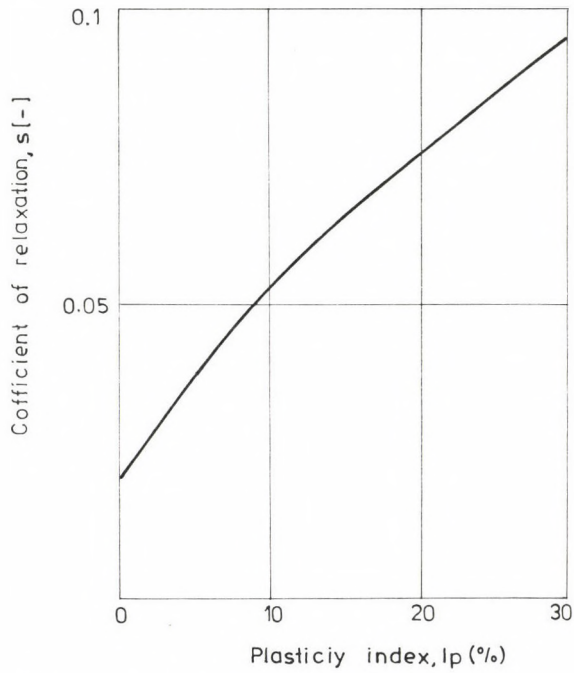

Fig. 10. Empirical relationship of Lacerda (1972) between the coefficient of relaxations and plasticity index I_p

According to the results, the radial total stress showed monotonic decreasing tendency for every value of the time irrespective of the value of the coefficients of consolidation and relaxation (Fig. 11), since both part-models resulted in a decreasing tendency.

Regarding the radial effective stress, the above-mentioned behaviour concerning a small permeability soil (Fig. 8) could be observed in the case of 10^{-10} $m^2/s < c_v < 10^{-5}$ m^2/s only. In the range of 10^{-4} $m^2/s < c_v < 10^{-1}$ m^2/s, the effective stress increased up to the moment when the pore water pressure became negligible, then it decreased (Fig. 12). These results can be attributed to the fact that the consolidation part-model resulted in an increase, while the relaxation part-model resulted in a decrease (Fig. 7, Eq. (13)). In addition, the time derivative of the consolidation part-model solution varied within a considerably greater range than that of the relaxation part-model, and may have vanished in a relatively short time period.

By comparison, it should be noted that the consolidation theories available assume a constant total stress state, and result in a radial

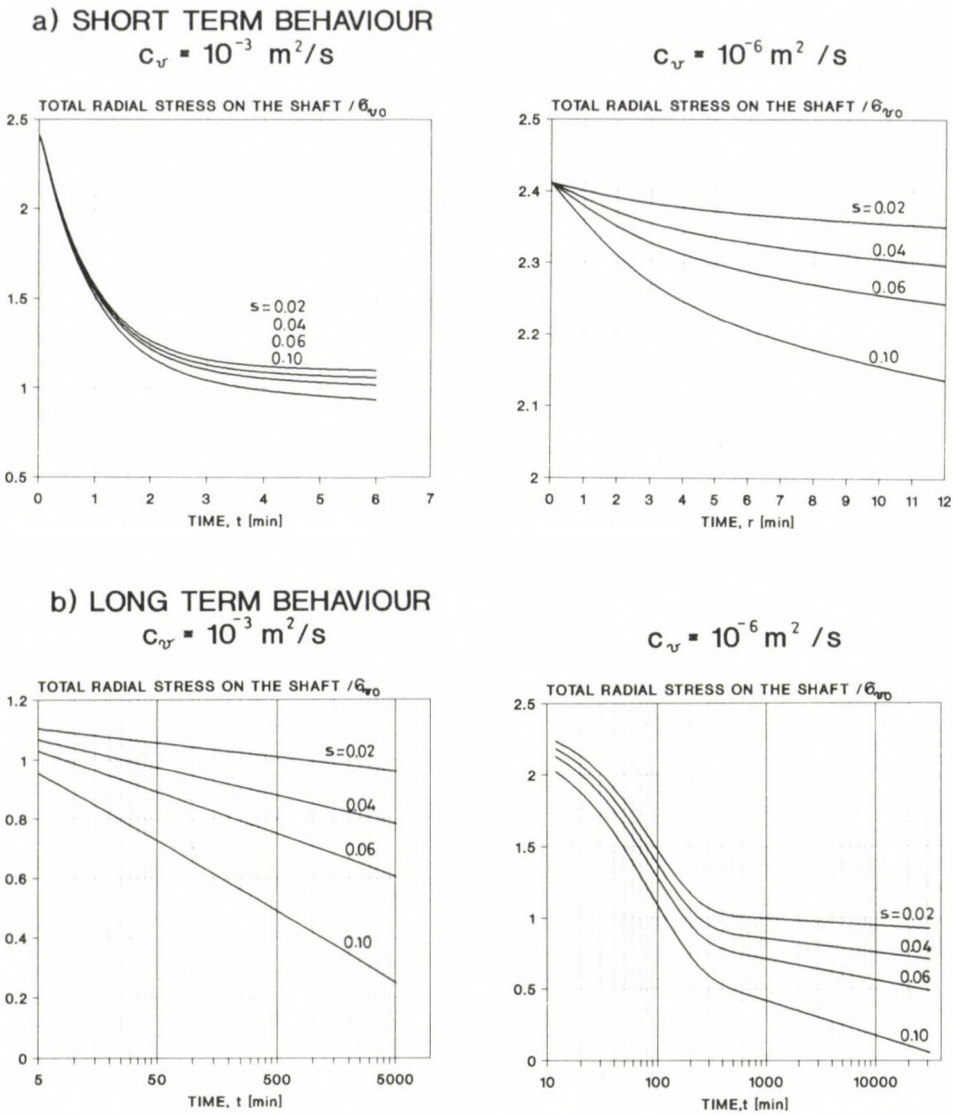

Fig. 11. Total radial stress on the shaft: results of a parametric analysis

effective stress at the same place with monotonous increasing tendency irrespective of the soil type.

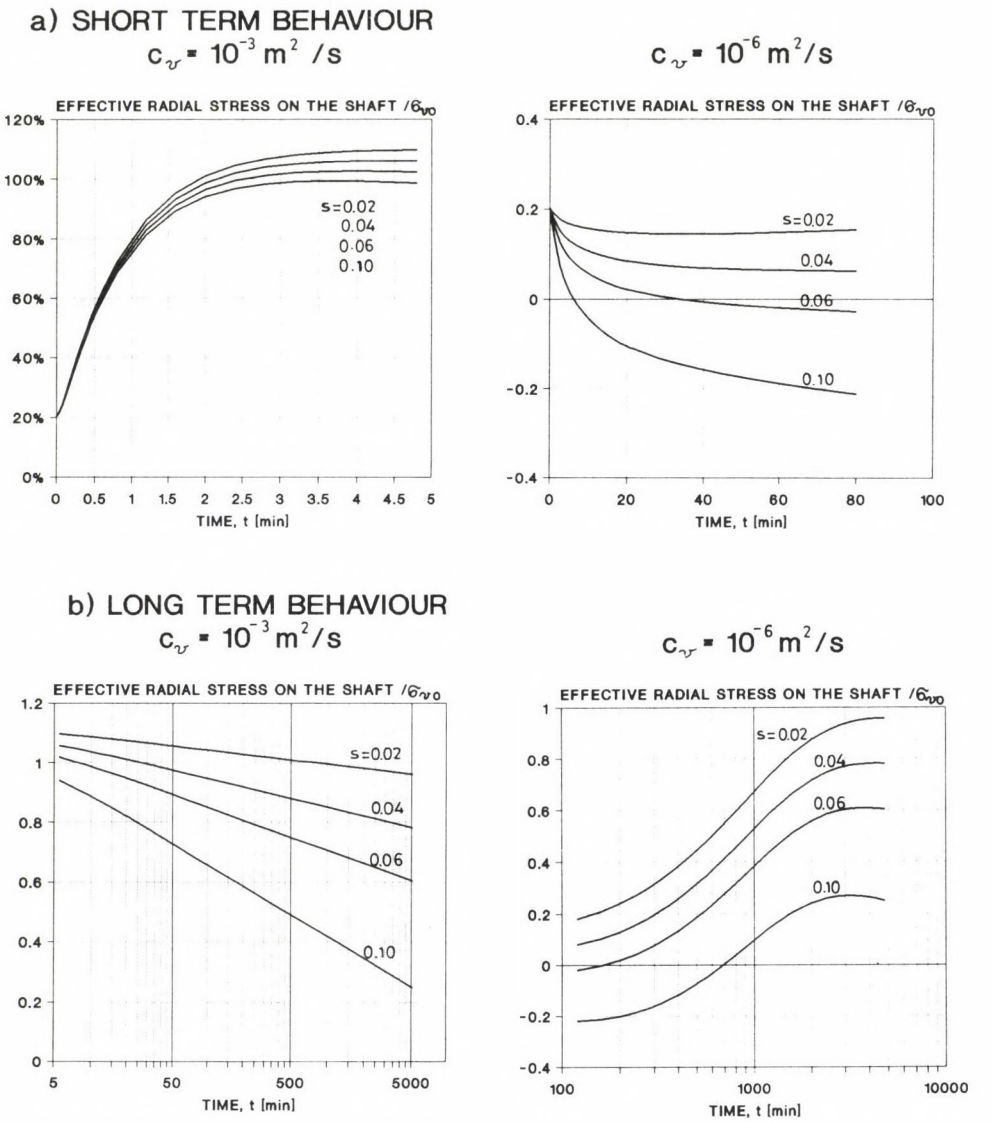

Fig. 12. Effective radial stress on the shaft: results of a parametric analysis

5. Discussion

(1) The steady-state part of the coupled consolidation part-model is identical to the linear elastic cylindrical cavity expansion problem, thus it can be interpreted as the stress and strain states arisen from a drained cavity expansion. Since this part of the solution is time-independent, it arises exclusively from penetration. It follows, that only the transient part of the consolidation part-model is influenced by the consolidation process. Since this part is identically equal to zero at infinite time, it can be stated that consolidation has no effect on the final stress and strain states.

(2) In case of soft clays with small permeability, very little volumetric change takes place during penetration. If a rough estimation is applied that the steady-state part is negligible in Eq (17)-(19),[9] the stress and strain states at the time when the pore water pressure vanishes are about equal to the ones before penetration:

$$\sigma_{ij}(\infty,r,z) \cong \sigma^{w}_{ij}(z) \tag{20}$$

$$\sigma'_{ij}(\infty,r,z) \cong \sigma^{w}_{ij}(z) \tag{21}$$

$$\varepsilon_{ij}(\infty,r,z) \cong \varepsilon^{w}_{ij}(z) \tag{22}$$

It follows that in case of soft clays, the skin friction can not be increased considerably by the application of displacement piles, since the compactness of the soil practically can not be changed either by penetration or by the subsequent consolidation.

(3) The consolidation part-model prescribes constant displacement in the surface normal direction across the whole boundary of the displacement domain. It follows that its volume is constant during consolidation. By comparison, it can be mentioned that the existing theories result in a volumetric decrease of the displacement domain. This follows from the fact that in the case of the uncoupled theory, the final effective stresses are higher than in case of the consolidation part-model presented herein by

---

[9] In the case of the solution presented in Section 4.2, the time-independent part was of 47%, its steady state part was of 5.7-18.2% (increasing with a decreasing value of K_0), the relaxation part was of 20%. Every percentage was ment in terms of the initial radial total stress at the shaft-soil interface.

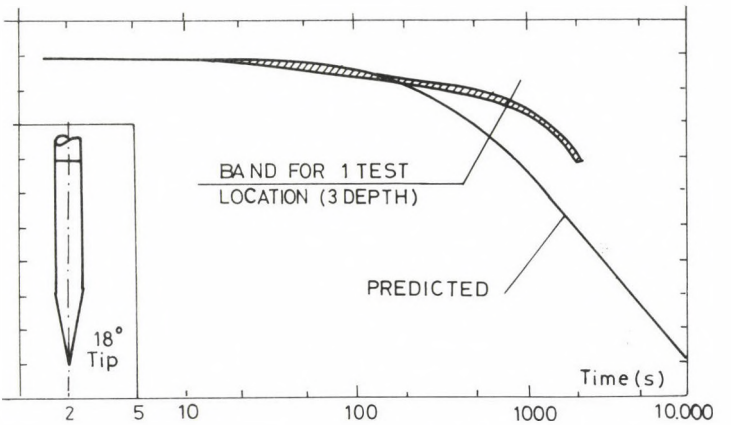

Fig. 13. Evaluation of linear 2D uncoupled predictions in Boston Blue Clay (from Baligh and Levadoux, 1986)

the value of the initial transient total stress ($\sigma^{t}_{ij}(0,r)$) at every point since the total stress state is assumed to be constant.

(4) Solutions to the joined model presented in Figs 6, 8 can be compared with dissipation test records (Fig. 13, Baligh and Levadoux, 1986) and with the results of the piezo-lateral stress cell measurement (Baligh et al., 1985; Fig. 1).[10] The calculated and the measured curves show a very similar character.

In situ undrained strength measurements around piles driven into soft clay (Roy-Lemieux, 1986) imply that the effective stress state in the vicinity of the pile at the end of the pore water pressure dissipation is about equal to the one valid prior to penetration. This result agrees with the corrollary of the joined model mentioned in Section 5(2) (and with the piezo-lateral stress cell measurement made in Boston Blue Clay (Fig. 1)).

Resuls of the rheological test made by Sz832 type CPT[11] imply that the radial effective stress at the shaft-soil interface increases in sand,

---

[10] The pore water pressure at the shaft-soil interface resulted from the strain path method and measured by the piezo-lateral stress cell are about equal, consequently not only the initial radial effective, but also the total stress was equal for the calculation and measurement. The coefficient of consolidation (c_v) applied for the calculation ($5.1 \cdot 10^{-6}$ m^2/s) is close to the range valid for the Boston Blue Clay (($2\text{-}4 \cdot 10^{-6}$ m^2/s) Baligh and Levadoux, 1986). In the lack of data zero for the pore water pressure prior penetration, and 0.06 for the coefficient of relaxation (s) were assumed probably slightly underpredicting the solution to the relaxation part-model.

[11] The considerable decrease in the total stress predicted by the joined model is in agreement with the total stress decrease experienced during the rheological test of the

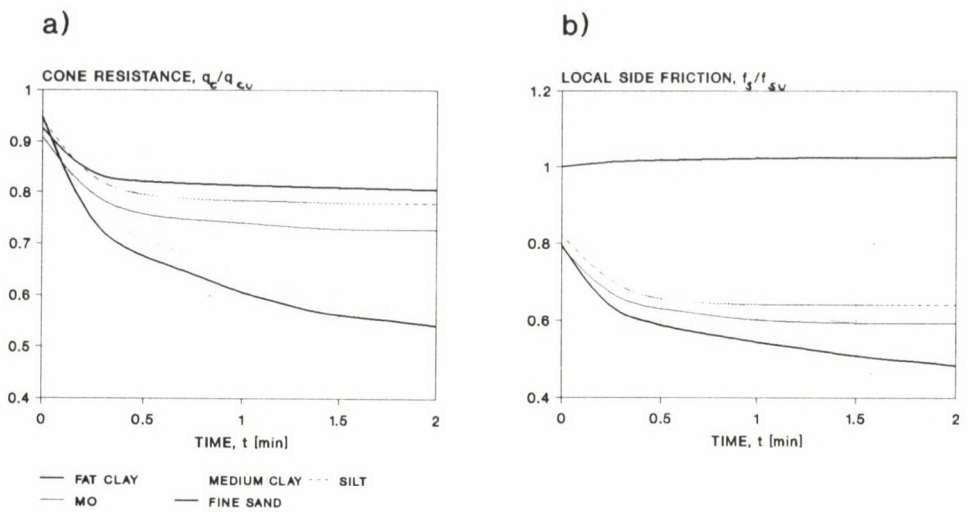

Fig. 14. Typical rheological type CPT test results for various soils from Szeged and Debrecen a) The time variation of cone resistance; b) The time variation of local side friction

decreases in clay during the first minutes after the end of penetration (Fig. 14). Difference between driving resistances measured at the end of the first driving and at the beginning of the re-driving (Yang, 1956) imply that the radial effective stress at the shaft-soil interface decreases in sand and increases in clay between a period of some minutes and some days. These results agree with the time variation tendencies of the radial effective stress determined by the joined model (Fig. 12).

6. Conclusions

The joined model is supported by the observations verifying the application of the kinematic type boundary condition at the shaft-soil interface.

It can be concluded that (i) theories assuming constant radial total stress for the shaft-soil interface can be applied to the consolidation modelling in the soil around expanding deep foundations where the radial total stress is actually controlled as constant; (ii) it is very probable,

---

Sz832 CPT (Fig. 11a, Fig. 14a) (it is reasonable to be assumed that the results of the one-dimensional and two-dimensional versions of the joined model are qualitatively similar to each other).

that the joined model can be used to describe the rheological processes in the soil which take place around rigid piles (and cone penetrometers) with vertical wall and axial load well above the tip after penetration; (iii) the joined model may contribute both to the solution of bearing capacity problems and to the evaluation of rheological type CPT tests.

ACKNOWLEDGEMENT

The author wishes to thank dr. Pál Rózsa for giving valuable pieces of advice on the analytical solutions to the coupled consolidation part-model.

Author is also grateful to dr. László Rétháti and dr. Péter Scharle for their precious information on the research sponsored by the Hungarian Research Fund.

Appendix 1: Definitions

Consolidation is a time-dependent seepage process which takes place unless the distribution of the total hydraulic head is identically equal to the solution of the Laplace equation with the given hydrodynamic boundary conditions.

Consolidation is treated as an uncoupled or a coupled problem. Uncoupled theories (Terzaghi, 1948) are based on continuity condition, describing pore water pressure variation assuming constant total stress state. Coupled theories - which couple stresses and displacements - (Biot, 1941) fulfil continuity, equilibrium and compatibility conditions. Not too many attempts are known verifying coupled theories (Cryer, 1963).

Burgers and Scott-Blair (1948) define thixotropy as a "process of softening caused by remolding, followed by a time-dependent return to the original harder state". The process is completely reversible.

Creep and relaxation are observed in the boundaries of a soil body as follows: if one state parameter (i.e. either the total stress or the displacement) is kept constant in a part of the boundary, then its dual counterpart will vary with time.

Immediate relaxation is experienced after fast monotonic increasing (partly) drained loading. It comprises a fast total stress decrease which terminates within a definite (relatively short) time period depending on the loading rate (Whitman, 1957; Konder-Stallknecht, 1961; Imre et al., 1989; Imre, 1990c).

Time dependent relaxation is experienced after monotonic increasing loading. Its phenomenological equation determined on the basis of triaxial relaxation tests results is as follows (Lacerda, 1972):

$$D(t)/D(t_0) = 1 - s \log(t^*/t_0^*) \quad t^* \geq t_0^* \tag{1}$$

The phenomenological equation of the time-dependent relaxation is changed if partial unloading occurs before the relaxation test (Lacerda, 1977).

Rheological CPT tests are performed after stopping the continuous penetration. The measured quantities are: (i) dissipation test - pore water pressure (Jamiolkowski et al., 1985); (ii) test made with the piezo-lateral stress cell - radial total stress and pore water pressure (Baligh et al., 1985); (iii) test made with the Sz832 penetrometer - local side friction and cone resistance (Imre et al., 1989). The dissipation test is performed to assess the in situ permeability/or coefficient of consolidation of soils. The two other tests are used for research purposes only in the lack of a proper evaluation theory.

Appendix 2: The self-weight part-model

The following equation can be written for a soil element characterized by assumptions (1), (2), (3):

Equilibrium equation:

$$\frac{\partial \sigma_z}{\partial z} + \gamma_t = 0 \, . \tag{1}$$

Geometrical equation:

$$\varepsilon_z = \frac{\partial w}{\partial z} \tag{2}$$

Effective stress equality:

$$\sigma_z = \sigma'_z + u \tag{3}$$

Constitutive equations:

$$\sigma'_r = - 2G \frac{\nu}{1-2\nu} \frac{\partial w}{\partial z} \tag{4a}$$

$$\sigma'_z = - 2G \frac{1-\nu}{1-2\nu} \frac{\partial w}{\partial z} \tag{4b}$$

Compiling Eqs (1)-(4), and taking into account that $\partial u / \partial z = \gamma'_t$:

$$2G \frac{1-\nu}{1-2\nu} \frac{\partial w^2}{\partial z^2} = \gamma_t - \frac{\partial u}{\partial z} = \gamma'_t . \tag{5}$$

The boundary conditions can be written as follows:

$$\sigma'_z(0) = - 2G \frac{1-\nu}{1-2\nu} \frac{\partial w(0)}{\partial z} = 0 , \tag{6}$$

$$w(z_d) = 0 . \tag{7}$$

Solution to differential equation (5) with (6), (7):

$$w(z) = 2G \frac{1-\nu}{1-2\nu} \frac{\gamma'_t}{2} (z^2 - z_d^2) . \tag{8}$$

Appendix 3: The coupled consolidation part-model

System of equations

The following equations can be written for a soil element assuming that assumptions (4)-(9) hold.

Equilibrium equation:

$$\frac{\partial \sigma_r}{\partial r} + \frac{\sigma_r - \sigma_\phi}{r} = 0 \tag{1}$$

Continuity equation:

$$\frac{\partial q}{\partial r} + \frac{\partial \varepsilon_r}{\partial t} + \frac{\partial \varepsilon_\phi}{\partial t} = 0 \tag{2}$$

Geometrical equations:

$$\varepsilon_r = \frac{\partial v}{\partial r} \tag{3a}$$

$$\varepsilon_\phi = \frac{v}{r} \tag{3b}$$

$$\varepsilon = \frac{\partial v}{\partial r} + \frac{v}{r} \tag{3c}$$

Generalized Darcy's law:

$$\frac{\partial q}{\partial r} = -\frac{k}{\gamma_v}\left(\frac{\partial u}{r\,\partial r} + \frac{\partial^2 u}{\partial r^2}\right), \tag{4}$$

Effective stress equality:

$$\sigma_r = \sigma_r' + u,\ \sigma_\phi = \sigma_\phi' + u,\ \sigma_z = \sigma_z' + u \tag{5}$$

Constitutive equations:[12]

$$\sigma_r' = -2G\left[\frac{\partial v}{\partial r}\left(1 + \frac{\nu}{1-2\nu}\right) + \frac{v}{r}\frac{\nu}{1-2\nu}\right] \tag{6a}$$

$$\sigma_\phi' = -2G\left[\frac{v}{r}\left(1 + \frac{\nu}{1-2\nu}\right) + \frac{\partial v}{\partial r}\frac{\nu}{1-2\nu}\right] \tag{6b}$$

$$\sigma_z' = -2G\nu\left[\frac{\partial v}{\partial r}\left(1 + \frac{2\nu}{1-2\nu}\right) + \frac{v}{r}\left(1 + \frac{2\nu}{1-2\nu}\right)\right] \tag{6c}$$

$$\sigma' = -K\varepsilon \tag{6d}$$

Equation (1) can be written in the following form using Eqs (5) and (6):

$$m\left(\frac{\partial^2 v}{\partial r^2} + \frac{1}{r}\frac{\partial v}{\partial r} - \frac{1}{r^2}v\right) = \frac{\partial u}{\partial r}\ . \tag{7}$$

---

[12] Compression stress is taken as positive.

Equation (2) combined with Eqs (3) and (4):

$$-\frac{k}{\gamma_v}\left[\frac{1}{r}\frac{\partial u}{\partial r}+\frac{\partial^2 u}{\partial r^2}\right]+\frac{\partial^2 v}{\partial r\,\partial t}+\frac{1}{r}\frac{\partial v}{\partial t}=0 \qquad (8)$$

Compiling Eqs (7) and (8):

$$\frac{\partial^2 v}{\partial r\partial t}+\frac{1}{r}\frac{\partial v}{\partial t}-c_v\left(\frac{\partial^3 v}{\partial r^3}+\frac{2}{r}\frac{\partial^2 v}{\partial r^2}-\frac{1}{r^2}\frac{\partial v}{\partial r}+\frac{1}{r^3}v\right)=0 \qquad (9)$$

Effect of the initial condition

Being Eqs (7) and (9) linear, various initial conditions for the pore water pressure with the same normalized distribution result in the same normalized solution for the pore water pressure and the radial displacement. This statement holds for every component of the transient stress and strain tensors since according to Eqs (3), (5), (6), (7) they are the sum of terms which are proportional to either $\bar{v}^t(t,r)$ or $\partial/\partial r\ \bar{v}^t(t,r)$ and derivation is a linear operator.

Expressions for the stress and strain tensor invariants

The following expressions can be written using Eqs (3), (5), (6), (7) and the boundary conditions:

$$\partial/\partial r\left[r\bar{v}^t(t,r)\right]=r\bar{\varepsilon}^t(t,r)=A\,r\bar{u}(t,r)-B\int_{r_0}^{r_i}3r\bar{u}(t,r)\,dr\,, \qquad (10)$$

$$r\bar{\sigma}'^t(t,r)=-\left[C\,r\bar{u}(t,r)-D\int_{r_0}^{r_1}3r\bar{u}(t,r)\,dr\right], \qquad (11)$$

$$r\bar{\sigma}^t(t,r)=E\,r\bar{u}(t,r)+F\int_{r_0}^{r_1}3r\bar{u}(t,r)\,dr\,. \qquad (12)$$

Appendix 4: The calculation of the initial condition

(a) Transient part

The transient part of the initial condition, normalized by σ'_{mo} was calculated on the basis of the excess pore water pressure results of the strain path method (Baligh, 1986, p. 494, Fig. 4) associated with an arbitrary depth along the shaft.

(b) Steady-state part

The steady-state part of the initial condition, normalized by σ'_{vo} was determined as follows. The normalized initial condition for the radial effective stress at the shaft-soil interface:

$$\frac{\sigma'_r(0,r_0,z)}{\sigma'_{vo}(z)} = \frac{1+2K_0}{3}\frac{\sigma'^{t}_r(0,r_0)}{\sigma'_{mo}(z)} + \frac{\sigma'^{w}_r(z)}{\sigma'_{vo}(z)} + \frac{\sigma'^{s}_r(r_0)}{\sigma'_{vo}(z)} \qquad (1)$$

where

$$\sigma'_{vo}(z) = \sigma'_z(z) = \gamma'_t z \ , \qquad (2)$$

$$\sigma'_{mo}(z) = (1+2K_0)/3 \ \ \sigma'^{w}_z(z) \ . \qquad (3)$$

In Eq. (1), the effect of variable z on the steady-state part and the transient part of the initial condition was neglected since the consolidation part-model solutions did not depend on z.

The known terms in Eq. (1) were as follows:

(i) Left-hand side of Eq. (1) was considered to be equal to the initial radial effective stress measured by the piezo-lateral stress cell at the shaft-soil interface in an unknown depth (Baligh et al., 1985, Fig. 1)

(ii) Term $(1+2K_0)/3$ was assumed to be equal to 1.

(iii) The value mentioned in (a) was substituted for the transient component on the right-hand side of Eq. (1) normalized by σ'_{mo}.

At first, the sum of the unknown terms of Eq. (1) (the steady-state and the self-weight parts of the solution) was calculated. The non-homogeneous boundary condition v_0 of the steady-state part was calculated with the use of Eq. (4) and assuming various K_0 values:

$$\frac{\sigma'^{w}_r}{\sigma'_{v0}} + \frac{\sigma'^{s}_r(r_0)}{\sigma'_{v0}} = K_0 + \frac{2Gv_0}{r_0} \qquad (4)$$

since

$$\sigma'^{s}_r(r) = 2G\,\frac{v_0 r_0}{r^2} \ , \qquad (5)$$

$$\sigma'^{w}_r(z) = K_0 \ \gamma'_t z \ . \qquad (6)$$

Finally, the spatial distribution of the steady-state part of the solution was determined with the use of the analytical solution, as a function of K_0.

(c) The joined model

By adding up the different components, the initial and final stress states of the joined model normalized by σ_{vo} were calculated assuming that term $(1+2K_0)/3$ is equal to 1. Zero for u_0 was substituted.

It can be noted that this set of initial conditions is veritable in one point (at the shaft-soil interface) and for the radial normal stress components only. In any other cases, the effect of inconsistencies should be taken into account, that (i) the strain path prediction assumes $K_0 = 1$ condition and the measurement concerns $K_0 < 1$ case; (ii) $K_0 = 1$ was assumed for the calculation of the multiplier in the right-hand side of Eq. (1) (the normalization units of the calculated and the measured data became equal), and different K_0 values were assumed for Eq. (4); (iii) the effect of the depth variation in the initial condition was neglected.

REFERENCES

1. Baguelin, F.-Jézéquel, J.F.-Shields, D.H. (1978): The pressuremeter and foundation engineering. Trans. Tech. Publications. p. 617
2. Baligh, M.M. (1985): Strain path method. Journal of Geotechnical Engineering. ASCE, Vol. 111, Gt9, 1108-1136
3. Baligh, M.M.-Martin, R.T.-Azzouz, A.S.-Morrisson, M.J. (1985): The piezo-lateral stress cell. Proc. of XIth ICSMFE, San Francisco, Vol. 2, 841-844
4. Baligh, M.M. (1986): Undrained deep penetration, II: pore pressures. Geotechnique, Vol. XXXVI, No. 4, 487-503
5. Baligh, M.M.-Levadoux, J.N. (1986): Consolidation after undrained penetration. II: Interpretation. Journal of Geotechnical Engineering. ASCE, Vol. 112, no. 7, 727-747
6. Biot, M.A. (1941): General theory of three dimensional consolidation. Journal of Appl. Phys. Vol. XII, 155-164
7. Burgers, J.M.-Scott Blair, G.W. (1948): Report on the Principles of Rheological Nomenclature. Joint Committee on Rheology of the Int. Council of Scientific Unions, Proceedings, Int. Rheologic Congress, Amsterdam, 1948
8. Cryer, C.W. (1963): A comparison of three dimensional theories of Biot and Terzaghi. Q.J. Mech. Appl. Maths. 16, 401-412
9. Imre, E.-Tarcsai, Gy.-né-Györffy, J.-Csizmás, F. (1989): Rheological tests with cone penetrometer. Proc. of the XIIth ICSMFE, Rio de Janeiro. Vol. 1, 239-242
10. Imre, E. (1989): Discussion. Proc. of the XIIth ICSMFE, Rio de Janeiro. Vol. 5.
11. Imre, E. (1990a): Stress changes in soil after pile penetration. 9th Danube-European Conference on Soil Mechanics and Foundation Engineering. October 2-5. 1990. Budapest
12. Imre, E. (1990b): Consolidation around piles. Proc. of the IX. National Conference on Soil Mechanics and Foundation Engineering. Cracow, 1990. 10. 9-11, 55-62

13. Imre, E. (1990c): Multistage oedometric relaxation test. Proc. of the IX. National Conference on Soil Mechanics and Foundation Engineering, Cracow, 1990. 10. 9-11, 171-179

14. Imre, E. (1990): Evaluation of the oedometric relaxation test. Diploma work for the postgraduate engineering - mathematical course, Mechanical Engineering, Department of Civil Engineering, Technical University of Budapest, pp. 31

15. Jamiolkowski, M.-Ladd, C.C.-Germaine, J.T.-Lancelotta, R. (1985): New developments in field and laboratory testing. Proc. of XIth ICSMFE, San Francisco, Vol. 1, 57-155

16. Kondner, R.L.-Stallknecht, A.R. (1961): Stress Relaxation in Soil Compaction. Proc. of Highway Research Board. Vol. 40, 617-630

17. Lacerda, W.A. (1972): Stress Relaxation and Creep Effects in Soil Deformation. Ph. D. Thesis. University of California, Berkeley

18. Lacerda, W.A. (1977): Stress Relaxation after Partial Unloading. Proc. of IXth ICSMFE, Tokyo, Vol. 1, 117-179

19. Levadoux, J.-Baligh, M.M. (1986): Consolidation after undrained penetration. I: Prediction. Journal of Geotechnical Engineering, ASCE, Vol. 112, No. 7. 707-727

20. Massarsch, K.R.-Broms, B.B. (1977): Fracturing of Soil Caused by Pile Driving in Clay. Proc. of the IXth ICSMFE,Tokyo, Vol. 1, 197-200

21. Roy, M.-Lemieux, M. (1986): Long-term behaviour of reconsolidated clay around a driven pile. Canadian Geotechnical Journal. Vol. 18, No. 2, 67-86

22. Sills, G.C. (1975): Some conditions under which Biot's Equations of Consolidation Reduce to Terzaghi's Equation. Geotechnique, London 25(1), 129-132

23. Soderberg, L.O. (1962): Consolidation Theory Applied to Foundation Pile Time Effects. Geotechnique, 12, 217-232

24. Terzaghi, K. (1948): Theoretical Soil mechanics. Vth printing, June, Wiley, 510

25. Whitman, R.V. (1957): The Behavior of Soil under Transient Loading. Proc. of Third ICSMFE, Vol. 1, 207-210

26. Yang, N.-C. (1956): Redriving characteristics of piles. ASCE. Journal of Soil Mechanics and Foundation Division, Vol. 82, No. SM3, p. 17

Acta Technica Acad.Sci.Hung., 104(1-3), pp. 125-185 (1991/92)

BUCKLING OF BARS ON ELASTIC FOUNDATION, SUBJECTED TO UNIFORMLY DISTRIBUTED AXIAL LOADS

JANKÓ, L.*

(Received: 14 August 1990)

Equilibrium method has been used to solve the simple branching problem of two-hinged bars, cantilevers and bars fixed at both ends of linearly elastic material, considered to be geometrically perfect, supported by Winkler's linear translational type foundation (bed). By means of the analytical process described in this paper, a system of diagrams ideal for use also in practice has been set up. Investigation of the effect of different boundary conditions has been instructive also from a theoretical point of view. E.g. the critical load for the two-hinged bar was found to lie below that for the cantilever (except for two-hinged bars on soft foundation).

1. Introduction, assumptions

The abundant literature on stability is rich in problems of bars on elastic foundation /1, 4, 6, 7-8, 10/ but no solution is found to the problems outlined below.

The plane two-hinged bar, cantilever and bar fixed at both ends illustrated in Fig. 1 are considered to be geometrically perfect. Equilibrium method is used to solve the simple branching problem of bars of linearly elastic material, supported by a foundation of linearly elastic spring law (Winkler's translational foundation) to secure it against translation.

Although our analytical process designed a priori for computer is voluminous as compared with the importance of the problem, the results obtained can be treated simply and they are an important aid in investigation of important structures used in practice. Such a structure is e.g. the plate or shell edge beam upon which the plate or the shell has an interactive effect.

Analysis of the different buckling modes permitted the branching phenomenon to be investigated thoroughly.

*Jankó, László, H-1091 Budapest, Üllői út 117, Hungary

Akadémiai Kiadó, Budapest

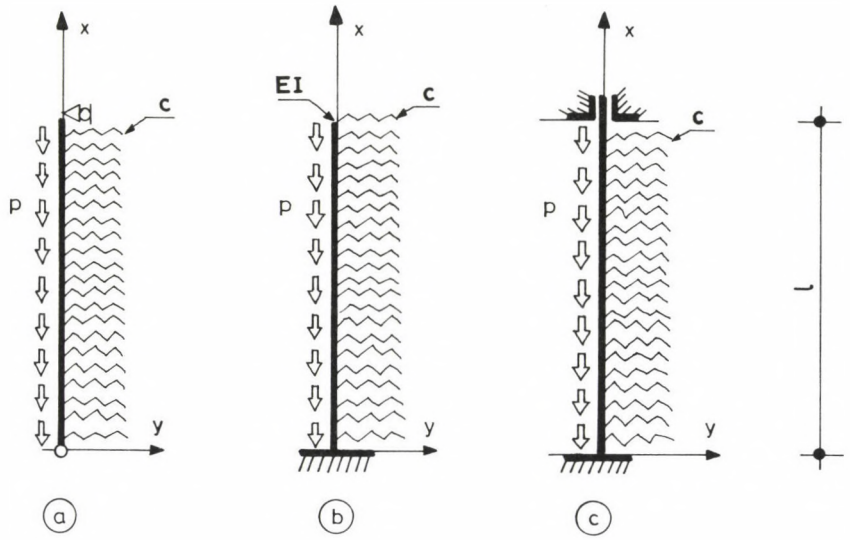

Fig. 1. General arrangement

From a theoretical point of view, the special effect of the different boundary conditions, rather unusual also in the field of the stability of bars, is peculiar: in the present case, the eigenvalues of the two-hinged bar are smaller than those of the cantilever (except for a small range).

2. Solution using equilibrium method

2.1 The differential equation and its solution

After differentiation of equation b) on page 101 of /10/ and addition of term cy for the elastic foundation, the differential equation of the problem can be written as follows (where c is the foundation coefficient):

$$EIy^{IV} + p\,[(\ell - x)y'' - y'] \quad cy = 0 \,. \tag{2.1}$$

Let the following notation be introduced:

$$x = \xi\,\ell \,, \tag{2.2}$$

$$y' = \frac{1}{\ell} y^{\cdot}, \ \ldots, \ y^{IV} = \frac{1}{\ell^4} y^{::} \ . \qquad (2.3\ a\text{-}d)$$

$$\lambda_o = \frac{p\,\ell^3}{EI} \ , \qquad (2.4)$$

$$\lambda = \frac{p\,\ell}{P_{crE}} = \frac{\lambda_o}{\pi^2} \ , \qquad (2.5)$$

$$P_{crE} = \pi^2 \frac{EI}{\ell^2} \ , \qquad (2.6)$$

$$u^2 = \frac{c\,\ell^4}{EI} \ . \qquad (2.7)$$

The problem becomes an eigenvalue problem with the boundary conditions according to par 2.2.

By use of quantities (2.2 thru 2.7) equation (2.1) can be written in parametric form as follows (the dot denoting derivation with respectto ξ):

$$y^{::} + \lambda_o \left[(1-\xi)y^{\cdot\cdot} - y^{\cdot}\right] + u^2 y = 0 \ . \qquad (2.8)$$

To find the general solution of differential equation (2.8) we use the following power series:

$$y = \sum_{k=0}^{\infty} c_k \frac{\xi^k}{k!} \ . \qquad (2.9)$$

For calculation of unknown coefficients c_k, the following recursive formula has been obtained using the method of indefinite coefficients:

$$c_k = -\lambda_o \left[c_{k-2} - (k-3)c_{k-3}\right] - u^2 c_{k-4} \ , \qquad (2.10)$$

$$k \geq 4 \ .$$

Then, with relationship (2.10) substituted into (2.9), an expression is obtained for y where each term is written as a function of max four coefficients unknown for the time being (c_0, c_1, c_2, c_3):

$$y = c_0 + \frac{c_1}{1!}\xi + \frac{c_2}{2!}\xi^2 + \frac{c_3}{3!}\xi^3 - \left\{\lambda_o\left[c_2 - 1c_1\right] + u^2 c_0\right\}\frac{\xi^4}{4!} -$$
$$- \left\{\lambda_o\left[c_3 - 2c_2\right] + u^2 c_1\right\}\frac{\xi^5}{5!} - \ldots = y(c_0, c_1, c_2, c_3) \ . \qquad (2.11)$$

In this way, each one of coefficients c_0, c_1, c_2, c_3 can be picked out independently and put before a subseries (and its magnitude can be assumed optionally in accordance with the boundary conditions).

The functions (subseries) associated with these coefficients are certainly linearly independent as a result of the existence and uniqueness theorem. Hence, the general solution of differential equation (2.8) has been produced:

$$y = \sum_{j=0}^{3} c_j f_j = c_0 f_0 + c_1 f_1 + c_2 f_2 + c_3 f_3 \ . \qquad (2.12)$$

The corresponding linearly independent particular solutions:

$$f_j = \sum_{k=0}^{\infty} c_k^j \frac{\xi^k}{k!} \ , \quad j = 0,1,2,3 \ . \qquad (2.13)$$

With the "starting" values given below, the recursive formula according to (2.10) unambiguously gives coefficients c_k^j of the series according to (2.13):

$$\begin{array}{|cccc|} \hline c_0^0 & c_1^0 & c_2^0 & c_3^0 \\ \hline c_0^1 & c_1^1 & c_2^1 & c_3^1 \\ \hline c_0^2 & c_1^2 & c_2^2 & c_3^2 \\ \hline c_0^3 & c_1^3 & c_2^3 & c_3^3 \\ \hline \end{array} = \begin{array}{|cccc|} \hline 1 & & & \\ \hline & 1 & & \\ \hline & & 1 & \\ \hline & & & 1 \\ \hline \end{array} \ . \qquad (2.14)$$

These coefficients are not arbitrary but unique values determined on the basis of written subseries mentioned when discussing equation (2.11).

2.2 Boundary conditions, eigenvalue equations

Hereinafter we are looking for the least positive eigenvalue λ_{cr} from among the discrete values of parameter λ, determined by the boundary conditions (the critical state being indicated by subscript cr).

Let first the derivatives of functions (2.13) with respect to ξ (cf. (2.2)) be written:

$$f_j' = \sum_k c_k^j \frac{\xi^{k-1}}{(k-1)!} , \quad j = 0,1,2,3 \tag{3.1}$$

$$f_j'' = \sum_k c_k^j \frac{\xi^{k-2}}{(k-2)!} , \tag{3.2}$$

$$f_j''' = \sum_k c_k^j \frac{\xi^{k-3}}{(k-3)!} , \tag{3.3}$$

$$f_j^{IV} = \sum_k c_k^j \frac{\xi^{k-4}}{(k-4)!} \tag{3.4}$$

$$j = 0,1,2,3$$

2.2.1 Two-hinged bar

Boundary condition relationships:

$$y(0) = y''(0) = 0 , \tag{3.5 a-b}$$

$$y(1) = y''(1) = 0 . \tag{3.6 a-b}$$

It follows from conditions (3.5 a-b) that

$$c_0 = c_2 = 0 . \tag{3.7 a-b}$$

Complying with conditions (3.6 a-b) are the following eigenvalue equations (boundary condition equations):

$$\begin{aligned} c_1 f_1(1) + c_3 f_3(1) &= 0 , \\ c_1 f_1''(1) + c_3 f_3''(1) &= 0 . \end{aligned} \tag{3.8 a-b}$$

2.2.2 Cantilever

Boundary condition relationships:

$$y(0) = y'(0) = 0 , \tag{3.9 a-b}$$

$$y''(1) = y'''(1) = 0 . \tag{3.10 a-b}$$

It follows from (3.9 a-b) that

$$c_0 = c_1 = 0 \ . \tag{3.11 a-b}$$

Eigenvalue equations according to conditions (3.10 a-b):

$$\begin{aligned} c_2 f_2''(1) + c_3 f_3''(1) &= 0 \ , \\ c_2 f_2'''(1) + c_3 f_3'''(1) &= 0 \ . \end{aligned} \tag{3.12 a-b}$$

2.2.3 Bar fixed at both ends

In a way similar to what has been said above, we obtain:

$$y(0) = y'(0) = 0 \ , \tag{3.13 a-b}$$

$$y(1) = y'(1) = 0 \ , \tag{3.14 a-b}$$

$$c_0 = c_1 = 0 \ , \tag{3.15 a-b}$$

$$\begin{aligned} c_2 f_2(1) + c_3 f_3(1) &= 0 \ , \\ c_2 f_2'(1) + c_3 f_3'(1) &= 0 \ . \end{aligned} \tag{3.16 a-b}$$

2.2.4 Determination of eigengalues and eigenfunctions

Critical load parameters (eigenvalues) λ_{cr} have been obtained from the zero-valuedness of the determinants of the coefficient matrices corresponding to equations (3.8 a-b), (3.12 a-b) and (3.16 a-b) by means of a numerical method. Our program written for IBM computer produces also eigenfunction (2.12) and its differential functions (3.1) thru (3.4). To test the process, it has been determined in any case whether equation (2.8) is satisfied.

Note that, for the sake of the required accuracy, series of more than hundred terms were needed in case of Figs 2 thru 6 ($u \leq 200$). For the high values of parameter u according to Fig. 7, series of several hundred terms were required to ensure convergence.

Because of the numerical difficulties encountered, double-point arithmetic has been adopted and some "tricks" ensuring the numerical

stability of the process were used (e.g. c_k^j/k has been stored in vectors instead of coefficients c_k^j of functions (2.13), etc.).

It has been numerically proved that series (2.13) and (3.1) thru (3.4) are absolute and uniformly convergent in the range of $\xi \leq 1$ /11/.

3. Results

Readers are reminded that parameter λ_{cr} = (2.5) is the parameter of total critical load.

3.1 Diagrams of critical load parameters

Critical load parameter λ_{cr} of the two-hinged bar in Fig. 1a changes according to diagram a in Fig. 2.

It can also be seen that the characteristic of the eigenfunction differs fundamentally for the initial quasi-sinusoidal function (u = 0) as the values of foundation parameter u ("characteristic length" parameter) increase. Otherwise the approximate curve presented in par 4 and illustrated by broken line (4.7) in Figs 2 and 6 could be obtained on the basis of a one-term sinusoidal basic function (upper limit). The tendency can be observed according to which the deflections are much less in the upper region of the bar than in the lower region as the value of u increases. The eigenfunctions are discussed in detail in par 3.2 in relation to Fig. 8.

The thin continuous line down in Fig. 2 is the solution for concentrated force /7/.

The "garland" curve of the cantilever according to Fig. 1b is illustrated as curve b in Fig. 3.

The upper thin broken line denoted by (4.13) shows the approximate solution based on the one-term basic function in par 4 (upper limit). See also Fig. 6.

In Fig. 3, also the solution for the concentrated force on top according to /5/ has been illustrated by the thin line down in the Figure.

As follows from the nature of the phenomenon, increasingly dominant cantilever end deflections are associated with the concentrated load on top increasing simultaneously with the increase of parameter u. However, in case of distributed load, the effect of the cantilever end diminishes

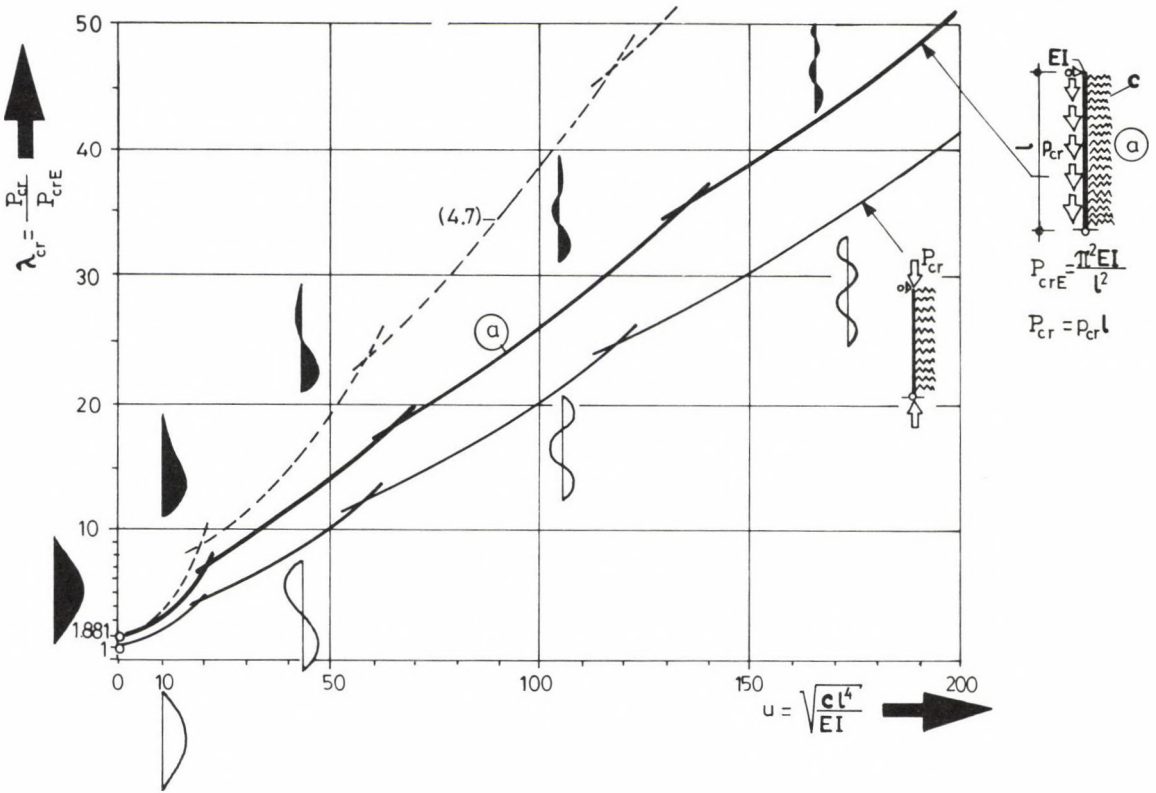

Fig. 2. Critical load parameters of a two-hinged bar

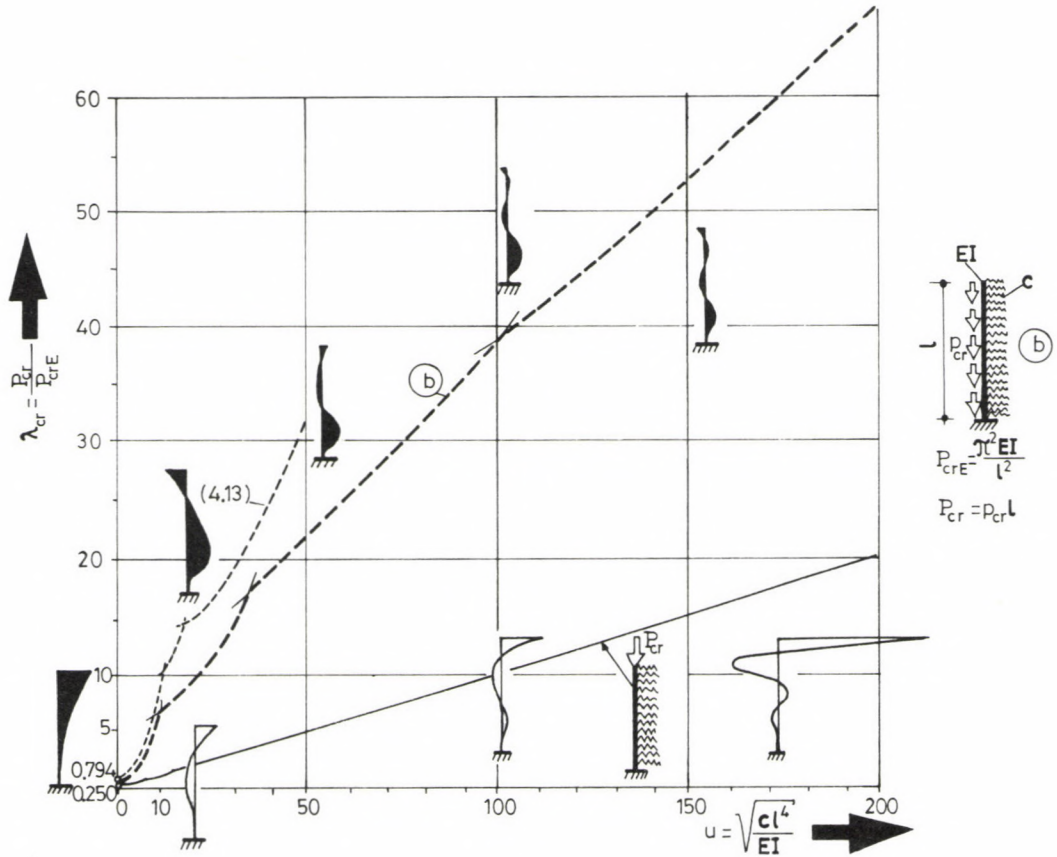

Fig. 3. Critical load parameters of a cantilever

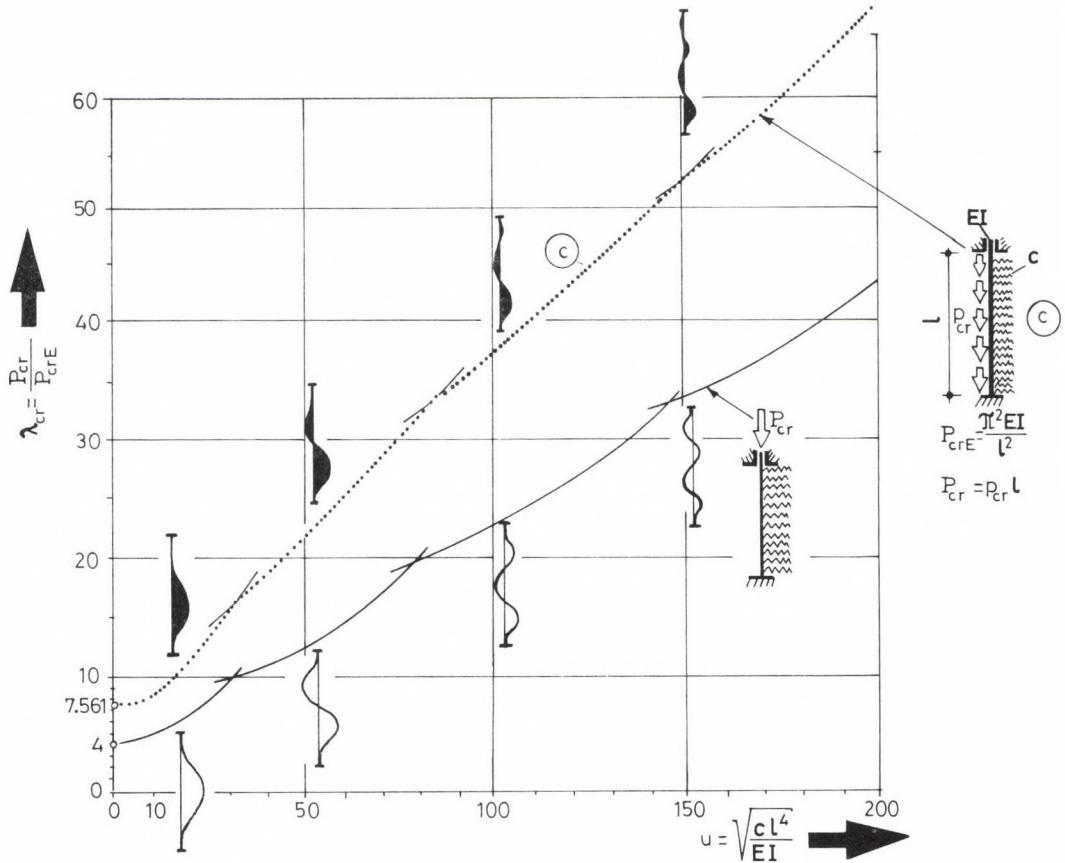

Fig. 4. Critical load parameters of a bar fixed at both ends

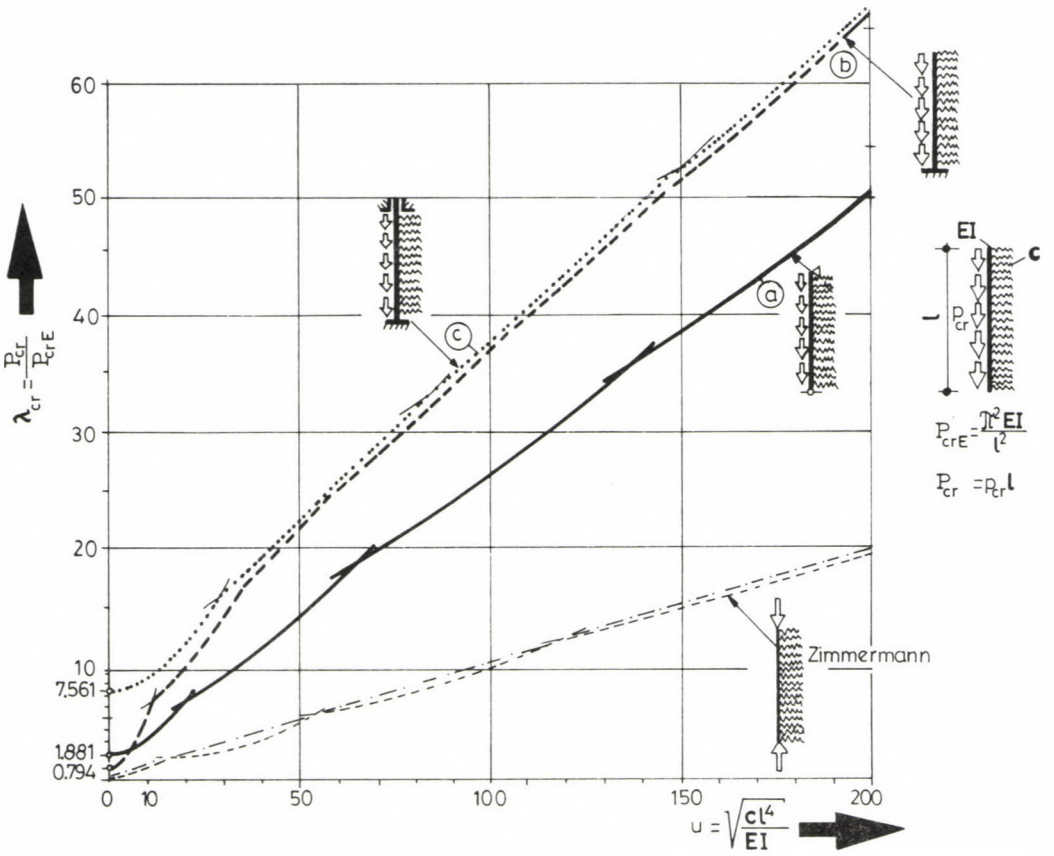

Fig. 5. Comparison of different boundary condition cases

increasingly with the effect of buckling deflection developing in the lower region of the bar predominating (see also Fig. 8).

The results obtained for the bar fixed at both ends according to Fig. 1c are illustrated by curve c in Fig. 4.

The solution in relation to concentrated force on top has been taken from /7/.

Concerning the character of the eigenfunctions, it can be seen again that the ordinates of the buckling mode, occurring in the lower region of the bar, are predominant again as the value of foundation parameter u increases (see also Fig. 8).

It can also be seen that as compared with the cantilever and bar fixed at both ends, the value of total critical load of a two-hinged bar lies much nearer to the critical value of concentrated load.

Interesting conclusions can be drawn from Fig. 5 where the curves of Figs 2, 3 and 4 are illustrated next to each other.

An appreciable difference between the critical load parameters of the cantilever (b) and the bar fixed at both ends (c) is found in the range of about $u < 40$ only. For higher values of foundation parameter u, the two curves are almost coincident, indicating that the effect of the upper edge is fading away. Obviously, this behaviour is similar to that of a "high-walled" cylindrical shell.

The same behaviour has been observed in investigation of cantilever on elastic foundation under concentrated load /5/.

However, the position of curves a and b as compared with each other is rather unusual: in the present case, the critical load parameters of the two-hinged bar lie below those of the cantilever! An exception is only the initial $u \leqslant 5$ range. Comments on the character of eigenfunctions imply explanation of the phenomenon: the load bearing capacity of the structure is fundamentally determined by the type of the lower edge with the effect of the upper edge fading away as the values of parameter u increase. This phenomenon is discussed in detail in par 3.2.

Also, we point out that the Southwell's theorem (principle of partial stiffening) applies also to our case in that the effect of elastic foundation (u) appears as an additive term as compared with the critical load of Euler in case of bars without foundation with, however, this latter term being very small in the present case. Of course, the critical load parameters of the bar without foundation ($u = 0$) have been determined similarly by means of the process described to obtain the well-known values according to literature.

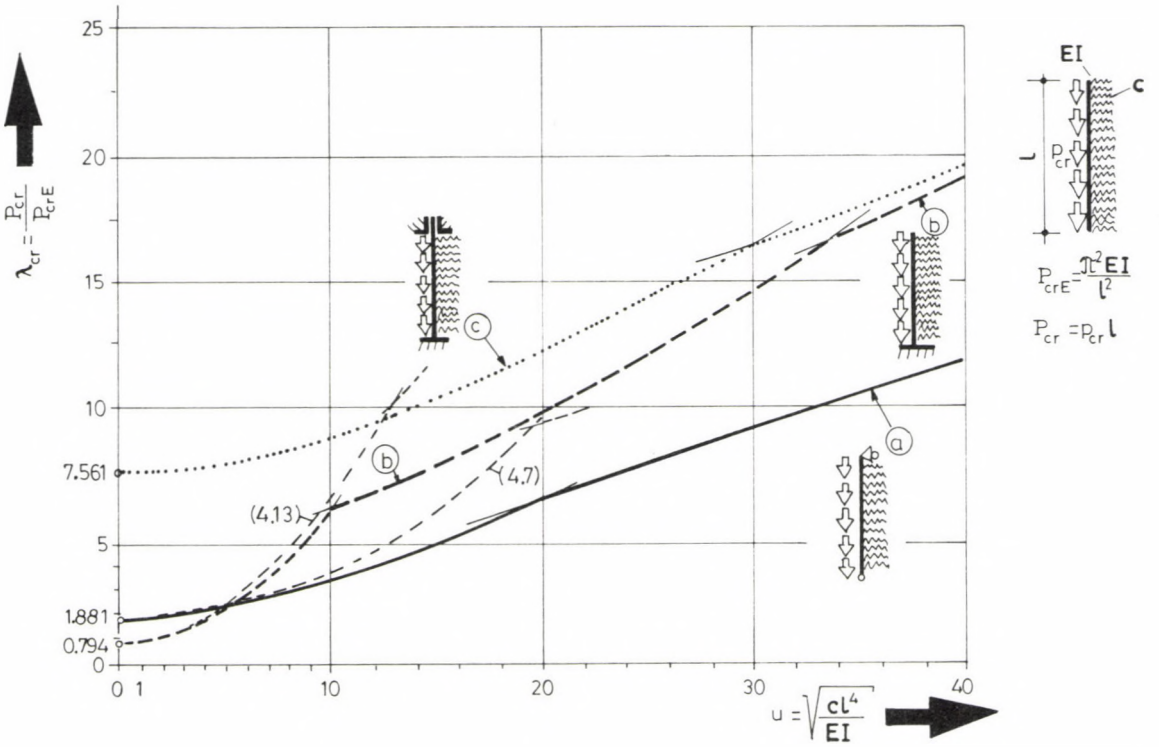

Fig. 6. Soft elastic foundation and/or short bar

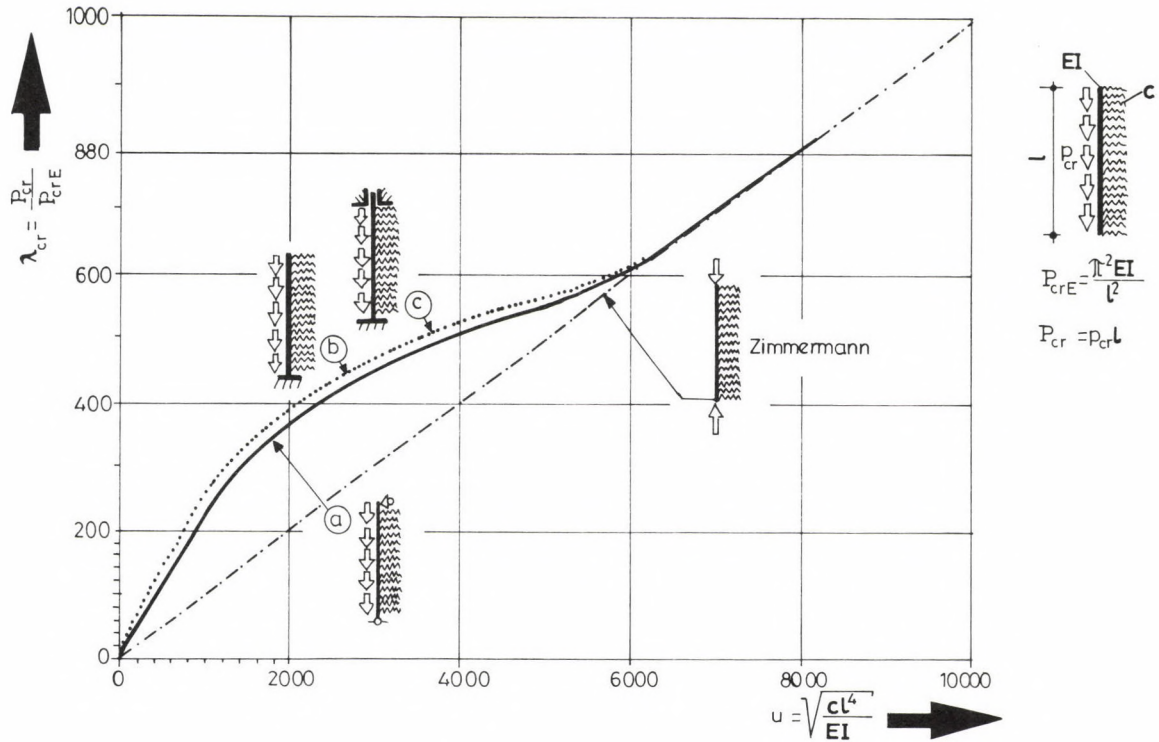

Fig. 7. Hard elastic foundation and/or long bar

Figure 6 has been plotted for relatively low values of foundation parameter u (soft elastic foundation or short bar or high bending rigidity) to facilitate practical application.

Figure 7 is important first of all from a theoretical point of view. Our intention was to show that in case of very high values of foundation parameter u ($u \longrightarrow \infty$), the curves approximated the solution for the Zimmermann bar free at the ends, under concentrated load /4, 8, 10/. The physical explanation of this phenomenon is that in case of a bar of infinite length ($\ell \longrightarrow \infty$ i.e. $u \longrightarrow \infty$), the lower section of the bar can be considered as a Zimmermann bar of infinite length, free at the ends, under load corresponding to the concentrated resultant of distributed loads (see also par 4).

3.2 Eigenfunctions

The shape of eigenfunctions for buckling presented in Fig. 8 is in agreement with what has been said so far about critical parameters λ_{cr}.

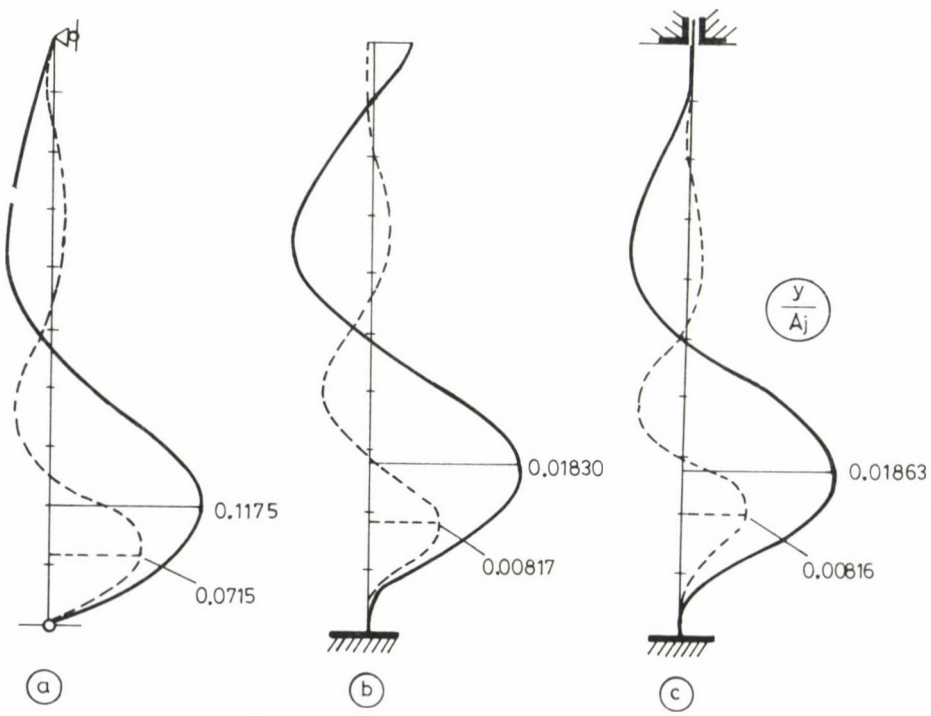

Fig. 8. Typical buckling modes (u = 50 ——; u = 150 -----)

This similarity of the eigenfunctions for buckling of the cantilever (b) and the bar fixed at both ends (c) obviously complies with the almost perfect coincidence of curves b and c for $u > 40$ in Fig. 5. In this domain, the nature of the buckling phenomenon is determined by the lower boundary conditions, the effect of the upper boundaries being negligible ("long" bar).

The buckling mode develops predominantly in the portion of the bar near the lower boundary, a statement applying to the two-hinged bar (a) as well. The characteristic of the eigenfunction of case a is similar to that associated with cases b and c but, considering the hinge at the bottom, the load bearing capacity of the bar is less than that of the cantilever (a in Fig. 5).

Although imperfection-sensitivity and/or post-critical behaviour are not dealt with in this study, the readers' attention is directed to possible problems nonlinear studies at a later data.

Curves found in the literature for two-hinged bar and bar fixed at both ends under concentrated load, illustrated on the basis of /7/ in Figs 2 and 4, respectively, have a common feature in that symmetric and antimetric eigenfunctions follow by turn.

The eigenvalues associated with two different buckling modes at the intersections of "garland" curves are identical and thus also a combination of two different buckling modes is possible (compound branching). This is important in investigation of the imperfection-sensitivity according to /2/, /9/ because the coincidence, or near-coincidence of two critical loads belonging to a stable-symmetric point of bifurcation each, the structure is very sensitive to structural imperfections. Moreover, the (critical) point of bifurcation of a two-hinged bar on elastic foundation under concentrated load is stable-symmetric in a rather narrow range of parameters u; it is unstable-symmetric in general /3/, /9/ or two symmetric (stable or unstable) branchings occur simultaneously at the intersections of "garland" curves /3/.

The case of cantilever under concentrated load /5/ seems to be more favourable according to Fig. 3. Namely, a "garland" character of the curve can be observed only in the initial domain of parameters u in this case and thus investigation of the possibility of simultaneous branchings seems to be less important.

The imperfection and postcriticality investigation will certainly be much more labour-intensive and require more caution in the cases discussed

in this work and illustrated in Fig. 1 than e.g. the case of the two-hinged bar on elastic foundation under concentrated load /3/ as suggested also by the much more complicated eigenfunction (2.12) associated with the cases illustrated in Fig. 1 as compared with the one-term sinusoidal functions, the exact eigenfunction of the two-hinged bar under concentrated load according to Fig. 2. This difference in difficulty will certainly increase in case of nonlinear problems (imperfection, postcriticality) and it seems to be expedient therefore to find some numerical solution (e.g. finite element method).

Note that, on the basis of considerations according to par 4, an analytical nonlinear approach may also be successful in the range of $u < 10$.

4. Approximate methods

Presented in this Chapter are some simple approximate relationships by means of the Ritz-method to prove that there exists a small domain of foundation parameter u ($u \leq 10$) where the accuracy of simple relationships (4.7) and (4.13) is sufficiently high for practical application (Fig. 6) on the one hand while on the contrary, to show that dissimilarly to bar stability problems of quite a number, no practicable result can be obtained by means of a one-term basic function (energy method) in the range of $u > 10$ on the other hand. It is unnecessary to assume two or more trigonometric terms because of the availability of the exact solution and a formula easy to treat in practice can not be obtained in this way either.

Let the one-term basic function given below be approximate eigenfunction of the two-hinged bar:

$$y = y_i \sin \frac{i\pi}{\ell} x , \quad i = 1,2,3,... \tag{4.1}$$

The second variation of potential energy per term (b: bending, c: elastic foundation, p: load):

$$V_{ii}^{b} = \frac{1}{2} EI \int_0^{\ell} y''^2 \, dx = \frac{\pi^4 EI}{4\ell^3} i^4 y_i^2, \tag{4.2}$$

$$V_{ii}^{c} = \frac{1}{2} c \int_0^{\ell} y^2 \, dx = \frac{1}{4} c \ell y_i^2 , \tag{4.3}$$

$$V_{ii}^{p} = -\frac{1}{2} p \int_{0}^{\ell} y'^{2} (\ell - x)\, dx = -\frac{\pi^2}{8} p\, i^2\, y_i^2 , \tag{4.4}$$

$$V_{ii} = V_{ii}^{b} + V_{ii}^{c} + V_{ii}^{p} . \tag{4.5}$$

Variation problem

$$\delta V_{ii} = 0 \tag{4.6}$$

shall usually be solved to find the critical equilibrium state (branching). This is simple in our case, the result being

$$\lambda_{cr} = \frac{P_{cr}\,\ell}{P_{crE}} \approx 1.881 \left(i^2 + \frac{u^2}{\pi^4}\,\frac{1}{i^2}\right) \tag{4.7}$$

$$i = 1,2,3,\ldots$$

(see Figs 2 and 6). Note that the value of the multiplier in formula (4.7) is actually 2 instead of 1.881 because the process is an approximation. A multiplier of 1.881 has been used as a correction to provide continuous transition for the accurate solution of case u = 0.

Similarly, the following relationships are obtained for cantilever:

$$y = y_i\left(1 - \cos\frac{i\pi}{2\ell} x\right) , \tag{4.8}$$

$$i = 1,\ 3,\ 5,\ \ldots$$

$$V_{ii}^{b} = \frac{\pi^4 EI}{64\,\ell^3}\, i^4\, y_i^2 , \tag{4.9}$$

$$V_{ii}^{c} = \frac{1}{2} c\,\ell \left(\frac{3}{2} + k\frac{4}{\pi i}\right) y_i^2 , \tag{4.10}$$

$$k = -1 \quad \text{if} \quad i = 1,\ 5,\ 9,\ \ldots$$
$$k = 1 \quad \text{if} \quad i = 3,\ 7,\ 11,\ \ldots \tag{4.11 a-b}$$

$$V_{ii}^{p} = -p\,\frac{\pi^2}{8}\left(\frac{i^2}{4} - \frac{1}{\pi^2}\right) y_i^2 , \tag{4.12}$$

$$\lambda_{cr} \approx 0.4722\, \frac{i^4 + \frac{32}{\pi^4}\left(\frac{3}{2} + k\frac{4}{\pi i}\right) u^2}{i^2 - \frac{4}{\pi^2}} . \tag{4.13}$$

(See Figs 3, 6.)

$$i = 1,3,5,\ldots$$

Here also, the actual multiplier in formula (4.13) is 0.5 instead of 0.4722. Correction has been used again to provide continuous transition to case u = 0.

The following simple curves can be used to approximate curves a and b in Fig. 2 and 3, respectively:

For two-hinged bar (a in Fig. 2):

$$\lambda_{cr} \approx 1.881 + 0.05410\, u^{\frac{3}{2}} , \qquad (4.14a)$$

$$0 \leqslant u < 20$$

$$\lambda_{cr} \approx 6.72 + 0.2444\,(u - 20) . \qquad (4.14b)$$

$$20 < u \leqslant 200$$

For cantilever (b in Fig. 3):

$$\lambda_{cr} \approx 0.794 + 0.0535\, u^{2} , \qquad (4.15a)$$

$$0 \leqslant u \leqslant 10$$

$$\lambda_{cr} \approx 6.14 + 0.4327(u - 10) , \qquad (4.15b)$$

$$10 \leqslant u \leqslant 40$$

$$\lambda_{cr} \approx 19.12 + 0.2985\,(u - 40) . \qquad (4.15c)$$

$$40 \leqslant u \leqslant 200$$

Finally, note that the solution associated with $u \longrightarrow \infty$ for the Zimmermann bar free at the end mentioned in par 3.1 can be obtained also by means of the model illustrated in Fig. 9. Since this model follows from what has been said in pars 3.1 and 3.2, our result can be considered as a marginal case associated with $u \longrightarrow \infty$, and/or a lower limit, of the solutions of problems given in Figs 1a thru c (Fig. 7).

The details can be neglected here since all what we have to do is to apply the method, defined by formulae (4.1) thru (4.7), to the model in Fig. 9 accordingly. Length ℓ_1 is included in the solution and thus the extreme value shall be found with respect to length ℓ_1 as well:

$$\frac{\partial p_{cr}}{\partial \ell_1} = 0 \ . \tag{4.16}$$

With the calculation of limit value $u \longrightarrow \infty$ applied to the formula obtained for p_{cr} we obtain

$$\lambda_{cr} = \frac{u}{\pi^2} \ . \tag{4.17}$$

which is, in fact, the solution of the Zimmermann bar for $u \longrightarrow \infty$ /7/, (Figs 5 and 7).

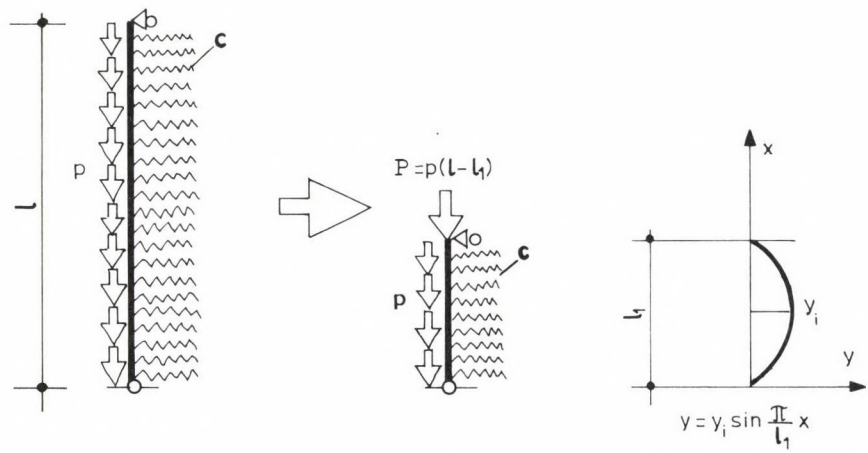

Fig. 9. Approximate method for the case $u \longrightarrow \infty$

ACKNOWLEDGEMENT

The research leading to this paper was supported by a grant of the National Scientific Research Council of Hungary (OTKA 684).

REFERENCES

1. Column Research Committee of Japan. Handbook of structural stability. Corona Company, Tokyo 1971

2. Gáspár, Zs.: Imperfection-sensitivity at near-coincidence of two critical points. Journal of Struct. Mechanics 13, 1984

3. Gioncu, V.-Ivan, M.: Bazele calculului structurilor la stabilitate. Facla, Timişoara 1983

4. Hetényi, M.: Beams on elastic foundation. Ann Arbor, Michigan, London, Oxford 1955

5. Jankó, L.: Buckling of a cantilever on elastic foundation loaded on top by concentrated force. Acta Techn. Acad. Sci. Hung. 104/1-2, (1991) 147-158

6. Petersen, C.: Statik und Stabilität der Baukonstruktionen. Vieweg & Sohn, Braunschweig, Wiesbaden 1982

7. Pflüger, A.: Stabilitätsprobleme der Elastostatik. Springer Verlag, Berlin - Heidelberg 1975

8. Ratzersdorfer, J.: Die Knickfestigkeit von Stäben und Stabwerken. Springer Verlag, Wien 1936

9. Thompson, J.M.T.-Hunt, G.W.: A general theory of elastic stability. John Wiley & Sons, London, New York 1973

10. Timoshenko, S.P.-Gere, J.M.: Theory of elastic stability. McGraw Hill Company, New York, Toronto 1961

11. Tuma, J.J.: Engineering mathematics handbook. McGraw-Hill Company, New York-Toronto 1985

Acta Technica Acad.Sci.Hung., 104(1-3), pp. 147-158 (1991/92)

BUCKLING OF A CANTILEVER ON ELASTIC FOUNDATION LOADED ON TOP BY CONCENTRATED FORCE

JANKÓ, L.*

(Received: 14 August 1990)

Equilibrium method was used to solve the simple branching problem of a cantilever of linearly elastic material on Winkler's linear translational type foundation (bed), considered to be geometrically perfect. The analytical process presented provided rather simple results ideal for use in practical work as well.

1. Introduction, basic assumptions

The ample literature on stability is rich in solutions to problems in relation to bars on elastic foundation /1, 4-7, 9/ but no solution to the problem illustrated schematically in Fig. 1 is found there.

The bar is considered to be geometrically perfect. Equilibrium method is used to solve the simple planar branching problem of a cantilever of linearly elastic material, supported against translation by a foundation o. linearly elastic behaviour (Winkler's elastic foundation).

Although the analytical process presented is relatively tiresome as compared with the importance of the problem, it provides results easy to handle and ideal for use in practical work.

The analysis of buckling modes permitted the nature of the branching phenomenon to be studied thoroughly.

We also studied the behaviour of the cantilever in question as compared with a beam on elastic foundation, free at both ends.

*Jankó, László, H-1091 Budapest, Üllői út 117, Hungary

Akadémiai Kiadó, Budapest

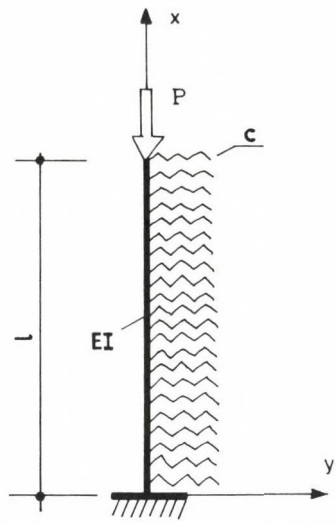

Fig. 1. General arrangement

2. Solution using equilibrium method

2.1 Differential equation and its solution

The differential equation of the problem can be written with some modification (substitution of -cy in place of q, where c is the foundation coefficient) of equation (1-5) on page 2 of /9/, as follows (Fig. 1):

$$EIy^{IV} + Py'' + cy = 0 \ . \tag{2.1}$$

Let notation

$$\lambda_0 = \frac{P}{EI} = \lambda \frac{\pi^2}{\ell^2} \ , \tag{2.2}$$

$$\lambda = \frac{P}{P_{crE}} \ , \tag{2.3}$$

$$P_{crE} = \frac{\pi^2 EI}{\ell^2} \ , \tag{2.4}$$

$$q_0 = \frac{c}{EI} = \frac{u^2}{\ell^4} \ , \tag{2.5}$$

$$u = \sqrt{\frac{c\,\ell^4}{EI}}\ , \tag{2.6}$$

be introduced to obtain the following formula from (2.1):

$$y^{IV} + \lambda_0 y'' + q_0 y = 0\ . \tag{2.7}$$

Quantities λ_0, q_0 in equation (2.7) are real numbers.

According to page 182 of /10/, the solution of differential equation (2.7) depends on the sign of discriminant

$$D = \lambda_0^2 - 4q_0\ . \tag{2.8}$$

Discriminant D is obtained in the course of solution of the characteristic equation.

Parameter λ_0 is unknown for the time being. Let the possibilities of solution for the different values of λ_0 and D be investigated.

Detailed investigations showed that in case of the present problem, case $D < 0$ (two pairs of complex conjugate roots) was associated with the least value of λ_0 over almost the entire domain of foundation parameter u ('characteristic length' parameter, see (2.6)).

Therefore, the solutions obtained for the case $D = 0$ (two coincident imaginary roots for each) and case $D > 0$ (four different imaginary roots) are not presented here (but they are included in the computer process).

Solution for $D < 0$ on the basis of /10/:

$$y = C_1 a_1(\xi) + C_2 a_2(\xi) + C_3 a_3(\xi) + C_4 a_4(\ )\ , \tag{2.9}$$

where

$$a_1(\xi) = \cos\alpha\xi\ \mathrm{sh}\beta\xi\ , \tag{2.10}$$

$$a_2(\xi) = \sin\alpha\xi\ \mathrm{ch}\beta\xi\ , \tag{2.11}$$

$$a_3(\xi) = \sin\alpha\xi\ \mathrm{sh}\beta\xi\ , \tag{2.12}$$

$$a_4(\xi) = \cos\alpha\xi\ \mathrm{ch}\beta\xi\ , \tag{2.13}$$

$$\xi = \frac{x}{\ell}\ , \tag{2.14}$$

$$\alpha = \sqrt{\frac{1}{2}\left(u + \frac{\pi^2}{2}\lambda\right)}\ , \tag{2.15}$$

$$\beta = \sqrt{\frac{1}{2}\left(u - \frac{\pi 2}{2}\lambda\right)}. \tag{2.16}$$

According to condition $D < 0$, the above relationships will apply if

$$\lambda < 2\frac{u}{\pi 2} \tag{2.17}$$

(as shown also by (2.16)). The solution applying in a very narrow domain ($u < 1.4$) corresponding to $D > 0$ is discussed in par 3.

2.2 Boundary conditions. Eigenvalue equation

To be found from among the discrete values of parameter λ, determined by the boundary conditions, is now the least positive eigenvalue λ_{cr} where subscript cr indicates the critical state.

The well-known boundary conditions are:

$$y(0) = 0 , \tag{2.18}$$

$$y'(0) = 0 , \tag{2.19}$$

$$y''(\ell) = 0 , \tag{2.20}$$

$$EIy'''(\ell) + P_{cr}y'(\ell) = 0 . \tag{2.21}$$

Theoretically, dimensionless eigenvalue λ_{cr} (see (2.3)) is supplied by the singularity condition of matrix $\underline{U}$ of size 4x4.

Since, however,

$$C_4 = 0 \tag{2.22}$$

according to equation (2.18) and

$$C_2 = -\frac{\beta}{\alpha} C_1 , \tag{2.23}$$

according to condition (2.19), we are looking for the eigenvalues of a matrix $\underline{U}$ of size 2x2 corresponding to a coefficient vector consisting of constants C_1, C_3. Written in detail:

$$\underline{\underline{U}} \begin{bmatrix} C_1 \\ C_2 \end{bmatrix} = \begin{bmatrix} u_1 & u_3 \\ v_1 & v_3 \end{bmatrix} \begin{bmatrix} C_1 \\ C_3 \end{bmatrix} = \underline{0} \ , \qquad (2.24\text{-}25)$$

where

$$Q = \frac{\alpha^2 + \beta^2}{\alpha} \ , \qquad (2.26)$$

$$u_1 = -Q \left[a_1(1)\alpha + a_2(1)\beta \right] \frac{1}{\ell^2} \ , \qquad (2.27)$$

$$u_3 = \left[a_3(1)(\beta^2 - \alpha^2) + 2a_4(1)\alpha\beta \right] \frac{1}{\ell^2} \ , \qquad (2.28)$$

$$v_1 = -Q \left[a_3(1)(\lambda_{cr} \pi^2 - \alpha^2 + \beta^2) + 2a_4(1)\alpha\beta \right] \frac{1}{\ell^3} \ , \qquad (2.29)$$

$$v_3 = \left[a_1(1)\alpha(\lambda_{cr} \pi^2 - \alpha^2 + 3\beta^2) + a_2(1)\beta (\lambda_{cr} \pi^2 - 3\alpha^2 + \beta^2) \right] \frac{1}{\ell^3} \ . \qquad (2.30)$$

It seems more practicable to determine the roots of transcendent equation

$$|\underline{\underline{U}}| = u_1 v_3 - u_3 v_1 = 0 \qquad (2.31)$$

that is the eigenvalues of λ_{cr} numerically by means of a computer since the computer method is a general method (that can be used for other cases as well) and, on the other hand, it resulted not only in a numerical solution but also in a very simple closed formula as will be seen later in par 3.

3. Results

3.1 Critical load parameters

The least positive solutions of equation (2.31) are given in Fig. 2. From about $u > 20$ on, function λ_{cr} can be considerred straight line.

Some 'garland' curve character is still perceivable in domain $u < 20$ but the slight deviation of the curve from straight line can be hardly perceived in Fig. 2.

As has been mentioned, only the solution complying with condition (2.17) is written in par 2 because it is valid for almost the entire domain of parameter u. The vertical broken line plotted for small values of parameter u ($u = 1.4$) corresponds to the zero valuedness of discriminant (2.8). By means of the computer program, we determined the solution also

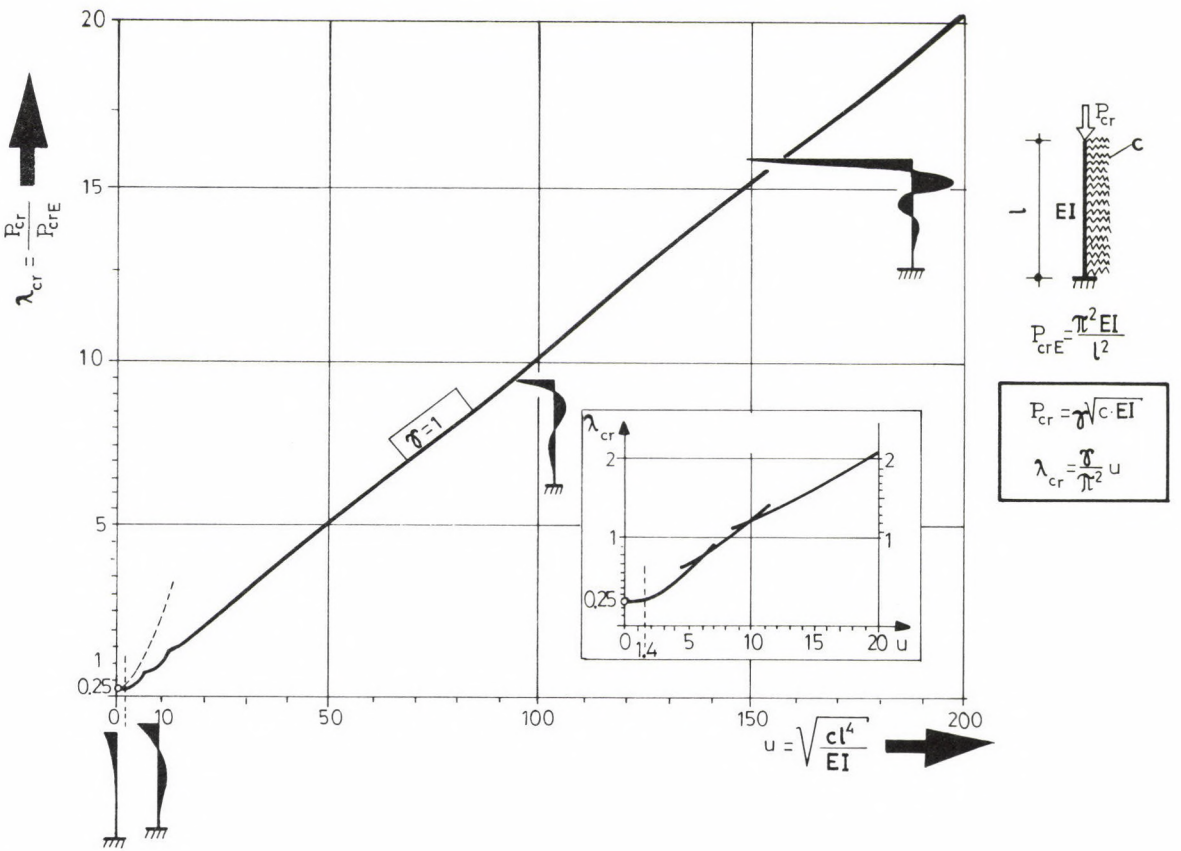

Fig. 2. Critical load parameters

in the very narrow domain complying with condition $D > 0$. This went continuously into the solution for minimum critical load parameter $\lambda_{cr} = 0.25$ of the cantilever without foundation.

On the basis of what has been said above, use of the following relationship (where $\gamma = 1$) is recommended in calculation for critical loads:

$$\lambda_{cr} = \frac{\gamma}{\pi^2} u \ . \tag{3.1}$$

Of this, the formula of critical force can be calculated by means of relationships (2.2) thru (2.6):

$$P_{cr} = \gamma \sqrt{c\ EI} \ . \tag{3.2}$$

These relationships are sufficiently accurate in the domain of about $u \geq 20$. In domain $0 > u > 20$, linear interpolation between the values of $\lambda_{cr} = 0.25 \div 2.094$ is permissible (Fig. 2).

3.2 On the eigenfunctions

Indicated in Figure 2 are also the geometrically true eigenfunctions for some special cases. As seen, the buckling made for small values of u similar to the first buckling mode of the cantilever becomes an exponentially declining curve of strongly variable curvature as foundation parameter u ('characteristic length' parameter) increases. A similar curve is shown also in Fig. 3.

Note that, to control the process, also the first four derivatives of the eigenfunction have been determined by computer to make sure that the obtained eigenfunction meets the boundary conditions and satisfies the differential equation (2.7) alike.

As is well known, the critical load of a bar without foundation can be determined in an exact way also by means of an energy method on the basis of one single basic function 1-cos x (see page 87 of /9/). Since the buckling mode of the bar on foundation is a rather complicated geometry according to Fig. 3, a satisfactory solution to the present case could be obtained by energy method using trigonometric basic functions only at the expense of a very large number of terms (especially if we want to meet all the four boundary conditions).

This is confirmed also by the curve illustrated by broken line in Fig. 2, starting from critical load parameter $\lambda_{cr} = 0.25$ of the bar with-

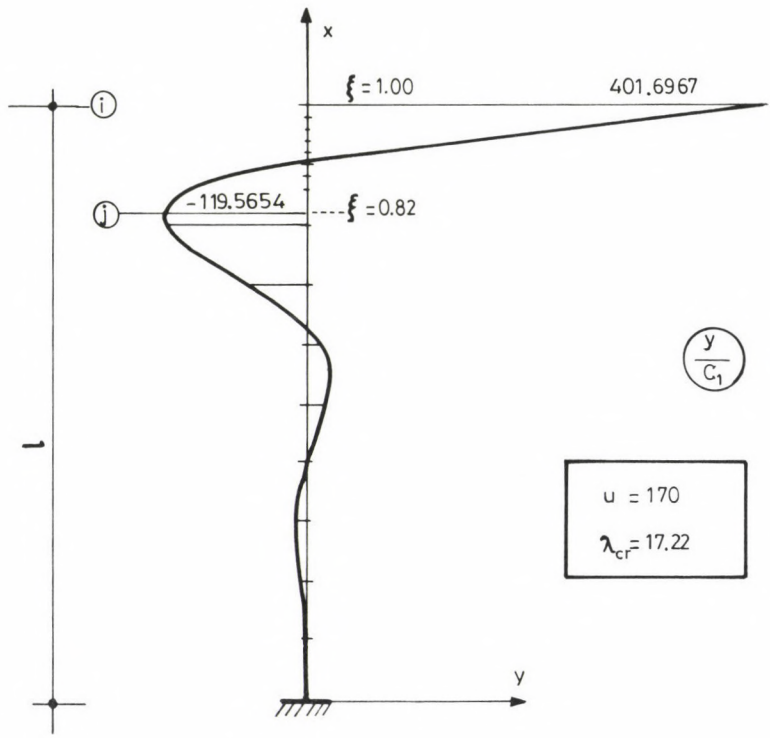

Fig. 3. Typical buckling mode

out foundation. A one-term buckling mode 1-cos x (basic function) has been used to obtain this curve.

4. Comparison

Like in case of other elastic foundation problems, the parameter describing the essentials of the phenomenon (λ_{cr} in the present case) depends on the geometrical length ℓ multiplied by the fourth root of rigidity ratio c/EI (u (2.6)).

Figure 4 where also the Engesser solution of a two-hinged bar on elastic foundation and the Zimmerman solution of the bar free at both ends have been indicated on the basis of /4,6,7,9/ explains why the shape of formulae (3.1) thru (3.3) is found so familiar. As is well known, the

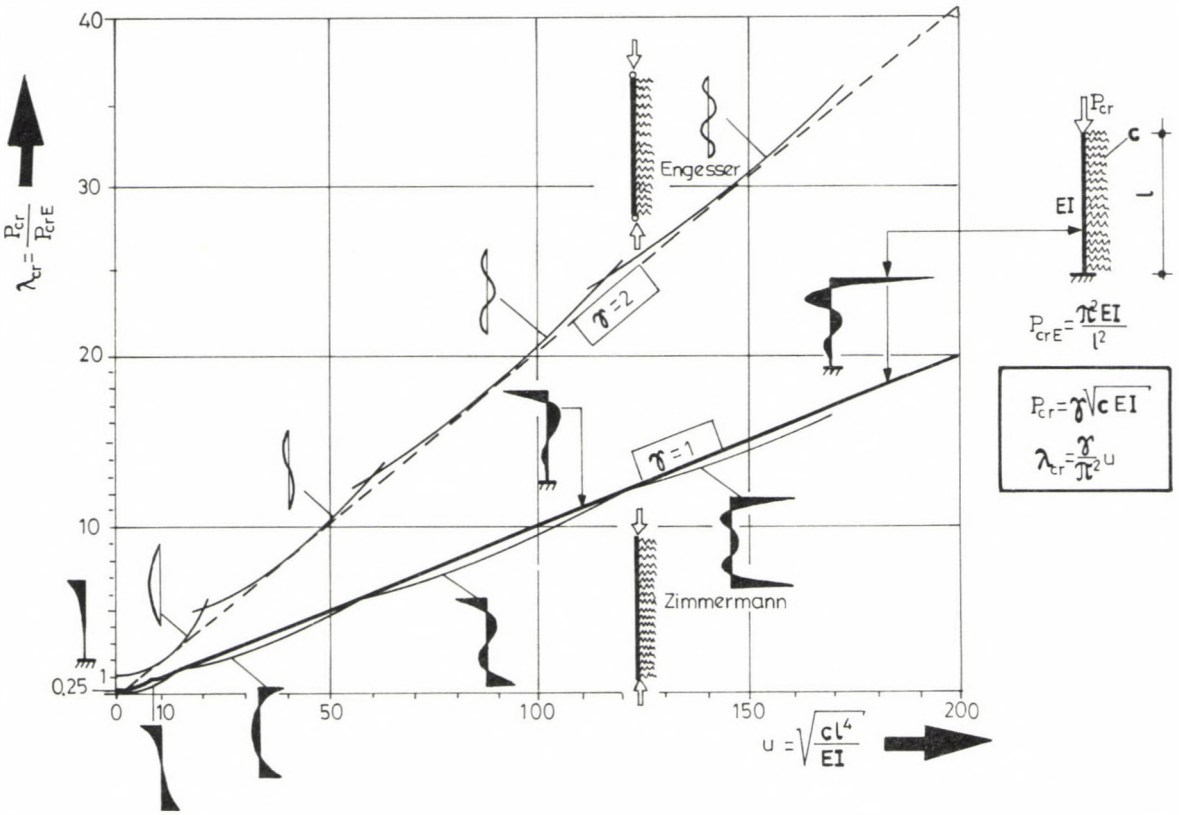

Fig. 4. Comparison of different cases of boundary conditions

Engesser 'garland' curve is usually replaced with the enveloping straight line of parameter $\gamma = 2$ (cf. (3.2)).

Hence, parameter $\gamma = 1$ of the cantilever on elastic foundation is just half as compared with the previous value. Note that a straight line of parameter $\gamma = 1$ can be used also in place of the 'garland' curves of Zimmerman's bar according to the approximate recommendation given in /6/. As clearly shown in Fig. 4, this approximation considerably reduces the safety here and there in domain $u < 12$.

The difference between Zimmermann's 'garland' curve and the straight line of the cantilever with parameter $\gamma = 1$ is small also for low values of u. Accordingly, the behaviour of the cantilever in a significant part of domain u is similar to that of a 'high-walled' cylindrical shell in that the edge disturbance type effect does not affect the other edge. At the same time, the cantilever acts as a 'low-walled' cylindrical shell in domain $u < 12$ that is the two edges affect each other considerably. In this domain, the bar free at both ends should by no means be investigated by use of a straight line of parameter $\gamma = 1$ and vice versa, use of Zimmermann's bar also in domain $u < 12$ on the basis of knowledge acquired so far to investigate the cantilever is a rough approximation to the benefit of safety.

We also point out that in the sense of Southwell's theorem (principle of partial stiffening), it is true also in the present case that the effect of elastic foundation appears as an additive term that is, the formula of critical load is

$$P_{cr} = P^{E}_{cr} + f(c) ,$$

where P^{E}_{cr} - Euler's critical force of the bar without foundation and
c - foundation coefficient

with, however, term P^{E}_{cr} being very small in the present case and not appearing therefore in equation (3.2). Although analysis of imperfection-sensitivity and/or postcritical behaviour are not dealt with in this work, possible problems occurring in nonlinear investigations later should still be mentioned here.

The most important common characteristic of the curves of the two-hinged bar and the bar free at the ends is that symmetric and antimetric eigenfunctions alternate with each other. The two eigenvalues associated with a different buckling mode each at the intersections of 'garland' curves are identical and thus a combination of both buckling modes (simul-

taneous branching/compound branching) is also possible.This might be important in analysis of imperfection-sensitivity according to /2, 8/ because in case of coincidence or near-coincidence of two critical loads belonging to a stable-symmetric point of bifurcation each, the structure is very sensitive to imperfections. Moreover, the (critical) point of bifurcation of a two-hinged bar on elastic foundation is usually unstable symmetric while it is stable symmetric in a certain narrow domain of parameter u only /3, 8/ or two symmetric (stable or unstable) branchings occur about at the intersections of 'garland' curves simultaneously /3/.

Considering that the exact eigenfunction of a two-hinged bar on elastic foundation consists of one-term simple sine functions (of variable shape in domain u) while in the present case, the eigenfunction is described by a much more complicated expression (2.9), it is quite obvious that much caution and work are required in nonlinear (imperfection-sensitivity and postcritical) investigations. It seems somewhat favourable in this respect that a 'garland' character is perceivable only at the initial section of the curve according to Fig. 2 and thus investigation of the possibility of simultaneous branchings seems to be less important.

In the last analysis, use of some numerical method (e.g. finite element method) seems to be most reasonable in future nonlinear investigations. According to our preliminary research, the relatively simply energy method (using trigonometric basic functions of 1-2 term(s)) promises practicable results in the domain $u < (5\text{-}10)$ only.

ACKNOWLEDGEMENT

The research leading to this paper was supported by a grant of the National Scientific Research Council of Hungary (OTKA 684).

REFERENCES

1. Column Research Committee of Japan. Handbook of Structural Stability. Corona Company, Tokyo 1971

2. Gáspár, Zs.: Imperfection-sensitivity at near-coincidence of two critical points. Journal of Struct. Mechanics, 13 (1984)

3. Gioncu, V.-Ivan, M.: Bazele calculului structurilor la stabilitate. Facla, Timişoara 1983

4. Hetényi, M.: Beams on elastic foundation. Ann Arbor, Michigan, London, Oxford 1955

5. Petersen, C.: Statik und Stabilität der Baukonstruktionen. Vieweg & Sohn, Braunschweig, Wiesbaden 1982

6. Pflüger, A.: Stabilitätsprobleme der Elastostatik. Springer Verlag, Berlin, Heidelberg 1975

7. Ratzersdorfer, J.: Die Knickfestigkeit von Stäben und Stabwerken. Springer Verlag, Wien 1936

8. Thompson, J.M.T.-Hunt, G.W.: A general theory of elastic stability. John Wiley & Sons, London, New York 1973

9. Timoshenko, S.P.-Gere, J.M.: Theory of elastic stability. McGraw-Hill Company, New York, London 1961

10. Tuma, J.J.: Engineering mathematics handbook. McGraw-Hill Company, New York-Toronto 1987

Acta Technica Acad.Sci.Hung., 104(1-3), pp. 159-185 (1991/92)

BUCKLING OF THE EDGE BEAMS OF A HYPERBOLIC PARABOLOID SHELL SUPPORTED ALONG THE GENERATRICES

JANKÓ, L.*

(Received: 14 August 1990)

The purpose of this work has been to investigate to what an extent are buckling hyperbolic paraboloid shell edge beams stiffened by the shell interacting with them. As compared with the literature, a much more accurate solution is given for the two-hinged edge beam. A process is described in this work, which is essentially a stopgap in case of cantilever edge beam structures.

Although the method used is somewhat circumstantial, it has yielded in the last analysis results which are simply applicable and easy to handle.

1. Introduction

Investigation of the classic (simple) branching problem of a geometrically perfect, flat, rectangular or oblique, isotropic (or orthotropic) hyperbolic paraboloid shell (hypar) supported along the generatrices of linearly elastic material under load uniformly distributed over the horizontal plan can be considered as a field that has been closed /2-5, 7, 11-14/.

However, buckling of edge beams is a problem that needs further investigation.

As is well known, a combination of hyperbolic paraboloid shells permits aesthetically attractive roofs of various types to be constructed. Two typical structures of this type are shown in Fig. 1.

Buckling of the hinged edge beam shown in Fig. 1a has been investigated by Dayaratnam and Gerstle /1/. These authors obtained approximate results only and to make the solution for the two-hinged edge beam much more accurate in this work was therefore most desirable.

Cantilever edge beams are often used in practice (Fig. 1b). The re-

*Jankó, László, H-1091 Budapest, Üllői út 117, Hungary

Akadémiai Kiadó, Budapest

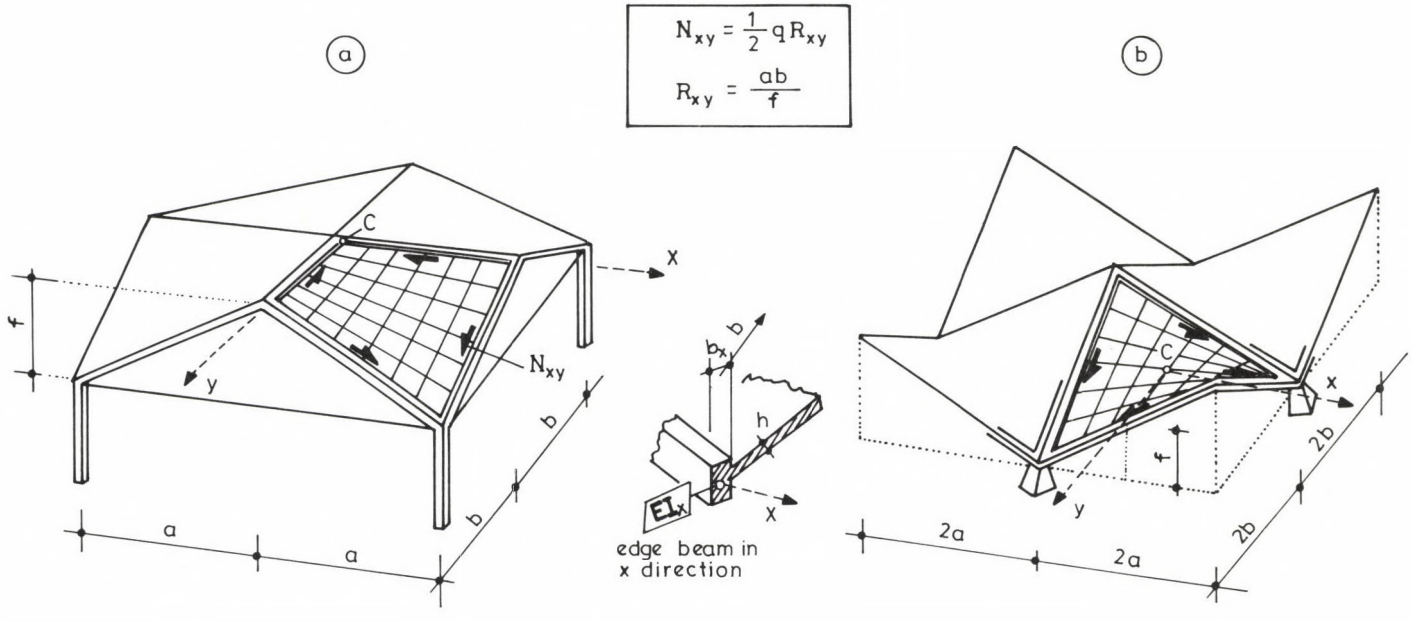

Fig. 1. Geometry, general arrangement

Fig. 2. Eigenfunctions

sults obtained in investigation of buckling of such structures are presented in this work.

Note that we produced the exact solution of buckling of two-hinged and cantilever beams on Winkler's translational type elastic foundation in our earlier works /9, 10/.

The cardinal idea of the present process is to determine, on the basis of /9, 10/, the rigidity of the elastic foundation brought about by the shell interacting with the buckling edge beam to relieve the edge beam.

Finally, our results are compared with the experimental results of Leet /12/ to illustrate the feasibility of our process.

2. Basic assumptions

Our work is based on the usual assumptions in majority. Still, it seems reasonable to list the assumptions taken as a basis for the investigation.

The flat shell bears a total surface load of intensity q and direction z, distributed uniformly over the horizontal plan.

Right angle is included by the generatrices of the hypar. The shell and the edge beam are geometrically perfect.

The structures are made of homogeneous, isotropic, linearly elastic material. The translational foundation is similarly elastic, a Winkler type foundation.

The edge beam on a foundation (stiffened by the shell) is considered to be a common two-hinged beam or cantilever. No joint forces are taken into account at joints of common deflection at the edge of the cantilever.

We take into account only bending rigidity EI_x of the edge beams applying to the horizontal principal axis of inertia (the bar being treated as a prismatic bar). As shown also by Leet's /12/ experiments, it is the moment of inertia I_x acting upon the horizontal principal axis that affects the phenomenon decisively.

Discussed below in detail are the simple planar buckling of the edge beams (and the simple branching phenomenon of the shell) within the framework of the usual small-displacement second-order theory (linear buckling theory).

At the same time, we point out that our process is suited also for investigation of the possibility of a simultaneous loss of stability of the shell and edge beam (see also par 4.2).

The transverse contraction factor μ is neglected (see also par 4.2).

The effect of deformations before loss of stability (subscript o, prebuckling) upon the present structures is negligible ($w_o = \emptyset$).

Let the Bleich-Salvadori hypothesis be adopted, according to which tangential translations $\bar{u}$, $\bar{v}$ taking place in the course of buckling of the hypothesis be proved at the same time /1/, see par 4.2.

For the sake of simplicity, let the geometry of the so-called first-type hyperbolic paraboloid shell shown in Figs 2a, b be taken into consideration. In this case, dimensions a, b, f referred to the hypar centre C of horizontal tangential plane are the full side lengths and rise of the hypar (dissimilarly to the so-called second-type hyperbolic paraboloid shell shown in Fig. 1b).

3. Buckling of two-hinged edge beam

Investigated are the beams schematically illustrated in Figs 1a and 2a.

3.1 Basic equations

Dayaratnam and Gerstle /1/ assumed the following functions for variations of deflections in normal direction of the buckling shell, $\bar{w}_{sh}$ and buckling edge beams, $\bar{w}_e$:

$$w = w_o + \bar{w} , \tag{3.1}$$

$$w_o = w_{osh} = w_{oe} = 0 , \tag{3.2}$$

$$\bar{w} = \bar{w}_{sh} + \bar{w}_e , \tag{3.3}$$

$$\bar{w}_{sh} = \sum_{i}^{\infty} \sum_{j}^{\infty} A_{ij} \sin \frac{i\pi}{a} x \sin \frac{j\pi}{b} y , \tag{3.4}$$

$$i,j = 1, 3, 5, \ldots$$

$$\bar{w}_e = \sum_{i}^{\infty} B_i \sin \frac{i\pi}{a} x + \sum_{j}^{\infty} C_j \sin \frac{j\pi}{b} y . \tag{3.5}$$

$$i,j \sim k,\ell$$

Note that, in the process described in par 4, we make a distinction between buckling half-wave numbers k, ℓ of the buckling edge beams and buckling half-wave numbers i, j of the buckling shell. Since the case is different in /1/, we used symbol $\sim$ after formula (3.5).

The well-known formula of tangential shearing force N_{xyo} resulting from surface load q, uniformly distributed over the horizontal plane, of the shell of membrane behaviour before buckling (subscript o), expressed by radius of curvature R_{xy} (Fig. 1):

$$R_{xy} = \frac{ab}{f}, \tag{3.6}$$

$$N_{xy} = N_{xyo} = \frac{1}{2} qR_{xy} = \frac{1}{2} q \frac{ab}{f} . \tag{3.7}$$

In case of a square ground plan (a = b and (3.11), (3.12)):

$$N_{xyo} = \frac{1}{2} qa \frac{\omega}{\rho} . \tag{3.8}$$

Dayaratnam and Gerstle /1/, using the Ritz method and taking one term of formula (3.5) into consideration, obtained the following expression for critical surface load resulting in buckling of the edge beam (i = j = k) in case of square ground plan (a = b) and symmetrical edge beam configuration ($I_x = I_y = I$):

$$\frac{q_{cr}}{E} = \frac{\rho}{\omega^4} \left[\frac{\pi^2}{6} (1+2\alpha)k^2 + \frac{4}{\pi^2} \rho^2 \frac{1}{k^2} \right], \tag{3.9}$$

where

$$\alpha = \frac{EI}{Ba} = \frac{12I}{h^3 a} , \tag{3.10}$$

$$\rho = \frac{f}{h} , \tag{3.11}$$

$$\omega = \frac{a}{h} , \tag{3.12}$$

$$B = \frac{Eh^3}{12} . \tag{3.13}$$

Minimization according to k resulted in the following relationships in /1/:

$$k^2 = \frac{2\sqrt{6}}{\pi^2} \frac{\rho}{\sqrt{1+2\alpha}} , \tag{3.14}$$

$$\frac{q_{cr}}{E} = \sqrt{2}\,\frac{2}{\sqrt{3}}\,\frac{\rho^2}{\omega^4}\,\sqrt{1 + 2\alpha} \quad . \tag{3.15}$$

3.2 Buckling of the shell

The process described in /1/ can not be used to investigate this phenomenon. The classic solution of the buckling of shell is given by Reissner /14/ and Ralston /13/:

$$\frac{q_{crR}}{E} = \frac{2}{\sqrt{3(1-\mu^2)}}\,\frac{h^2}{R_{xy}^2} = \frac{2}{\sqrt{3(1-\mu^2)}}\,\frac{\rho^2}{\omega^4} \quad . \tag{3.16}$$

A detailed analysis of the problem is found in the book of Kollár and Dulácska /11/. We refer to the above well-known relationship repeatedly later in this work.

3.3 Critical remarks

This analysis is necessary because, on the one hand, the definition of the results according to par 3.1 is not always correct in the literature and because, on the other hand, the process for investigation of buckling of two-hinged edge beams has to be improved so as to be more accurate (see par 3.4).

Above all, we don't believe that in case of $\alpha = 0$, relationship (3.15) has to go into relationship (3.16) dissimilarly to what is believed sometimes in the literature, certainly because in /1/, the isolated shell-buckling (here: par 3.2) is not investigated but, instead, the eigenvalue of the structure of buckling mode $\overline{w}_e$ according to Fig. 2a, consisting of the sum of two cylinders of sinusoidal directrix (Eq. (3.5)) is determined. Since the effective buckling mode of the shell is not described by (3.5) but it is given by (3.4), see /13/, Eq. (3.15) can not go into (3.16) either.

Accordingly, the simultaneous loss of stability of the shell and edge beam is not investigated in /1/ either.

The Bleich-Salvadori hypothesis mentioned in par 1 has been rightly adopted as will be explained in par 4.2.

The case of different side lengths ($a \neq b$) is taken into consideration in the process within certain limits only; this case is not contained in the final results. Remember that the same applies to the classic solution of the buckling of shell according to par 3.2 (except for the lower enveloping straight line according to (3.6)).

The actual error in the solution of Dayaratnam and Gerstle /1/ lies not in what has been said above but rather in that the results obtained by one-term expression (3.5) are only a rough approximation of most of the values of rigidity of the foundation brought about by the shell (u (3.26)) to relieve the structure, moreover, to the detriment of safety.

3.4 Solution of the edge beam-buckling problem

Remember: the exact solution of buckling of common two-hinged beam on Winkler's translational type elastic foundation has been produced in /10/.

Relying upon this solution, the cardinal idea in our process is to determine the rigidity of elastic foundation (u (3.26)) brought about by the shell interacting with the edge beam to relieve the edge beam.

The exact solution according to /10/ is illustrated by thick continuous "garland" curve a in Fig. 3. This solution has been obtained numerically by means of an equilibrium method, using the method of indefinite coefficients. Figure 3 shows also the character of eigenfunctions.

Approximate one-term basic function

$$w = w_k \sin \frac{k\pi}{\ell} x, \quad k = 1, 2, 3, \ldots \tag{3.17}$$

has been used to produce also an approximate relationship for critical load parameter λ_{cr} a two-hinged beam of length ℓ under uniformly distributed load $p(p_{cr})$:

$$\lambda_{cr} = \frac{p_{cr}\ell}{P_{crE}} \quad 2\left(k^2 + \frac{u^2}{\pi^4} \frac{1}{k^2}\right), \tag{3.18}$$

$$k = 1, 2, 3, \ldots$$

where

$$u = \sqrt{\frac{c\,\ell^4}{EI}}, \tag{3.19}$$

$$P_{crE} = \frac{\pi^2 EI}{\ell^2}. \tag{3.20}$$

In the common beam problem, c is the elastic foundation coefficient.

Extreme value calculation according to buckling half-wave number k results in

$$k = \frac{\sqrt{u}}{\pi}, \tag{3.21}$$

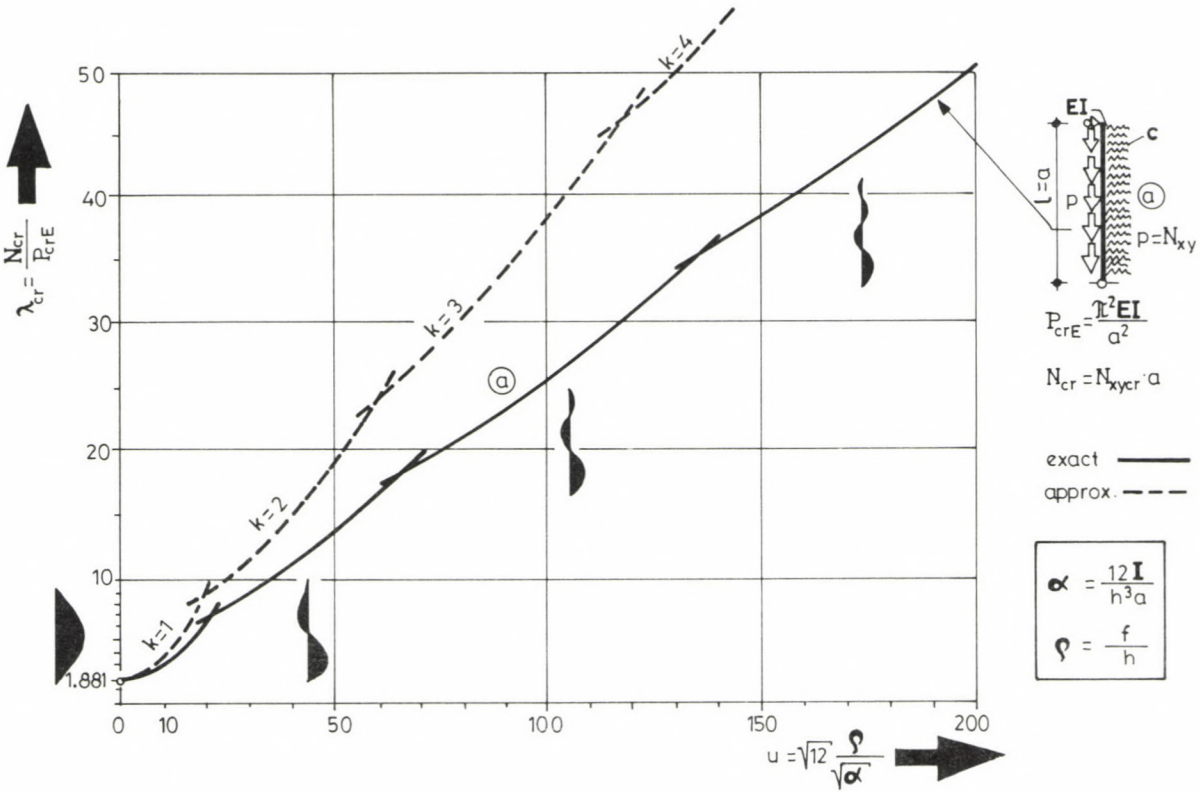

Fig. 3. Critical load parameters of two-hinged bar

$$\lambda_{cr} \approx \frac{4}{\pi^2} u \ . \tag{3.22}$$

Note that in Figure 3, relationship (3.18) is illustrated by broken line with 1.881 written in place of 2 as a multiplier (for the sake of transition to the exact solution of case $u = \emptyset$).

In the edge beam problem investigated, the critical value of specific tangential shearing force N_{xy} (3.7) corresponds to specific critical distributed load p_{cr}. Similarly, ℓ a if the structure is sufficiently flat, otherwise the length $\underline{\ell}$ is the actual length of the edge beam.

Let equality

$$p_{cr} = \lambda_{cr} p_{crE} \frac{1}{\ell} = N_{xycr} \tag{3.23}$$

be written first on the basis of what has been said above ($\ell = a$), where, according to (3.22),

$$p_{cr} = \frac{1}{3} Ea \frac{\alpha}{\omega^3} u \ , \tag{3.24}$$

and, on the basis of (3.15) and (3.7),

$$N_{xycr} = E a \sqrt{\frac{2}{3} \frac{\rho}{\omega^3}} \sqrt{1 + 2\alpha} \ . \tag{3.25}$$

On the basis of (3.23) thru (3.25), the foundation parameter u ('characteristic length' parameter) can be calculated from shell parameters (3.11), (3.12):

$$u = \sqrt{12} \frac{\rho}{\sqrt{\alpha}} \ . \tag{3.26}$$

Note that the same result will be obtained if the coefficients of buckling half-wave number k of expression N_{xycr} according to (3.9) and (3.7) are compared with the appropriate coefficients of expression (3.18).

By means of formulae (3.11), (3.12), (3.26) as well as Fig. 3, determination of critical load N_{xycr} of the buckling edge beam is a rather simple job.

Critical load parameter $\lambda_{cr} = \lambda(u)$ according to Fig. 3 supplies the specific critical load p_{cr} in accordance with the left side of relationship (3.23). The critical value of N_{xy} according to (3.7) is equal to this p_{cr}:

$$N_{xycr} = p_{cr} \quad . \tag{3.27}$$

Surface load q_{cr} shall be calculated by means of (3.7).

Note that in certain cases, the following formulae, an approximation of function a in Fig. 3, can be successfully used?

$$\lambda_{cr} \approx 1.881 + 0.05410.u^{\frac{3}{2}} \quad , \qquad 0 \leq u \leq 20 \tag{3.28 a}$$

$$\lambda_{cr} \approx 6.72 + 0.2444(u - 20) \quad . \qquad 20 \leq u \leq 200 \tag{3.28 b}$$

It is necessary to mention that the thin broken curve in Fig. 3 (Eq. (3.18)) is to thick curve a giving the exact solution of the simple bar problem as the approximate solution according to Dayaratnam and Gerstle /1/ (3.9) is to the exact solution of the shell edge beam problem. Thus Fig. 3 shows at the same time that our solution (Eq. (3.27)) yields values even 30–50% (or even more) lower for higher values of parameter u than Eq. (3.15) being in error to the detriment of safety.

Attention: Recommended are for use in practice essentially the relationships according to par 5.

4. Buckling of cantilever edge beam

Investigated are the beams illustrated in Fig. 2b.

4.1 Basic equations

Relationships (3.1), (3.2) apply also in this case.

The following functions have been assumed for deflections $\bar{w}_{sh}$ of the shell and $\bar{w}_e$ of the edge beams, respectively, in normal direction:

$$\bar{w}_{sh} = \sum_{i}^{\infty} \sum_{j}^{\infty} A_{ij} \sin \frac{i\pi}{a} x \sin \frac{j\pi}{b} y \quad , \tag{4.1}$$

$$i,j = 1, 2, 3, \ldots$$

$$\bar{w}_e = B_{k\ell} \left[\left(1 - \cos \frac{k\pi}{2a} x\right) \left(1 - \sin \frac{\ell\pi}{2b} y\right) + \right.$$

$$\left. + \left(1 - \sin \frac{k\pi}{2a} x\right) \left(1 - \cos \frac{\ell\pi}{2b} y\right) \right] \quad , \tag{4.2}$$

$$k,\ell = 1, 3, 5, \ldots$$

$$\bar{w} = \bar{w}_{sh} + \bar{w}_e \ . \tag{4.3}$$

4.1.2 Boundary conditions

4.1.2.1 Shell

Well-known geometrical ($\bar{w}_{sh}$) and physical ($\bar{w}''_{sh}$, $\bar{w}^{\cdot\cdot}_{sh}$) boundary conditions of the shell:

$$\bar{w}_{sh}(x = 0, a) = 0 \ ,$$

$$\bar{w}_{sh}(y = 0, b) = 0, \tag{4.4. a-d}$$

$$\bar{w}''_{sh}(x = 0, a) = 0 \ ,$$

$$\bar{w}^{\cdot\cdot}_{sh}(y = 0, b) = 0 \ . \tag{4.5 a-d}$$

The stress function derivative, $F^{\cdot}_{o}{}' = N_{xyo}$, in prebuckling state is the value according to equation (3.7).

As shown below, no special boundary conditions are required for stress function variation $\bar{F}$ associated with the buckling process since we have adopted the Bleich-Salvadori hypothesis /1/ mentioned in par 2. Namely, as follows from assumption $\bar{u} = \bar{v} = \emptyset$ (and also from (3.2)),

$$\bar{\varepsilon}_x = \bar{u}' - \bar{w}z'' = 0 \ ,$$

$$\bar{\varepsilon}_y = \bar{v}^{\cdot} - \bar{w}z^{\cdot\cdot} = 0 \ , \tag{4.6 a-c}$$

$$\bar{\gamma}_{xy} = \bar{u}^{\cdot} + \bar{v}' - 2\,\bar{w}z^{\cdot}{}' = -2\,\bar{w}\,\frac{f}{ab} \ .$$

Here the following equation of the middle surface is included in the formula (to be simple, in the co-ordinate system according to Fig. 1b):

$$z = \frac{f}{ab}\,xy \ . \tag{4.7}$$

It follows from what has been said above that

$$\bar{F}^{\cdot}{}' = -\bar{N}_{xy} = \frac{1}{2}\,D\,\bar{\gamma}_{xy} = -D\bar{w}\,\frac{f}{ab} \tag{4.8}$$

where D is the extensional rigidity:

$$D = Eh \ . \tag{4.9}$$

Equation (4.8) shows that no special boundary conditions can be stipulated for stress function $\bar{F}$. It is also remarkable that compatibility equation /7, 16/

$$\Delta\Delta\bar{F} - 2D\bar{w}'_{,z''} = 0 \tag{4.10}$$

is now trivially (identically) satisfied.

The correctness of the Bleich-Salvadori hypothesis is backed up not only by the literature /1/ but also by our investigations, see par 4.2.

4.1.2.2 Edge beams

According to our basic assumptions (par 2), the edge beams are considered to be common cantilevers independent of each other. It seems reasonable to omit to give the long list of well-known boundary conditions relevant to the problem here in this work.

4.1.3 Energy expressions

The following equations of the second variation of potential energy have been written here for application of the Ritz method. Deflection variation $\bar{w}$ of normal direction appearing in these equations is shown in Eq. (4.3).

Sum of energy:

$$V = V_b^{sh} + V_s^{sh} + V_b^{e} + V_s^{e} + V_q \ . \tag{4.11}$$

Second variation of the bending (b) potential energy of the shell:

$$V_b^{sh} = \frac{1}{2} B \int_0^a \int_0^b \left[\bar{w}''^2 + \bar{w}_{,}^{\cdot\cdot 2} + 2\bar{w}'^{2}_{,\cdot}\right] dxdy \ . \tag{4.12}$$

Here bending rigidity B is defined by equation (3.13). Second variation of the extensional (s) potential energy of the shell:

$$V_s^{sh} = \frac{1}{2} \int_0^a \int_0^b \left[\frac{2}{D}\bar{F}'^{2}_{,\cdot} - 2N_{xyo}\,\bar{w}'\bar{w}'\right] dxdy \ . \tag{4.13}$$

Extensional rigidity D can be obtained according to (4.9), specific tangenital shearing force is defined by equation (3.7) while $\overline{F}''$ is given in formula (4.8).

Second variation of the bending (b) potential energy of the edge beams (2 in each direction) of width b_x and b_y:

$$V_b^e = \frac{EI_x}{b_x} \int_0^a \int_0^{b_x} \overline{w}''^2 (y=0)\, dxdy + \frac{EI_y}{b_y} \int_0^{b_y} \int_0^{b} \overline{w}''^2 (x=0)\, dxdy \quad . \tag{4.14}$$

Appropriate part for extensional energy:

$$V_s^e = -\frac{1}{b_x} \int_0^a \int_0^{b_x} N_{yxo} \times \overline{w}'^2 (y=0)\, dxdy - \frac{1}{b_y} \int_0^{b_y} \int_0^{b} N_{xyo} y\, \overline{w}'^2 (x=0) dxdy. \tag{4.15}$$

Second variation of the potential enegy of the external load q is zero:

$$V_q = 0 \quad . \tag{4.16}$$

The following variation problem shall be solved to find the critical equilibrium position (branching):

$$\delta V = 0 \quad , \tag{4.17}$$

with magnification factor

$$C = \frac{a^3}{B\, b} \tag{4.18}$$

introduced, the expression for the bending potential energy of the shell can be written in a more detailed form, as follows:

$$C\, V_b^{sh} = \frac{\pi^4}{8} \sum_i \sum_j A_{ij}^2 \left(\frac{i^2}{\gamma^2} + j^2\right)^2 \gamma^4 + B_{k\ell}^2\, b_1 + \sum_i \sum_j A_{ij} B_{k\ell}\, b_2, \tag{4.19}$$

where

$$b_1 = \frac{\pi^4}{32} \left| k^4 b_{k\ell} + \ell^4 \gamma^4\, b_{\ell k} + k^2 \ell^2 \gamma^2 \left(1 + \frac{2}{\pi^2} \frac{1}{k\ell}\right) \right|, \tag{4.20}$$

$$b_{k\ell} = \left(\frac{3}{2} - \frac{4}{\pi} \frac{1}{\ell}\right) + \frac{2}{k\pi} \left(1 - \frac{3}{\pi} \frac{1}{\ell}\right), \tag{4.21}$$

$$b_2 = 4\pi^2 \left| i^2 k^2 \left(\frac{-i}{j\, a_{ik}} + \frac{2ij}{a_{ik} a_{j\ell}}\right) + j^2 \ell^2 \gamma^4 \left(\frac{-j}{i a_{j\ell}} + \frac{2ij}{a_{ik}\, a_{j\ell}}\right) + \right.$$

$$\left. + ijk\ell\, \gamma^2 \frac{k\ell}{a_{ik}\, a_{j\ell}} \right], \tag{4.22}$$

$$a_{ik} = 4i^2 - k^2 , \tag{4.23}$$

$$a_{j\ell} = 4j^2 - \ell^2 , \tag{4.24}$$

$$\gamma = \frac{a}{b} . \tag{4.25}$$

In quantity $b_{\ell k}$, ℓ and k change places as compared with $b_{k\ell}$. After the required operations have been performed, the second variation of the extensional potential energy of the shell (see 4.13)) takes the following shape:

$$CV_s^{sh} = 3\sum_i\sum_j A_{ij}^2 \gamma^2 \rho^2 + B_{k\ell}^2 c_1 + \sum_i\sum_j A_{ij} B_{k\ell} c_2 - 6 \frac{q}{E} \frac{\omega^4}{\rho} c_3 , \tag{4.26}$$

where

$$c_1 = 6\gamma^2 \rho^2 (13 - \frac{36}{\pi}\frac{1}{k} - \frac{36}{\pi}\frac{1}{\ell} + \frac{100}{2}\frac{1}{k\ell} , \tag{4.27}$$

$$c_2 = \frac{192}{\pi^2}\gamma^2 \rho^2 \left[\frac{1}{ij} - 2 \frac{i^2 a_{j\ell} + j^2 a_{ik} - 2 i^2 j^2}{ij a_{ik} a_{j\ell}} \right] , \tag{4.28}$$

$$c_3 = 4\sum_i \sum_j \sum_p \sum_q A_{ij} A_{pq} \frac{ijpq}{(i^2-p^2)(j^2-q^2)} + 16 \sum_i \sum_j A_{ij} B_{k\ell} \frac{ijk\ell}{a_{ik} a_{j\ell}} , \tag{4.29}$$

$$i \pm p = 3, 5, \ldots \quad j \pm q = 3, 5, \ldots \quad i,j = 1,2,3,\ldots$$

$$\rho = \frac{f}{h} , \tag{4.30}$$

$$\omega = \frac{a}{h} . \tag{4.31}$$

Second variation of the bending potential energy of the edge beams after the operations according to (4.14) have been performed:

$$C V_b^e = B_{k\ell}^2 \frac{\pi^4}{32} [\alpha \gamma k^4 + \beta \gamma^4 \ell^4] , \tag{4.32}$$

where

$$\alpha = \frac{EI_x}{B\,a} \quad , \tag{4.33}$$

$$\beta = \frac{EI_y}{B\,a} \quad , \tag{4.34}$$

Later also the following expression will be used:

$$d_1 = C\,V_b^e\,\frac{1}{B_{k\ell}^2} \quad . \tag{4.35}$$

Second variation of the extensional potential energy of the edge beams written in detail:

$$C\,V_s^e = -\frac{3\,\pi^2}{4}\,\frac{q}{E}\,\frac{\omega^4}{\rho}\,B_{k\ell}^2\left[\frac{1}{2}\,(k^2+\ell^2) - \frac{4}{\pi^2}\right] \quad . \tag{4.36}$$

Hereinafter we refer to the following expression:

$$e_1 = C\,V_s^e\,\frac{1}{B_{k\ell}^2} \quad . \tag{4.37}$$

4.2 Buckling of the shell

In this actual case, condition (4.17) takes the following shape:

$$\frac{\partial V}{\partial A_{ij}} = 0 \quad . \tag{4.38}$$

The equation below follows from (4.38):

$$\overline{a}_{11} = A_{ij}\left[\frac{\pi^4}{4}\left(\frac{i^2}{\gamma^2}+j^2\right)^2\gamma^4 + 6\,\gamma^2\,\rho^2\right] - 48\,\frac{q}{E}\,\frac{\omega^4}{\rho}\sum_{p}\sum_{q} A_{pq}\,\frac{i\,j\,p\,q}{(i^2-p^2)(j^2-q^2)} = 0 \quad . \tag{4.39}$$

$$i \pm p = 3,5,\ldots \qquad j \pm q = 3,5,\ldots \qquad i,j = 1,2,3,\ldots$$

The linear equation system according to (4.39) can be divided in two groups. i + j is even number in the first group while odd number in the other group.

It is easy to recognize that equation system (4.39) is exactly identical with Ralston's /13/ equation system /15/ set up by use of the Galerkin method. Accordingly, with the eigenvalues of equation system (4.39) de-

termined, then the lower enveloping straight line of the appropriate "garland" curve taken, relationship (3.16) would be obtained (with $\mu = \emptyset$).

The Bleich-Salvadori hypothesis (par 2, Eq. (4.6 a-c)) is true in this case as has been proved again by what has been said above since the process ignoring this hypothesis /13/ also leads to results identical with (4.39).

It can also be seen that negligence of the transverse contraction factor ($\mu = \emptyset$) results in a negligible error that can be corrected subsequently as follows from (3.16) accordingly.

Of course, Eq. (4.39) is not solved here since the solution is known.

Also, we omit to investigate the effect of deformations of the edge beam modifying the critical branching load (Eq. (3.16)) of the shell by use of the process according to par 4.13. We can do so all the more because /2, 3 and 11/ showed that the linear critical buckling load of the shell was only slightly affected by the boundary condition. This can be attributed to the fact that the buckling mode of the hypar is, according to /11/, page 112, similar to that seen in the middle of Fig. 2 ($\bar{w}_{sh}$).

The results according to pars 4.3 and 5 (that is (4.51) and (5.4)), respectively, can not be taken over to (3.16) for reasons similar to what has been said in par 3.3.

4.3 Buckling of edge beam

Ritz's equation

$$\frac{\partial V}{\partial B_{k\ell}} = 0 \tag{4.40}$$

complying with variation conditions (4.17) can be briefly written, as follows:

$$a_{22} = 2(b_1 + c_1 + d_1 + e_1) = 0 \ . \tag{4.41}$$

The quantities included in the formula are given in relationships (4.20), (4.27), (4.35), (4.37). After substitution and reduction, the function of the critical load of the edge beam is defined by the following expression:

$$\frac{q_{cr}}{E} = \frac{\pi^2}{24} \frac{1}{f_{k\ell}} \frac{\rho}{\omega^4} \left\{ \left[\alpha \gamma k^4 + \beta \gamma^4 \ell^4 \right] + \frac{32}{\pi^4} (b_1 + c_1) \right\}, \tag{4.42}$$

where

$$f_{k\ell} = \frac{1}{2}(k^2 + \ell^2) - \frac{4}{\pi^2} . \qquad (4.43)$$

Equation (4.42) is valid for k, ℓ = 1, 5, 9, ... (while some modification is required for k, ℓ = 3, 7, ...).

For a hypar over a square ground plan (γ = a/b =1) with symmetrical edge beam configuration ($I_x = I_y = I$), the following equation has been obtained for k = ℓ = 1:

$$\frac{q_{cr}}{E} = \frac{\rho}{\omega^4}\left[1.3830\alpha + 0.2914\varrho^2\right. . \qquad (4.44)$$

Using equation (3.7), the critical tangential shearing force corresponding to surface load q_{cr}:

$$N_{xycr} = \frac{1}{2} E a \frac{1}{\omega^3}\left[1.3830\alpha + 0.2914\varrho^2\right. . \qquad (4.45)$$

In the present case, it was practicable to determine N_{xycr} associated with k = 1 (see par 3.4), then to produce foundation rigidity u (4.50) associated with it. The reason for this is that the error of the approximate one-term solution (broken line) of the accurate 'garland' curve (b in Fig. 4) of the simple cantilever on elastic foundation is minimum in domain u associated with k = 1. Accordingly, the value so calculated for foundation parameter u associated with the accurate curve u will be best suited.

Like in par 3.4, approximate method is used to determine foundation rigidity parameter u expressing the stiffening effect of the shell for accurate solutions taken from /10/ (see Figs 3, 4). This is considered to be justified considering the ample work required for what has been discussed so far.

Hereinafter we rely upon the results produced in /10/ and illustrated in Fig. 4 (cf. par 3.4). These results give critical load parameter λ_{cr} or specific critical distributed load p_{cr} of the simple cantilever of length ℓ on Winkler's translational foundation (u (3.9)). P_{crE} is Euler's critical force (buckling load) of the two-hinged bar (Eq. (3.20)).

Also an approximate method has been produced by means of the Ritz method in /10/ with the one-term buckling mode taken as a basis (broken line in Fig. 4).

One-term approximate basic function:

$$w = w_k \left(1 - \cos \frac{k\pi}{2\ell} x\right) . \tag{4.46}$$

$$k = 1,3,5,\ldots$$

Parameter of the total critical load:

$$\lambda_{cr} = \frac{p_{cr}\ell}{P_{crE}} \approx \frac{1}{2} \frac{k^4 + \frac{32}{\pi 4}\left(\frac{3}{2} + \varkappa \frac{4}{\pi k}\right) u^2}{k^2 - \frac{4}{\pi^2}} . \tag{4.47}$$

$$k = 1,3,5,\ldots$$

$$\varkappa = -1 \quad \text{if} \quad k = 1,5,9,\ldots$$

$$\varkappa = 1 \quad \text{if} \quad k = 3,7,11,\ldots$$

u and P_{crE} are defined by Eq. (3.19) and (3.20), respectively.

Broken line has been used in Fig. 4 to illustrate equation (4.47) in such a way that 0.4722 is used in place of $\frac{1}{2}$ as a multiplier (for the sake of transition to the accurate solution of case $u = \emptyset$).

In the above relationships, the critical value of specific tangential shearing force N_{xy} (3.7) corresponds to specific critical distributed load p_{cr}. Similarly, $\ell \approx a$ in case of a sufficiently flat structure, otherwise the length ℓ is the actual length of the edge beam.

On the basis of what has been said above, let first equality

$$p_{cr} = \lambda_{cr} P_{crE} \frac{1}{\ell} = N_{xycr} \tag{4.48}$$

be written. On the basis of (4.47), we obtain

$$p_{cr} = 0.6915\ Ea \frac{\alpha}{\omega^3} (1 + 0.07449\ u^2) \tag{4.49}$$

for $k = 1$.

With relationships (4.45) and (4.49) substituted into (4.48), the wanted foundation rigidity parameter, u, is obtained for use:

$$u = 1.682 \frac{\rho}{\sqrt{\alpha}} . \tag{4.50}$$

With this compared with (3.26), the cantilever edge beam was found to be much less stiffened by the shell than the two-hinged edge beam.

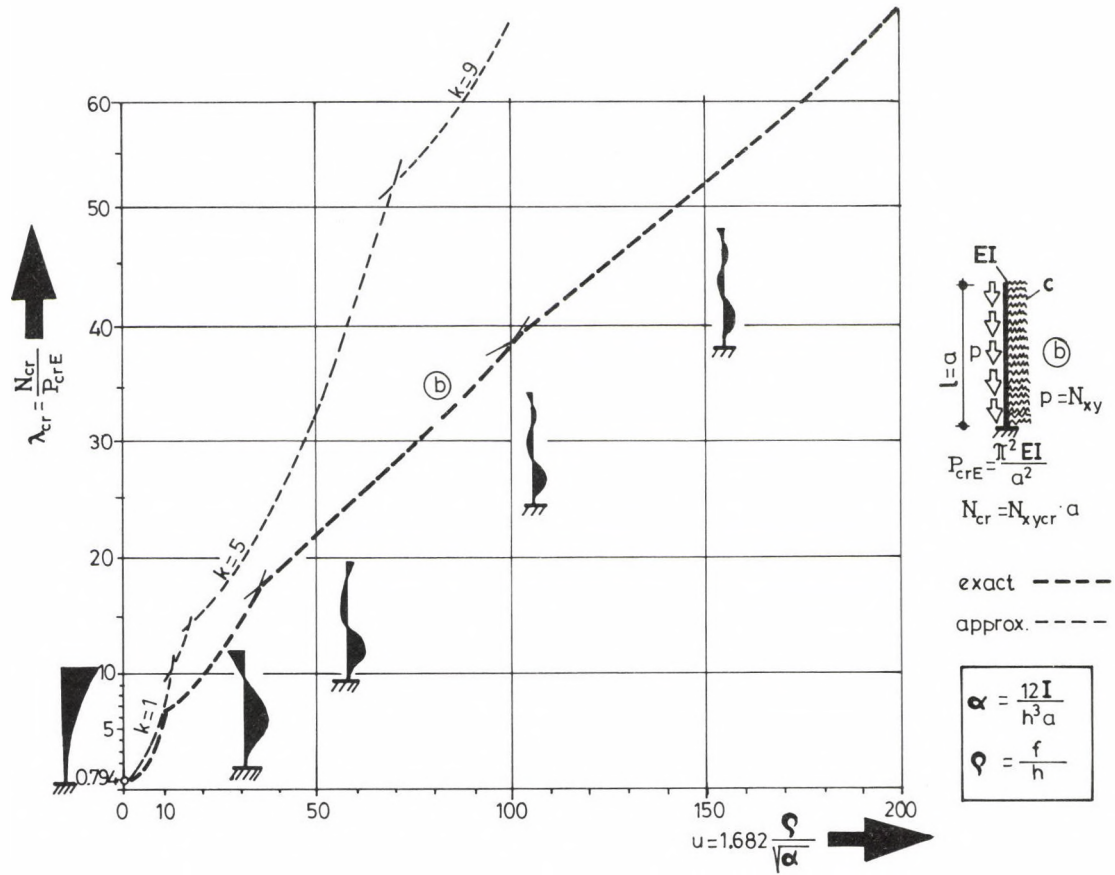

Fig. 4. Critical load parameters of cantilever

The critical load of the buckling edge beam, N_{xycr}, can be determined very simply using formulae (3.11), (3.12), (4.50) as well as Fig. 4.

Critical eigenvalue parameter $\lambda_{cr} = \lambda(u)$ supplies specific critical load p_{cr} according to the left side of Eq. (4.48). Thus the critical value N_{xycr} in expression (3.7) is equal to p_{cr}:

$$N_{xycr} = p_{cr} . \tag{4.51}$$

Surface load q_{cr} shell be calculated according to (3.7). Note that, in certain cases, the approximate formula for function b of Fig. 4 can be successfully used:

$$\lambda_{cr} \approx 0.794 + 0.0535\, u^2 , \tag{4.52a}$$

$$0 \leqslant u \leqslant 10$$

$$\lambda_{cr} \approx 6.14 + 0.4327\,(u-10) , \tag{4.52b}$$

$$10 \leqslant u \leqslant 40$$

$$\lambda_{cr} \approx 19.12 + 0.2985\,(u-40) . \tag{4.52c}$$

$$40 < u \leqslant 200$$

Figure 5 has been produced for small values of foundation parameter u (short rigid bar or/and soft foundation).

The comparative Figure 6 has been taken from /10/. In that work, we explained in detail that the load bearing capacity of bars of different boundary condition (a, b, c) was essentially determined by the conditions of support of the lower edge (lying in the direction of load).

This explains the higher critical load of the cantilever in domain $u > 5$ as compared with the two-hinged bar according to Fig. 6. Of course, this true only in case of identical values of u. As a matter of fact, one can not say that, in case of a hypar, the cantilever edge beam is stronger. According to our engineering view, the contrary is true as clearly shown by (3.26) and (4.50) according to which the cantilever is less stiffened by the shell than the two-hinged bar. This can be clearly seen also in Fig. 7 indicating our final relationships recommended for use in practice.

5. Recommendations

Use of the following, rather simple relationships is recommended in practice (Fig. 7).

5.1 Two-hinged bar

Curve a in Figure 3, plotted as a function of $\rho/\sqrt{\alpha}$, has been transformed using formula (3.26). Then, with the lower enveloping straight line of the curve (which is almost a straight line determined, the following expression has been obtained for calculation of the critical load parameter:

$$\lambda_{cr} = 1.881 + 0.846 \frac{\rho}{\sqrt{\alpha}} . \tag{5.1}$$

Equation of the critical surface load (by means of (3.23) and (3.7)

$$\frac{q_{cr}}{E} = \frac{\rho}{\omega 4} (3.094\ \alpha + 1.391\ \rho\sqrt{\alpha}) . \tag{5.2}$$

Here α, ρ, ω are parameters according to (3.10) thru (3.12).

5.2 Cantilever

With curve b in Fig. 4 transformed in the way outlined in par 5.1 transformed using relationship (4.50), the equation of the lower enveloping straight line has been obtained as

$$\lambda_{cr} = 0.794 + 0.629 \frac{\rho}{\sqrt{\alpha}} . \tag{5.3}$$

Formula of the critical surface load (by means of (4.48) and (3.7):

$$\frac{q_{cr}}{E} = \frac{\rho}{\omega 4} (1.306\ \alpha + 1.035\ \rho\sqrt{\alpha}) . \tag{5.4}$$

6. Numerical results

Leet /12/ used plastic specimens to determine the critical load of two-hinged and cantilever edge beam experimentally. Specimen No. 5 used by Leet is suited to simulate our case. Specifications:

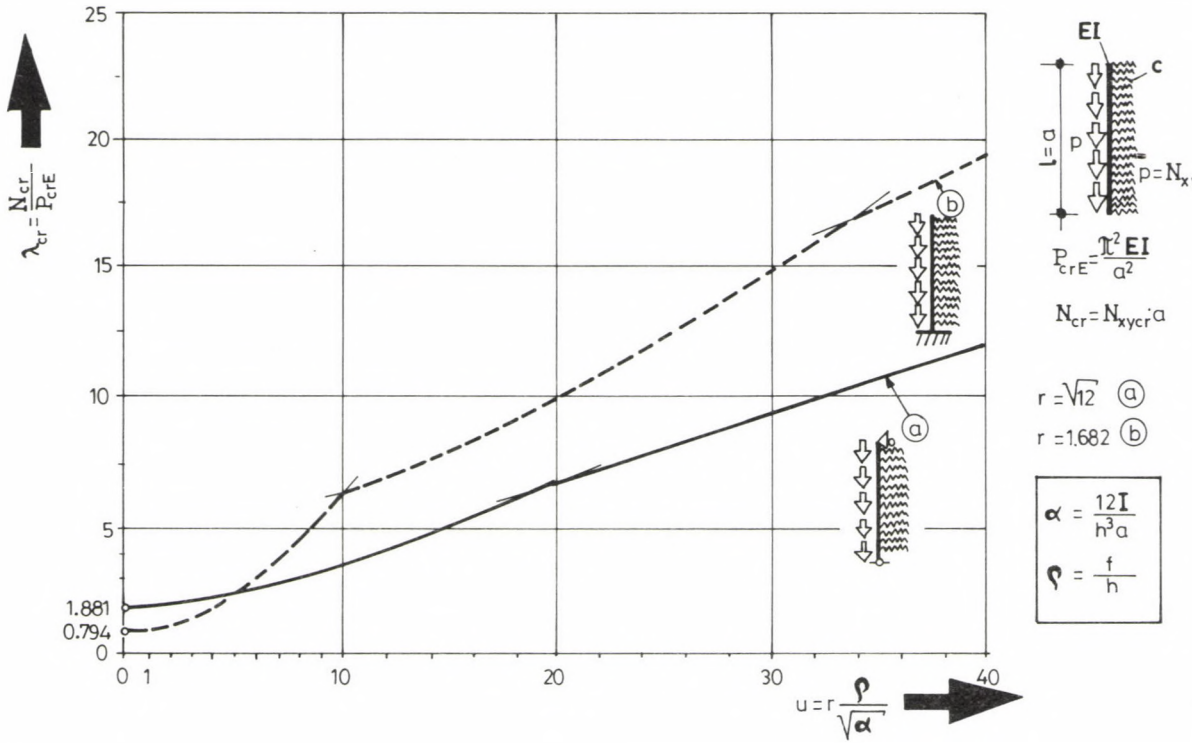

Fig. 5. Soft elastic foundation

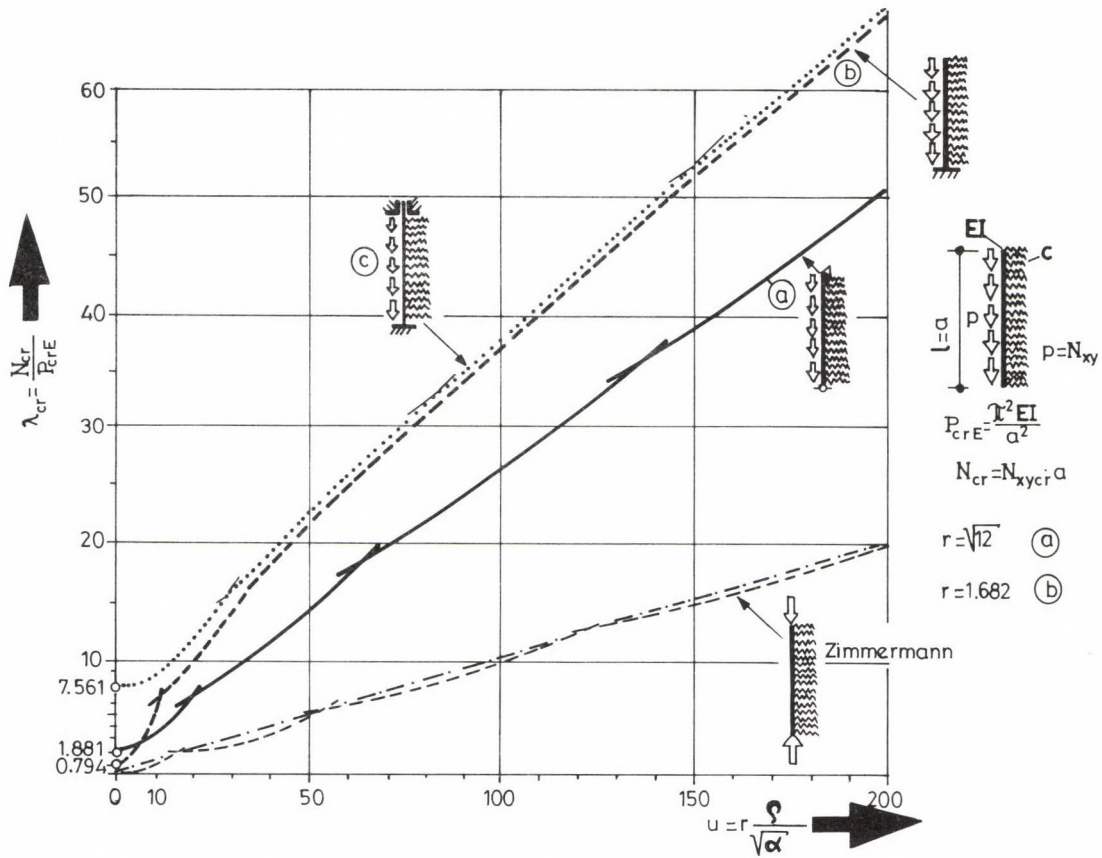

Fig. 6. Critical load parameters of beams of different boundary conditions

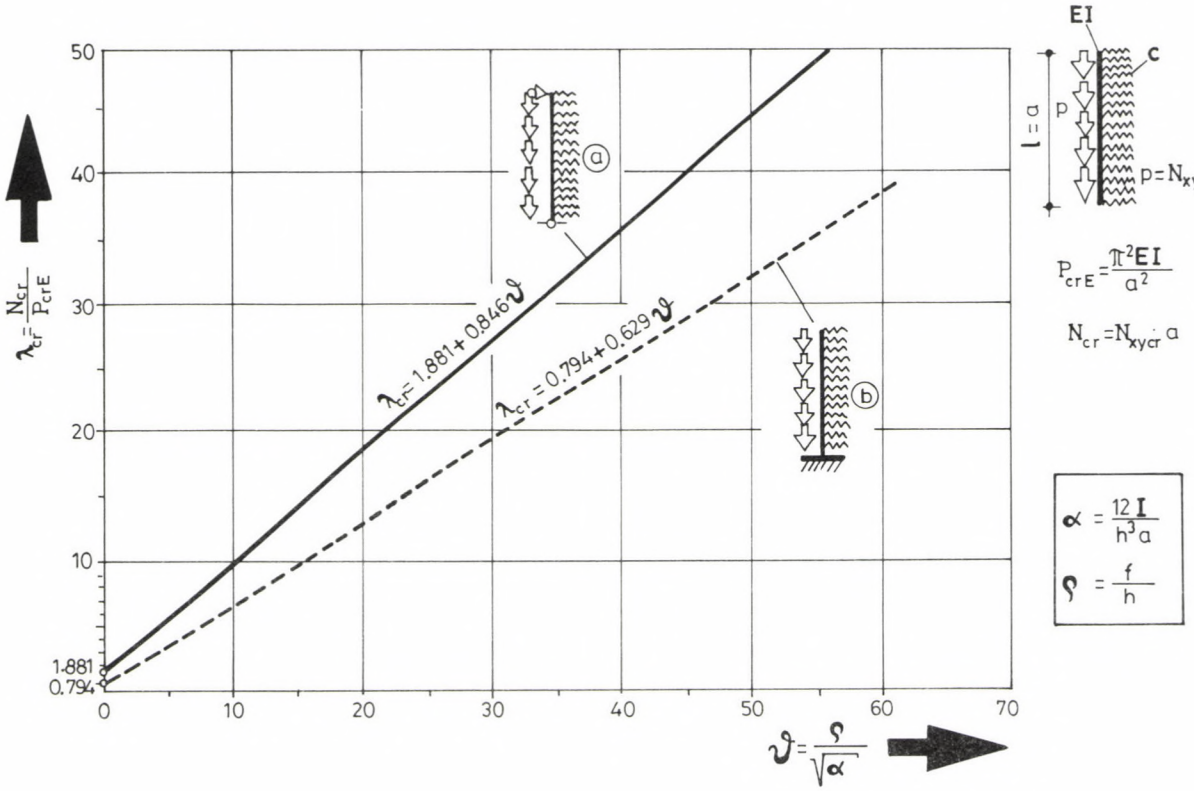

Fig. 7. Recommended design diagrams

$a = b = 16$ inch $= 406.4$ mm,

$f = 4$ inch $= 101.6$ mm,

$h = 0.0305$ inch $= 0.7747$ mm,

$I_x = I_y = I = 1.33\ 10^{-3}$ inch^4 $= 553.6$ mm^4 .

As can be read from Figs 19 and 20 of /12/, the ratio of critical loads of the cantilever and two-hinged edge beam is 95/146 = 0.65.

Of course, the experimental results contain effects which have not been taken into consideration in our calculations, such as geometrical imperfection, relatively large deformations, rigidities of the bar left out of consideration,etc. Note that at points A and D in Fig. 2, the support of the specimens was somewhat stronger in case of the hinged bar.

Leet used essentially an edge beam supported at point B of Fig. 2 ("supported") and one with free end at point B ("cantilever").

On the basis of what has been said above, it seems reasonable to compare the ratio of critical loads instead of the actual values in our case.

Parameters used in our work:

$$(3.10) \quad \alpha = 35.157,$$

$$(3.11) \quad \rho = 131.148,$$

$$(3.12) \quad \omega = 524.59.$$

Critical load parameter of the two-hinged edge beam:

$$(5.1) \quad \lambda_{cr} = 20.59.$$

Critical load parameter of the cantilever:

$$(5.3) \quad \lambda_{cr} = 14.71.$$

Ratio of critical loads: 14.71/20.59 = 0.71.

Considering that experimental value 0.65 contains also the distorting effects mentioned (e.g. geometrical imperfection,etc.), the ratio, between the theoretical and experimental value (0.71 and 0.65, respectively) is considered to be satisfactory.

ACKNOWLEDGEMENT

The research leading to this paper was supported by a grant of the National Scientific Research Council of Hungary (OTKA 684).

REFERENCES

1. Dayaratnam, P.-Gerstle, K.H.: Buckling of hyperbolic paraboloids. World Conference on Shell Structures, San Francisco, 1962, 289-296
2. Dulácska, E.: Stability of anisotropic hyperbolic paraboloid shells. Acta Techn. Acad. Sci. Hung. 59, 1967, 123-130
3. Dulácska, E.: Vibration and stability of anisotropic shallow shells. Acta Techn. Acad. Sci. Hung. 65, 1969, 225-260
4. Fischer, M.: Das Beulproblem der flachen, orthotropen, hyperbolischen Paraboloidschale. Der Stahlbau, 1974, 52-61
5. Gergely, P.: Buckling of orthotropic hyperbolic paraboloid shells. Journ. Struct. Div. (Proc. ASCE) 98, 1972, 395-399
6. Gioncu, V.-Ivan, M.: Instabilitatea Structurilor din Plâci Curbe Subţiri. (Buckling of shell structures.) Ed. Acad. Rep. Soc. Romania 1978
7. Gioncu, V.: Thin reinforced concrete shells. Ed. Acad. Rep. Soc. Romania - J. Willey, Chichester, Toronto 1979
8. Hruban, K.: Die Biegetheorie der Translationsflächen und ihre Anwendung im Hallenbau. Acta Techn. Acad. Sci. Hung. 7, 1953, 425-464
9. Jankó, L.: Buckling a of cantilever on elastic foundation loaded on top by concentrated force. Acta Techn. Acad. Sci. Hung. 104/1-2, (1991) 147-158
10. Jankó, L.: Buckling of bars on elastic foundation subjected to uniformly distributed axial loads. Acta Techn. Acad. Sci. Hung. 104/1-2, (1991) 125-145
11. Kollár, L.-Dulácska, E.: Buckling of shells for engineers. Akadémiai Kiadó, Budapest 1984
12. Leet, K.M.: Study of stability in the hyperbolic paraboloid. Journ. Eng. Mech. Divis. (Proc. ASCE) 92, 1966, 121-142
13. Ralston, A.: On the problem of buckling of a hyperbolic paraboloidal shell loaded by its own weight. Journ. Math. Phys. 35, 1956, 53-59
14. Reissner, E.: On some aspects of the theory of thin elastic shells. Journ. Boston Soc. Civil Eng. 17, 1955, 100-133
15. Timoshenko, S.P., Gere, J.M.: Theory of elastic stability. McGraw-Hill Book Company, New York, Toronto, London, 1961
16. Wolmir, A.S.. Biegsame Platten und Schalen. VEB Verlag für Bauwesen, Berlin 1962

Acta Technica Acad.Sci.Hung., 104(1-3), pp. 187-209 (1991/92)

CALCULATION OF PLANE FRAMES BRACED BY SHEAR WALLS FOR SEISMIC LOAD

KOLLÁR, L.P.*

(Received: 25 July 1990)

The paper investigates the vibration of the continuum model of plane frames braced by shear walls. It presents charts and tables with the aid of which the seismic load and the initial stresses of frames and shear walls due to earthquakes can be calculated.

1. Introduction

The determination of seismic loads is even in case of simple structures very complicated. Using a continuum model of frames and braced frames, relatively simple results can be derived. The aim of this paper is to determine some charts and numerical tables with the aid of which the continuum model of braced frames can be analyzed.

2. The investigated model

A replacement continuum for braced frames could be a sandwich column with thick faces /8, 9, 11/, nevertheless in many cases simpler models can be accurate enough. For example /1/, introduces the following four bar models for the investigation of multi storey buildings:

1) Simple bar having flexural deformation only (Fig. 1a). This can be the model of a (high and solid) shear wall.

2) Simple bar having shearing deformation only (Fig. 1b). This can be the model of a multi storey plane frame.

3) Bar having shearing and flexural deformation as well (Fig. 1c). This can be the model of coupled shear walls.

*Kollár, László, H-1122 Budapest, Karap u. 9, Hungary

Akadémiai Kiadó, Budapest

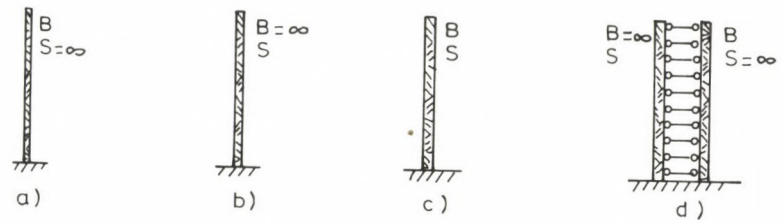

Fig. 1. Bar models used in the analysis of buildings

4) Bar consists of a bar having shearing, and another having flexural deformation only (Fig. 1d). This can be the model of frames braced by shear walls.

All these models can be derived from the general three-layer sandwich bar with thick faces /9/.

In this paper the fourth model will be treated. This model was first introduced by P. Csonka /6/ for the analysis of multi storey frames, hence it is called 'Csonka-type bar'.

The determination of the rigidities of the replacement bar can be found e.g. in /1, 7, 10/.

The bending rigidity (EI) in this paper will be denoted by B, the shearing rigidity (AG/n) by S. The bars having flexural deformation only will be called B-bars, and those having shearing deformation only will be called S-bars. The Csonka-type bar consists of a B-, and an S-bar connected to each other in a way that the displacements of the two bars are the same.

3. Basic expressions for calculation of seismic load

A widespread approximate method for the investigation of seismic load the 'Response Modal Analysis' /1, 5/, which is used in many standards (e.g. in DIN 4149 /1/, or in the Hungarian directive /4/). The Response Modal Analysis splits the calculation into two steps: first the 'Response-Spectrum' is analyzed with the simplest hounting model, which is a single mass on a cantilever beam, then this result is applied for the model of the building, which is - as a rule - a discrete model with multi degree of freedom.

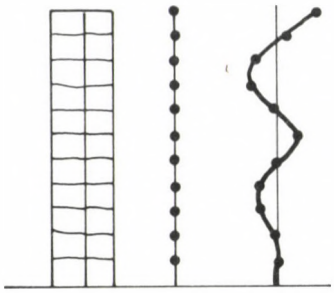

Fig. 2. Discrete model and the i-th mode of vibration of a frame

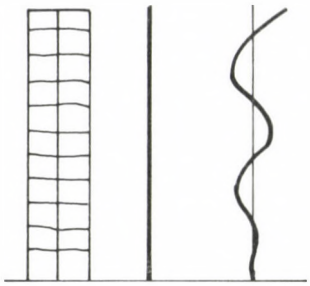

Fig. 3. Continuum model and the i-th mode of vibration of a frame

The build-up of the expression for the horizontal loads on this discrete model of a structure due to the i-th normal mode of vibration is the following /1/ (Fig. 2):

$$H_{j,i} = K\, m_j\, \rho\, \psi_{j,i} \frac{\sum_{k=1}^{n} m_k\, \psi_{k,i}}{\sum_{k=1}^{n} m_k\, \psi_{k,i}^2}\, \beta_i\,, \tag{3.1}$$

where

$H_{j,i}$ - is the force acting on the j-th mass point,

K - is a multiplicator depends on the geographic area, on the soil, on the ductility of the structure, etc.,

m_j - is themass of the j-th point,

ρ - is the acceleration of gravity,

$\psi_{j,i}$ - is the horizontal displacement of the j-th point due to the i-th mode of vibration,

n - is the number of mass points,

β_i - is the value of the normed response spectrum, which depends on the naturalperiod of vibration T_i.

In the case of a continuum model (Fig. 3), with uniform distribution of mass Eq. (3.1) becomes the following expression:

$$H_i(x) = K\, m\, \rho\, w_i(x) \frac{\int_0^H w_i(x)}{\int_0^H w_i^2(x)}\, \beta_i\,, \tag{3.2}$$

where

$H_i(x)$ - is a distributed horizontal load due to the i-th mode of vibration,

m - is the mass of the unit length of the building,

$w_i(x)$ - is the i-th mode of vibration.

Expression (3.2) does not depend on the magnitude of the mode of vibration.

In the following normed modes of vibration denoted by $\overline{w}_i(x)$ are used, that is, the top displacements are considered the unit. Also introducing the following notation

$$\phi_i = \frac{\int_0^1 \overline{w}_i(\xi)}{\int_0^1 \overline{w}_i^2(\xi)} , \tag{3.3}$$

where $\xi = \frac{x}{H}$, we obtain from (3.2):

$$H_i(\xi) = K\, m\, \rho\, \phi_i\, \beta_i\, \overline{w}_i(\xi) . \tag{3.4}$$

In the following sections we will determine $\overline{w}_i(x)$, ϕ_i, T_i (the last one for calculating β_i), and some other parameters for the determination of bending moment and shearing force diagrams of the replacement bar of braced frames.

4. The basic differential equation and its solution

The equilibrium equation of horizontal forces acting on a 'Csonka-type' bar is /8/

$$B\, w''''(x) - S\, w''(x) - m\, \omega^2\, w(x) = 0 , \tag{4.1}$$

which is a homogeneous differential equation of the forth order. The last term contains the D'Alembert force,

$$\omega = \frac{2\pi}{T} , \tag{4.2}$$

this is the circular frequency. ( )' denotes the derivation with respect to x.

The bending moment, and the shearing force on the component B-bar (bar having flexural deformation only):

$$M_B(x) = -B\, w''(x) \,, \tag{4.3}$$

$$Q_B(x) = -B\, w'''(x) \tag{4.4}$$

and those on the S-bar (bar having shearing deformation only) /8/:

$$M_S(x) = M_0 + S\, w(x) \,, \tag{4.5}$$

$$Q_S(x) = S\, w'(x) \,, \tag{4.6}$$

The boundary conditions are as follows:

$$w(H) = 0 \,, \tag{4.7a}$$

$$w'(H) = 0 \,, \tag{4.7b}$$

$$M_B(0) = 0 \,, \quad \text{i.e.} \quad w''(0) = 0 \,, \tag{4.7c}$$

$$Q_B(0) + Q_S(0) = 0 \,, \quad \text{i.e.} \quad -B\, w'''(0) + S\, w'(0) = 0 \,. \tag{4.7d}$$

$$M_S(0) = 0 \,, \quad \text{i.e.} \quad M_0 + S\, w(0) = 0 \,. \tag{4.8}$$

The general solution of Eq. (4.1) is the sum of two trigonometrical and hyperbolic functions, however, to obtain a numerically stable solution the following form is more usable:

$$w(\xi) = C_1 e^{-\lambda_1 \xi} + C_2 e^{-\lambda_1 (1-\xi)} + C_3 \cos(\lambda_2 \xi) + C_4 \sin(\lambda_2 \xi) \,, \tag{4.9}$$

where λ_1 and λ_2 can be calculated from the roots of the characteristic equation

$$\frac{B}{H^4}\,\lambda^4 - \frac{S}{H^2}\,\lambda^2 - m\,\omega^2 = 0$$

as follows:

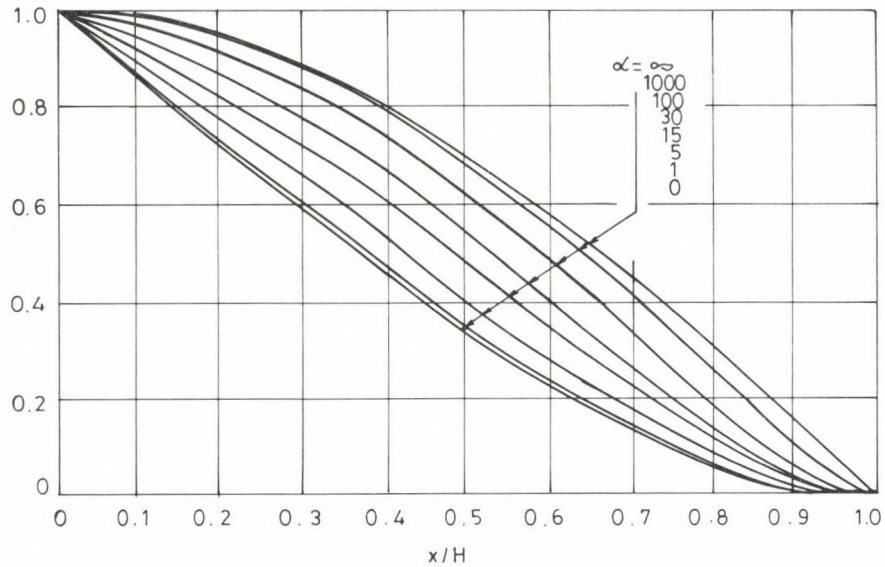
1.0
0.8
0.6
0.4
0.2
0
0 0.1 0.2 0.3 0.4 0.5 0.6 0.7 0.8 0.9 1.0
x/H
α = ∞
1000
100
30
15
5
1
0

Fig. 4a.

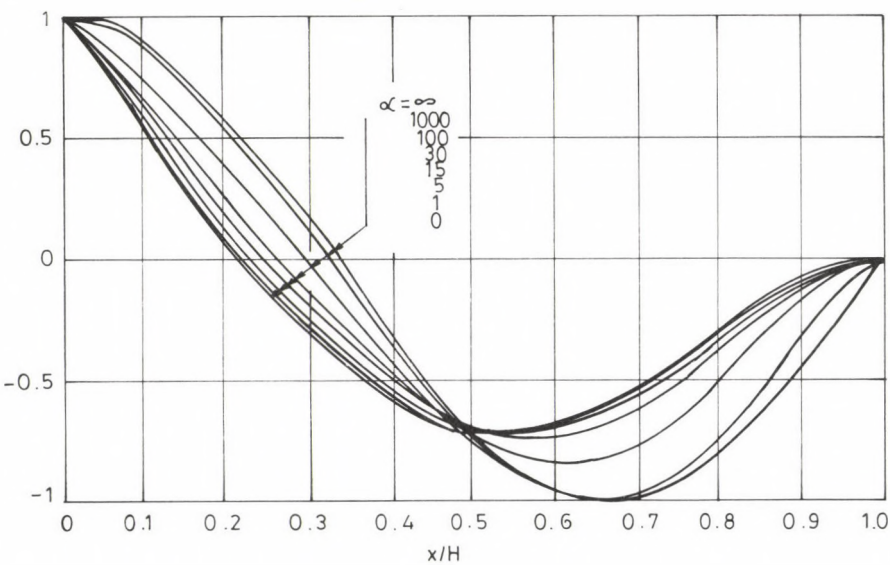
1
0.5
0
-0.5
-1
0 0.1 0.2 0.3 0.4 0.5 0.6 0.7 0.8 0.9 1.0
x/H
α = ∞
1000
100
30
15
5
1
0

Fig. 4b.

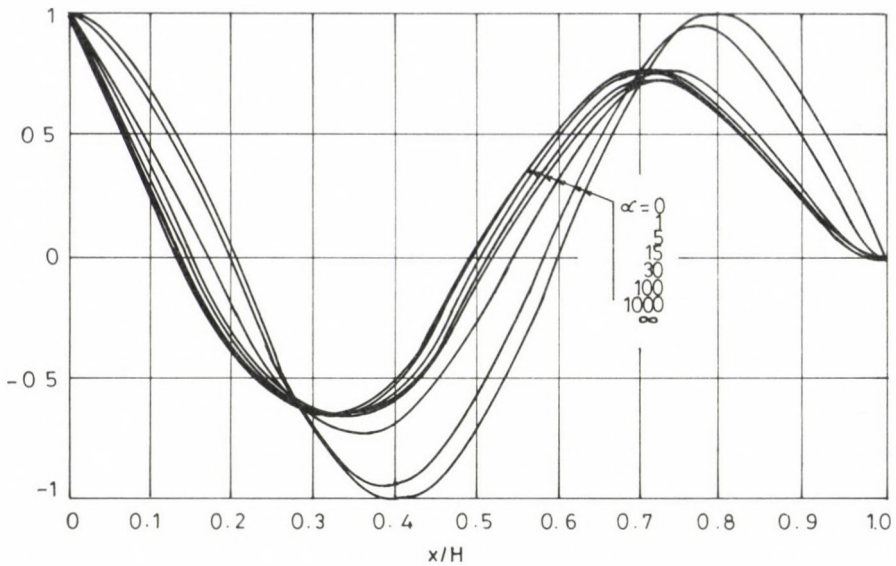

Fig. 4c.

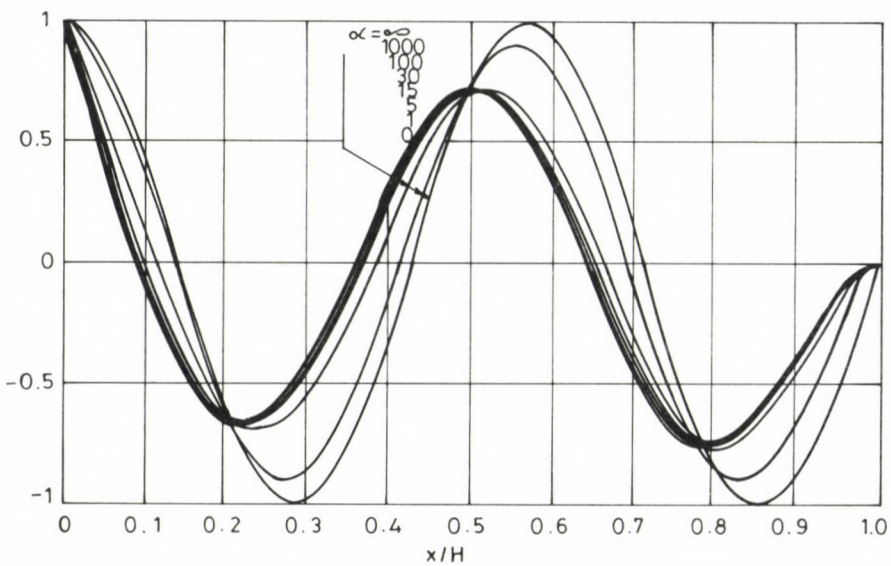

Fig. 4d.

Fig. 4. Modes of vibration $\bar{w}_i(\xi)$ (These functions are necessary for the calculation of the load in expression (3.4). a) i = 1; b) i = 2; c) i = 3; d) i = 4)

$$\lambda_1 = \sqrt{\frac{\alpha}{2} + \sqrt{\frac{\alpha^2}{4} + \frac{m\omega^2 H^4}{B}}}\,, \tag{4.10}$$

$$\lambda_2 = \sqrt{-\frac{\alpha}{2} + \sqrt{\frac{\alpha^2}{4} + \frac{m\omega^2 H^4}{B}}}\,. \tag{4.11}$$

In these expressions

$$\alpha = \frac{S H^2}{B}\,. \tag{4.12}$$

M_0 can be determined from Eq. (4.8), and (4.7a-d) constitute a homogeneous linear equation system for C_1, C_2, C_3, and C_4. The condition for non-trivial solution is the singularity of the coefficient matrix, which means a non-linear equation for ω. After the determination of ω (or T), the ratio of C_1, C_2, C_3, and C_4 can be calculated and, assuming that the displacement at x = 0 equals to the unity, also their absolute values. We made this calculation for 8 different values of ω, for the first four modes of vibration. The modes of vibration are plotted in Figs 4a-d, the period of vibration can be calculated from the following expression:

$$T = \frac{2\pi H}{c}\sqrt{\frac{m}{B}} = \frac{2\pi H\sqrt{\alpha}}{c}\sqrt{\frac{m}{S}}\,. \tag{4.13}$$

c and $c/\sqrt{\alpha}$ can be found in Table 1.

Table 1

Values of c for the calculation of T in expression (4.13)

i/α	10^{-8}	1	5	15	30	100	1000	10^{9}
1	3.516	4.110	5.768	8.250	10.688	17.611	51.354	49.670
2	22.035	22.757	25.406	30.839	37.157	56.499	155.479	149.020
3	61.697	62.321	64.751	70.432	78.071	105.501	263.774	248.370
4	120.902	121.491	123.821	129.453	137.433	169.149	378.787	347.720

Values of $c/\sqrt{\alpha}$ for the calculation of T in expression (4.13)

1/α	10^{-8}	1	5	15	30	100	1000	10^{9}
1	111.200	4.110	2.580	2.130	1.951	1.761	1.624	1.571
2	696.800	22.757	11.362	7.963	6.784	5.650	4.917	4.713
3	1.951.000	62.321	28.958	18.185	14.254	10.550	8.341	7.854
4	3.823.300	121.491	55.374	33.425	25.092	16.915	11.978	10.996

If $\alpha < 10^{-3}$ then the bar can be considered as if it were a B-bar (bar having flexural rigidity only) and if $\alpha > 10^{5}$ then the bar can be considered as if it were an S-bar (bar having shearing deformation only). In the second case the modes of vibration are

$$\bar{w}_i(\xi) = \cos\left(\frac{\pi(2i-1)}{4}\xi\right). \qquad (4.14)$$

5. The internal forces

For the analysis of the internal forces the values of ϕ_i should be calculated. These are given in Table 2. The loads are carried partly by the B-, and partly by the S-bar. The loads carried by the S-bar will be given by expression (5.6). It has to be mentioned, that a concentrated force acts on the top between the S- and B-bar, the value of which is equal to the shearing force on the top of the B-bar.

Table 2

Values of ϕ for the calculation of the load in the expression (3.4)

i/α	10^{-8}	1	5	15	30	100	1000	10^{9}
1	1.566	1.552	1.506	1.434	1.381	1.315	1.278	1.273
2	0.868	0.853	0.801	0.716	0.644	0.530	0.438	0.425
3	0.509	0.507	0.501	0.483	0.459	0.386	0.277	0.255
4	0.364	0.363	0.362	0.357	0.348	0.312	0.211	0.182

Table 3

The values of M_{Bi} in the expression (5.1)

1/α	10^{-8}	1	5	15	30	100	1000	10^{9}
1	0.2844	0.2306	0.1567	0.1124	0.0893	0.0560	0.0194	0.0000
2	0.0454	0.0430	0.0363	0.0283	0.0233	0.0162	0.0064	0.0000
3	0.0162	0.0159	0.0149	0.0131	0.0113	0.0083	0.0037	0.0000
4	0.0083	0.0082	0.0079	0.0073	0.0067	0.0051	0.0025	0.0000

Table 3 (cont.)
The values of $M_{Bi}\sqrt{\alpha}$ in the expression (5.1)

i/α	10^{-8}	1	5	15	30	100	1000	10^{9}
1	0.0000	0.2306	0.3505	0.4353	0.4893	0.5597	0.6150	0.6366
2	0.0000	0.0430	0.0812	0.1096	0.1278	0.1621	0.2011	0.2122
3	0.0000	0.0159	0.0333	0.0506	0.0621	0.0828	0.1164	0.1273
4	0.0000	0.0082	0.0177	0.0284	0.0366	0.0513	0.0792	0.0909

First the internal forces on the B-bar are determined. The bending moment (taking the expression of the load in Eq. (4.1) and in Eq. (3.4) into consideration) is as follows:

$$M_{Bi}(\xi) = -B\, w_i''(x) = -\frac{B}{H^2}\, w_i^{\cdot\cdot}(\xi) = -K\, m\, \rho\, \phi_i\, \beta_i\, H^2 \frac{\overline{w}_i^{\cdot\cdot}(\xi)}{c_i^2} =$$

$$= -K\, m\, \rho\, \phi_i\, \beta_i\, H^2\, M_{Bi}\, m_{Bi}(\xi) =$$

$$= -K\, m\, \rho\, \phi_i\, \beta_i\, H \sqrt{\frac{B}{S}} \left(M_{Bi}\sqrt{\alpha} \right) m_{Bi}(\xi) \qquad (5.1)$$

where ( ) denotes the derivation with respect to ξ.

The values of M_{Bi} and $M_{Bi}\sqrt{\alpha}$ are given in Table 3, the diagrams of $m_{Bi}(\xi)$ are seen in Figs 5a-d. The function of the shearing force on the B-bar is:

$$Q_{Bi}(\xi) = -B\, w_i'''(x) = -\frac{B}{H^3}\, w_i^{\cdot\cdot\cdot}(\xi) = -K\, m\, \rho\, \phi_i\, \beta_i\, H \frac{\overline{w}_i^{\cdot\cdot\cdot}(\xi)}{c_i^2} =$$

$$= -K\, m\, \rho\, \phi_i\, \beta_i\, H\, Q_{Bi}\, q_{Bi}(\xi)\,. \qquad (5.2)$$

The values of Q_{Bi} and are given in Table 4, the diagrams of $q_{Bi}(\xi)$ are shown in Figs 6a-d.

The internal forces on the S-bar are as follows. The bending moment:

$$M_{Si}(\xi) = -S\, w_i(0) + S\, w_i(x) = K\, m\, \rho\, \phi_i\, \beta_i\, H^4 \frac{S}{B}\frac{1}{c_i^2} \left(\overline{w}_i(\xi) - 1 \right) \qquad (5.3)$$

The diagrams of $\overline{w}_i(\xi)$ are presented in Figs 4a-d.

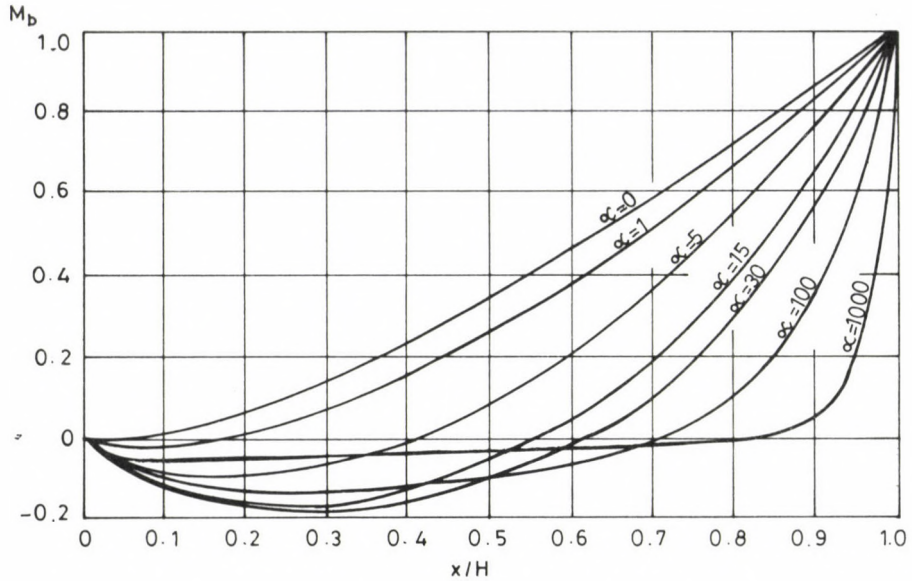
M_b
1.0
0.8
0.6
0.4
0.2
0
-0.2
0 0.1 0.2 0.3 0.4 0.5 0.6 0.7 0.8 0.9 1.0
x/H
α=0
α=1
α=5
α=15
α=30
α=100
α=1000

Fig. 5a.

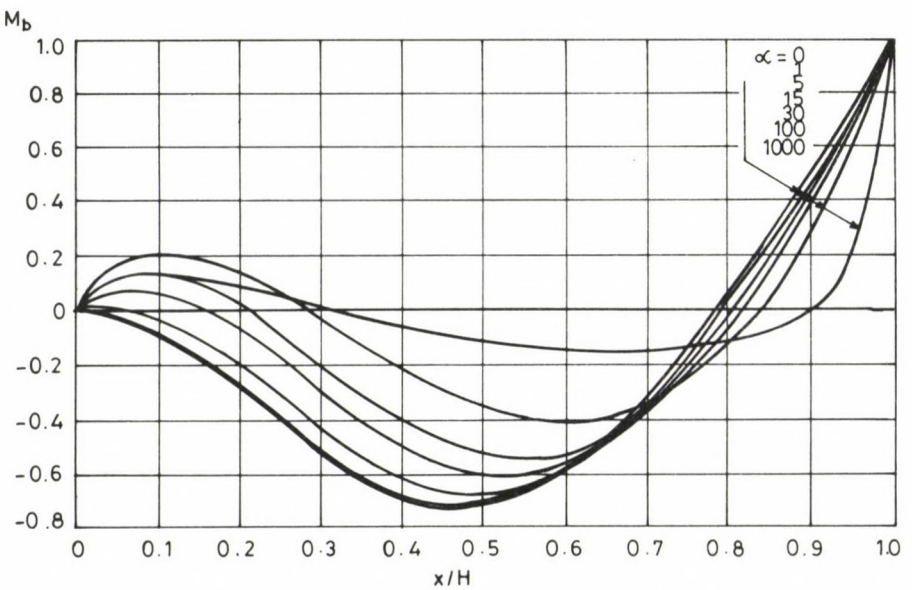
M_b
1.0
0.8
0.6
0.4
0.2
0
-0.2
-0.4
-0.6
-0.8
0 0.1 0.2 0.3 0.4 0.5 0.6 0.7 0.8 0.9 1.0
x/H
α = 0
1
5
15
30
100
1000

Fig. 5b.

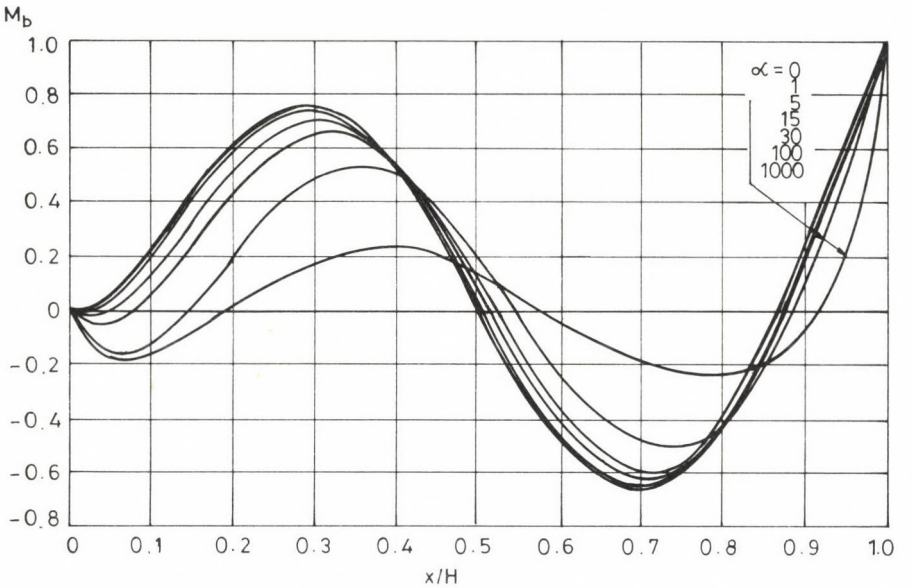

Fig. 5c.

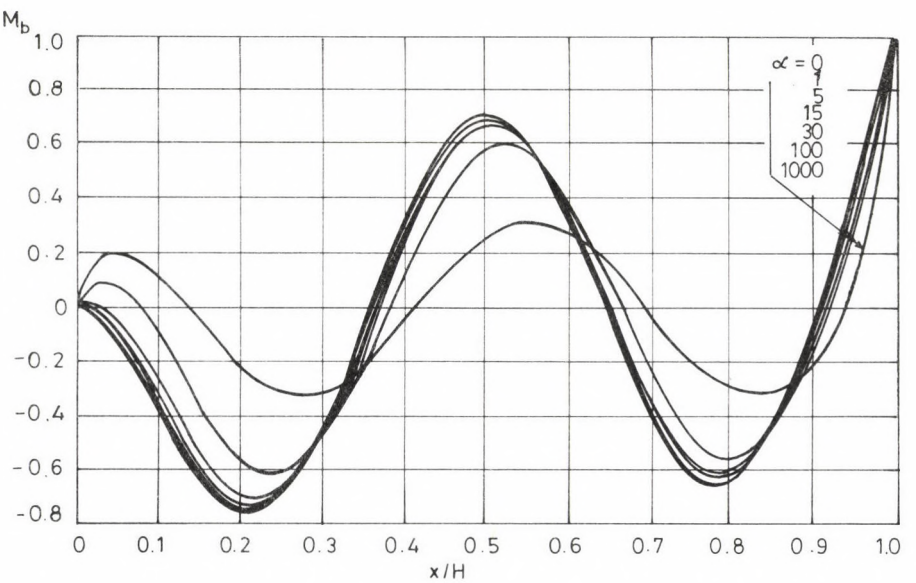

Fig. 5d.

Fig. 5. $m_{Bi}(\xi)$ for the determination of the bending moment $M_{Bi}(\xi)$ (5.1) on the B-bar (a) i = 1; b) i = 2; c) i = 3; d) i = 4)

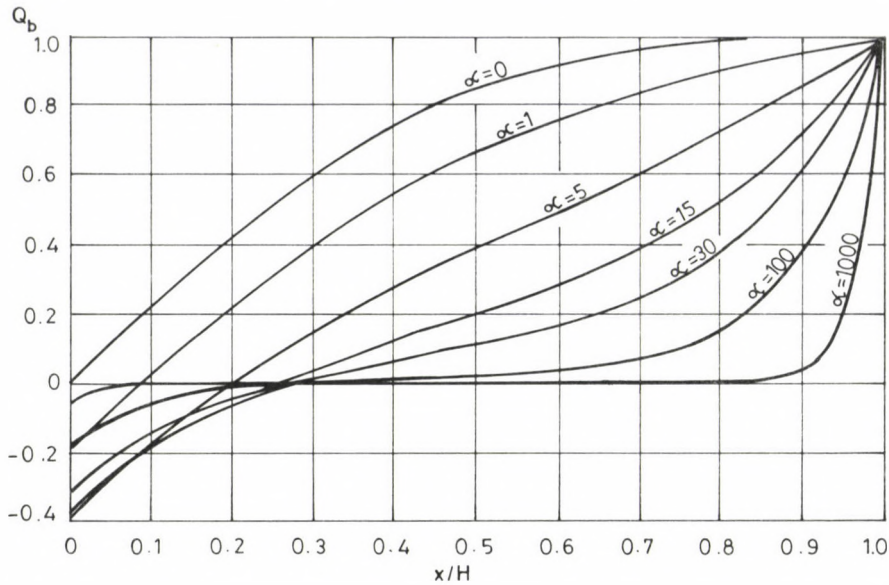
Q_b
1.0
0.8
0.6
0.4
0.2
0
-0.2
-0.4
0
0.1
0.2
0.3
0.4
0.5
0.6
0.7
0.8
0.9
1.0
x/H
α=0
α=1
α=5
α=15
α=30
α=100
α=1000

Fig. 6b.

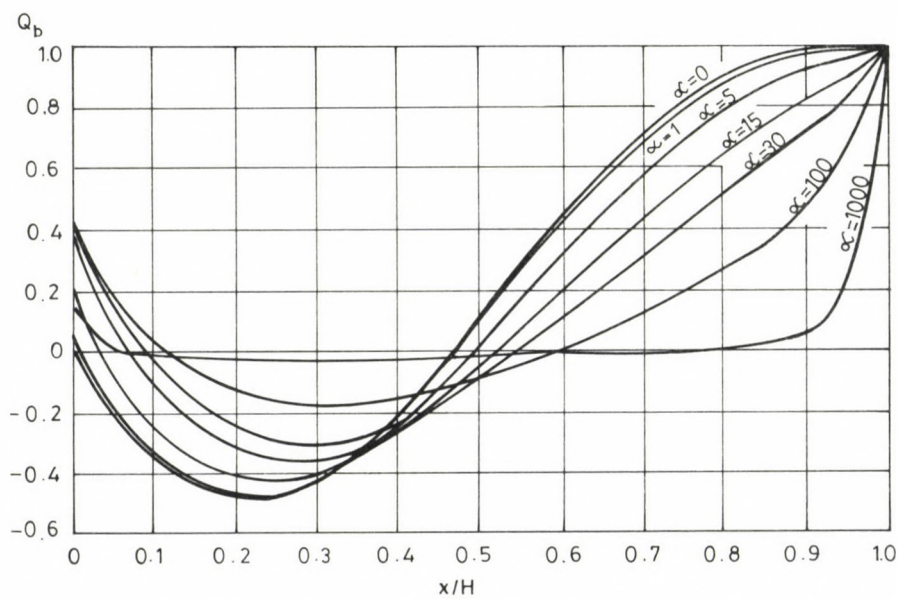
Q_b
1.0
0.8
0.6
0.4
0.2
0
-0.2
-0.4
-0.6
0
0.1
0.2
0.3
0.4
0.5
0.6
0.7
0.8
0.9
1.0
x/H
α=0
α=1
α=5
α=15
α=30
α=100
α=1000

Fig. 6a.

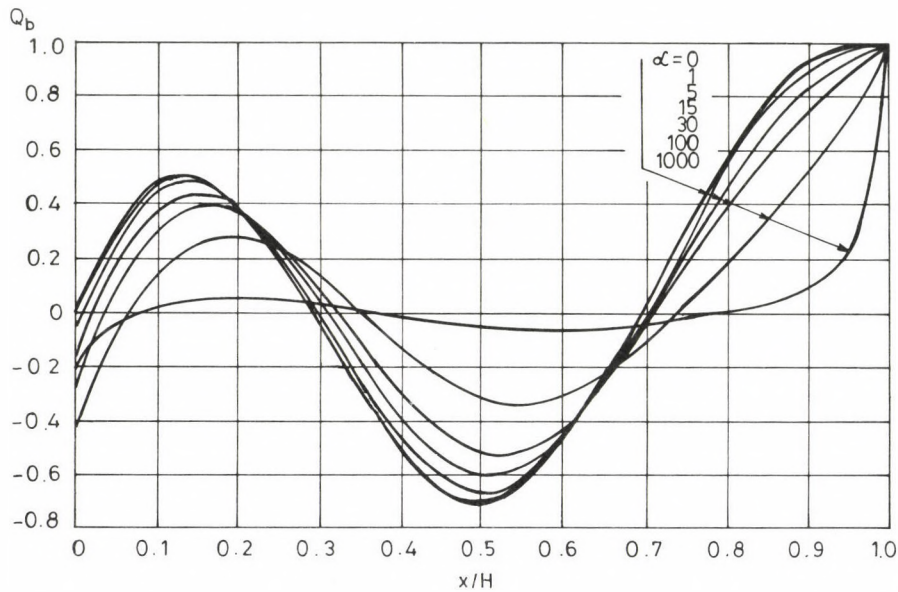

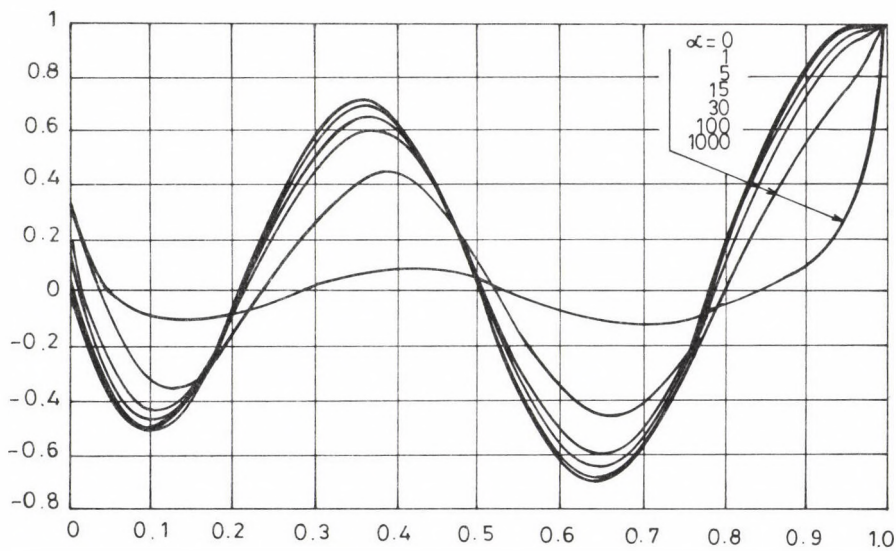

Fig. 6d.

Fig. 6. $q_{Bi}(\xi)$ for the determination of the shearing force $Q_{Bi}(\xi)$ (given by Eq. (5.2)) on the B-bar, a) i = 1; b) i = 2; c) i = 3; d) i = 4)

The shearing force on the S-bar is as follows:

$$Q_{Si}(\xi) = S\, w_i'(x) = K\, m\, \rho\ \ \phi_i\ \ \beta_i H^3 \frac{S}{B} \frac{1}{c_i^2} \bar{w}_i^{\cdot}(\xi) \ . \qquad (5.4)$$

The total shearing force is the sum of $Q_{Bi}(\xi)$ and $Q_{Si}(\xi)$:

$$Q_i(\xi) = Q_{Bi}(\xi) + Q_{Si}(\xi) = -K\, m\, \rho\ \ \phi_i\ \ \beta_i\ H \frac{1}{c_i^2} \left(\bar{w}_i^{\cdot\cdot\cdot}(\xi) - \alpha \bar{w}_i^{\cdot}(\xi) \right) =$$

$$= -K\, m\, \rho\ \ \phi_i\ \ \beta_i\ H\, Q_{Bi} q_i(\xi) \ . \qquad (5.5)$$

Table 4

The values of Q_{Bi} in the expression (5.2)

i/α	10^{-8}	1	5	15	30	100	1000	10^{9}
1	0.3915	0.4011	0.4322	0.4793	0.5153	0.5681	0.6158	0.6366
2	0.2170	0.2108	0.1941	0.1779	0.1733	0.1815	0.2034	0.2122
3	0.1272	0.1261	0.1222	0.1155	0.1102	0.1067	0.1201	0.1273
4	0.0909	0.0905	0.0890	0.0860	0.0827	0.0772	0.0841	0.0909

The values of Q_{Bi} are given in Table 4, the diagrams of $q_i(\xi)$ are seen in Figs 7a-d. After the determination of $Q_i(x)$ the shearing force $Q_{Si}(x)$ on the S-bar can be determined as the difference of $Q_i(x)$ and $Q_{Bi}(x)$.

The load carried by the S-bar is the first derivative of shearing force (5.4) as follows:

$$H_{Si}(\xi) = S\, w_i''(x) = K\, m\, \rho\ \ \phi_i\ \ \beta_i\, \alpha \frac{1}{c_i^2} \bar{w}_i^{\cdot\cdot}(\xi) =$$

$$= K\, m\, \rho\ \ \phi_i\, \beta_i\, h_{Si}(\xi) \ . \qquad (5.6)$$

The curves of $h_{Si}(\xi)$ are given in Figs 8a-d.

6. Paradox of the calculations due to some standards

Let us consider a shear wall the model of which is a bar without shearing deformation. In an interval β_i

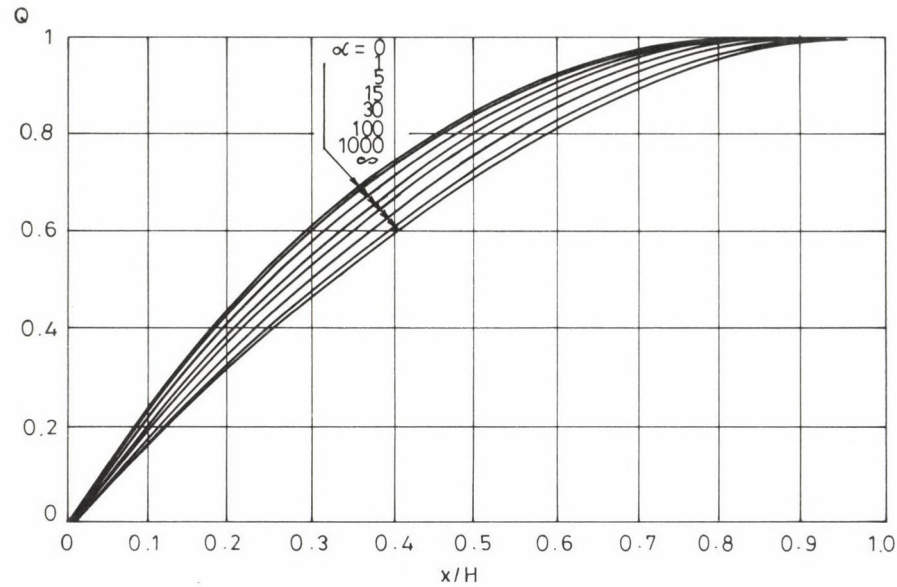
Q
1
0.8
0.6
0.4
0.2
0
α = 0
1
5
15
30
100
1000
∞
0 0.1 0.2 0.3 0.4 0.5 0.6 0.7 0.8 0.9 1.0
x/H

Fig. 7a.

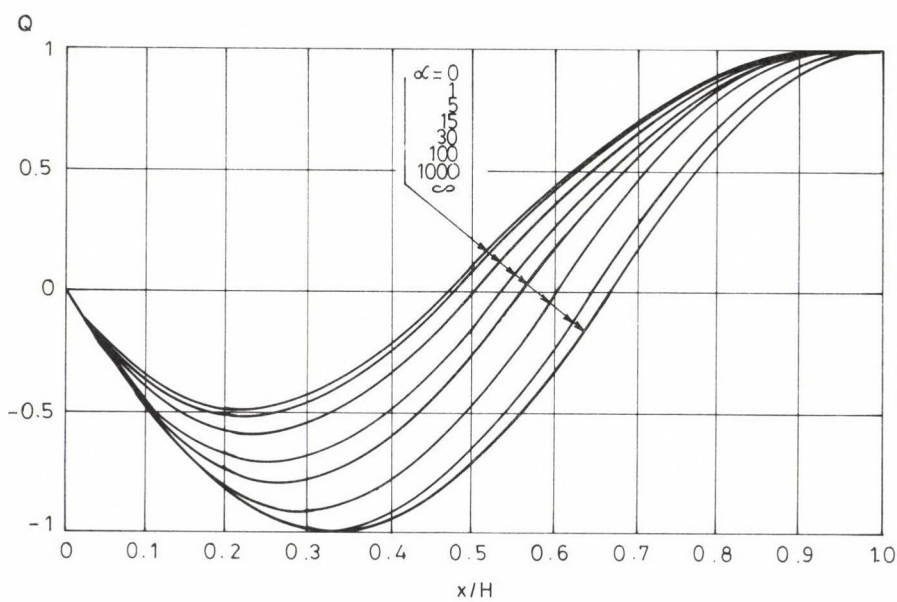
Q
1
0.5
0
-0.5
-1
α = 0
1
5
15
30
100
1000
∞
0 0.1 0.2 0.3 0.4 0.5 0.6 0.7 0.8 0.9 1.0
x/H

Fig. 7b.

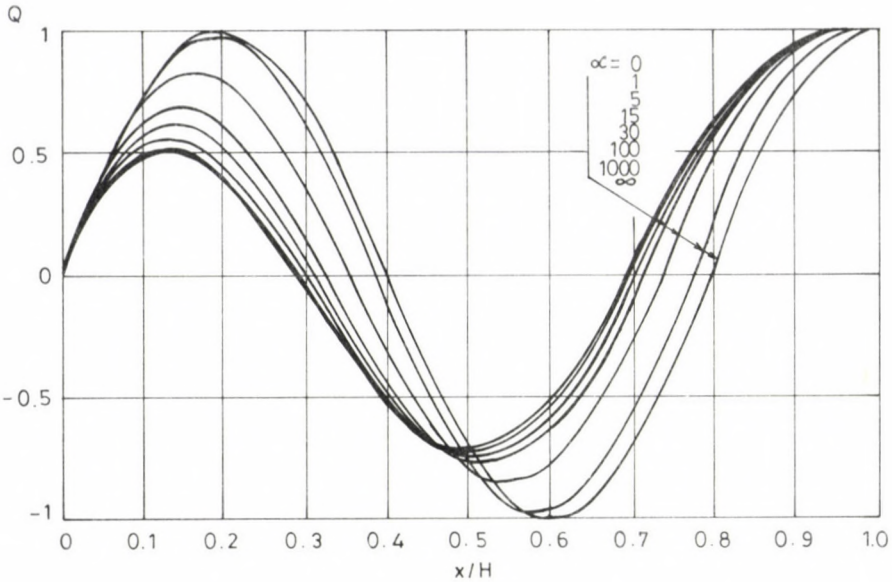

Fig. 7c.

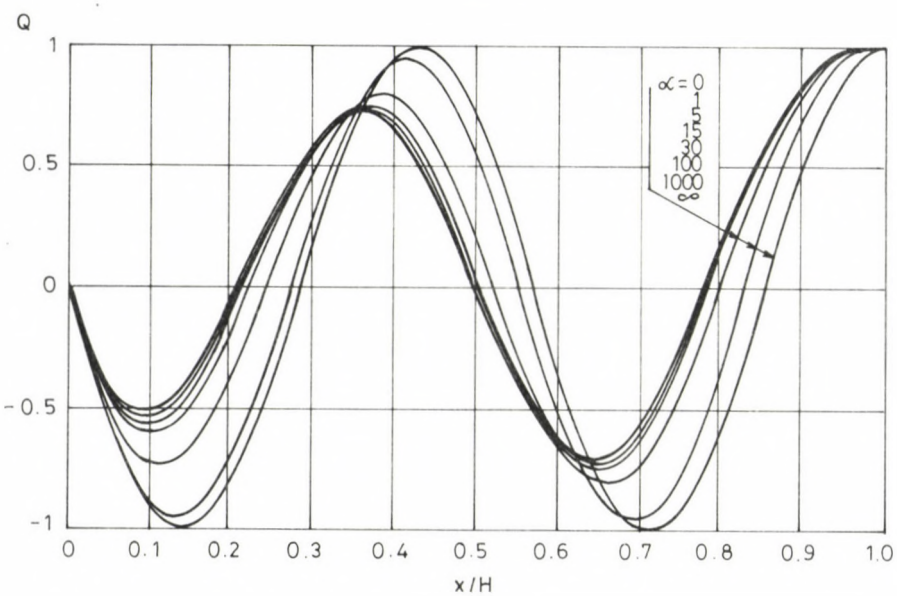

Fig. 7d.

Fig. 7. $q_i(\xi)$ for the determination of the total shearing force $Q_i(\xi)$ (given by Eq. (5.4)), (a) i = 1; b) i = 2; c) i = 3; d) i = 4)

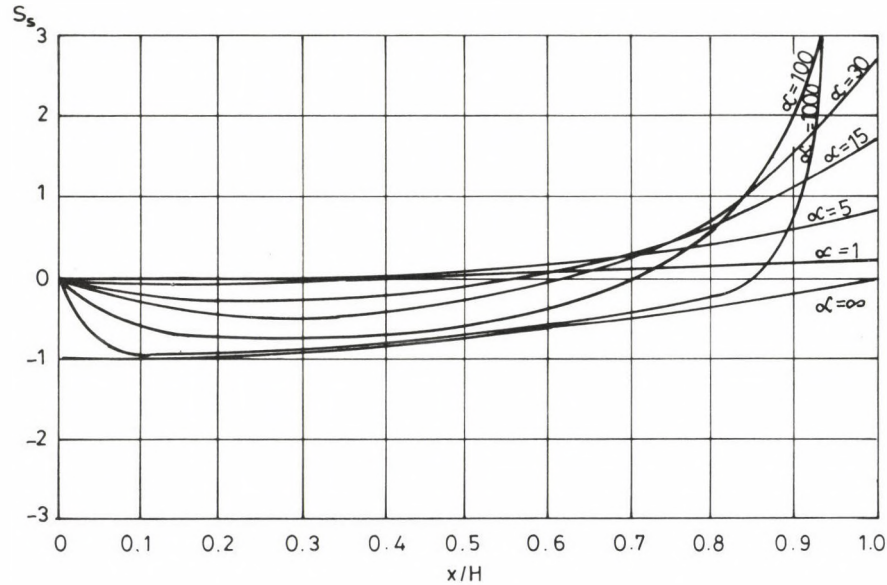
S_s
3
2
1
0
-1
-2
-3
0
0.1
0.2
0.3
0.4
0.5
0.6
0.7
0.8
0.9
1.0
x/H
α=100
α=30
α=15
α=5
α=1
α=∞

Fig. 8a.

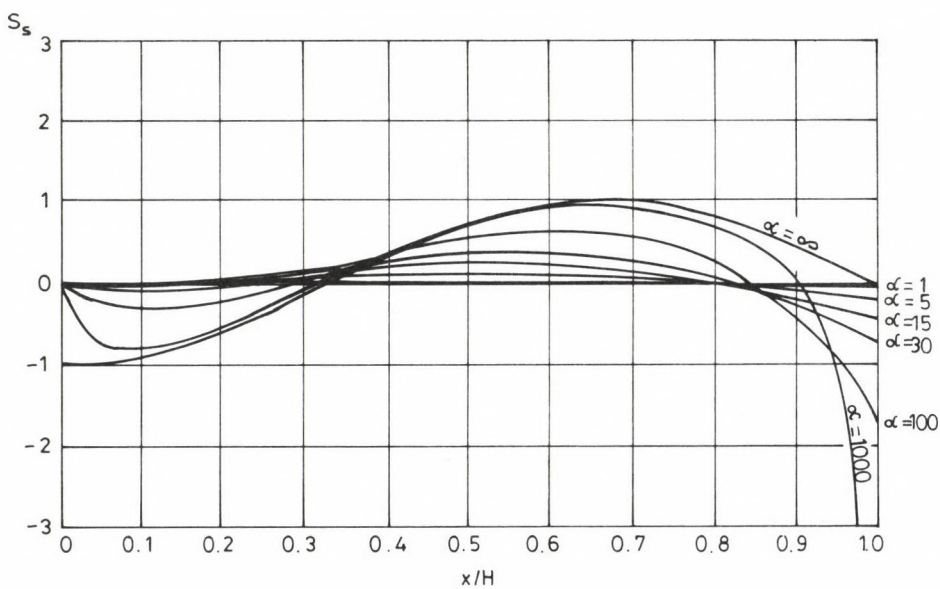
S_s
3
2
1
0
-1
-2
-3
0
0.1
0.2
0.3
0.4
0.5
0.6
0.7
0.8
0.9
1.0
x/H
α=∞
α=1
α=5
α=15
α=30
α=100
α=1000

Fig. 8b.

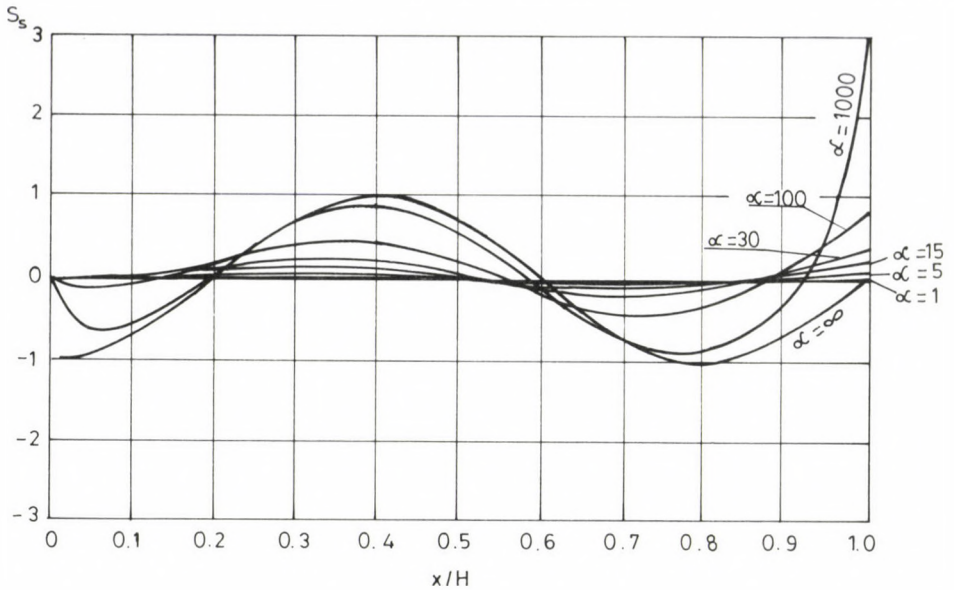

Fig. 8c.

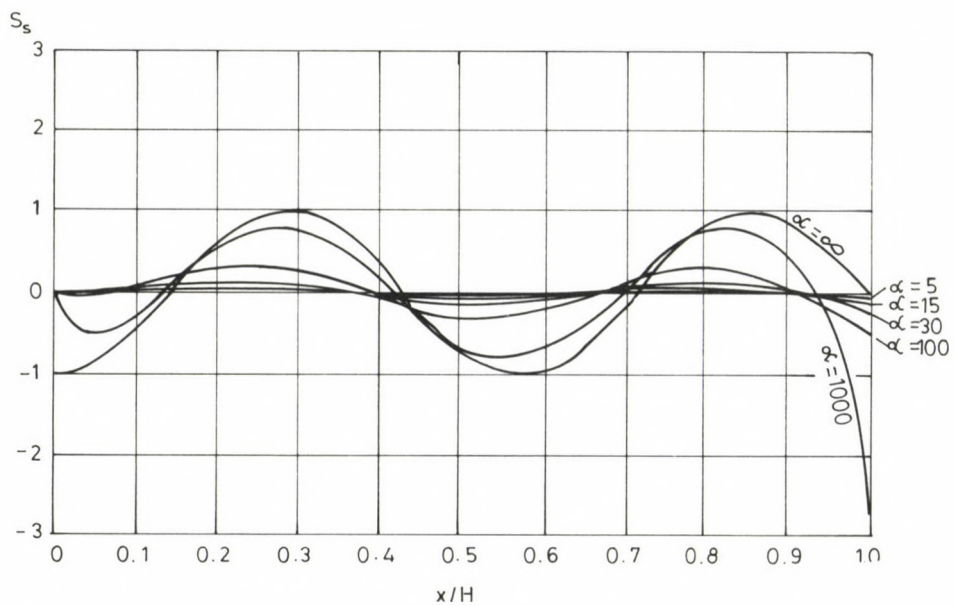

Fig. 8d.

Fig. 8. $h_{Si}(\xi)$ for the determination of the load $H_{Si}(\xi)$ (5.6) on the S-bar
(a) i = 1; b) i = 2; c) i = 3; d) i = 4)

- due to the Hungarian directive - is proportional to T_i^{-1},
- due to the DIN 4149 - is proportional to $T_i^{-0.8}$.

The natural period of vibration depends on H^2 (4.13), hence the intensity of the load, which depends on β_i (3.4), is proportional to H^{-2}, and $H^{-1.6}$, respectively. The maximum value of the shearing force on the bottom depends on H^{-1} and $H^{-0.6}$, respectively, which means that there is an interval, where the higher the building the greater the safety of the building against shear, or with other words if the safety of the building is not great enough, then it should be enhanced with some storeys.

7. Numerical example

The building the plan of which is given in Fig. 9 consists four plane frames and it is braced by four solid shear walls in the x direction. Let us determine the seismic load and the bending moments of the walls in the x direction on the basis of /4/, taking only the first mode of vibration into account. The height of the building is H = 82.3 m, the mass is $m = 2.65 \times 10^5$ kg/m. Let the factor K = .01. (This can be calculated from tables of /4/.) The expression of β_i is the following:

$$\beta_i = T_i^{-1} \text{ , but } .6 < \beta_i < 3 \text{ .}$$

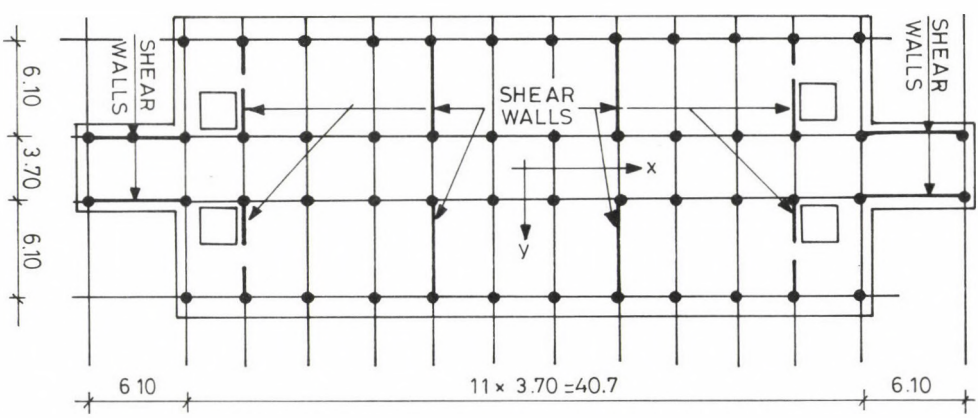

Fig. 9. Plan of the investigated building

i) Let us assume that the connection of frames are not rigid, hence, only the walls resist the seismic load. In this case $\alpha = 0$.

The inertia of a shear wall $I = 7.64\ m^4$, and its Young's modulus $E = 19.5 \times 10^9\ N/m^2$. From Table 1 we obtain $c = 3.516$, hence the period of vibration (4.13)

$$T_1 = \frac{2\ \pi\ 82.3^2}{3.516} \sqrt{\frac{2.66 \times 10^5}{4 \times 19.5 \times 10^9}} = 8.068 \text{ sec} .$$

From the previous expression we obtain $\beta_1 = 0.6$, and from Table 2 $\phi_1 = 1.566$. The function of the seismic load (3.4) is the following:

$$H(x) = 0.01 \times 1.66 \times 10^5 \times 9.81 \times 1.566 \times 0.6\ \overline{w}(x) = 24520\ \overline{w}_1(x) \quad N/m .$$

The bending moment (5.1) taking $M_{B1} = 0.2844$ from Table 3a into account is the following:

$$M_{B1}(x) = 0.01\ \frac{2.66 \times 10^5 \times 9.81}{4}\ 1.566 \times 0.6 \times 82.3^2 \times 2844\ m_{B1}(x) =$$

$$= 11.808 \times 10^6\ m_{B1}(x) \quad Nm .$$

The functions $m_{B1}(x)$ and $\overline{w}_1(x)$ can be found in Figs 4a and 5a, respectively.

ii) We assume that the frames take part in load bearing. The height of the floors is $h = 2.97$ m, the length of the beams is $l = 3.70$ m, the inertia of the beams and columns are $I_b = 0.579 \times 10^{-3}\ m^4$, and $I_c = 2.133 \times 10^{-3}\ m^4$, respectively. The Young's modulus of the frame is $E_f = 23 \times 10^9\ N/m^2$. The number of beams and columns are the same $n = 44$, $m = 44$. The replacement shearing rigidity of the frame is the following /1, 10/:

$$S = \left(S_c^{-1} + S_b^{-1} \right)^{-1} = \left(2.936^{-1} + 0.640^{-1} \right)^{-1} \times 10^9 = 0.525 \times 10^9\ N ,$$

where

$$S_c = m\ E_f\ \frac{12\ I_c}{h^2} = 44 \times 23 \times 10^9\ \frac{12 \times 2.133 \times 10^{-9}}{2.97^2} = 2.936 \times 10^9\ N ,$$

$$S_b = n\ E_f\ \frac{12\ I_b}{l\ h} = 44 \times 23 \times 10^9\ \frac{12 \times 0.579 \times 10^{-3}}{3.7 \times 2.97} = 0.640 \times 10^9\ N.$$

From expression (4.12) we obtain:

$$\alpha = \frac{0.525 \times 10^9 \times 82.3^2}{4 \times 7.64 \times 19.5 \times 10^9} = 5.97 ,$$

and from the first three tables the following values can be calculated: $c_1 = 6.08$, $\phi_1 = 1.50$, $M_{B1} = 0.150$, hence the period of vibration (4.13)

$$T_1 = \frac{2\pi 82.3^2}{6.08} \sqrt{\frac{2.66 \times 10^5}{4 \times 19.5 \times 10^9}} = 4.67 \text{ sec},$$

and $\beta = 0.6$. The function of the seismic load 83.49 is the following:

$$H(x) = 0.01 \times 2.66 \times 10 \times 9.81 \times 1.50 \times 0.6 \, \bar{w}(x) = 23480 \, \bar{w}_1(x) \quad \text{N/ml} .$$

(This load is less than in case i) in spite of the fact that the structure is more rigid than in the previous case, which is a paradox as well. This occurred because of the simplified calculation of β.) The bending moment is the following:

$$M_{B1}(x) = 0.01 \frac{2.66 \times 10^5 \times 9.81}{4} 1.50 \times 0.6 \times 82.3^2 \times 150 \, m_{B1}(x) =$$

$$= 5.966 \times 10^6 \, m_{B1}(x) \, [\text{Nm}],$$

which is the half of the previous one. The functions $\bar{w}_1(x)$ and $m_{B1}(x)$ are very close to those given in Figs 4a and 5a at $\alpha = 5$, respectively.

REFERENCES

1. Müller, F.P.-Keintzel, E.: Erdbebensicherung von Hochbauten. W. Ernst & Sohn, Berlin, etc. 1978
2. Dowrick, D.J.: Earth resistant design. John Wiley & Sons, London, etc. 1977
3. Green, N.B.: Earth quake resistant building deisgn and construction. Van Nostrand Reinhold Company, New York, etc. 1981
4. Directives of analysis for earthquakes. (In Hungarian.) MI-04.133-81. Építésügyi Tájékoztatási Központ, Budapest, 1981
5. Hunyadi, F.: Analysis of buildings for earthquake in Hungary. (In Hungarian.) Mélyépítéstudományi szemle. 21 (1971), 279-282
6. Csonka, P.: Beitrag zur Berechnung waagrecht belasteter Stockwerkrahmen. Die Bautechnik. 39, (1962), 237-240

7. Szerémi, L.: Calculation of stiffening systems of buildings. (In Hungarian.) Mérnöki Kézikönyv II. Ed. Palotás László, Műszaki Könyvkiadó, Budapest, 1984

8. Hegedűs, I.-Kollár, P.: Application of the sandwich theory for the stability analysis of engineering structures. (A chapter of the book: Special Problems of Structural Stability, in Hungarian.) Akadémiai Kiadó, Budapest, 1991

9. Hegedűs, I.-Kollár, P.: Generalized bar models and their physical interpretation. Acta Technica Hung. Civil Eng. 101 (1988), 67-93

10. Hegedűs, I.-Kollár, P.: Stabilitätsuntersuchung von Rahmen und Wandscheiben mit der Sandwichtheorie. Bautechnik (West-Berlin), 64 (1987), 420-425

11. Kollár, P.: Stability analysis of frames and shear-walls by the method of difference equations and by the continuum method. (In Hungarian.) Dissertation TU Budapest, 1986

Acta Technica Acad.Sci.Hung., 104(1-3), pp. 211-236 (1991/92)

ESTIMATION OF TORSIONAL RIGIDITY BY MEANS OF THE FINITE ELEMENT METHOD

PÁCZELT, I.* - SZABÓ, T.**

(Received: 15 November 1991)

The upper and lower limit of the torsional rigidity of a compound bar cross section of anisotropic material with, however, homogeneous subdomains is determined by means of the finite element method, making use of the extremal principles of complementary energy and potential energy. Stress function U and warping function ϕ are used as approximation fields. Formally, the coefficient matrices of the equation systems obtained as a result of discretization of the functionals to be minimized are identical in respect of difference of the matrices of the material constants while slightly different as far as the loading sides are concerned. The boundary condition can be simply provided for U in case of a multiply connected domain by means of 'following' point techniques along the holes.

Isoparametric elements are used as a finite element. According to the results of calculations, a very small value is obtained for the difference between the upper and lower limit of torsional rigidity provided elements of a sufficient number are assumed.

Introduction

Since St. Venant, researchers have paid, and are still paying, significant attention to investigation of the problem of torsion of prismatic bars /1, 2/ and /3, 4, 7/, respectively.

Use of variation principles of the theory of elasticity /5/ offers a reasonable way to estimate the torsional rigidity of the cross section through the upper and lower limits.

This work uses the finite element method /6/ to analyze the torsion problem of prismatic bars of anisotropic material by means of variation principles. The mechanical boundary value problem is formulated for stress function U and warping function ϕ /2/, then, by means of variation principles based on total complementary energy and potential energy minimum

*Pácelt, István, H-3529 Miskolc, Perczel Mór u. 30, Hungary

**Szabó, Tamás, H-3529 Miskolc, Aulich u. 26, Hungary

Akadémiai Kiadó, Budapest

principles, the boundary and fitting conditions for the approximation fields to be 'a priori' satisfied are cleared.

The finite element method is taken as a basis for approximation of the fields, giving the relationships to produce the matrices and vectors in the equations to be solved as well as the method to calculate torsional rigidity.

From the relationships applying to the cross section composed of different materials, also the formulae applying to the cross section of homogeneous isotropic material are derived simply. The finite elements presented can be easily built into the usual finite element program systems.

Basic relationships

The mechanical problem resulting from the St.Venant torsion of a prismatic bar of axis z, consisting of different materials (e = 1, ..., E) sticked together, unloaded over the external surfaces but loaded at both ends, can be discussed on the basis of stress function $U = U(x,y)$ on the one hand while warping function $\phi = \phi(x,y)$ on the other hand.

The stressed state of the body is described by stress vector $\underline{\tau} = \tau_{xz}\underline{i} + \tau_{yz}\underline{j}$ while its displacement field by displacement vector $\underline{u} = u\underline{i} + v\underline{j} + w\underline{k} = z(\underline{k} \times \underline{R}) + w\underline{k}$, where ϑ is the angle of twist per unit length and $\underline{R} = x\underline{i} + y\underline{j}$ is position vector.

The shear stress arisen, $\underline{\tau}$, can be calculated as

$$\underline{\tau} = \vartheta(\nabla U \times \underline{k}), \quad \underline{\tau} = \underline{\underline{D}} \cdot (\nabla\phi + \underline{k} \times \underline{R})\,\vartheta\,, \tag{1}$$

where

$\underline{\underline{D}} = \underline{\underline{C}}^{-1}$ - second-order tensor of material constants.

Assuming elastic material shear strain vector $\underline{\gamma} = \gamma_{xz}\underline{i} + \gamma_{yz}\underline{j}$ composed of specific shear strains γ_{xz}, γ_{yz} is:

$$\underline{\gamma} = \underline{\underline{C}} \cdot \underline{\tau} \qquad \underline{\gamma} = \nabla w + (\underline{k} \times \underline{R})\,\vartheta\,; \quad w = \vartheta\phi \tag{2}$$

$$\underline{\tau} = \underline{\underline{D}} \cdot \underline{\gamma}\,.$$

With no mass forces existing, equilibrium equation

$$\nabla \cdot \underline{\tau} = 0 \tag{3}$$

is automatically satisfied by U while equation

$$\nabla \cdot \underline{\underline{D}} \cdot (\nabla \phi + \underline{k} \times \underline{R}) = \underline{0} \qquad \underline{R} \in A \tag{4a}$$

applies to ϕ.

According to the Beltrami-Michel compatibility equation, the basic equation for U is

$$(\nabla \cdot \underline{\underline{C}} \cdot (\nabla U)) = -2 \qquad \underline{R} \in A \ . \tag{4b}$$

With external normal $\underline{n}$ introduced because the external surfaces are unloaded,

$$\underline{\tau} \cdot \underline{n} = 0 \ , \tag{5}$$

where U = const,
boundary condition

$$\underline{n} \cdot \underline{\underline{D}} \cdot \nabla \phi - \underline{t} \cdot \underline{\underline{D}} \cdot \underline{R} = 0 \qquad \underline{R} \in A$$

applies to the boundary of the cross section.
Here

$$\underline{t} = \underline{k} \times \underline{n}$$

is a tangential unit vector.

The following dynamic fitting condition applies to the boundary of the prismatic bodies of different material properties constituting the bar (see Fig. 1):

$$\underline{\tau}^e \cdot \underline{n}^e + \underline{\tau}^j \cdot \underline{n}^j = 0 \ , \qquad \underline{R} \in \Gamma_c^{ej}$$

that is

$$\nabla U^e \cdot \underline{t}^e + \nabla U^j \cdot \underline{t}^j = 0 \qquad \underline{n}^e \cdot \underline{\underline{D}}^e \cdot \nabla \phi^e + \underline{n}^j \cdot \underline{\underline{D}}^e \cdot \nabla \phi^j -$$

$$- (\underline{t}^e \cdot \underline{\underline{D}}^e + \underline{t}^j \cdot \underline{\underline{D}}^j) \cdot \underline{R} = 0 \ , \tag{6}$$

while the continuity (equivalence) of the displacement is ensured by the existence of conditions

$$\underline{n}^e \cdot \underline{\underline{C}}^e \cdot \nabla U^e + \underline{n}^j \cdot \underline{\underline{C}}^j \cdot \nabla U^j = 0 \ , \qquad \phi^e = \phi^j \qquad \underline{R} \in \Gamma_c^{ej} \ . \tag{7}$$

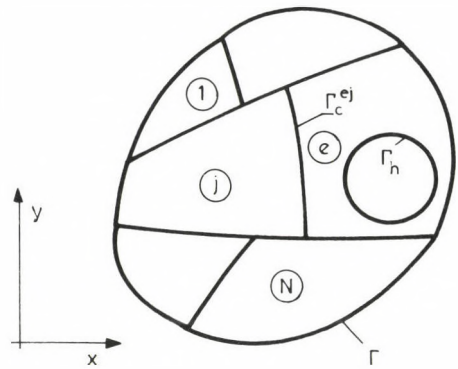

Fig. 1. Cross section consisting of homogenepus anisotropic subdomains of number N (Γ - boundary, Γ_h - boundary of hole, Γ_c^{ej} - joint between elements e and j)

In case a hole is present, the following integral relationship is existing:

$$\oint_{\Gamma_h} \underline{n} \cdot \underline{\underline{C}} \cdot \nabla U \, ds = 2A_h \,, \tag{8}$$

where A_h is the surface of the hole.

In the knowledge of torsional moment M_T acting upon the cross section, torsional rigidity I_T can be defined, as follows:

$$M_T = \underline{k} \cdot \int \underline{R} \times \underline{\underline{I}} \, dA = \vartheta I_T \,, \tag{9}$$

which is

$$I_T = 2\left(\int_{(A)} U \, dA + \sum_h A_h U_h\right) , \tag{10}$$

on the one hand, where U_h is the value of function U arising on the boundary of the hole and, using function

$$I_T = \int_{(A)} \underline{R} \times \underline{\underline{D}} \cdot (\nabla \phi + \underline{k} \times \underline{R}) \, dA \,. \tag{11}$$

on the other hand.

Use of variation principles

For the approximate solution of the above boundary value problem, the total complementary energy minimum principle is used on the basis of U while the total potential energy minimum principle on the basis of ϕ /5/.

Suppose sideplate z = 0 of the bar is rigidly clamped while endplate

$z = L$ is displaced angularly like a rigid body. Thus the complementary energy:

$$\pi_C = \frac{1}{2}\,\vartheta^2 \int_0^L dz \sum_e \int_{(A^e)} (\nabla U \times \underline{k}) \cdot \underline{\underline{C}} \cdot (\nabla U \times \underline{k})\, dA$$

$$- \vartheta^2 L \sum_e \int_{(Ae)} (\underline{k} \times \underline{R}) \cdot (\nabla U \times \underline{k})\, dA$$

$$= \frac{1}{2}\,\vartheta^2 L \left(\sum_e \int_{(A^e)} \nabla U \cdot \underline{\underline{C}} \cdot \nabla U\, dA + 2 \sum_e \int_{(A^e)} \nabla U \cdot \underline{R}\, dA \right) \qquad (12)$$

The Gauss-Ostrogradski integral transformation theorem can be used to prove that, in case of U satisfying the boundary value problem,

$$J = \frac{\pi_C}{\vartheta^2 L} = -\frac{I_T}{2}\,, \qquad (13)$$

and, on the other hand, in stationary position, $\delta \pi_C = 0$, of functional (12), the relationships given in (4) thru (8) are existing in case of a continuous U and compliance with the boundary condition according to (5) (see Appendix A.1).

Total potential energy associated with the problem:

$$\pi_p = \frac{1}{2} \int_0^L dz \sum_e \int_{(A^e)} \underline{\gamma} \cdot \underline{\underline{D}} \cdot \underline{\gamma}\, dA =$$

$$= \vartheta^2 L \frac{1}{2} \sum_e \int_{(A^e)} (\nabla\phi + \underline{k} \times \underline{R}) \cdot \underline{\underline{D}} \cdot (\nabla\phi + \underline{k} \times \underline{R})\, dA = \vartheta^2 L \frac{I_T}{2}$$

Accordingly,

$$\mathcal{L} = \frac{\pi_p}{\vartheta^2 L} = \frac{I_T}{2}\,. \qquad (14)$$

For variation equation $\delta \pi_p = 0$, it can be shown (see Appendix A.2) that, with the continuity of ϕ 'a priori' satisfied, the equations as well as the boundary and fitting conditions of the boundary value problem for ϕ are existing /3/ thru /6/.

Due to inequality

$$-\pi_c(U^*) \leqslant -\pi_c(U) = \pi_p(\phi) \leqslant \pi_p(\phi^*) ,$$

where U^*, ϕ^* are approximation fields, inequality

$$I_T(U^*) \leqslant I_T \leqslant I_T(\phi^*) \tag{15}$$

applies to torsional rigidity.

Use of the finite element method for minimization of J

The functional defined under /12, 13/ shall be minimized by field U which is continuous and resulting in a continuous value at the boundaries.

With approximation functions $N_i(x,y)$ (e.g. isoparametric elements) selected as is usual in the finite element method and approximation

$$U^* = \sum_i N_i(x,y)\, U_i = \underline{\underline{N}}\, \underline{u} \tag{16}$$

used, where U_i is the nodal stress function, the gradient will be

$$\nabla U^* = \sum_i (P_i^X(x,y)\, U_i\, \underline{i} + P_i^Y(x,y)\, U_i\, \underline{j}) \Rightarrow$$

$$\nabla U^* \Rightarrow \begin{bmatrix} \frac{\partial U^*}{\partial x} \\ \\ \frac{\partial U^*}{\partial y} \end{bmatrix} = \sum_i \begin{bmatrix} P_i^X \\ \\ P_i^Y \end{bmatrix} U_i = \begin{bmatrix} \underline{\underline{P}}^{XT} \\ \\ \underline{\underline{P}}^{YT} \end{bmatrix} \underline{u} = \underline{\underline{B}}\, \underline{u} , \tag{17}$$

while the vector containing the tangential stresses

$$\underline{\tau} = \begin{bmatrix} \tau_{xz} \\ \tau_{yz} \end{bmatrix} = \vartheta \begin{bmatrix} \underline{\underline{P}}^{YT} \\ -\underline{\underline{P}}^{XT} \end{bmatrix} \underline{u} = \vartheta\, \underline{\underline{\tilde{B}}}\, \underline{u} \tag{18}$$

where $P^{XT} = [P_1^X \ldots P_i^X \ldots P_N^X]$ $\quad X \leftrightarrow Y$

$$P_i^X = \frac{\partial N_i}{\partial x}, \qquad P_i^Y = \frac{\partial N_i}{\partial y}$$

$$\underline{u}^T = [U_1 \ \ldots \ U_i \ \ldots \ U_N]$$

vector of nodal stress function. Then, using the above relationships,

$$J = \frac{1}{2} \underline{u}^T \underline{S} \underline{u} - \underline{u}^T \underline{f} \tag{19}$$

where the rigidity matrixis

$$\underline{S} = \int_{(A)} \underline{B}^T \underline{C} \underline{B} \, dA \tag{20}$$

and the loading vector:

$$\underline{f} = -\int_{(A)} \begin{bmatrix} P_1^X x + P_1^Y yx \\ \vdots \\ P_i^X x + P_i^Y y \\ \vdots \end{bmatrix} dA \tag{21}$$

According to the minimum condition,

$$\underline{S} \underline{u} = \underline{f} \tag{22}$$

and

$$J = -\frac{1}{2} \underline{u}^T \underline{f} \tag{23}$$

On the basis of (9), (13), (15),

$$I_T(U^*) = \underline{u}^T \underline{f} = \frac{M_T}{\vartheta} . \tag{24}$$

Accordingly, using (17), the tangential stress resulting from torsional moment M_T acting upon the axis:

$$\underline{\tau} = \frac{M_T}{\underline{u}^T \underline{f}} \underline{\tilde{B}} \underline{u} . \tag{25}$$

Use of the finite element method for minimization of $\mathcal{L}$

After simple reduction, functional $\mathcal{L}$ according to (14) takes the following shape:

$$\mathcal{L} = \sum_e \left(\frac{1}{2} \int_{(A^e)} \nabla\phi \cdot \underline{\underline{D}} \cdot \nabla\phi \, dA + \int_{(A^e)} (\underline{k} \times \underline{R}) \cdot \underline{\underline{D}} \cdot \nabla\phi \, dA \right) +$$

$$+ \sum_e \frac{1}{2} \int_{(A^e)} \underline{R} \cdot \underline{\underline{D}} \cdot \underline{R} \, dA \, . \tag{26}$$

Using the approximation according to (16) for the warping function,

$$\phi^* = \sum_i N_i(x,y) \; \phi_i = \underline{\underline{N}} \; \underline{\phi} \, , \tag{27}$$

where $\underline{\underline{N}}$ - approximation matrix,

$\underline{\phi}$ - vector of nodal warpings.

$$\nabla\phi \Rightarrow \begin{bmatrix} \dfrac{\partial \phi}{\partial x} \\ \\ \dfrac{\partial \phi}{\partial y} \end{bmatrix} = \sum_i \begin{bmatrix} P_i^X(x,y) \\ \\ P_i^Y(x,y) \end{bmatrix} \phi_i = \underline{\underline{B}} \; \underline{\phi} \, . \tag{28}$$

Thus

$$\mathcal{L} = \frac{1}{2} \underline{\phi}^T \underline{\underline{K}} \, \underline{\phi} - \underline{\phi}^T \underline{g} + \frac{I_p^*}{2} \tag{29}$$

where, with the matrix of material constants of dimension $\underline{\underline{D}}(2x2)$ introduced,

$$\underline{\underline{K}} = \int_{(A)} \underline{\underline{B}}^T \underline{\underline{D}} \, \underline{\underline{B}} \, dA \tag{30}$$

$$\underline{g} = - \int_{(A)} \underline{\underline{B}}^T \begin{bmatrix} - D_{11} \, y + D_{12} \, x \\ \\ - D_{21} \, y + D_{22} \, x \end{bmatrix} dA \tag{31}$$

$$I_p^* = \int_{(A)} \underline{\underline{R}}^T \underline{\underline{D}} \underline{\underline{R}} \, dA \; ; \qquad \underline{\underline{R}} = \begin{bmatrix} x \\ \\ y \end{bmatrix} . \tag{32}$$

Due to the minimum condition,

$$\underline{\underline{K}} \, \underline{\phi} = \underline{g} \tag{33}$$

and thus

$$\mathcal{L} = -\frac{1}{2} \underline{\phi}^T \underline{g} + \frac{I_p^*}{2} = \frac{I_T(\phi^*)}{2} , \tag{34}$$

that is the upper limit of torsional rigidity is:

$$I_T(\phi^*) = I_p^* - \underline{\phi}^T \underline{g} = \frac{M_T}{\vartheta} . \tag{35}$$

The shear stresses (1) taking into consideration of (28) can be expressed as

$$\underline{\tau} = \frac{M_T}{I_T} \underline{\underline{D}} \left(\underline{\underline{B}} \, \underline{\phi} + \begin{bmatrix} -y \\ \\ x \end{bmatrix} \right) , \tag{36}$$

The position co-ordinates of the centre of gravity of the cross section, the value of 'polar' second-order moment I_p^* according to (32) are determined by numerical integration, using isoparametric elements.

The case of a homogeneous cross section of isotropic material

In this case, stress $\underline{\tau}$ according to (1) shall most reasonably be calculated by introducing shear elasticity factor G:

$$\underline{\tau} = G \vartheta (\nabla \tilde{U} \times \underline{k}), \quad \text{or} \quad \underline{\tau} = G \vartheta (\nabla \phi + \underline{k} \times \underline{R}) , \tag{37}$$

that is

$$U = G\tilde{U} \; ; \quad \underline{\underline{D}} = G \, \underline{\underline{I}} \; ; \quad \underline{\underline{C}} = \frac{1}{G} \underline{\underline{I}} \tag{38}$$

as follows from a comparison of (37) and (1),
where $\underline{\underline{I}}$ - identity tensor.

Now, according to (4a, b),

$$\nabla^2 \tilde{U} = -2, \qquad \nabla^2 \phi = 0 \qquad \underline{R} \in A \tag{39}$$

while at the boundary,

$$\tilde{U} = \text{const}, \qquad \nabla\phi \cdot \underline{n} = \underline{R} \cdot \underline{t} \qquad \underline{R} \in \Gamma \tag{40}$$

Assuming the cross section to be of identical material,

$$M_T = G\vartheta\, I_T \tag{41}$$

can be written in place of (9),
where

$$I_T = 2\left(\int_{(A)} \tilde{U}\, dA + \sum_h A_h \tilde{U}_h \right) \tag{42a}$$

or

$$I_T = \int_{(A)} \underline{R} \times (\nabla\phi + \underline{k} \times \underline{R})\, dA \,. \tag{42b}$$

With (38) taken into consideration,

$$J = \frac{\pi_C}{G\vartheta^2 L} = -\frac{I_T}{2}; \qquad \mathcal{L} = \frac{\pi_P}{G\vartheta^2 L} = \frac{I_T}{2} \tag{43}$$

that is,

$$I_T(\tilde{U}^*) \leq I_T \leq I_T(\phi^*) \,. \tag{44}$$

applies.

Now the rigidity matrices according to (20) and (30) are identical,

$$\underline{\underline{S}} = \int_{(A)} \underline{\underline{B}}^T \underline{\underline{I}}\, \underline{\underline{B}}\, dA = \underline{\underline{K}} \,, \tag{45}$$

loading vector $\underline{f}$ is identical with that according to (21), while

$$\underline{g} = -\int_{(A)} \begin{bmatrix} P_1^Y x - P_1^X y \\ \vdots \\ P_i^Y x - P_i^X y \\ \vdots \end{bmatrix} dA \,, \tag{46}$$

$$I_p^* = \int_{(A)} \underline{\underline{R}}^2 \, dA \text{ being polar second-order moment,} \tag{47}$$

and

$$I_T(\tilde{U}^*) = \underline{\underline{u}}^T \, \underline{\underline{f}} = \frac{M_T}{G\vartheta} \tag{48}$$

$$I_T(\phi^*) = I_p^* - \underline{\underline{\phi}}^T \, \underline{\underline{g}} = \frac{M_T}{G\vartheta} \quad . \tag{49}$$

Stress $\underline{\underline{\tau}}$ is calculated according to (25), (36) invariably.

Examples

Example 1

To illustrate what has been said above, let torsional rigidity I_T of the cross section schematically illustrated in Fig. 2 be determined by means of a process based on functions U and ϕ. Limits

$$1{,}3860 \cdot 10^8 \leq I_T \leq 1{,}3861 \cdot 10^8$$

have been obtained for torsional rigidity with the finite element mesh according to Fig. 3a. In calculations taking U as a basis, boundary condition U = 0 is assumed for boundary 1 while the condition $U|_\Gamma$ = const is met by subordinating the nodal points to point * at boundary 2.

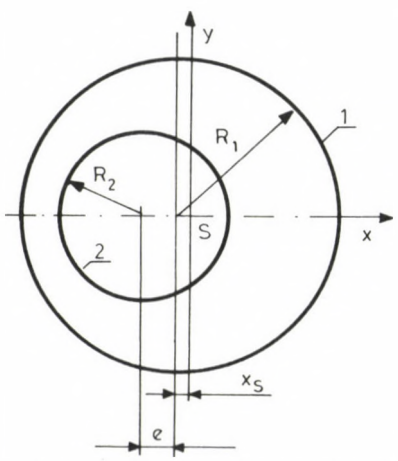

Fig. 2. Cross section with a hole in it

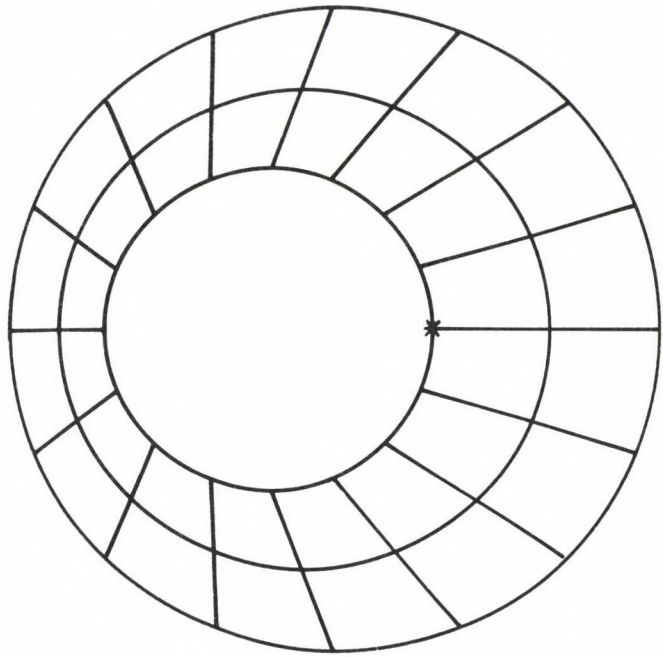

Fig. 3a. Mesh of cross section

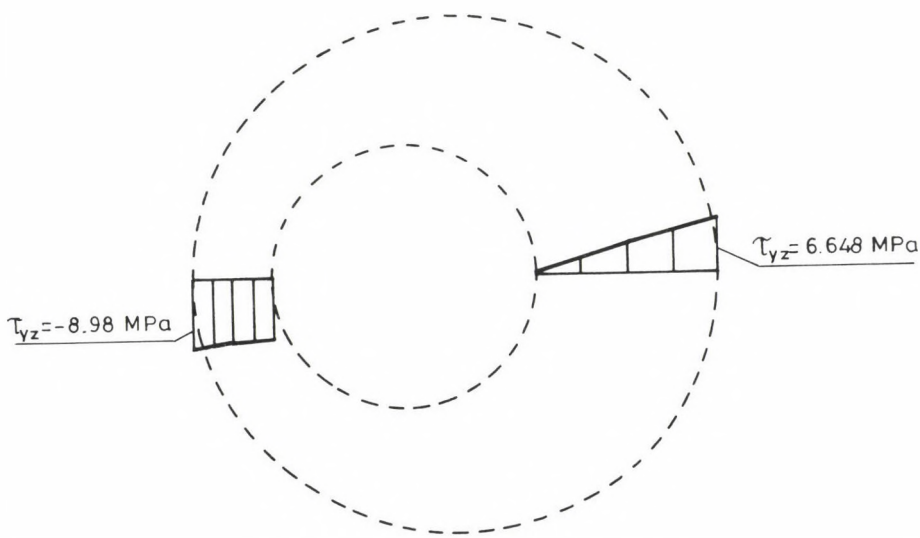

Fig. 3b. Stress distribution τ_{yz} along y = 0

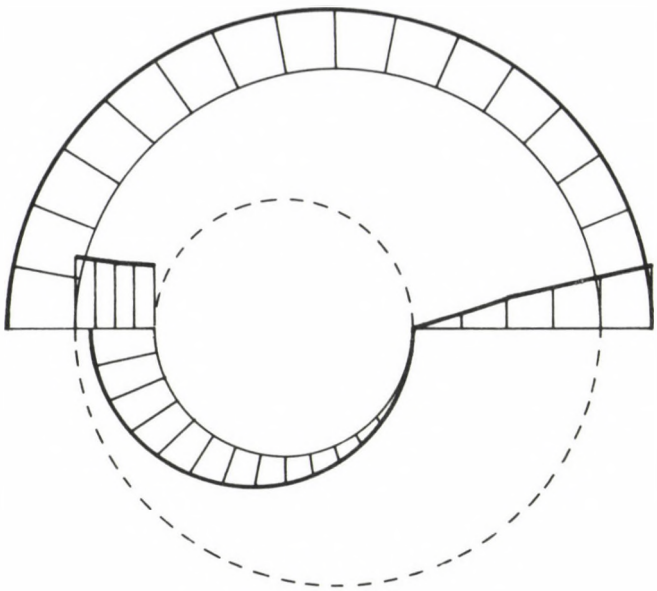

Fig. 3c. Distribution of stress δ_{red}

In calculations based on ϕ, it is enough to assume $\phi = 0$ at one point. In this case, deplanation w of the cross section appears in relation to this point ($w = \vartheta\phi$ (x,y).

The shear stress arising along axis x in case of moment $M_T = 10^6$ and stress δ_{red} at the boundary and axis x of the cross section are illustrated in Figs 3b and 3c, respectively.

Example 2

The second example is the St. Venant torsion problem for a square cross section of sides of a length of a = 100 mm illustrated in Fig. 4. The values of torsional rigidity obtained for a finite element mesh according to Figs 4a-d as well as the maximum values of shear stress arising at the midpoint of the sides in case of a torsional rigidity of $M_T = 10^6$ Nmm are tabulated in Table 1.

Polar second-order moment of the cross section: $I_p = 16{,}666 \cdot 10^6$ mm^4. It can be clearly seen that inequality (12) and conditions $I_T \leq I_p$ are satisfied. The mesh according to 4d supplies practically the exact solution.

With the same cross section divided in two along axis y, assumed to

Table 1

Finite element mesh	$I_T/10^6$ (mm^4)		τ_{max} (MPa)	
	$\tilde{U}$	ϕ	$\tilde{U}$	ϕ
4a	-	16.666	-	3.00
4b	13.971	14.167	5.579	5.294
4c	14.049	14.063	4.810	4.847
4d	14.057	14.058	4.806	4.806

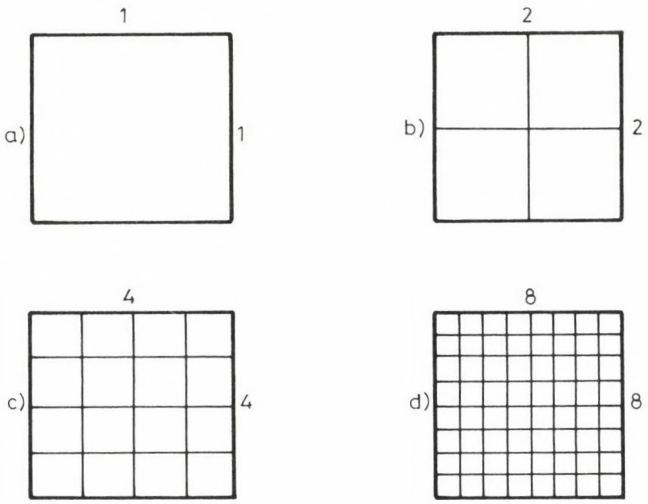

Fig. 4. Torsion of a square cross section in case of different finite element meshes

consist of two different materials with material constants $G=G_1=38461.538$ MPa, $G_2=2G_1$, inequality

$$I_T(U^*) = 7{,}5752 \cdot 10^{11} \leq I_T \leq I_T(\phi^*) = 7{,}5758 \cdot 10^{11}$$

is obtained in case of mesh according to 4d. By means of relaxation method, Ely, I.F. and Zienkiewicz, O.C. /7/ obtained a value of $0{,}1941\ GL^4 = 7{,}4654 \cdot 10^{11}$ for I_T while Ecsedi, I. /3/ estimated $I_T(U^*) = 0{,}1515\ GL^4 = 5{,}8269 \cdot 10^{11}$, $I_T(\phi^*) = 0{,}25\ GL^4 = 9{,}615 \cdot 10^{11}$. Here L is the length of the side of the square. It can be seen that practically exact solution has been supplied by the finite element method also in this case.

Example 3

The beam schematically illustrated in Fig. 5 is reinforced by a compact cylinder of radius R_3 and/or a pipe of radius R_3, R_2 in such a way that the elastic coefficient of E_2 will considerably exceed that of the original cross section that is

$$E_1 = 2{,}14 \cdot 10^5 \text{ MPa}, \quad E_2 = 5{,}8 \cdot 10^5 \text{ MPa}, \quad \nu = 0{,}3 .$$

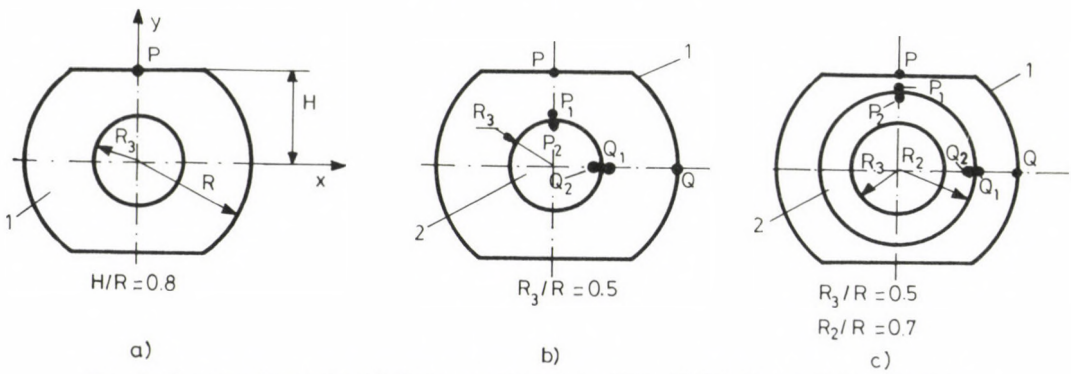

Fig. 5. Torsion of spindle (a) Homogeneous cross section; b) Reinforcement by cylindric, compact, high-strength core; c) Reinforcement with No. 2 high-strength pipe)

Table 2

Structure	5a	5b	5c
$I_T(U^*)$ /Nmm^2/	$0.99336 \cdot 10^{13}$	$1.1357 \cdot 10^{13}$	$1.3150 \cdot 10^{13}$
$I_T(\phi^*)$ /Nmm^2/	$0.99364 \cdot 10^{13}$	$1.1360 \cdot 10^{13}$	$1.3153 \cdot 10^{13}$
P	1.697 (1.698 U)	1.446 (1.4457 U)	1.1765
P_1	0.9479	0.7334	0.9553
σ_{red} /MPa/ P_2	0.9485	1.986	2.5906
Q	1.336	1.185	1.0252
Q_1	0.5966	0.5749	0.6821
Q_2	0.5966	1.558	1.8485

The values of torsional rigidity according to (24) and (35) in case of R = 100 mm together with the values of stress obtained at some points for a torsional rigidity of $M_T = 10^6$ Nmm are tabulated in Table 2.

The values determined by calculaton on the basis of U and ϕ differ from each other in the fourth digit. The values of stress according to 5a

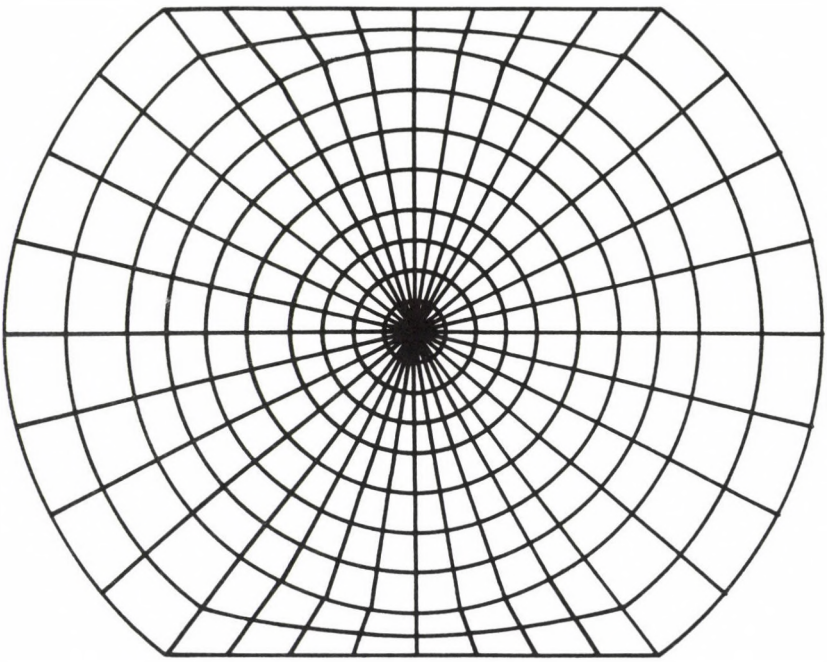

Fig. 6a. Finite element mesh of spindle

and 5b have been determined on the basis of U while those according to 5c on the basis of ϕ. The upper and lower limits obtained for torsional rigidity are practically identical. The area of the cross section is $A = 2{,}8146 \cdot 10^{14}$ mm^2 while the values of intertia calculated for axes x and y are $I_x = 5{,}3084 \cdot 10^7$ mm^4 and $I_y = 7.6124 \cdot 10^7$ mm^4, respectively. In the case denoted by 5a, there exists inequality $I_T < I_p = I_x + I_y$.

The finite element mesh associated with structures 5a and 5b is illustrated in Fig. 6a while stress σ_{red} arising along the typical lines of structural elements 1 and 2 in case 5b is given in Figs 6b and 6c, respectively. Higher stresses arise in the internal cylinder of higher rigidity, $E_2 > E_1$, than in the external body.

In case of cross section 5c, Fig. 7a shows the mesh while Figs 7b, c indicate stress σ_{red}. The values of stress are higher in the internal pipe than in the external body also in this case, moreover, the maximum of σ_{red} in the internal pipe is higher than the value in case of 5b. The stresses at point P, Q of the external body reduced as compared with the state according to 5a while those at points P_2, Q_2 increased considerably (approximately threefold).

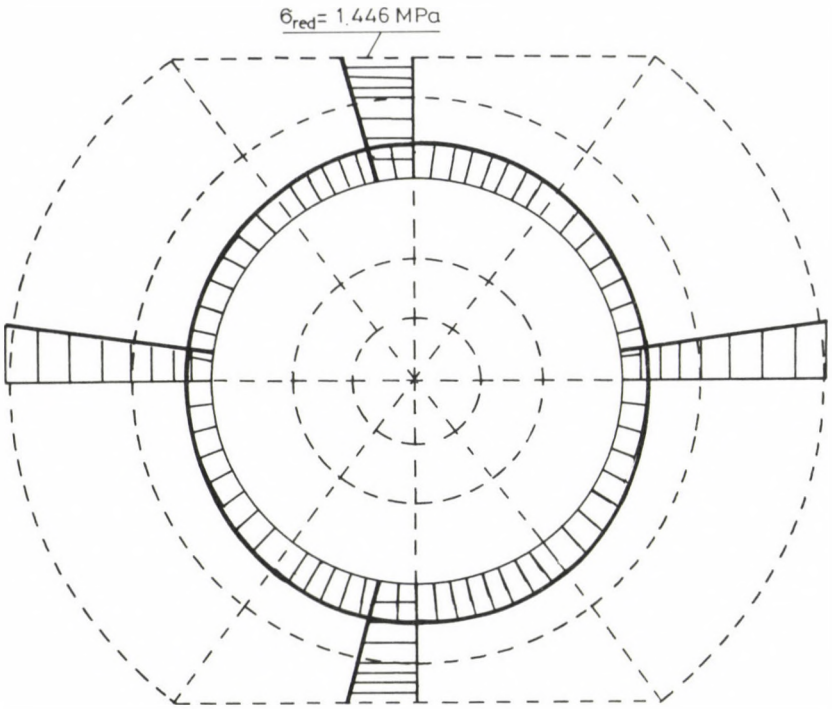

Fig. 6b. Stress σ_{red} arising in structure shown in Fig. 5b along typical lines of the external body

Conclusions

Solution of the St. Venant torsion problem permits the torsional rigidity of any arbitrary cross section to be determined. Using the classic variation principles of the theory of elasticity, local approximation (finite element approximation) provides satisfactory limites for torsional rigidity.

The numerical examples presented above given, in fact, a proof of what has been said above. For the calculations, the 'torsional' finite elements can be simply built into the usual finite element program systems.

The elements built into FEM-3D program system are isoparametric elements of 8 or 6 nodes. To illustrate the stressed state graphically, the

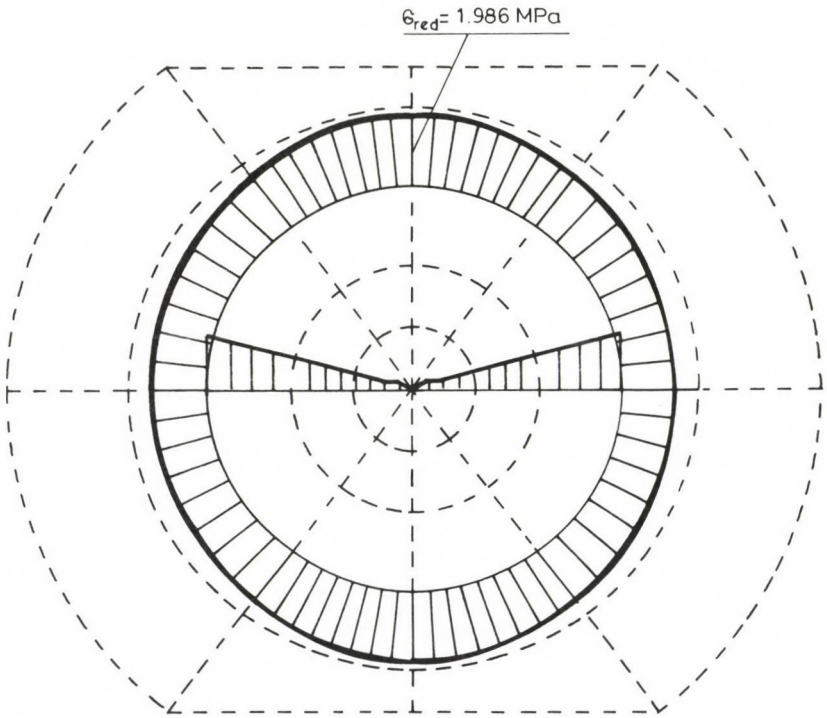

Fig. 6c. Stress σ_{red} arising in structure shown in Fig 5b along typical lines of the internal body

cross section is divided in subdomains of a different material each. In this way, the gap in stressed state at the boundary of subdomains of different material can be illustrated in a convenient way.

Appendix

A.1 Stationarity of total complementary energy

Complementary energy of a prismatic bar made of different materials, unloaded over the external surfaces, with given displacement at endplate $z = L$:

$$\pi_C = \frac{1}{2} \int_0^L dz \sum_e \int_{(A^e)} \underline{\tau} \cdot \underline{\gamma} \, dA \, dz - \sum_e \int_{(A_L^e)} \underline{\tau} \cdot \underline{u} \, dA \,, \qquad (A.1)$$

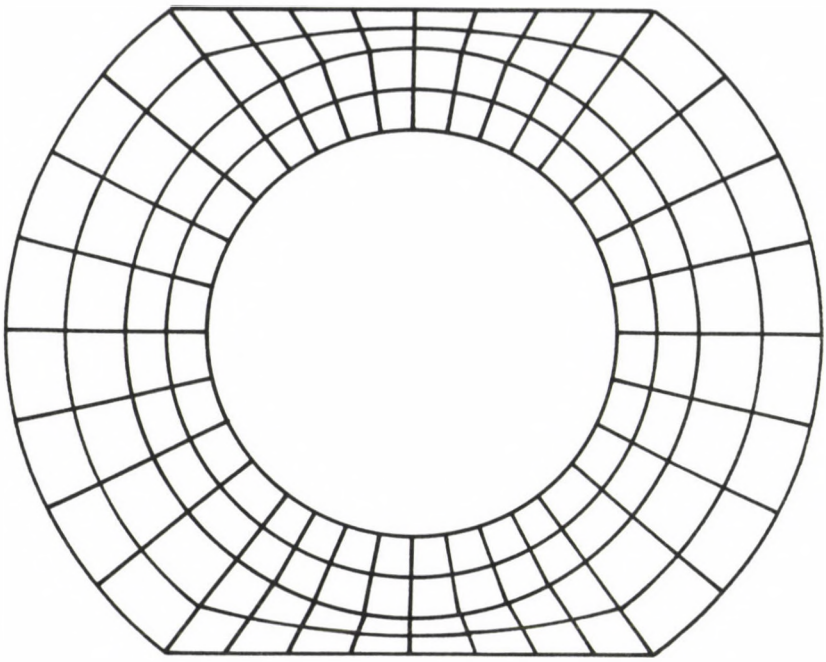

Fig. 7a. Finite element mesh of spindle according to Fig. 5c

where $\sum_{e}$ - summation of subdomains of number N constituting the cross section.

With stress function U, stress $\underline{\tau}$ and shear strain vectors $\underline{\gamma}$:

$$\underline{\tau} = \tau_{xz}\,\underline{i} + \tau_{yz}\,\underline{j} = \vartheta\,(\nabla U \times \underline{k})\,,$$
$$\underline{\gamma} = \gamma_{xz}\,\underline{i} + \gamma_{yz}\,\underline{j} = \underline{\underline{C}} \cdot \underline{\tau}\,, \tag{A.2}$$

where $\underline{\underline{C}}$ - fourth-order tensor of material constants,

∇ - Hamilton's differential operator.

Displacement taking place in the bar:

$$\underline{u} = u\,\underline{i} + v\,\underline{j} + w\,\underline{k}\,,$$
$$\underline{u} = w\underline{k} + \vartheta\, z\,(\underline{k} \times \underline{R})\,, \tag{A.3}$$

where the first term results from warping of the cross section while the

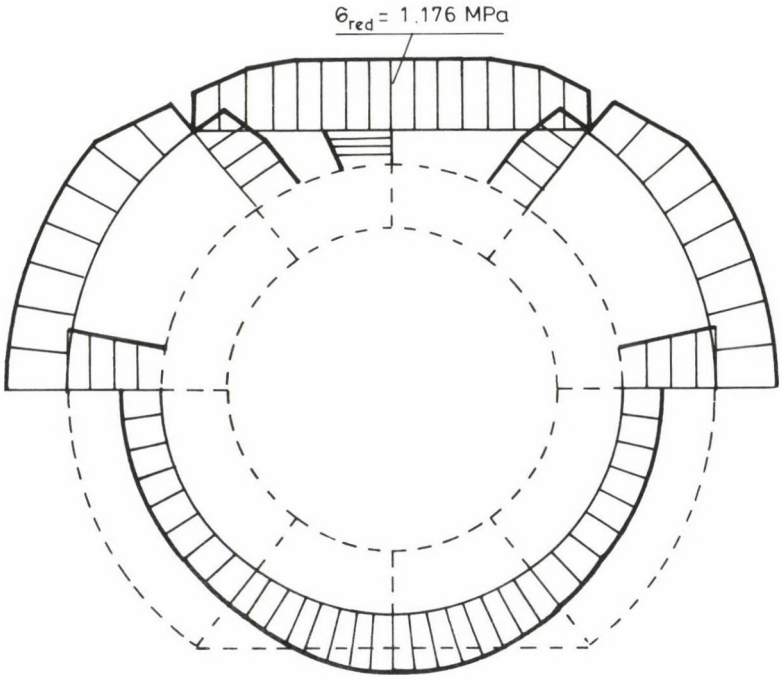

Fig. 7b. Stress σ_{red} arising in the external body of structure shown in Fig. 5c

second term stands for the rigid-body type angular displacement of the cross section,

ϑ - angle of twist per unit length,

$\underline{R}=x\underline{i}+y\underline{j}$ - position vector in the cross section,

z - co-ordinate of the bar along the longitudinal axis.

Using the displacement field,

$$\underline{\gamma} = \nabla w + (\underline{k} \times \underline{R}) \quad \vartheta \,. \tag{A.4}$$

With (A.2), (A.3) taken into consideration,

$$\pi_c = \frac{1}{2} \vartheta^2 L \left(\sum_e \int_{(A^e)} \nabla U \,.\, \underline{\underline{C}} \,.\, \nabla U \, dA + 2 \sum_e \int_{(A^e)} \nabla U \,.\, \underline{R} \, dA \right) \tag{A.5}$$

and with the first variation of π_c taken,

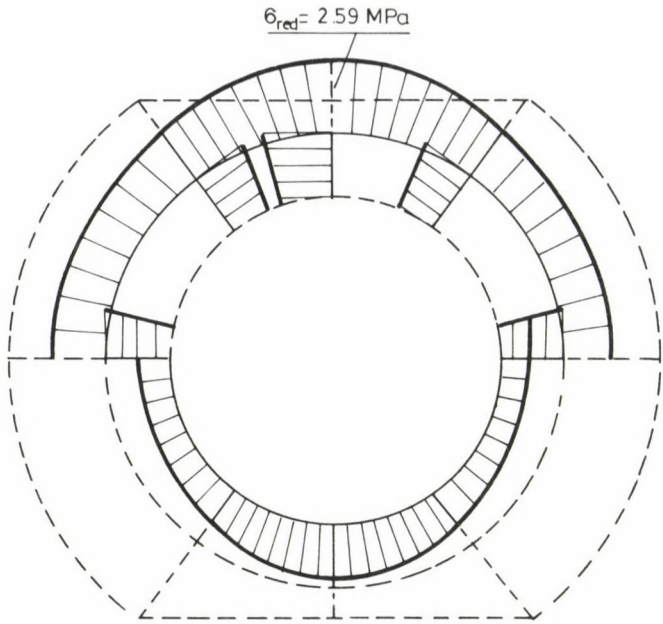

Fig. 7c. Stress σ_{red} arising in the internal body of structure shown in Fig. 5c

$$\delta\pi_c = \vartheta^2 L \sum_e \int_{(A^e)} (\delta\nabla U \,.\, \underline{\underline{C}} \,.\, \nabla U + \delta\nabla U \,.\, \underline{R})\, dA \,,$$

then, with also identities

$$\delta\nabla U \,.\, \underline{\underline{C}} \,.\, \nabla U = (\nabla\delta U) \,.\, \underline{\underline{C}} \,.\, \nabla U = (\nabla\delta U \,.\, \underline{\underline{C}} \,.\, \nabla U) - \delta U(\nabla \,.\, \underline{\underline{C}} \,.\, \nabla U)$$

$$\delta\nabla U \,.\, \underline{R} = (\nabla\delta U) \,.\, \underline{R} = (\nabla\delta U \,.\, \underline{R}) - \delta U\,(\nabla \,.\, \underline{R}) = (\nabla\delta U \,.\, \underline{R}) - \delta U \,.\, 2 \,,$$

and/or the Gauss integral transformation theorem

$$\int_{A^e} \nabla \,.\, (\,)\, dA = \int_{\Gamma^e} \underline{n} \,.\, (\,)\, ds$$

taken into consideration, we can write:

$$\delta J = \frac{\delta\pi_c}{\vartheta^2 L} = \sum_e \Big\langle \int_{\Gamma^e} (\underline{n} \,.\, \underline{\underline{C}} \,.\, \nabla U)\, \delta U\, ds + \int_{\Gamma^e} \underline{n} \,.\, \underline{R}\, \delta U\, ds -$$

$$- \int_{(A^e)} \delta U \left[(\nabla U \,.\, \underline{\underline{C}}\nabla U) + 2 \right] dA \Big\rangle \,.$$

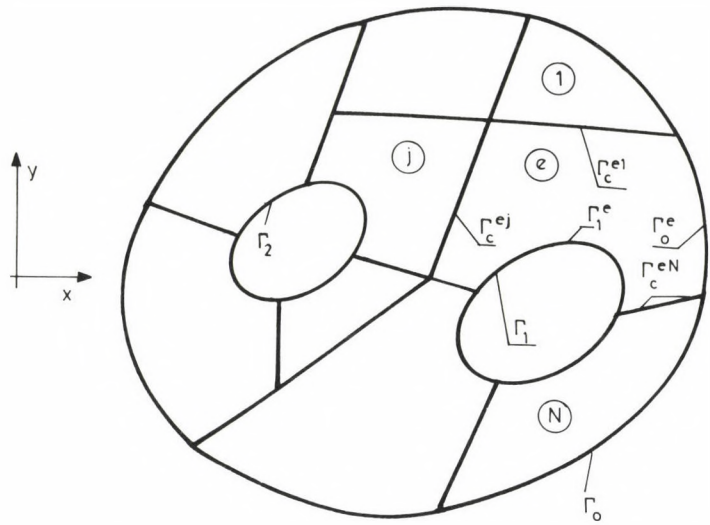

Fig. A.1. Geometrical characteristics of a compound cross section
(N - number of subdomain; boundaries: Γ_o - external, $\Gamma_h = \Gamma_1 + \Gamma_2$ - hole;
joint between subdomains: $\Gamma_c^e = \Gamma_c^{e1} + \ldots + \Gamma_c^{ej} + \ldots + \Gamma_c^{eN}$, e = 1, ..., n)

Considering that Γ^e can be divided in boundary sections Γ_o^e (external), Γ_c^e (joining) and Γ_h^e (hole) (see Fig. A.1)

$$\Gamma^e = \Gamma_o^e + \Gamma_c^e + \Gamma_h^e ,$$

and

$$\underline{\tau} \cdot \underline{n} = 0 \Rightarrow U \text{ const}$$

at the free boundaries (Γ_o^e, Γ_h^e),

$$\delta J = \sum_e \left\langle \int_{e_c} (\underline{n} \cdot \underline{\underline{C}} \cdot \nabla U + \underline{n} \cdot \underline{R})\ \delta U\ ds + \right.$$

$$+ \int_{e_h} (\underline{n} \cdot \underline{\underline{C}} \cdot \nabla U + \underline{n} \cdot \underline{R})\ \delta U\ ds - \qquad (A.6)$$

$$\left. - \int_{(A^e)} \left[\delta U\ (\nabla \cdot \underline{\underline{C}} \cdot \nabla U) + 2 \right] dA \right\rangle = 0 .$$

With the continuity of U ensured, dynamic fitting condition

$$\underline{\tau}^e \cdot \underline{n}^e + \underline{\tau}^j \cdot \underline{n}^j = 0$$

is automatically existing at the boundary of the elements since, in the knowledge of (A.2),

$$\vartheta\left[(\nabla U \times \underline{k}^e) \cdot \underline{n}^e + (\nabla U \times \underline{k})^j \cdot \underline{n}^j \right] = 0$$

$$\nabla U^e \cdot \underline{t} - \nabla U^j \cdot \underline{t} = 0 \ ,$$

that means that the directional derivatives along the boundary are identical

$$\left.\frac{\partial U}{\partial s}\right|_e = \left.\frac{\partial U}{\partial s}\right|_j \ ,$$

a condition always satisfied in case of continuity $U^e = U^j$.

The integrals according to (A.6) disappear as a result of the arbitrary variation of field U. As a result, the basic equation for U is obtained with the last term while additional considerations are necessary to clear the physical content of the first two integrals.

Let the joint effect of elements e and j be denoted by Γ_c^{ej} . Now, considering only continuity U instead of the first integral, we can write that

$$\sum_e \int_{\Gamma_c^e} ds = \ldots + \int_{\Gamma_c^{ej}} \delta U \, (\underline{n}^e \cdot \underline{\underline{C}} \cdot \nabla U^e + \underline{n}^j \cdot \underline{\underline{C}}^j \cdot \nabla U^j) \, ds + \ldots$$

the integral disappearing, since δU is arbitrary, in such a way that the expression in parantheses under the integrand is zero. The equation obtained expresses the equivalence of the displacement. Actually, taking the relationships according to (A.4), (A.2) as a starting point,

$$\underline{\underline{C}} \cdot \underline{\tau} = \vartheta \, \underline{\underline{C}} \cdot (\nabla U \times \underline{k}) = \nabla w + \vartheta \, (\underline{k} \times \underline{R})$$

which, after multiplication by tangentional unit vector $\underline{t}^e$ or $\underline{t}^j$ leads to expressions

$$-\vartheta (\nabla U \cdot \underline{\underline{C}})^e \cdot \underline{n}^e = \nabla w^e \cdot \underline{t}^e + \underline{n}^e \cdot \underline{R} \, \vartheta \quad \text{and}$$

$$-\vartheta \, (\nabla U \cdot \underline{\underline{C}})^j \cdot \underline{n}^j = \nabla w^j \cdot \underline{t}^j + \underline{n}^j \cdot \underline{R} \, \vartheta$$

with respect to

$$\underline{n}^s = \underline{t}^s \times \underline{k} = -\underline{k} \times \underline{t}^s \quad (s = e,j) .$$

With the equations obtained added, we arrive at the equation expressing equivalence of the displacement,

$$(\nabla U \cdot \underline{\underline{C}} \cdot \underline{n})^e + (\nabla U \cdot \underline{\underline{C}} \cdot \underline{n})^j = 0 \quad \underline{R} \in \Gamma_c^{ej}$$

with respect to the continuity of deplanation w as well as to the opposite orientation of the normals ($\underline{n}^e = -\underline{n}^j$).

The second integral according to (A.6), assumed at the boundary of the holes,

$$\sum_e \int_h^e (\underline{n} \cdot \underline{\underline{C}} \cdot \nabla U + \underline{n} \cdot \underline{R}) \delta U \, ds =$$

$$= \sum_h \delta U \int_{\Gamma_h} (\underline{n} \cdot \underline{\underline{C}} \cdot \nabla U) \, ds - 2A_h = 0 ,$$

supplies, except for constant ϑ, the circulation theorem:

$$\oint_{\Gamma_h} \underline{\gamma} \cdot d\underline{R} = 2 \vartheta A_h ,$$

since along the hole, the variation of U is arbitrary but everywhere identical.

To sum up, to be 'a priori' ensured is the constancy at boundaries Γ_o, Γ_h, while the continuity at the boundary of the subdomains, of stress function U in the calculation based on π_c. The fields satisfying variation equation $\delta\pi_c = 0$ correspond to actual field since they provide the basic equation according to (4b) as well as the continuity and compatibility of displacement field w. Continuity U, if 'apriori' assumed, will automatically satisfy the dynamic fitting condition automatically.

A.2 Stationarity of total potential energy

If the deplanation,

$$w = \vartheta \phi$$

is expressed through warping function ϕ, the vector of specific shear strains $\underline{\gamma}$ will be

$$\underline{\gamma} = \vartheta \, (\nabla \phi + \underline{k} \times \underline{R}) \tag{A.7}$$

while that of the shear stresses

$$\underline{\tau} = \underline{\underline{D}} \, \underline{\gamma} \qquad (\underline{\underline{D}} = \underline{\underline{C}}^{-1}) \, . \tag{A.8}$$

Considering that the external surfaces are unloaded while endplate z + L corresponds to a surface of given displacement, the potential energy for the bar under torsion is

$$\pi_p = \frac{1}{2} \int_0^L dz \sum_e \int_{(A^e)} \underline{\gamma} \cdot \underline{\underline{D}} \cdot \underline{\gamma} \, dA \, .$$

After substitution and reduction:

$$\mathcal{L} = \frac{\pi_p}{\vartheta^2 L} = \frac{1}{2} \sum_e \int_{(A^e)} \left| \nabla \phi \cdot \underline{\underline{D}} \cdot \nabla \phi + 2(\underline{k} \times \underline{R}) \cdot \underline{\underline{D}} \cdot \nabla \phi \right| dA + \text{const} \, . \tag{A.9}$$

With the rule concerning derivation of products and the Gauss integral transformation theorem used repeatedly, the first variation of $\mathcal{L}$ is

$$\delta \mathcal{L} = \sum_e \oint_{\Gamma^e} \delta \phi (\underline{n} \cdot \underline{\underline{D}} \cdot \nabla \phi + \underline{n} \cdot \underline{\underline{D}} \cdot (\underline{k} \times \underline{R}) \, ds -$$

$$- \sum_e \int_{(A^e)} \delta \phi \, (\nabla \cdot \underline{\underline{D}} \cdot \nabla \phi) + (\nabla \cdot \underline{\underline{D}} \cdot (\underline{k} \times \underline{R})) \quad dA = 0 \, .$$

basic equation)

In place of the second term of the first integral, also

$$- \oint_{\Gamma^e} \delta\phi \, (\underline{t} \cdot \underline{\underline{D}} \cdot \underline{R}) \, ds$$

can be written and thus, with the continuity of ϕ ensured in case of an arbitrary value of $\delta\phi$, the disappearance of the integral results in dynamic fitting condition

$$(\underline{n} \cdot \underline{\underline{D}} \cdot \nabla\phi)^e + (\underline{n} \cdot \underline{\underline{D}} \cdot \nabla\phi)^j - (\underline{t}^e \cdot \underline{\underline{D}}^e + \underline{t}^j \cdot \underline{\underline{D}}^j) \cdot \underline{R} = 0$$

at boundary Γ_c^{ej}, dynamic boundary condition

$$\underline{\tau} \cdot \underline{n} = 0 \Rightarrow$$

$$\underline{n} \cdot \underline{\underline{D}} \cdot \nabla\phi - \underline{t} \cdot \underline{\underline{D}} \cdot \underline{R} = 0$$

at boundaries Γ_o and Γ_h while the disappearance of the integral over subdomain A^e yields the basic equation expressing the value of the quantity in brackets.

It follows from what has been said above is that, in addition to derivability, the only requirement to be 'a priori' met by ϕ is continuity while in calculation based on U, ϕ is also expected to be constant at boundaries Γ_o, Γ_h.

REFERENCES

1. Arutiunian, N.H.-Abramian, B.L.: Krucenie uprugih tel (in Russian). 'Fismatgis' Moskow 1963
2. Lehnicki, S.G.: Krucenie anisotopnih tel i neodnorodnih stershnei (in Russian). Isd. 'Nauka', M. 1971
3. Ecsedi, I.: Variation method giving the solution to the torsion problem of prismatic bars of composite material. Acta Techn. Acad. Sci. Hung. 85(1-2), (1977), 147-177
4. Karayannis, C.G.-Soulis, J.V.: A numerical method for torsional analysis of structural elements. Computers & Structures, 36. No. 4 (1990), 755-768
5. Lurie, A.I.: Teoria uprugosti (in Russian). Nauka, Moskow 1970
6. Zienkiewicz, O.C.: Finite element methods in engineering. McGraw-Hill, New York 1971
7. Gofman, M.N.: Naprjashennoie sostoianie armirovannovo vala besshponotshnovo soedenia pri krutshenii (in Russian). Detail masin, 46, Tehnika (1988)
8. Ely, I.F.-Zienkiewicz, O.C.: Torsion of compound bars. Int. J. of Mech. Sic. 1 (1960), 356-365

Acta Technica Acad.Sci.Hung., 104(1-3), pp. 237-256 (1991/92)

TRICKLE LATERAL MAXIMUM LENGTH FOR SELECTED FLOW UNIFORMITY

SHARAF, G.A.*

(Received: 14 August 1990)

The purpose of this paper is to present an analytical expression for the physical variables in lateral line design based on principles of fluid mechanics and dependent on hydraulic characteristics of emitter and lateral line, in addition to demonstrate a relationship can help in limiting lateral length for a selected flow uniformity. The final resulted formula while complex in form including all variables involved in the design process which are, lateral diameter, emitter characteristics and operating pressure, spacing requirement, tube friction, emitter connection losses, emitter connection type, discharge uniformity, and landslope. To demonstrate the effect of some of these variables, graphic solutions will be presented based on computer solution.

NOTATION

Symbols	Explanation	Units
b	Emitter barb diameter	mm
d	Inside lateral diameter	mm
D	Inside lateral diameter	m
f	Pipe friction factor	-
fe	Emitter connection loss as an equivalent length	m
F	Reduction coefficient for friction loss in multiple outlet pipe	-
g	Acceleration of gravity	m/s^2
hf	Lateral friction loss	m
H	Pressure head at the emitter	m
HE	Elevation differences between inlet and far end of the lateral	m
HF	Total pressure loss	m
hfe	Emitter connection pressure loss	m
HMAX	Maximum operating pressure for an emitter	m
HMIN	Minimum operating pressure for an emitter	m
HN	Pressure head at inlet of lateral	m
HO	Pressure head at far end of lateral	m
i	Subscript identifying a particular length ratio	l/L
l	Given length measured from head end of the line	m
L	Total Lateral line length	m
L'	Equivalent length of lateral with emitters	m

*Sharaf, G.A., Research Associate Aspirant, Department of Water Management and Land Reclamation, University of Agricultural Sciences, H-2100 Gödöllő, Nyisztor tér 1, Hungary

Akadémiai Kiadó, Budapest

Symbols	Explanation	Units
m	Flow rate exponent	-
N	Number of emitters on lateral	-
p	Emitter flow variation	%
q	Emitter flow rate	l/h
Q	Lateral flow rate	l/h
Re	Reynolds number	-
s	Land slope	-
se	Emitter spacing on lateral line	m
V	Flow velocity	m/s
V_m	Coefficient of manufacturing variation	-
V_q	Coefficient of variation of emitter flow due to hydraulics	-
V_t	Total coefficient of variation of emitter flow	-
x	Emitter discharge exponent	-

Introduction

Trickle irrigation uses small diameter plastic pipes or tubes with water emission devices at necessary spacing to deliver water to soil surface near the plants. The sizing of tubes for a trickle irrigation lateral is a decision-making process based on numerous factors. They are crop water neads, climate, soil properties, hydraulic principles, emitter flow characteristics, field size and topography, irrigation and tube economics, and criteria of water application uniformity. The relationship among all the factors is complex. Current lateral design practice has evolved from relationships that were developed for design of other types of irrigation systems. Recent research on several aspects of small tube hydraulics has provided new information that can improve the energy, water, material and giving system designers better information on which to base decision.

The design of single drip irrigation lateral lines considering hydraulic variation has been presented by various researchers. Meyers and Bucks, 1975, and Wu and Gitlin, 1974 derived the hydraulic energy gradient line for determining the emitter flow variation and uniformity along a lateral line. Howell and Hiler, 1974, and Warrick and Yitayew, 1988 developed lateral line design equations based upon specific uniformity criteria. Watters and Keller, 1979 developed a general friction curve can be used for graphical solutions assnciated with laterals and manifolds. Keller and Radrigo, 1979 used this principle to develop numerical solutions for both single and pairs of nontaperd laterals on uniforme slopes. Paco, 1985 developed a procedure to determine the length of sections in the case of lateral lines with two diameters. Benami and Ofen, 1984, and Wu, I. P.,

1985 referred to use polyplot for solving trickle lateral optimum diameters and corresponding length for flat or sloping surfaces.

Emitter characteristics

The emitter is a most important part of a trickle irrigation system. In lateral design it is not possible to discuss lateral sizing separate from emitter characteristics. Many emitters are sensitive to pressure variation. As the pressure along the lateral line varies due to pipe friction, elevation, or accidental restrictions, so does the discharge from the emitter. This casues a non-uniform application of water. The sensitivity to pressure can impose serious limitations on lateral line length for a specified uniformity of irrigation, especially on sloping land.

The mitter discharge rate is a function of operating pressure related by the equation

$$q = k\, H^{x} , \qquad (1)$$

in which q - emitter flow rate

H - operating pressure

k - proportionality factor dependant on the emitter and units of q and H

x - exponent in emitter discharge relationship.

The magnitude of (x) characterizes the discharge versus pressure relationship. It is the measure of how sensitive the discharge is to pressure. The value of (x) will typically fall between 1 and 0 depending on the design of the emission device. For an emitter with laminar flow conditions, (x) will theoretically equal 1. If flow is fully turbulant, the value of (x) should be 0.5, a perfect pressure compensating emitter will have a value of (x) equal to 0.

Emitter flow variation

The variation or nonuniformity of emitter discharge in trickle lateral is the result of a number of factors. Themost important of these factors is the hydraulic variation and emitter discharge variation. The hydraulic

variation along the lateral line is a function of land slope, length and diameter of the pipe and emitter discharge relationship. Emitter variation at a given operating pressure is caused by manufacturing variability, emitter plugging, water temperature changes, number of emitters per plant, and emitter wear. If the hydraulic pressure at each emitter can be determined, it is possible to determine, the flow variation due to hydraulics along the lateral. The coefficient of hydraulic variation Vq can be found from the following (Bralts, Wu and Gitlin, 1981):

$$V_q = \frac{S_q}{q_m} , \qquad (2)$$

in which S_q - standard deviation of emitter flow rates due to hydraulics l/h

q_m - mean emitter discharge l/h.

Since no two emitter devices can be identically manufactured some variation will exist from emitter to emitter.Solomon, 1977 recommended adopting a measure of this variation called the coefficient of manufacturing variation Vm, given by the following relationship

$$V_m = \frac{S_m}{q_m} , \qquad (3)$$

in which S_m - standard deviation of the flow rates due to manufacturing l/h.

The values of Vm range from .02 to.2 for the various types of emitters (Solomon, 1977). The total emitter flow variation V_t which is affected by both hydraulics and manufacturing was determined statistically (Bralts, et al. 1981) and verified by a computer simulation (Wu, et al., 1985) as follows:

$$V_t = \left(V_q^2 + V_m^2 \right)^{.5} . \qquad (4)$$

The coefficient of flow variation V_t will also be affected by the cases that several emitters are irrigating a tree, or for row crops. This is called grouping effects which is generally expressed as follows (Wu, et al., 1988):

$$V_{tg} = V_t / n^{.5} , \qquad (5)$$

in which V_{tg} - coefficient of variation of emitter flow when n emitters are grouped together as an unit per plant.

The effect of temperature on emitter flow variation is not only due to entirely viscosity changes in the water, but also due to dimensional changes in the emitter with temperature. Benjamin and Tol, 1980 studied the effect of temperature on emitter discharge. The discharge sensitivity to temperature was found to be positive for helical long path emitter ($x > .5$), not significant for the labyrinth emitter ($x \simeq .5$), and negative for the vortex emitter ($x < .5$). The same results were confirmed by Decroix, 1985.

Lateral pressure relations

Emitters may have a designated operating pressure range for proper discharge, flushing action and safety from rupture. It should be recognized as pressure limits not to be exceeded in the field as shown in Fig. 1. A wide range of operating pressure CHMAX - HMINO is a desirable quality in an emitter. These limits should be stated by the manufacturers. Emitter operating pressure limits imply that HN < HMAX and HO > HMIN.

Howell and Hiller, 1974 modified Eq. (1) for the inlet pressure, (HN) and pressure head at the far end of lateral (HO) as follows:

$$HN = \left(q/k \left(1 + (p/100)\right)\right)^{1/x} \tag{6}$$

and

$$HO = \left(q/k \left(1 - (p/100)\right)\right)^{1/x}, \tag{7}$$

in which p - emitter flow variation allowed in a lateral line expressed as a percentage, for example $\pm$ 10% from (q) equals a (p) of 10. Equations (6) and (7) can be combined to obtain

$$\frac{HMIN}{HMAX} < \frac{HO}{HN} = \left| \frac{1 - (p/100)}{1 + (p/100)} \right|^{1/x} . \tag{8}$$

The above relationship relates emitter pressure ratio, lateral pressure limit, emitter flow variation and the emitter discharge exponent. A graphic solution to Eq. (8) introduced by Braud and Soon, 1979 in Fig. 2 shows that the selection of emission uniformity coefficient P and emitter discharge exponent x places a fix on the pressure ratio HO/HN allowable in the lateral. The limits of HO/HN must also lie within the maximum and mini-

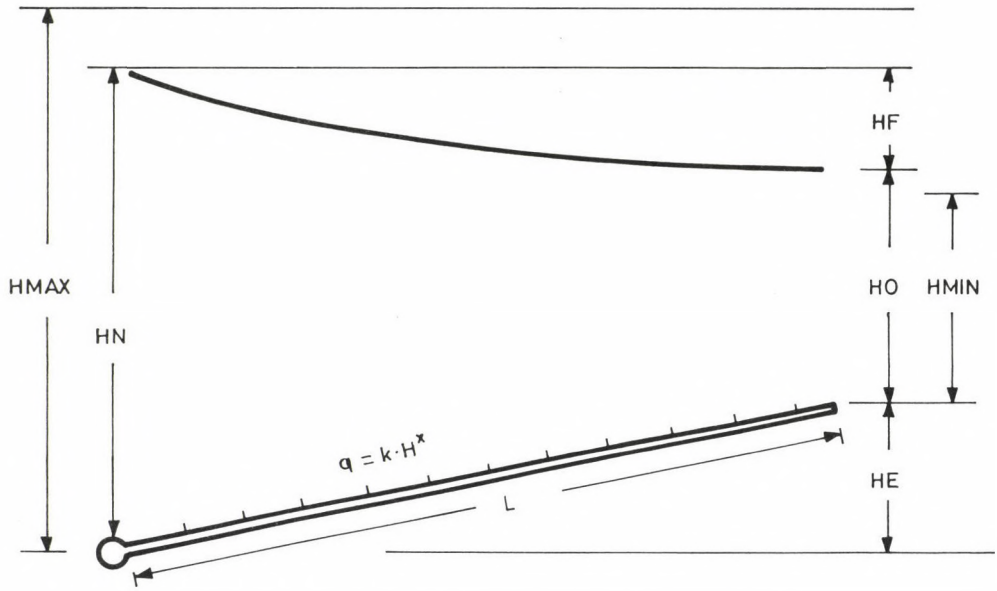

Fig. 1. Pressure head relationships shows lateral uphill
HMAX > HN; HMIN < HO; HE; HF

mum pressure heads required by the emitter for proper operation, HMIN < HO and HN < HMAX.

The pressure drop and elevation differences are what cause the difference in HO and HN. As diagramed in Fig. 1, pressure head relationships in a lateral then, can be described as follow:

$$HN = HF + HO \pm HE \ , \tag{9}$$

in which HE = pressure loss or gain due to elevation differences. (+) means that the lateral runs upslope and (-) downslope.

Dividing Eq. (9) by HN yields

$$\frac{HO}{HN} = 1 - \left(\frac{HF}{HN} \pm \frac{HE}{HN} \right) \tag{10}$$

Introducing the above Equation into Eq. (8) and solving for HF yields

$$HF = HN \left(1 - \left(\frac{1 - (p/100)}{1 + (p(100)} \right)^{1/x} \pm \frac{HE}{HN} \right) . \tag{11}$$

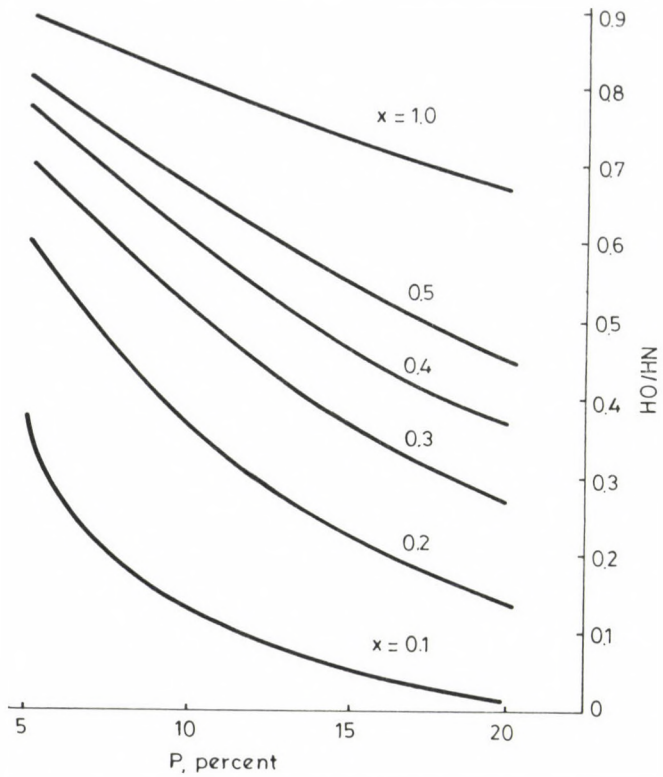

Fig. 2. Graphic solution to equation 8. Relation of HO/HN, P and x

The system pressure here is characterized by the lateral inlet pressure HN, the emitter flow variation (p), the emitter discharge exponent (x), and the elevation head HE, all of which impose a limit on the allowable lateral pressure loss HF.

Lateral pressure loss

Most trickle irrigation hydraulic analyses ignore any differences in pipe friction head loss computations for the laminar flow range. The turbulent flow formulas are generally used even in laminar flow range because velocities are so low that head losses are almost negligible. Hence, even large relative errors of 30% to 50% in computing the very small head losses occurring of the laminar flow portions of the system are negligible

(Watters and Keller, 1978). Many investigators have shown that for the small diameter smooth pipes usedin trickle laterals the Darcy Weisbach Equation combined with the Blasius Equation for f gives accurate predictions of lateral friction head loss. The Darcy Wiesbach equation is

$$hf = f \frac{L}{D} \frac{V^2}{2g} , \qquad (12)$$

in which hf - pipe friction head loss (m)

f - friction factor

L - pipe length (m)

D - inside diameter of pipe (m)

V - flow velocity in the pipe (m/s)

g - acceleration of gravity (m/s^2) .

According to the Blasius Equation

$$f = 0.23\ Re^{-.25} , \qquad (13)$$

in which Re = Reynolds number expressed as ($D\ V/\mu$), for $2 \times 10^3 < Re < 10^5$ μ = = kinematic viscosity (m^2/s), for water 1.033×10^{-6} at 20 ^{o}C.

Combining Eqs (12) and (13) yields

$$hf = 32\ (2g)^{-1}\ \mu^{.25}\ V^{1.75}\ D^{-1.75}\ L . \qquad (14)$$

Considering V = Q/A, where Q is the pipe flow rate (m^3/s), and A is the cross-sectional area of the pipe (m^2)

$$hf = .32\ (2g)^{-1}\ \mu^{.25}\ (4/3.14)^{1.75}\ D^{-4.75}\ Q^{1.75}\ L . \qquad (15)$$

Rearranging Eq. (15) becomes

$$hf = K\ D^{-4.75}\ Q^{1.75}\ L , \qquad (16)$$

in which K = constant, (7.87×10^{-4}) for water at 20 ^{o}C.

Head losses estimation in pipes with evenly spaced outlets each with uniform discharge must include a reduction coefficient F necessary to compensate for discharge decrease along the line. F values can be obtained from tables based on number of outlets or can be estimated by using Christiansen's Equation which is mainly used in sprinkler irrigation

$$F = \frac{1}{m+1} + \frac{1}{2N} + \frac{(m+1)^5}{6N^2}, \qquad (17)$$

in which N - number of emitters on the lateral

m - the exponent of the flow rate in the friction equation (1.75).

Considering Q = N q and N = L/se, then, Eq. (17) can be modified to be as follows:

$$hf = .4716\ d^{-4.75}\ F\ (q/se)^{1.75}\ L^{2.75}, \qquad (18)$$

in which hf - head loss due to friction (m)

d - lateral inside dimater (mm)

F - flow reduction coefficient

q - emitter flow rate (l/h)

se - emitter spacing (m)

L - lateral length (m).

Emitter connection losses in laterals

The emitter connector barb projects into the flow in lateral hose causes additional turbulance over and above normal pipe friction turbulance. Early studies on trickle irrigation laterals tended to confuse the emitter connection losses with the pipe friction loss. Howell and Barinas, 1978, Watters and Keller, 1979, Meshket and Warner, 1985, and Pitts et al., 1986, suggested that the energy losses across emitter connections should be considered in the lateral line design. Two methods for calculating emitter friction losse were proposed, one being the determination of equivalent additional lateral length and the other being an equivalent increase in the pipe roughness.

The method chosen to represent the additional minor losses contributed by the barbs is the equivalent pipe method. The head loss contributed by the barb is equivalenttothehead loss due to pipe friction in a length (fe) of the lateral hose. The spacing between emitters can then be increased by (fe) and the friction losses can be computed neglecting barbs but including the greater equivalent length. If the spacing of the emitters is (se), then for purpose of computing head loss, the length of the lateral (L) should be increased ot (L') where

$$L' = L \frac{se + fe}{se}, \qquad (19)$$

in which L' - the equivalent length of the lateral with emitters (m)
se - spacing between emitter connection along the lateral (m)
fe - emitter connection loss as an equivalent length of lateral. (m).

Watters and Keller, 1978 presented a graphic data on emitter barb losses for various pipe diameters and barb dimensions as shown in Fig. 3. The following Eq. (with a correlation coefficient of R = 0.99) was based on their results (formed by Pitts and Ferguson, 1986).

$$fe = 0.25\ b\ (19\ d^{-1.9}), \qquad (20)$$

in which fe - equivalent length of pipe (m)
b - emitter barb diameter (mm)
d - diameter of lateral (mm).

Equation (20) can be used to estimate the equivalent length of pipe only in case of on-line emitter connection with the same dimensions indicated in Fig. 3, while fe = 0.23 m in case of in-line type.

By introducing Eqs (19) and (20) to Eq. (18), the lateral total pressure loss (HF) then, can be estimated including both friction and minor

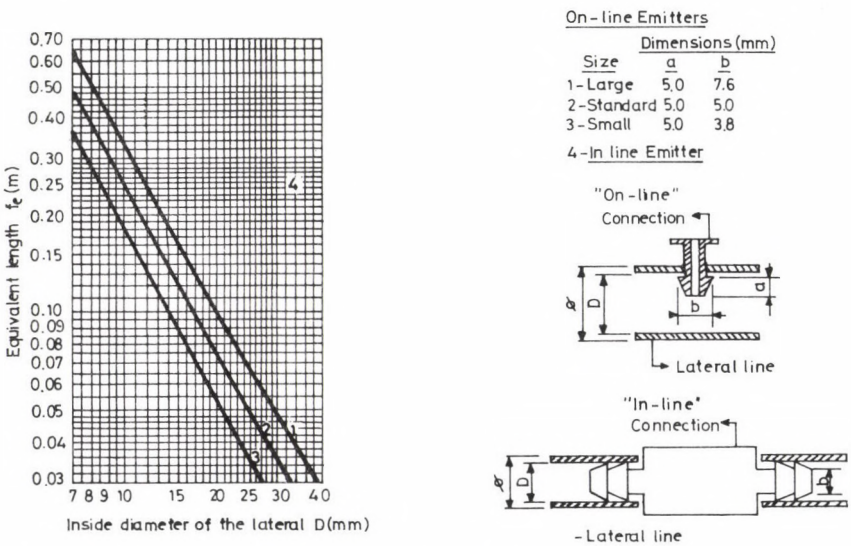

Fig. 3. Equivalent length of pipe

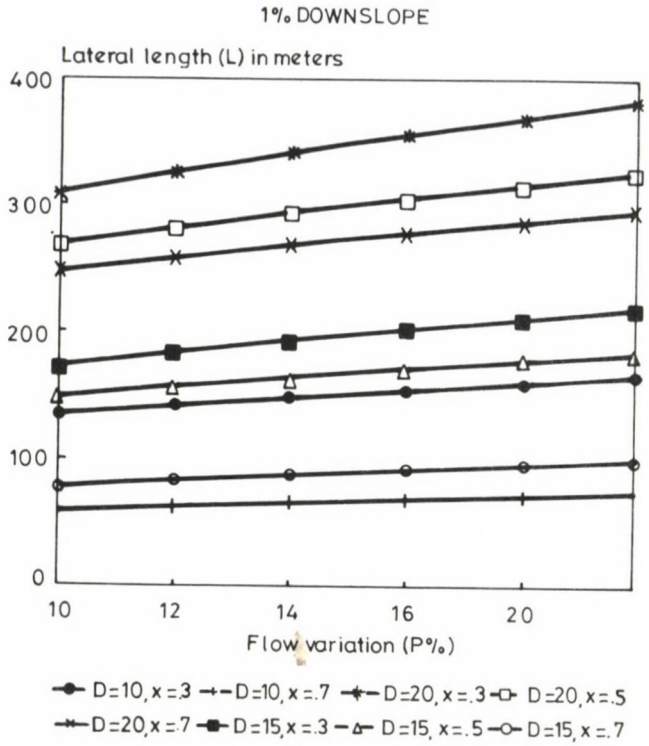

Fig. 4. Solution of equation (23)

losses as follows

$$HF = .4716\ d^{-4.75}\ F(q/se)^{1.75}\ L^{1.75}\ L \qquad (21)$$

or

$$HF = .4716\ d^{-4.75}\ F\ (q/se)^{1.75}\ L^{2.75}\ ((se+fe)/se)\ . \qquad (22)$$

The lateral maximum possible length, then can be obtained by combining Eqs (11) and (21) and solving for L

$$L = 1.314\ d^{1.727}(se/q)^{.636}\ \left[(F\ a)^{-1}\ HN\ (1 - c^{1/x} \pm (HE/HN)\right]^{.363}\ , \qquad (23)$$

in which L - lateral maximum possible length (m)

F - $(1=m+1) + (1/2N) + ((m+1)^5/6\ N^2)$

a - se/(se + fe)

c - (1 - P/100)/(1 + P/100)

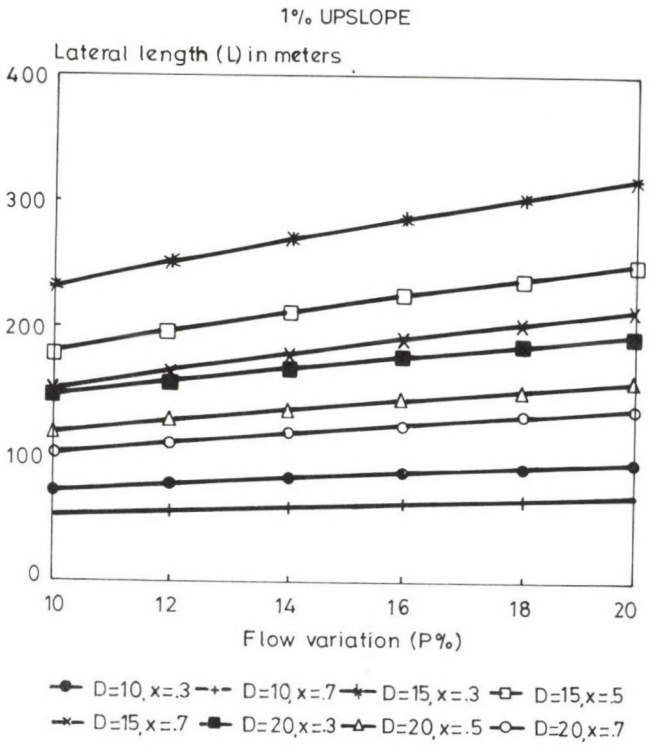

Fig. 5. Solution of equation (23)

HE- L.s

s - lateral slope (decimal).

Equation (23) includes all the variables involved in the design process. They are length, diameter, inlet pressure, emitter flow characteristics, lateral friction, emitter connection losses, emitter flow variation, spacing requirement, and land slope.

To indicate the effect of P, d, x, and s on limiting the lateral length, graphic solutions are presented for the lateral maximum length versus flow variation for three sizes of tubes 10, 15, and 20 mm, under three values of x (0.3, 0.5, and 0.7) in case of 1% downslope, 1% upslope, and leveled land as shown in Figs 4, 5 and 6, respectively.

Data were collected from literature for comparison and verification from Howell and Hiller, 1974, Jensen, 1980, and Warrick and Yitayew, 1988, respectively.The results are summarized in Table 1.

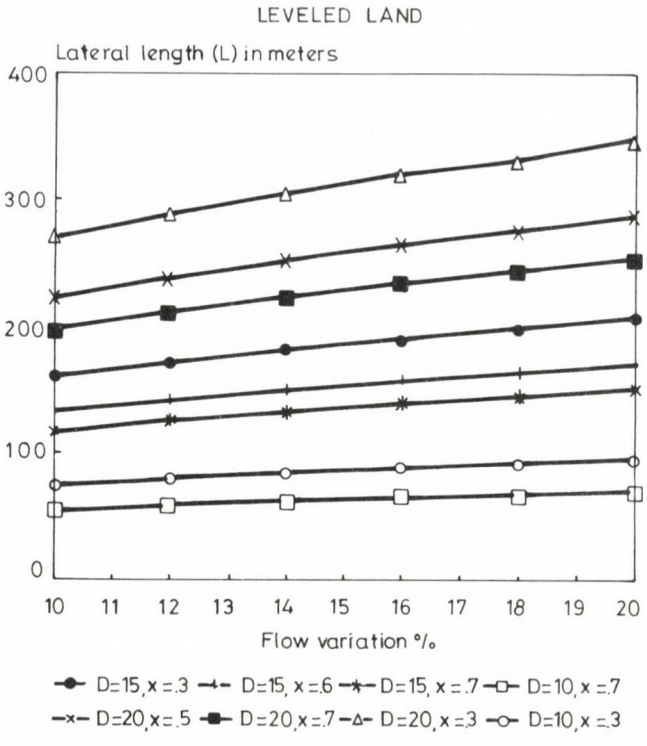

Fig. 6. Solution of equation (23)

To demonstrate the effect of spacing between emitters on lateral pressure loss, local loss caused by emitters as relative to lateral friction is illustrated versus spacing between emitter as shown in Fig. 7. The calculation of this curve based on the standard emitter dimensions for three tube sizes 10, 15, and 20 mm diameter.

Emitter flow profile along the lateral

As shown in Equation (1), the emitter flow is determined by the hydrostatic pressure at the emitter. This means whenever there is a pressure variation in the drip irrigation line there wilsl be an emitter flow variation along the irrigation line. If the length of the line is known, the pressure head gain or drop can be determined. If an input pressure is

Table 1

Input and output data for comparison

Design parameter	By		Procedure results	
	Howel and Hiler, 1974			
Input				
P =	9%	17%	9%	17%
q = 3.8 l/h				
x = 0.7				
se= 6.1 m				
d = 16 mm				
H = 5.1 m				
s = 0				
Output				
L =	347 m	434 m	337 m	425 m
HN =	5.82 m	6.4 m	5.77 m	6.4 m
HO =	4.46 m	3.91 m	4.43 m	3.85 m
HF =	1.3 m	2.24 m	1.31 m	2.48 m
hfe =	-	-	0.03 m	0.05 m
	Jensen, 1980			
Input				
P =	9%		9%	
q = 16 l/h				
x = 0.8				
se= 10				
d = 16 mm				
H = 10.1 m				
s = -1%				
Output				
L =	260 m		254 m	
HN =	12.2 m		11.25 m	
HO =	9.7 m		8.9 m	
HF =	5.1 m		4.86 m	
hfe =	-		0.07 m	
	Warrick and Yitayew, 1988			
Input				
P =	9%	17%	9%	17%
q = 4 16h				
x = 0.5				
se= 1 m				
H = 9.63 m				
d = 14 mm				
s = 0				
Output				
L =	126 m	172 m	112 m	141 m
HN =	10.6 m	11.7 m	11.4 m	13.1 m
HO =	-	-	7.89 m	6.5 m
HF =	-	-	3.07 m	5.8 m
hfe =	-	-	0.48 m	0.91 m

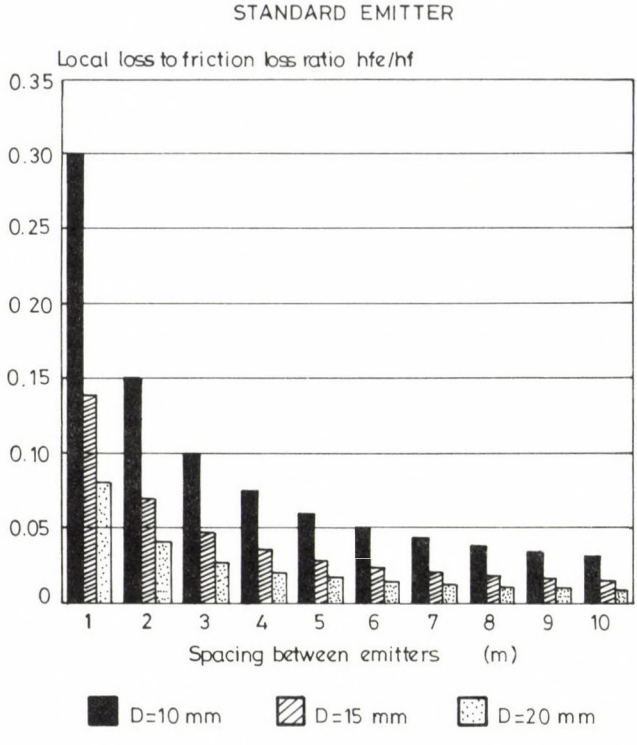

Fig. 7. Effect of spacing between emitters on lateral loss

given, the pressure distribution along a drip lateral can be expressed mathematically as follows (Jensen, 1960, and Nakayama and Bucks, 1965):

$$H_i = HN - HF_i \pm HE_i \ , \tag{24}$$

in which H_i - pressure expressed as hydrostatic head (m) at a given length ratio i,

HF_i - total pressure drop (m) at a given length ratio i,

HE_i - pressure head gain or loss (m) at a given length ratio i.

The emitter flow can be calculated by substituting the above Equation into the emitter flow Eq. (1)

$$q_i = k \left(HN - HF_i \pm HE_i\right)^x \ . \tag{25}$$

Removing k by dividing by the emitter flow at HN yields

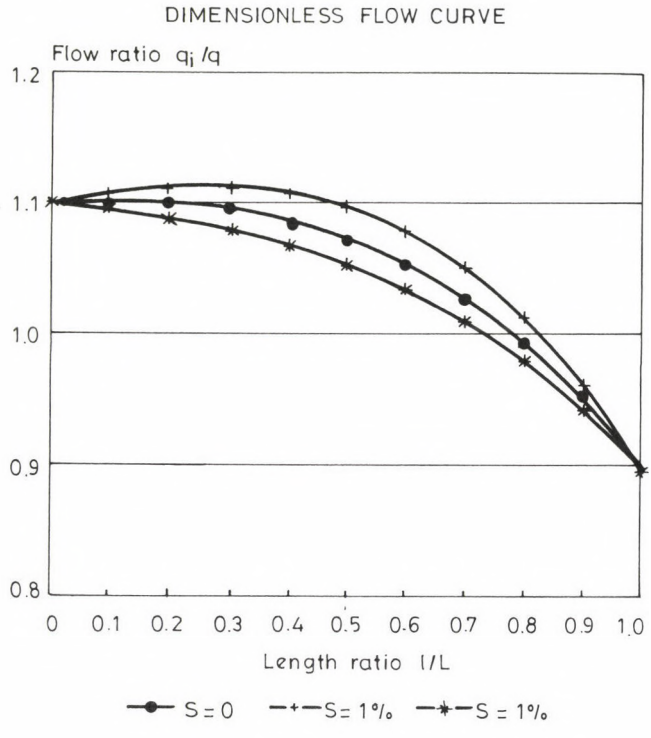

Fig. 8. Effect of slope on emitter flow profile

$$q_i = q_1 \left(1 - \frac{HF_i}{HN} \pm \frac{HE_i}{HN} \right)^x , \qquad (26)$$

in which q_i - emitter flow rate (l/h) at a length ratio i,

q_1 - emitter flow rate (l/h) at a pressure HN (first emitter).

The shape of the dimensionless emitter flow profile can be plotted from an emitter by emitter analyses. Figure 8 indicate the dimensionless emitter flow profile for emitter have function ($q = 1.21\ H^5$) for 1% downslope, leveled land, and 1% upslope. Figure 9 shows the dimensionless emitter flow profile for the same emitter along leveled lateral for selected emitter flow variation 5%, 10%, and 15%. Figure 10 indicate the effect of emitter discharge exponent x at constant emitter flow variation (10%) where s = 0 for three emitters have the same discharge with x = 0.2, 0.5, and 0.9.

A basic computer program was written to accomplish the design process. The program is able to estimate beside lateral maximum possible length for

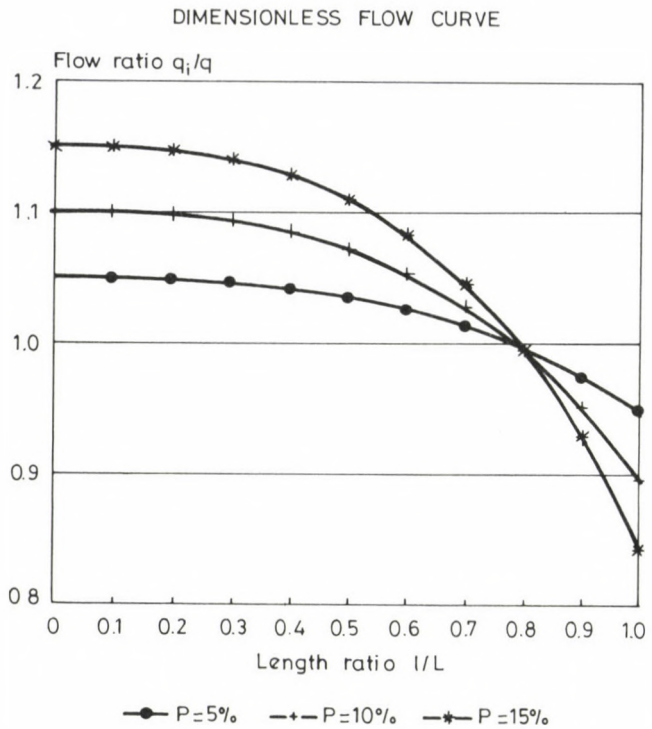

Fig. 9. Effect of flow variation on emitter flow profile

a given lateral design, overall pressure loss, pressure loss due to lateral friction, pressure loss due to emitter connections in case of on-line emitter connection or in-line emitter connection, lateral inlet pressure, pressure head at the far end of the lateral. In addition to pressure distribution and emitter flow profile along the lateral, if the following parameters are given: emitter operating presssure, lateral size, emitter flow variation, spacing of emitters along the lateral, emitter flow characteristics, emitter type connection emitter barb diameter, and land slope.

The design procedure is as follows:

1. Estimating of lateral inlet pressure (HN) and pressure head at the far end of the lateral (HO) based on the design criterion (p) and emitter flow function (x), (k) using Eqs (6) and (7), respectively.

2. Based on emitter type connection, emitter connection loss as an equivalent length (fe) will be estimated.

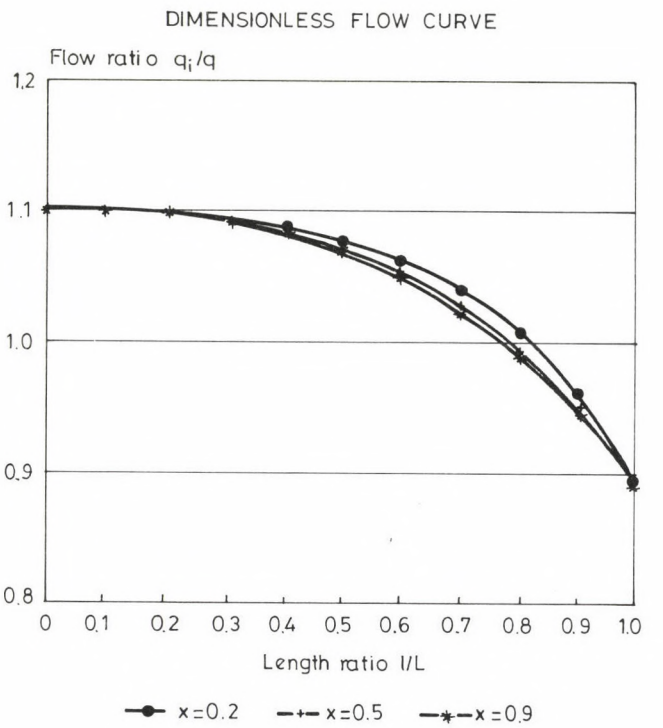

Fig. 10. Effect of discharge exponent on emitter flow profile

3. Assuming an initial lateral length for the selected lateral.

4. According to this guess, number of emitters (N), discharge reduction coefficient (F), and elevation difference (HE), will be calculated, consequently, the lateral length.

5. Comparing the calculated lateral length with the assumed value. The design is accepted when the difference is too small, otherwise, the length is rejected.

6. If the design is rejected, the calculated value will be assumed as an initial value to the lateral length and step 4, 5 wil be repeated until a proper length is found.

7. Once an approximate lateral length has been determined, the total pressure drop (HF) can be found using Eq. (22), pressure head loss due to friction (hf) using Eqs (18), and pressure loss due to emitter connection (hfe) as a difference between Eqs (22) and (18).

8. The last sequence of the design process is a loop that calculate

the pressure distribution along the lateral using Eq. (24), and emitter flow profile using Eq. (26).

Conclusions

Lateral size appears as a separate parameter in Equation (23). The lateral length is proportional to d power 1.727. This means the larger the diameter size the longer the length, if the rest of variables are constant.

In all cases the reduction in (x) value allows longer length in a given size for a given value of other variables. The advantage of using a pressure compensating emitters here is apparent.

It is seen that at high (p) values, the increase in lateral length tends to be insignificant such the effects of (x) and (d), especially in small diameter.

Local losses due to emitter connections in small distance between emitters (continuous wet strip of soil or row cultivation) have to be taken in consideration, especially in small lateral diameter while neglecting it, is possible in wide-spaced crops like orchards without significant effect on total lateral loss.

The effect of land slope, emitter flow variation, and emitter discharge exponent on dimensionless emitter flow profile have been studied. The effect of (x) seemed to be not significant from 0.2 to 0.9.

ACKNOWLEDGEMENT

I would acknowledge the sincere help and advices of Dr. László Vermes my supervisor. My sincere appreciation and thanks also to Prof. Dr. István Ijjas for his valuable consultation and continuous assistant.

REFERENCES

1. Benami, A.-Ofen, A.: Irrigation engineering. IESP, Haifa, Israel. Chapter (3), (1984), 147-192.

2. Benjamin, Z.-Tal, S.: Emitter discharge sensitivity to pressure and temperature. Journal of the Irrigation and Drainage Division ACSE 107 (IR1), (1981), 1-9

3. Bralts, V.F.-Wu, I.P.-Gitlin, H.M.: Manufacturing variation and drip irrigation uniformity. Transaction of ASAE 24 (1) (1981), 113-119

4. Braud, H.J.-Soon, A.M.: Trickle irrigation design for improved application uniformity. ASAE Paper No. 79 (1979) - 2581, St. Joseph, Michigan 49085

5. De Paco, J.L.: Lengths of sections of lateral of two diameters. Drip trickle irrigation in action, ASAE Proceedings of the Third International Drip/Tickle Irrigation Congress, Vol. I, (1985), 410-415

6. Decroix, M.-Malaval, A.: Laboratory evaluation of trickle irrigation equipment for filed system design. Drip/Trickle Irrigation in action, ASAE Proceedings of the Third International Drip/Trickle Irrigation Congress, Vol. I, (1985), 325-330

7. Howel, T.A.-Barinas, F.A.: Pressure losses across trickle irrigation fittings and emitters. ASAE Paper No. 78 (1978). - 2014, St. Joseph, Michigan 49085

8. Howel, T.A.-Hiller, E.A.: Design trickle irrigation laterals for uniformity. Journal of Irrigation and Drainage Division. ASCE 100 (IR4) (1974), 443-454

9. Jensen, M.E.: Design and operation of farm irrigation system. ASAE, St. Joseph, Michigan 49085, Chapter (16), (1980), 663-717

10. Keller, J.-Rodrigo, J.: Trickle irrigation lateral design. ASAE Paper No. 79, (1979) - 2570 St. Joseph, Michigan 49085

11. Meshkat, M.-Warner, R.C.: A user frindly interactive trickle irrigation design model. Drip/Trickle irrigation in action, ASAE proceedings of the Third International Drip/Trickle Irrigation Congress, Vol. I, (1985), 339-451

12. Myers, L.E.-Bucks, D.A.: Uniform irrigation with low pressure tirckle systems. Journal of the Irrigation and Drainage Division ASCE 98 (IR3) (1972), 341-346

13. Nakayama, F.S.-Duck, D.A.: Tirckle irrigation for crop production. Elsevier, Amsterdam, Chapter (29 (1986), 53-92

14. Pitts, D.J.-Ferguson, J.A.-Wright, R.E.: Tirckle irrigation lateral line design by computer analysis. Transaction of the ASAE, 29 (5), (1986), 1320-1324

15. Solomon, K.: Manufacturing variation of emitters in trickle irrigation system. ASAE Paper No. 77 (1977) - 2009, St. Joseph, Michigan 49085

16. Warrick, A.W.-Yitayew, M.: Tirckle lateral hydraulics. I: Analytical solution. Journal of the Irrigation and Drainage Division ASCE 114 (IR2), (1988), 281-288

17. Warrick, A.W.-Yitayew, M.: Tirckle lateral hydraulics, II: Design and examples. Journal of the Irrigation and Drainage Division ASCE 114 (IR2), (1988), 289-300

18. Watters, G.S.-Keller, J.: Trickle irrigation tubing hydraulics. ASAE Technical Paper No. 78, (1978) - 2015. St. Joseph, Michigan 49085

19. Wu, I.P.-Gitlin, H.M.: Energy gradient line for drip irrigation laterals. Journal of the Irrigation and Drainage Division ASCE 101 (IR4), (1975), 321-326

20. Wu, I.P.-Irudayaraj, M.J.-Feng, J.S.: Grouping effect on the uniformity of drip irrigation. Proceedings of the Fourth International Micro Irrigation Congress. IC-4 (1988)

21. Wu, I.P.-Yabusaki, K.Y.-Irduayarj, J.M.: Computer simulation of total emitter flow variation. Drip/Trickle Irrigation and Action. Proceedings of the Third International Drip/Trickle Irrigation Congress. Vol. II, (1985), 873-877

Acta Technica Acad.Sci.Hung., 104(1-3), pp. 257-276 (1991/92)

FINAL SETTLER BIOLOGICAL ACTIVITY IN ACTIVATED SLUDGE PROCESS

SOROUR, M.T.*

(Received: 20 June 1991)

The main objective of this study was to develop a mathematical model for the activated sludge process, which can predict the biological activity of the final settler. The initial models were taken from the literature and modified where necessary. Simulation results were shown in comparison with experimental data for the same plant.

Introduction

Activated sludge wastewater treatment plants can be described as a large complex system with inputs which are not always predictable, and with strong interactions among process units. Most activated sludge plant operate in a dynamically changing environment, it is common to observe large variations in wastewater flow rate, concentration, and composition. Experimental evidence has established that the dynamic response of final settlers to sudden changes in flow rate is nonlinear /1, 2, 3, 4/. Sudden increases in flow rate results in rapid increases in the concentration of effluent solids, but not necessary in the concentration of soluble substrate. Such findings support the hypothesis that the final settler serves as a bioreactor when the plant receives sudden increase in flow rate.

Mathematical modeling of wastewater treatment processes can serve many purposes. For the researcher, modeling serves as a conceptual framework upon which to build and test hypotheses, thereby extending knowledge. Because there is no consensus in the literature concerning the biological activity of the final settler, a study was undertaken to develop a model, which can predict the soluble organics removal in the final settler. For the purpose of this study, the scheme included only the biological reactor

*Sorour, Mohamed Tarek, Civil Eng. Dept. Faculty of Eng., Tanta University, Egypt

Akadémiai Kiadó, Budapest

and the final settler. The models for individual process units were taken from the literature and modified where necessary.

A review of the environmental engineering literature revealed no comprehensive mathematical models that postdate the one developed by the International Association of Water Pollution Research and Control (IAWPRC) group /5/. Consequently, it will be used as a base for developing the proposed model.

The original models

IAWPRC task group model

The activated sludge model employed is a reduced version of that proposed by the IAWPRC group. The reduced version incorporates only those features which relate to the utilization of carbonaceous material in an aerobic activated sludge system. It is presented in matrix format according to Pettersen /6/ in Table 1. The components modeled are (according to the notation proposed by Grau et al. /7/):

active biomass (X_B);
particulate products of biomass decay (X_p);
slowly biodegradable substrate (X_S);
inert particulate (X_I);
readily biodegradable substrate (S_s); and
dissolved oxygen (S_o)

all expressed as chemical oxygen demand (COD). In the following the slowly biodegradable substrate will be referred as particulate substrate and the readily biodegradable substrate as soluble substrate.

The processes modeled are:

1. Aerobic growth of biomass. Soluble substrate (S_s) is used for growth by the active biomass (X_B). There is an associated use of oxygen (S_o).

The process is modeled by the Monod expression together with a switching function which reduces the rate to zero in the absence of oxygen.

2. Death of active biomass: Organism decay is modeled according to the (Death-regeneration) hypothesis. The organism dies at a certain rate; a portion (f) of the material from death is non-degradable and adds to the particulate products of biomass decay (X_p) which the remainder (1-f) adds to the pool of biodegradable particulate COD (X_S).

Table 1

The reduced IAWPRC model for utilization of carbonaceous material in an aerobic activated sludge system

Component i	1	2	3	4	5	6	Rate expression
j Process	X_B	X_P	X_S	X_I	S_s	S_o	
1 Growth	1				$\frac{-1}{y}$	$\frac{-1(1-y)}{y}$	$\hat{\mu} X_B \frac{S_s}{(K_S+S_S)} \frac{S_s}{(K_o+S_o)}$
2 Decay	-1	f	(1-f)				$b\, X_B$
3 Hydrolysis			-1		1		$K_H \frac{X_S}{K_X+(X_S/X_B)} \frac{S_o}{K_o+S_o}$
Stoichiometric parameters:							Kinetic parameters:
True growth yield: Y							Maximum specific growth rate: $\hat{\mu}$
Fraction of biomass leading to particulate							Half saturation constants: K_S, K_o, K_X
Products: f	Active Biomass	Particulate Products of Biomass Decay	Slowly Biodegradable Substrate	Inert Particulates	Readily Biodegradable Substrate	Dissolved Oxygen Concentration	Specific decay rate: b

3. Hydrolysis of particulate COD: Biodegradable particulate COD in the influent is assumed to be enmeshed in the sludge mass within the system. The enmeshed material is broken down extracellularly, with the products of breakdown adding to the pool of readily biodegradable substrate (S_S) available to the organisms for synthesis purposes. This (hydrolysis/solubilisation) process is modeled on the basis of Levenspiel's surface reaction kinetics /8/.

The fundamental equation for a mass balance within any defined system boundary is:

$$\begin{matrix}\text{Rate} \\ \text{of} \\ \text{accumulation}\end{matrix} = \begin{matrix}\text{Rate} \\ \text{of} \\ \text{input}\end{matrix} - \begin{matrix}\text{Rate} \\ \text{of} \\ \text{output}\end{matrix} \pm \begin{matrix}\text{Rate of} \\ \text{production} \\ \text{by reaction}\end{matrix} \qquad (1)$$

The system reaction term usually denoted by r_i for compound i (r_i is the production of compound i per unit time per unit volume $[M_i\ (L^{-3}\ T^{-1})]$ must often account for the combined effect of a number of processes.

For example from Table 1, the rate of reaction for the compound biomass (X_B) at a point in the system would be:

$$r\,X_B = \hat{\mu}\,\frac{S_S}{K_S + S_S}\,\frac{S_O}{K_O + S_O}\,X_B + (-1)\,b_H\,X_B \qquad (2)$$

Similarly for the component soluble substate (S_S):

$$r\,S_S = \frac{-\hat{\mu}}{Y}\,\frac{S_S}{K_S + S_S}\,\frac{S_O}{K_O + S_O}\,X_B + K_H\,\frac{X_S}{K_X + (X_S/X_B)}\,\frac{S_O}{K_O + S_O} \qquad (3)$$

Typical values of the stoichiometric and kinetic parameters are given in Table 2 according to Henze et al. /5/.

However, it should be noted that the model of IAWPRC considers only the biological reactions in the treatment system and treats the settler as a separation point with no hold-up. For the purpose of this study it was necessary to link the IAWPRC to a settler model. The layered settler model of Vitasovic /9/ was chosen for this purpose.

The layered settler model of Vitasovic

This model is based on the flux theory and can be considered as the result of several years continuous development /3, 10, 11/.

Table 2

Typical parameter values at neutral Ph and 20 ^{o}C for domestic wastewater (Henzet et al., 1987)

Parameter	Symbol	Units	Value
	Stoichiometric parameter		
Truc growth yield	y	g cell COD_{-1} formed.(g COD oxidized)$^{-1}$	0.46 - 0.69
Fraction of biomass leading to particulate products	f	dimensionless	0.08
	Kinetic parameters		
Maximum biomass specific grow rate	$\hat{\mu}$	day^{-1}	3-13.2
Hydrolysis half-saturation coefficient	K_x^*	g COD.(g COD)$^{-1}$	0.15
Biomass half-saturation coefficient	K_s	g $COD.m^{-3}$	10-180
Oxygen half saturation coefficient	K_o	g $O_2 . m^{-3}$	0.01-0.15
Biomass decay coefficient	b	day^{-1}	0.09-0.15

*slowly biodegradable

As shown in Fig. 1 the influent flow enters the settler in the feed layer (f) and is assumed to be instantly and completely distributed in the layer. The model considers at this time one compound only: suspended solids. To handle the solids concentration of all the layers a vector of (n) element (X_i where i = 1...f...n) is set up. The concentration in the bottom layer provides the under-flow (recycle) concentration.

The solids are moving in the settler due to two effects: bulk fluid movement (upward and downward flow) and settling.

Solids fluxes due to bulk fluid movement are calculated by:

$$J_{up\ i} = \frac{Q_E \cdot X_i}{Ac} , \qquad (4)$$

where i - 1 to f

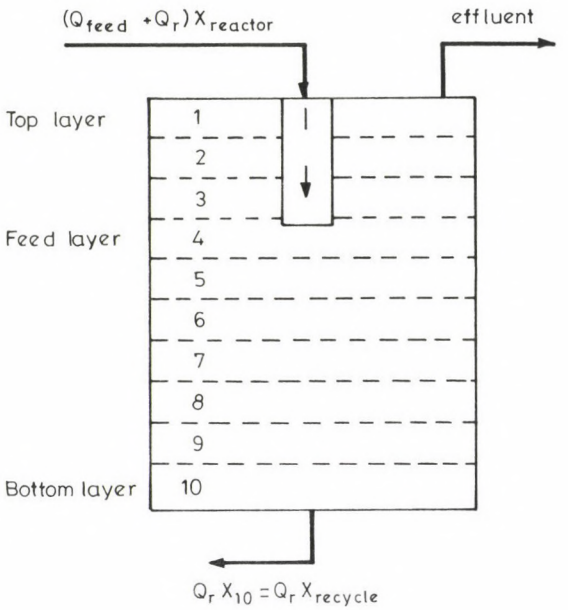

Fig. 1. Layered settler model

$J_{up\ i}$ - upward solids flux due to bulk fluid movement in layer (i) $(M/L^2/T)$,

Q_E - effluent flow rate (L^3/T),

Ac - surface area of clarifier (L^2)

and

$$J_{dn\ i} = \frac{Q_R \cdot X_i}{Ac} \quad , \tag{5}$$

where i - f to n

$J_{dn\ i}$ - downward solids flux due to bulk fluidmovement in a layer (i) $(M/L^2/T)$,

Q_R - recycle and waste flow rate (L^3/T).

Settling solids fluxes can be calculated by:

$$J_{si} = v_{si} \cdot X_i \quad , \tag{6}$$

where i - 1 to n,

J_{si} - solids flux due to settling in layer (i) $(M/L^2/T)$,

v_{si} - settling velocity in layer (i) (L/T).

Settling velocity can be calculated using the empirical relationship of

Vesilind /12/:

$$v_{si} = v_o \cdot e^{-b X_i}, \qquad (7)$$

v_o - Stokes settling velocity for a single discrete particle (L/T),
b - empirical parameter.

The material balance for the possible groups of layers within the settler are presented in the Appendix.

However, it should be indicated that Vesilind's settling velocity equation applies only to hindered settling conditions. As the solids concentration in the upper layers of the clarifier decreases below the hindered settling concentration, settling velocities predicted by Vesilind's equation will exceed the actual settling velocity of the floc particles as predicted by Li and Ganczarczyk /13/. For the mathematical representation of this phenomenon Takács and Patry /14/ proposed the following double exponential equation instead of Eq. (7)

$$v_{si} = v_o \left[e^{-r\ floc(X_o - X_{min})} - e^{-r\ coll(X_o - X_{min})}\right], \qquad (8)$$

v_o - Stokes settling velocity (L/T),
X_i - Suspended solids concentration, in layer (i) (ML^{-3}),
X_{min} - $f_{ns} \cdot X_o$ (ML^{-3}),
f_{ns} - non-settleable fraction of X_{in},
X_o - inflowing suspended solids to the settler (ML^{-3}),
r_{flox} - settling parameter for flocs,
r_{coll} - settling parameter for the slowly settleable material equation.

The first term $\left[v_o.e^{-r_{floc}(X_i - X_{min})}\right]$ in Eq. (8) reflects the settling velocity of the large, well flocculating particles.

On the other hand the second term $\left[v_o.e^{-r_{coll}(X_i - X_{min})}\right]$ of Eq. (8) is a velocity correction factor to account for the slowly settling colloidal particles.

The equation of Takács and Patry was used in this study.

The proposed model

At this point the linked model (IAWPRC + Vitasovic) is however still not capable of incorporating the biological reaction in the final settler. Both models assume that the process which occurs in the settling tank is merely one of physical character i.e. no reaction takes place.

The linked model was modified and extended by assuming that each

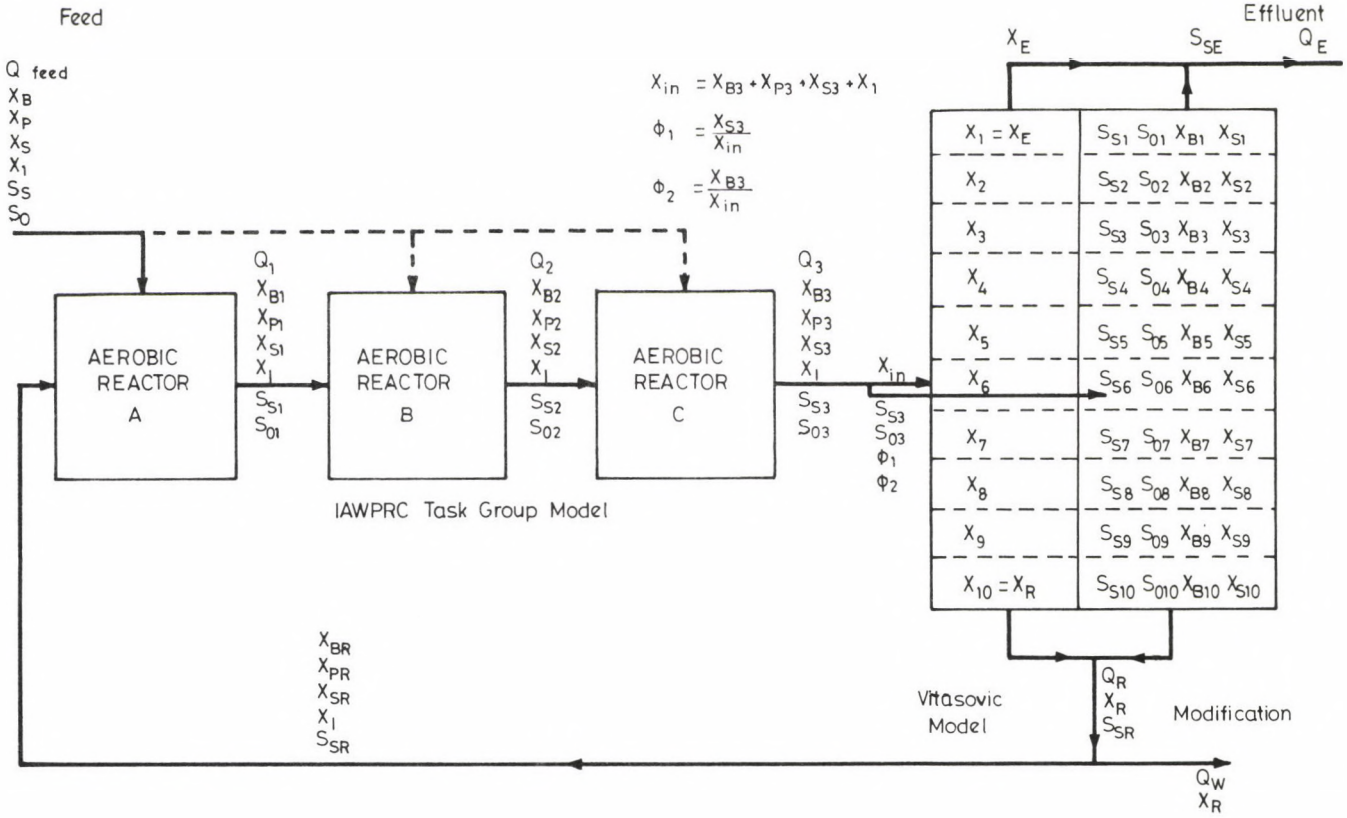

Fig. 2. System information flow diagram

layer acts as a complete mix reactor and also was modeled according to the IAWPRC model.

The model to be used in this study was based on 3 continuous stirred-tank reactors (CSTR) in series with step feed capability to create a range of contacting patterns, followed by a final settler with 10 layers as suggested by Vitasovic /9/.

The system information flow diagram is shown in Fig. 2. The material balance for soluble substrate in the five possible groups of layers in the settler are as follows (Fig. 3):

Feed layer (f)

$$V_f \frac{dS_{sf}}{dt} = (Q_E + Q_R)\, S_{s3} - Q_E\, S_{sf} - Q_R\, S_{sf} + rS_{sf}\, Vf \qquad (9)$$

V_f - volume of feed layer (L^3)

$$rS_{sf} = \frac{-\hat{\mu}}{Y} \frac{S_{sf}}{K_s+S_{sf}} X_{Bf} + \frac{K_H(X_{sf})}{K_x+(X_{sf}/X_B f)} \frac{S_{of}}{K_o+S_{of}} \qquad (10)$$

S_{sf} - soluble substrate concentration in feed layer ($M.L^{-3}$)

$$X_{sf} = \frac{X_{S3}}{\Sigma X} . X_f = \emptyset_1 \cdot X_f , \qquad (11)$$

$$X_{Bf} = \frac{X_{B3}}{\Sigma X} \cdot X_f = \emptyset_2 \cdot X_f \qquad (12)$$

X_f - solids concentration in feed layer ($M.L^{-3}$)

$$\Sigma X = X_{B3} + X_{S3} + X_3 + X_{P3} = MLSS3 \qquad (13)$$

$\emptyset$ - mixed-liquor suspended solids from the las reactor ($M.L^{-3}$).

Layers below the feed layer

$$V_i \frac{dS_{si}}{dt} = Q_R \cdot S_{si-1} - Q_R \cdot S_{si} + rS_{si} \cdot V_i \qquad (15)$$

V_i - volume of layer i (L^3),

i - f + 1 through n-1

S_{si} - soluble substrate concentration in layer i ($M.L^{-3}$).

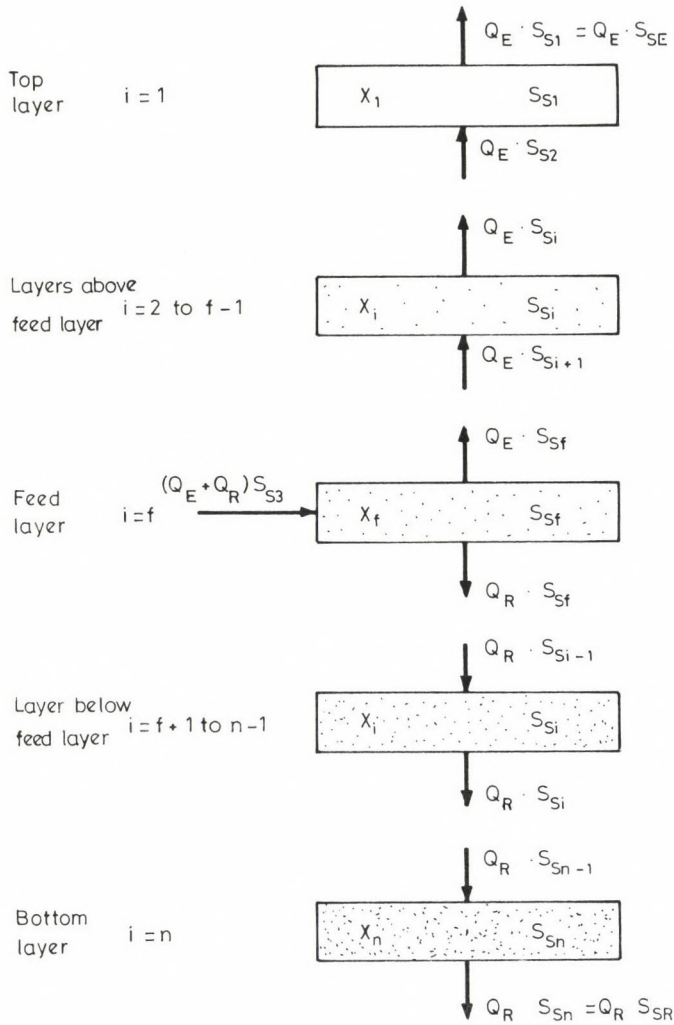

Fig. 3. Soluble substance balance across settler layers

$$rS_{si} = \frac{-\hat{\mu}}{Y} \frac{S_{si}}{K_s + S_{si}} X_{Bi} + \frac{K_H (X_{si})}{K_x + (X_{si}/X_{Bi})} \frac{S_{oi}}{K_o + S_{oi}} \qquad (16)$$

$X_{si} - \emptyset_1 \cdot X_i$

$X_{Bi} - \emptyset_2 \cdot X_i$

X_i - solids concentration in layer i ($M.L^{-3}$).

Bottom layer i = n

$$V_n \frac{dS_{sn}}{dt} = Q_R \cdot S_{s\,n-1} - Q_R S_{sn} + r S_{sn} \cdot V_n \qquad (17)$$

S_{sn} - soluble substrate concentration in last layer ($M.L^{-3}$).
Layers above feed layer

$$V_i \frac{dS_{si}}{dt} = Q_E \cdot S_{s\,i+1} - Q_E \cdot S_{si} + r S_{si} \cdot V_i \qquad (18)$$

i - 2 through f-1.
First layer - effluent layer i = 1

$$V_1 \frac{dS_{s1}}{dt} = Q_E \cdot S_{s2} - Q_E \cdot S_{s1} + r S_{s1} \cdot V_1 \qquad (19)$$

S_{s1} - effluent soluble substrate concentration ($M.L^{-3}$).

The overall proposed model (reactor + settler) can be described by 55 mass balance equations, 15 equations for the reactors; 10 equations for the solids in the settler; and 30 equations for soluble substrate, particulate substrate and oxygen in the final settler. There was no need to create mass balances for the other compounds in the settler.

The model was written in Simmon /15/ which is a continuous simulation language program ased on the MS.DOS operating system for the personal computers.

Experimental procedure

In order to examine the validity of the model laboratory experiments were performed. The experimental work was conducted on a laboratory pilot plant consisted of three 15 ℓ complete mix aeration tanks in-series followed by a 0.18 m diameter, 1.0 m deep settler. Figure 4 shows its general layout. Raw sewage from the Southern Budapest Treatment Plant was continuously pumped to the feed tank. The wastewater was screened to remove influent solids, including course material which would have clogged pumps and valves, the screen removed about 15% of the influent suspended solids. Influent total COD varied within a rage of 288 to 450 mg/ℓ. To reduce the effect of this wide range, influent COD concentration of 350 mg/ℓ ± 10% range was used for data analysis. Any data obtained with influent COD concentration outside this range was excluded from the analysis. The solids retention time (SRT) was maintained at 5 days to minimize nitrification.

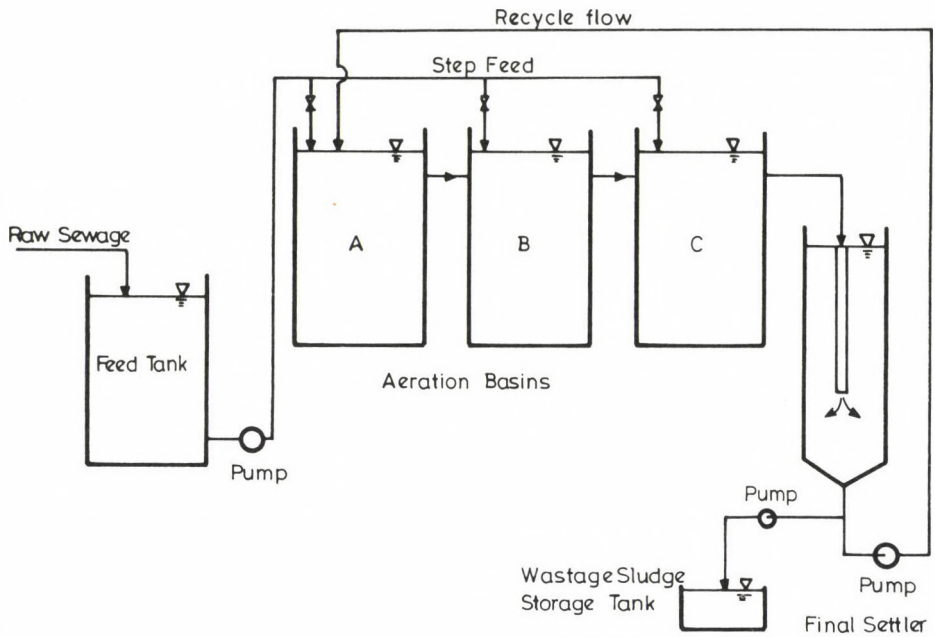

Fig. 4. Lay-out of activated sludge pilot plant

Wastewater was fed to the first reactor (A) at rate of 150 ℓ/d. Return activated sludge was always directed to reactor A at a constant flow rate of 100 ℓ/d. The system was operated for three weeks to reach steady-state, reaching the steady-state was indicated by the improvement and stabilization of the effluent quality.

The dissolved oxygen (DO) in the reactors varied but never fell below 3.0 mg/ℓ. The settler had a lower DO, ranging between 2.0 and 4.0 mg/ℓ, and was measured at 10 cm from the water surface. A detailed description of the pilot plant and measurement techniques is available /16/.

Three sets of dynamic experiments were carried out:

1. Step feed to reactor C at normal flow rate of 150 ℓ/d. The data of this set was used for model calibration.

2. Step feed to reactor B at peak flow rate of 250 ℓ/d.

3. Step feed to reactor C at peak flow rate of 250 ℓ/d.

The length of the dynamic action was about 24 h, at the end influent was returned to reactor A at the normal flow rate. Return activated sludge and air flow rates were maintained at constant levels for a minimum of 16 h before the experiment until the end of the experiment. Each set of ex-

periments was repeated 5 times to reduce the uncertainty associated with test results.

Simulation studies

Model calibration

Calibration of the model requires that the stoichiometric, kinetic and settling parameters be quantified. However, dealing with a model describing biological activities, and therefore being confronted with the problem of limited and uncertain data, confidence in sophisticated numerical calibration techniques may not be too well placed. The model was calibrated by varying some of the parameters to give the best fit with the data of the first set of experiments which has been selected for this purpose. Default stoichiometric, kinetic and settling parameters available in

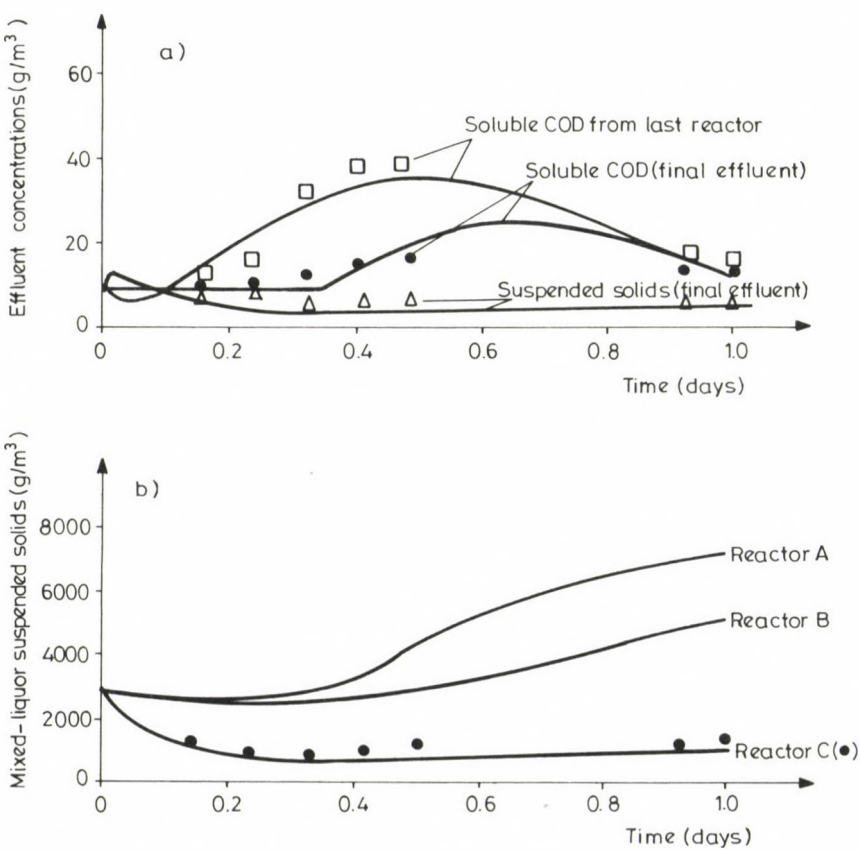

Fig. 5. Normal flow rate with step feed to reactor C

Table 3

Calibrated parameter values of the proposed model

Parameter	Value
Stoichiometric	
Y	0.65 g cell COD formed (g COD oxidized)$^{-1}$
f	0.08
Kinetic	
$\hat{\mu}$	4.0 day^{-1}
K_x	0.05 g slowly biodegradable COD (g COD)$^{-1}$
K_H	2.9 day^{-1}
K_s	5.8 g COD . m^{-3}
K_o	0.2 g O_2 . m^{-3}
b	0.66 day^{-1}
Final settler	
Number of Layers n	10
X_t	3000 g.m^{-3}
v_{max}	70 m.d^{-1}
r_{floc}	0.0008
r_{coll}	0.015
f_{ns}	0.005 g.m^{-3}

the literature were incorporated. Table 3 presents a summary of the values selected for model parameters. After having identified the parameters all simulations were performed without changing any of them. Figure 5 shows the actual data points with the calibrated simulation.

Model verification

The acceptability of the model is promoted if, on applying it to a range of situations, one can find consistency between observation and prediction.

The model was verified against two sets of experiments: 1) peak flow rate with step feed to reactor B; and 2) peak flow rate with step feed to reactor C. The analysis focused on solids concentration and soluble COD.

Peak flow rate with step feed to reactor B

Results of the simulation under step feed to reactor B are shown in Fig. 6 and compared with the recorded observations. Peak flow conditions was simulated by an abrupt change in flow rate from 150 to 250 ℓ/d, while the recycle flow rate was kept constant. An increase in the mixed liquor suspended solids concentration in reactor A and reduction in both B and C was observed in the model. This is in agreement with the experimental data and with the results of Thompson /17/.

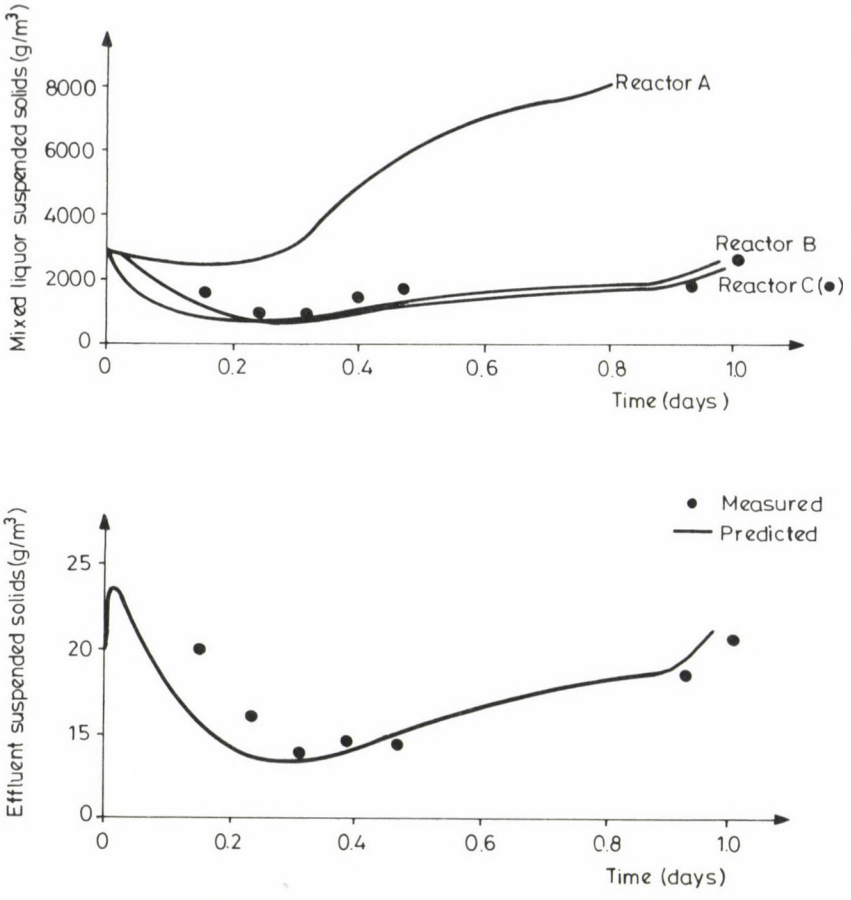

Fig. 6. Peak flow rate with step feed to reactor B

Peak flow rate with step feed to reactor C

Simulated and measured results are shown in Fig. 7. Step feed to reactor C caused an increase in mixed liquor concentration in reactor A and B, while solids from the third reactor were washed out from the system, decreasing the solids loading to the settler. A slight improvement in effluent suspended solids was also observed comparing with step feed to reactor B (Fig. 6b and 7b).

Original and modified models

Concerning the effluent soluble COD concentration a distinction must be made between the original and modified models.

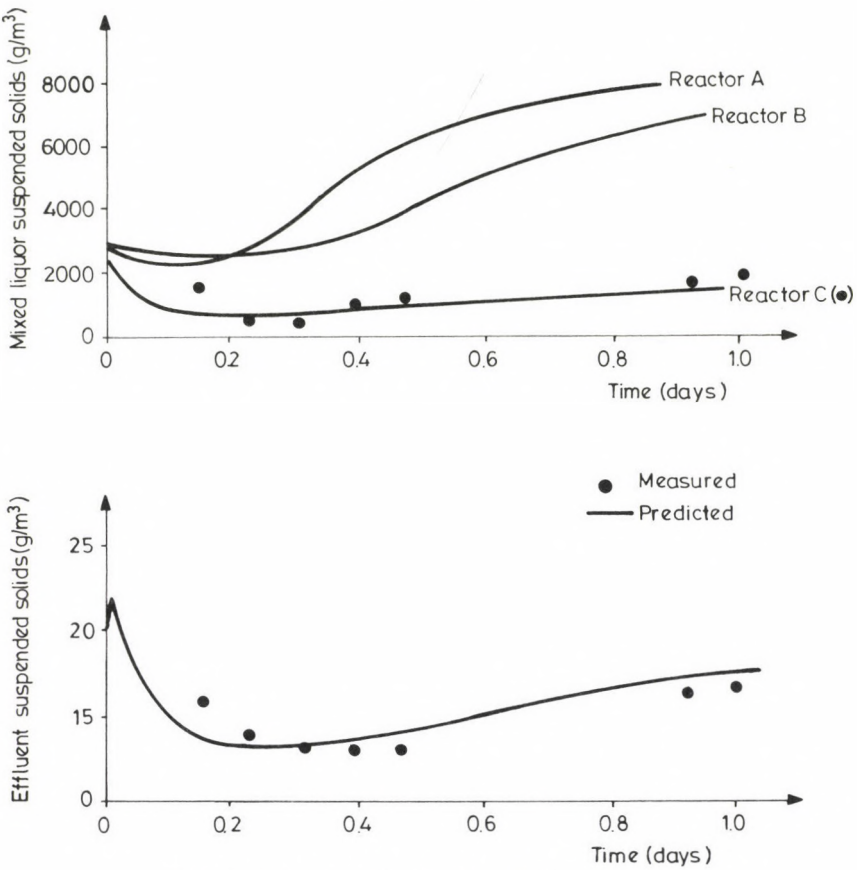

Fig. 7. Peak flow rate with step feed to reactor C

Figure 8 shows the measured and predicted values of soluble substrate in the final effluent of the two studied cases. Comparing the observed and predicted responses it is evident for both cases that the proposed model gave a better agreement with the experimental results than the original model did. The closeness with which the proposed model conforms to the observations constitues evidence for the acceptability of the model.

Simulations also show that the highest soluble COD removal in the final settler obtained by directing the peak flow to reactor C, Fig. 9. The short hydraulic retention time in the last reactor results in poor soluble COD removal, as a consequence the final settler functions as a bioreactor when if receives the biodegradable substrate.

The closer the feed point to the settler, the highest soluble COD removal in it for the same flow rate.

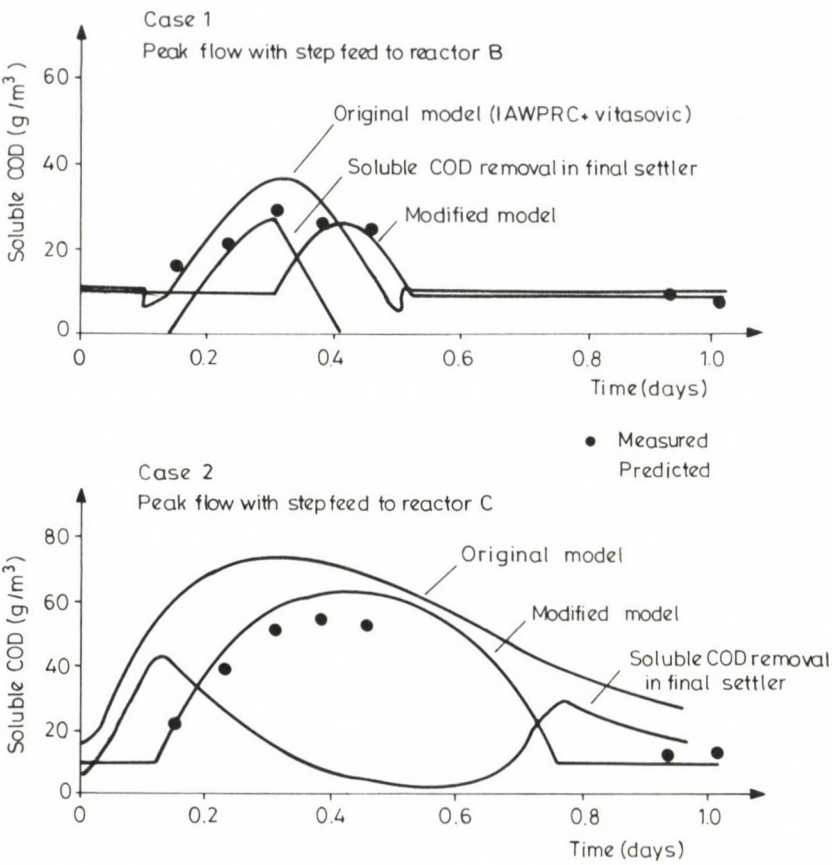

Fig. 8. Measured and predicted soluble COD concentrations in the final effluent

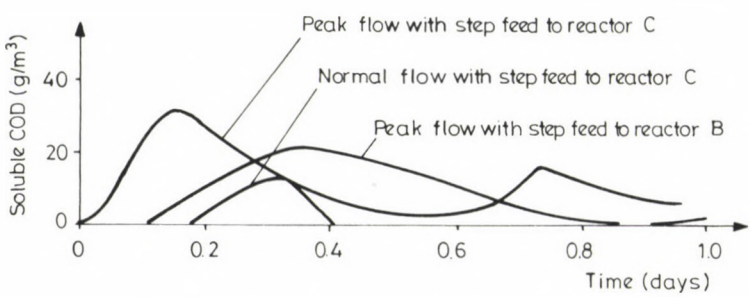

Fig. 9. Soluble COD removal in the final settler

Conclusions

A dynamic model for activated sludge process was presented. The original models for the process were taken from the literature and modified to predict the soluble substrate utilization in the final settler. The model was applied to laboratory experimental data with good results. The differences between the observed and simulated results fall with the expected range of accuracy of such complex models.

ACKNOWLEDGEMENTS

The author is grateful to Dr. László Somlyódy for his valuable advices during the course of this research.

Appendix

The material balances for the possible five group of layers within the settler are:

layer (1):

$$Z(1)\,\frac{dX(1)}{dt} = J_{up}(2) - J_{dn}(1) - J_s(1)$$

$$Z(1) = \text{height of layer 1 (L)}$$

$$J_s(1) = \min\left[V_s(1)\,.\,X(1),\ V_s(2)\,.\,X(2)\right] \text{ if } X(2) \quad Xt$$

$$Xt = 3000\ g/m^3$$

$$J_s(1) = V_s(1)\,.\,X(2) \text{ if } X(2) \quad Xt$$

layers 2 through (f-1):

$$Z(i)\,\frac{dX(i)}{dt} = J_{up}(i+1) - J_{up}(i) + J_s(i-1) - J_s(i)$$

$$Z(i) = \text{height of layer; (L)}$$
$$i = 2 \text{ through } f-1$$

$$J_s(i) = \min \left[V_s(i) \cdot X(i),\ V_s(i+1) \cdot X(i+1)\right] \text{if } X(i+1) \quad Xt$$

$$J_s(i) = V_s(i) \cdot X(i) \text{ if } X(i+1) \quad Xt$$

feed layer (f):

$$Z(f) \frac{dX(f)}{dt} = \frac{Q_E+Q_R}{Ac} \text{MLSS } U - J_{up}(f) - J_{dn}(f) + J_s(f-1) - J_s(f)$$

$$J_s(f) = \min V_s(f) \cdot X(f),\ V_s(f+1) \cdot X(f+1)$$

$$\text{MLSS} = X_B + X_E + X_S + X_I \text{ from the last reactor.}$$

layers (f+1) through (n-1):

$$Z(i) \frac{dX(i)}{dt} = J_{dn}(i-1) - J_{dn}(i) + J_s(i-1) - J_s(i)$$

$$i = f+1 \text{ through } n-1$$

last (bottom)layer (n):

$$Z(n) \frac{dX(n)}{dt} = J_{dn}(n-1) - J_{dn}(n) + J_s(n-1)$$

$$J_s(n-1) = \min \left[V_s(n-1) \cdot X(n-1),\ V_s(n) \cdot X(n)\right]$$

REFERENCES

1. Chapman, D.T.: Final settler performance during transient loading. Journal WPCF, Vol. 57, (1985), 227-234
2. Olsson, G.-Chapman, D.: Modeling the dynamics of clarifier behaviour in activated sludge system. Instrumentation and Control of Water and Wastewater Treatment and Transport Systems. R.A.R. Drake, editor, Pergamon Press, Oxford, U.K. 1985
3. Hill, R.D.: Dynamics and control of solids-liquid separation in activated sludge process. Ph.D. thesis, Rice University, Texas 1985
4. Dietz, J.D.-Keinath, T.M.: Dynamic response of final clarifiers. Presented at the 12th IAWPRC Biennial International Conference, Amsterdam, Sept. 1984
5. Henze, M.-Grady, Jr.-Gujer, W.-Marais, G.V.R.-Matsuo, T.: Activated sludge model No. 1. IAWPRC Scientific and Technical Report No. 1 (1987), IAWPRC, London, U.K.

6. Pettersen, E.E.: Chemical reaction analysis. Prentice Hall, Englewood Cliffs 1965

7. Grau, P.-Henze, M.-Elmaleh, S.-Grady, C.P.-Gujer, W.-Koller, K.: Recommended notation for use in the description of biological wastewater treatment processes. Water Research, Vol. 16 (1982), 1501-1505

8. Levenspiel, O.: Chemical reaction engineering (2nd Ed.). John Wiley and Sons, New York 1972

9. Vitasovic, Z.Z.: An integrated control strategy for the activated sludge process. Ph.D. thesis, Rice University, Texas 1986

10. Busby, J.-Andrews, J.F.: Dynamic modeling and control strategies for the activated sludge process. Journal WPCF, Vol. 41 (1975), 1055-1080

11. Stenstrom, M.K.: A dynamic model and computer compatible control strategies for wastewater treatment plants. Ph.D. thesis, Rice University, Texas 1976

12. Vesilind, A.: Discussion of "Evaluation of activated sludge thickening theories", by R.I. Dick, Journal Sanitary Engineering Division, ASCA, 94. (1968), 185-191

13. Ganczarczyk, J.J.-Li, D.: Stroboscopic determination of settling velocity, size and porosity of activated sludge flocs. Water Research, Vol. 21 (1987), 257-262

14. Takács, I.-Patry, G.G.: A generalized dynamic model of the thickening - clarification process. Journal Water Sci. Tech., Vol. 20. (1990), 487-494

15. Elmqvist, M.-Astrom, K.J.-Schonthal, T.: SIMNON-User's Guide for MS-DOS Computers. Department of Automatic Control., Lund Institute of Technology, Lund, Sweden 1990

16. Sorour, M.T.: Activated sludge modeling for operational control, an approach to step-feed system. Dissertation, Hungarian Academy of Sciences, Budapest 1991

17. Thompson, D.: Activated sludge: step feed control to minimize solids loss during storm flow. M. Eng. thesis, McMaster University, Department of Chemical Eng., Hamilton, Canada 1988

Acta Technica Acad.Sci.Hung., 104(1-3), pp. 277-296 (1991/92)

ON DERIVATION OF STRESS FUNCTIONS IN MICROPOLAR THEORY OF ELASTICITY

SZEIDL, GY.*

[Received: 26 May 1989]

The main result of the present work has been the proof of the possibility that for micropolar bodies the general and complete solution of equilibrium equations in terms of stress functions can be derived from the general primal form of principle of virtual work. The most important functionals of Lagrange's type have also been presented assuming that the micropolar body under consideration is linearly elastic. The vanishing of variations with respect to the strain fields of the functionals as a variational principle ensures, through stress functions, the fulfillment of equilibrium equations and stress boundary conditions.

1. Introduction, Preliminaries

1.1. Representation for equilibrated stress fields in terms of stress functions is one of the problems which has been solved in micropolar theory of elasticity. Stress function solution of simple structure for the equilibrium equations of micropolar theory was obtained by *M.Günther* in 1958 [4]. However he did not notice that the solution is complete only for such regions whose boundary consists of a single closed surface. If the region is bordered by more than one closed surface (multibordered region) which are assumed to be not intersecting then the solution is totally self-equilibrated on each surface therefore it can not be complete. By supplementing *Günther's* solution, but independently from each other, *H.Schaefer* and *D.Carlson* found formally different and complete solutions, however, they are equivalent [9,2].

1.2. Paper [11] by *M.Stippes* is devoted to the problem how to find equilibrated and compatible stress fields in classical theory of elasticity. Since he seeks the solution with the aid of stress functions chosen suitably, he regards the derivation of the general solution for the equilibrium equations of classical elasticity from a variational principle as a first step.

The paper [11], however,

- pays no attention to the analysis of surface integrals obtained by mathematical transformations; the author entirely leaves them out of consideration;
- does not investigate the role of body forces;
- includes no reference to the fact that for a region bordered by a single closed surface three stress functions are sufficient to the solution; perception of this requires the thorough investigation of the compatibility conditions as subsidiary conditions which was carried out by *I.Kozák* [5],[6].

Published in 1978 the book [1] written by *N.P.Abovski., N.P.Andreev* and *A.P.Deruga* provides a detailed representation of variational principles in classical elastostatics including those variational principles where the solutions of the equilibrium equations in terms of stress functions appear as *Euler* equations. In comparison

*Szeidl, György, H-3529 Miskolc, Derkovits u. 54, Hungary

Akadémiai Kiadó, Budapest

with paper [4] there is a step ahead in the treatment of the boundary surface but all the terms needed to have a complete solution for multibordered regions are missing. The reason for this comes from the assumption that the particular solutions of equilibrium equations are assumed to be known therefore difference between homogeneous and particular solutions i.e. self-equilibrated stresses are given by the above mentioned *Euler* equations.

1.3. In micropolar theory of elasticity, to the best of the author's knowledge, no attempt has been made to derive complete solutions to equilibrium equations resulted from a variational principle or an equivalent form of principle of virtual work.

1.4. In view of the foregoing the present paper aims at

(a) deriving the complete solution of equilibrium equations in micropolar theory of elasticity from the general primal form of principle of virtual work striving, at the same time, for accuracy in handling volume integrals and body forces as well as the number of necessary stress functions;

(b) the presentation of the corresponding variational principles and their functionals.

1.5. The variational principle which has a functional obtained from the *Lagrange* functional by applying the method of the *Lagrange* multipliers is regarded as a primal one. As regards details in connection with primal systems we refer to *E. Tonti's* work [12].

2. Complete Solution of Equilibrium Equations and Principle of Virtual Work

2.1. The region occupied by the body and the surface of the body are denoted respectively by V and S. For the sake of simplicity we assume that the region V is simple-connected. The surface S may, however, consist of not only one but more

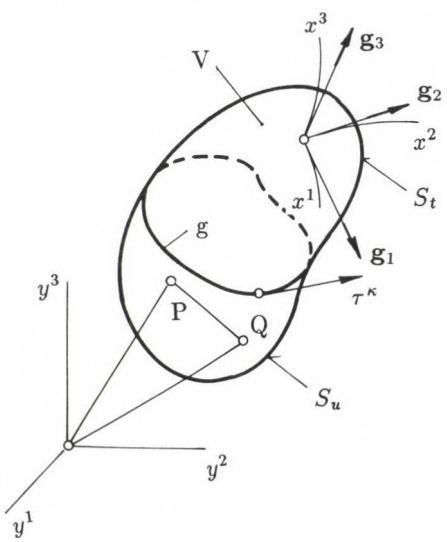

Fig. 1.

closed surfaces — multiply-bordered region — as well. The surface S is divided into parts S_u and S_t whose common bounding curve is denoted by g. The body represented in *Fig.1* is bordered by a single closed surface.

If the body is bordered by N closed regular surfaces ($N \geq 2$) and each surface is divided into two parts $S_u^{(i)}$, $S_t^{(i)}$ separated from each other by a bounding curve $g^{(i)}$ ($i = 1, \ldots, N$) then S_u, S_t and g are the unions of the subsurfaces $S_u^{(i)}$ and $S_t^{(i)}$ and the bounding curves g_i, respectively.

Any of the surfaces $[S_u]$ $\{S_u^{(i)}\}$ or $[S_t]$ $\{S_t^{(i)}\}$ may be an empty set.

2.2. Indicial notations and three coordinate systems,

— the $(y^1y^2y^3)$ Cartesian

— the $(x^1x^2x^3)$ curvilinear and

— the $(\xi^1\xi^2\xi^3)$ curvilinear, defined on the surface S,

are applied throughout this paper.

Scalars and tensors, unless the opposite is stated, are denoted independently of the coordinate system by the same letter. Distinction is helped by the indication of the arguments y, x and ξ used to denote the totality of the corresponding coordinates.

Volume integrals — except the formulas (2.10) — and surface integrals are considered, respectively, in the coordinate systems $(x^1x^2x^3)$ and $(\xi^1\xi^2\xi^3)$, consequently, in the case of integrals, arguments are omitted.

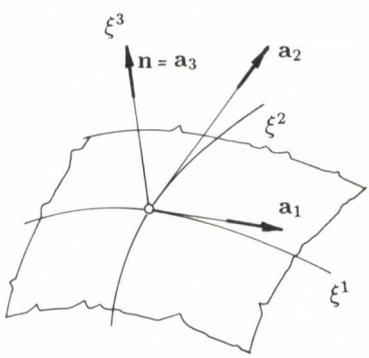

Fig. 2.

In accordance with the general rules of indicial notations summation over repeated indices is implied and subscripts preceded by a semicolon denote covariant differentiation with respect to the corresponding subscripts. Latin and Greek indices range over the integers 1, 2, 3 and 1, 2 respectively.

ϵ^{klm} and ϵ_{pqr} stand for the permutation tensors; δ_k^l is the *Kronecker* delta.

2.3. In Cartesian system $(y^1y^2y^3)$ $\mathbf{e}_1$, $\mathbf{e}_2$ and $\mathbf{e}_3$ are the base vectors, besides covariant and contravariant components of tensors are coinciding.

2.4. In the system of material coordinates $(x^1x^2x^3)$ $\mathbf{g}_k$ and $\mathbf{g}^l$ are the covariant and contravariant base vectors. The corresponding metric tensors are denoted by g_{kl} and g^{pq}.

2.5. By assumption there exists a one-to-one relationship $y^k = y^k(x^1, x^2, x^3)$ between the Cartesian coordinate y^k and the curvilinear coordinates x^1, x^2 and x^3

where y^k is differentiable with respect to x^l as many times as required. Consequently

$$J_{y,x} = \left| \frac{\partial y^k}{\partial x^l} \right| \neq 0.$$

Contravariant and covariant vector fields B^l and C_b are transformed in accordance with the rules

$$C_b(x) = C_p(y) \frac{\partial y^p}{\partial x^b} \qquad B^k(x) = B^p(y) \frac{\partial x^k}{\partial y^p} . \tag{2.1}$$

2.6. Equations and calculations can be better understood by introducing a suitable surface oriented coordinate system. Let $x^k = x^k(\xi^1, \xi^2)$ be the equation of the surface S where ξ^1 and ξ^2 are the surface coordinates. Let ξ^3 be the perpendicular distance measured on the outward unit normal $\mathbf{n}$ to the surface S. On S $\xi^3 = 0$. [Base vectors] {Metric tensors} on S are denoted by [$\mathbf{a}^k$ and $\mathbf{a}_k$] {a_{kl} and a^{kl}}. In the coordinate system $(\xi^1 \xi^2 \xi^3)$

$$\mathbf{n} = \mathbf{a}_3 = \mathbf{a}^3 , \qquad n^3 = 1 \qquad \text{and} \qquad n^\eta = 0.$$

The relationship $x^k = x^k(\xi^1, \xi^2, \xi^3)$ is assumed to be a one-to-one. Consequently the functional determinant is not vanishing:

$$J_{x,\xi} = \left| \frac{\partial x^k}{\partial \xi^l} \right| \neq 0.$$

Upon change of coordinates (x^1, x^2, x^3) and (ξ^1, ξ^2, ξ^3) a tensor $D^p_{.q}(x)$ of second order follows the transformation rules

$$D^k_{.l}(\xi) = D^p_{.q}(x) \frac{\partial \xi^k}{\partial x^p} \frac{\partial x^q}{\partial \xi^l} , \tag{2.2}_1$$

$$D^p_{.q}(x) = D^k_{.l}(\xi) \frac{\partial x^p}{\partial \xi^k} \frac{\partial \xi^p}{\partial x^k} \tag{2.2}_2$$

where

$$\frac{\partial x^k}{\partial \xi^l} \frac{\partial \xi^p}{\partial x^k} = \delta^p_l . \tag{2.2}_3$$

We shall assume that the vector and tensor fields involved in the investigations are sufficiently smooth.

2.7. Let u_k be the displacement field and φ^b be the rotation field (u_k and φ^b together are referred to as displacement fields or briefly, displacements). Furthermore let γ_{kl} be the asymmetric strain tensor and $\kappa_{a.}^{\ b}$ be the curvature twist tensor (together strain fields or briefly, strains).

By t^{kl} and $\mu^a_{.b}$ we denote, respectively, the asymmetric stress tensor and couple-stress tensor (together stress fields or briefly, stresses).

Displacements and strains will be assumed to be small.

Boundary conditions — inasmuch as there are some boundary conditions pre-

scribed — have the following forms:

Displacement boundary conditions:

$$u_k = \hat{u}_k\,, \qquad \varphi^b = \hat{\varphi}^b \qquad x \in S_u \tag{2.3}$$

Stress boundary conditions:

$$n_k t^{kl} = \hat{t}^l\,, \qquad \mu^a_{.b} = \hat{\mu}_b \qquad x \in S_t \tag{2.4}$$

where $\hat{u}_k$ and $\hat{\varphi}^b$ are respectively prescribed displacement and rotation; $\hat{t}^l$ and $\hat{\mu}_b$ are prescribed tractions.

2.8. By generalizing the results of *I.Kozák* [7] valid for classical case paper [10] systematize [the general primal forms] {the primal form ordered to prescribed boundary conditions} of principle of virtual work, the corresponding assertions and, in addition to this, it gives the missing [general dual forms] {dual forms ordered to prescribed boundary conditions} and dual assertions together with their proofs.

The line of thought of the present section is based on a well known assertion related to the general primal form of principle of virtual work and on a proper choice of the corresponding subsidiary conditions.

2.9. Strains $\gamma_{kl}(x)$ and $\kappa_{a.}^{\ b}(x)$ are said to be [compatible] {kinematically admissible} if the differential equations

$$\gamma_{kl}(x) = u_{l;k} + \epsilon_{lks}\varphi^s \qquad x \in V \qquad (2.5)_1$$

$$\kappa_{a.}^{\ b}(x) = \varphi^b_{.;a} \qquad x \in V \qquad (2.5)_2$$

have a single-valued solution for the displacements $u_l(x)$ and $\varphi^b(x)$ $x \in V$ and the solution [does not satisfy other conditions] {satisfies the displacement boundary conditions (2.3) }.

By applying the above term sufficiently smooth — differentiable at least twice — displacements $u_l(x)$ and $\varphi^b(x)$ will also be referred to as compatible.

2.10. Let b^l and c_b be the body forces and body couples. By definition the stresses $t^{kl}(x)$ and $\mu^a_{.b}(x)$ $x \in V$ are said to be [equilibrated]{statically admissible} if they satisfy the equilibrium equations

$$t^{kl}_{..;k}(x) + b^l = 0 \qquad x \in V \qquad (2.6)_1$$

$$\mu^a_{.b;a}(x) + \epsilon_{bkl}t^{kl} + c_b = 0 \qquad x \in V \qquad (2.6)_2$$

and [do not meet other conditions]{the stress boundary conditions (2.4)}.

2.11. For a linearly elastic body the boundary conditions (2.3), (2.4) and field equations (2.5) (2.6) should be supplemented by the stress-strain relations. By assuming a centrosymmetric material the stress strain relations have the form

$$t^{kl} = A^{klpq}\gamma_{pq} \qquad x \in V \qquad (2.7)_1$$

$$\mu^{ab} = B^{abpq}\kappa_{pq} \qquad x \in V \qquad (2.7)_2$$

where A^{klpq} and B^{abpq} are the tensors of elastic coefficients.

2.12. The equation

$$\int_V (t^{kl}\gamma_{kl} + \mu^a_{.b}\kappa_a{}^b)dV = \int_V (b^l u_l + c_b\varphi^b)dV + \int_S (n_3 t^{3l}u_l + n_3\mu^3_{.b}\varphi^b)dA \qquad (2.8)$$

is the general primal form of principle of virtual work.

To the above equation the following direct assertion can be ordered:

Suppose that $\gamma_{kl}(x)$ *and* $\kappa_a{}^b(x)$ *as compatible strain fields are obtained from* $(2.5)_{1,2}$. *If the equation* (2.8) *holds for any compatible displacement fields* $u_k(x)$, $\varphi^b(x)$ *then the stress fields* $t^{kl}(x)$, $\mu^a_{.b}(x)$ *are equilibrated.*

By substituting the kinematic equations $(2.5)_{1,2}$ as subsidiary conditions and performing partial integrations the assertion can easily be proved. Really, upon substitution of the integral

$$\int_V [t^{kl}(u_{l;k} + \epsilon_{lks}\varphi^s) + \mu^a_{.b}\varphi^b_{.;a}]dV = \int_S (n_3 t^{3l}u_l + n_3\mu^3_{.b}\varphi^b)dA + \int_V [t^{kl}_{..;k}u_l + (\mu^a_{.b;k} + \epsilon_{bkl}t^{kl})\varphi^b]dV$$

into (2.8) and subsequent rearrangement it follows the fulfillment of the equilibrium equations if we take into consideration that the coefficients u_k and φ^b in the resulting equation

$$\int_V (t^{kl}_{..;k} + b^l)u_l dV + \int_V (\mu^a_{.b;a} + \epsilon_{bkl}t^{kl} + c_b)\varphi^b dV = 0$$

are arbitrary in V.

2.13. It can be expected that the above assertion will remain valid when the subsidiary conditions (2.5) are replaced by such side conditions which have a different mathematical form but otherwise are equivalent to (2.5).

2.14. According to a fundamental result of potential theory [3] the body forces b^l and body couples c_b always admit the representation

$$b^l = -\Delta B^l = -g^{pq}B^l_{.;pq} \qquad x \in V \qquad (2.9)_1$$

$$c_b = -\Delta C^b = -g^{pq}C_{b;pq} \qquad x \in V \qquad (2.9)_2$$

where $B^l(x)$ and $C_b(x)$, provided that the integrals

$$B^l[y^r(Q)] = \frac{1}{4\pi}\int_V \frac{b^l[y^r(P)]}{|y^s(P) - y^s(Q)|}dV_P \qquad Q \in V \qquad (2.10)_1$$

$$C_b[y^r(Q)] = \frac{1}{4\pi}\int_V \frac{c_b[y^r(P)]}{|y^s(P) - y^s(Q)|}dV_P \qquad Q \in V \qquad (2.10)_2$$

have been determined first, are obtained from the transformation formulas (2.1). With reference to the above result we shall assume that the vector fields $B^l(x)$ and $C^b(x)$ are known.

2.15. After substituting the formulas (2.9) and using then *Gauss'* integral theorem the volume integral

$$I_V^{BC} = \int_V (b^l u_l + c_b \varphi^b) dV \tag{2.11}_1$$

is changed to

$$I_V^{BC} = -\int_S (g^{pq} B^l_{.;pq} u_l + g^{pq} C_{b;pq} \varphi^b) dA = \int_S (n_3 a^{3l} B^s_{.;l} u_s + n_3 a^{3l} C_{b;l} \varphi^b) dA$$
$$- \int_V \left[g^{kl} B^s_{.;l} (u_{s;k} + \epsilon_{skp} \varphi^p) + g^{kl} (\epsilon_{lps} B^s + C_{p;l}) \varphi^p_{.;k} \right] dV. \tag{2.11}_2$$

Upon substitution of the integral $(2.11)_2$ into (2.8) and with regard to the kinematic equations $(2.5)_{1,2}$ we obtain the equation

$$\int_V \left[(t^{kl} - g^{ks} B^l_{.;s}) \gamma_{kl} + + (\mu^a_{.b} - g^{al} (\epsilon_{lbs} B^s + C_{b;l})) \kappa_{a.}^{\ b} \right] dV =$$
$$\int_S \left[n_3 (t^{3l} - B^l_{.;3}) u_l + n_3 (\mu^3_{.b} - (\epsilon_{3b\sigma} B^\sigma + C_{b;3})) \varphi^b \right] dA \tag{2.12}$$

which is a transformation of the general primal form of principle of virtual work. It is noteworthy that in the above equation the kinematic variables appear

— either on the boundary S only as it is the case for u_l and φ^b

— or on the volume V as it is the case for γ_{kl} and $\kappa_{a.}^{\ b}$.

The paragraphs 2.16., 2.17. and 2.18 are devoted to the problem of how to find a proper form of the subsidiary conditions to the equation (2.18).

2.16. With reference to that what has been said in paragraph 2.13. we have to raise the following two questions:

(a) Under what conditions are the strains

$$\gamma_{kl},\ \kappa_{a.}^{\ b} \qquad x \in V$$

compatible?

(b) What further conditions are needed if we want the displacements

$$u_k,\ \varphi^v \qquad x \in V$$

to be obtained from the above mentioned compatible strains to coincide with those being in the surface integral in the right hand side of *(2.12)*.

2.17. Solution to problem (a) is presented here on the basis of paper [11]. To begin with, we have to introduce some new notations.

The index pairs that range over a subset of the nine possible values will be capitalized.

Let $\beta_{k.}^{\ l}$ and α_{ab} be arbitrary tensor fields on V. Furthermore let $r^l(x)$ and $w_b(x)$ $x \in V$ be two unknown vector fields.

By $_{K.}^{\ L}$ and $_{AB}$ we denote those subsets of the possible values of index pairs $_{k.}^{\ l}$ and $_{ab}$ for which the differential equations

$$r^L_{.;K} = \beta^L_{K.}(x) \qquad x \in V \tag{2.13}_1$$
$$w_{B;A} + \epsilon_{BAp} r^p = \alpha_{AB}(x) \qquad x \in V \tag{2.13}_2$$

have a solution for the vector fields $r^l(x)$ and $w_b(x)$.

It is obvious that the index pairs ${}^{L}_{K.}$ and $_{AB}$ may have only three-three different values.

Let $\{{}^{Y}_{X.}\}[_{ST}]$ be the supplementary subsets of index pairs the union of which with $\{{}^{L}_{K.}\}[_{AB}]$ is the set of index pairs $\{{}^{l}_{k.}\}[_{ab}]$.

It is clear, that the index pairs ${}^{Y}_{X.}$ and $_{ST}$ may have only six-six different values.

Tensors of incompatibility e^{mb} and $d^{m}_{.l}$ are defined by the equations

$$e^{mb}(x) = \epsilon^{mpa}\kappa_{a.;p}{}^{b} \qquad x \in V \qquad (2.14)_1$$

$$\begin{aligned} d^{m}_{.l}(x) &= \epsilon^{mpk}(\gamma_{kl;p} + \epsilon_{klb}\kappa_{p.}{}^{b}) \\ &= \epsilon^{mpk}\gamma_{kl;p} + \delta^{m}_{l}\kappa^{p}_{p.} - \kappa_{l.}{}^{m}\,. \end{aligned} \qquad x \in V \qquad (2.14)_2$$

Returning to question (a) the independent necessary and sufficient conditions for the strains γ_{kl} and $\kappa_{a.}^{b}$ to be compatible [8] in a simple-connected region V are the fulfillment of differential equations of compatibility

$$e^{XY}(x) = \epsilon^{Xpk}\kappa_{k.;p}{}^{Y} = 0\,, \qquad x \in V \qquad (2.15)_1$$

$$d^{S}_{.T}(x) = \epsilon^{Spq}(\gamma_{qT;p} + \epsilon_{qTb}\kappa_{p.}{}^{b}) = 0 \qquad x \in V \qquad (2.15)_2$$

and that of boundary conditions of compatibility

$$n_3 e^{3b}(\xi) = n_3\epsilon^{3\pi\chi}\kappa_{\chi.;\pi}{}^{b} = 0\,, \qquad \xi \in S \qquad (2.16)_1$$

$$n_3 d^{3}_{.l}(\xi) = n_3\epsilon^{3\pi\chi}(\gamma_{\chi l;\pi} + \epsilon_{\chi lb}\kappa_{\pi.}{}^{b}) = 0. \qquad \xi \in V \qquad (2.16)_2$$

We note, that $(2.15)_1$ and $(2.15)_2$ are equivalent to six-six scalar equations.

2.18. Referring again to [8] solution for problem (b) is provided by the following assertion:

Suppose that the strains $\gamma_{kl}(\xi)$ and $\kappa_{a.}^{b}(\xi)$ fulfil the kinematic boundary conditions

$$\kappa_{\eta.}{}^{b} - \varphi^{b}_{.;\eta} = 0\,, \qquad \xi \in S \qquad (2.17)_1$$

$$\gamma_{\chi l} - u_{l;\chi} - \epsilon_{l\chi b}\varphi^{b} = 0\,. \qquad \xi \in S \qquad (2.17)_2$$

Then

(1) the boundary conditions of compatibility $(2.16)_{1,2}$ are identically satisfied and

(2) the displacements $u_k(\xi)$, $\varphi^b(\xi)$ $\xi \in S$ can be determined in terms of strains $\gamma_{kl}(\xi)$, $\kappa_{a.}^{b}(\xi)$.

In paper [8] proof of part (1) of the assertion is not complete and that of part (2) is missing.

2.19. For the sake of completeness we shall overview the missing proofs. The main difficulty is inherent in the circumstance that the derivatives of displacements $u_k(\xi)$, $\varphi^b(\xi)$ $\xi \in S$ taken with respect to the normal will also appear in the formal transformations. As they cannot be calculated it is worth changing to symbolic notations mentioning that the normal derivatives are needed only apparently as it can

be shown analytically too by a sophisticated analysis of the rules that apply to the calculations of derivatives taken on a surface. In the present case the symbolic writing leads to the desired results more quickly. Using symbolic notations and marking dot products to be carried out after the derivations from equations $(2.16)_{1,2}$ we obtain:

$$e^{3b}\mathbf{a}_b = \mathbf{a}_\nu \cdot \epsilon^{3\pi\nu}\frac{\partial}{\partial\xi^\pi}(\kappa_{\eta\cdot}^{\ b}\mathbf{a}^\eta\mathbf{a_b}) = 0 \qquad \xi \in S \qquad (2.18)_1$$

$$d^3_{\cdot l} = \mathbf{a}_\nu \cdot \epsilon^{3\pi\nu}\frac{\partial}{\partial\xi^\pi}(\gamma_{\chi l}\mathbf{a}^\chi\mathbf{a}^l) + \delta^3_l\kappa_{\pi\cdot}^{\ \pi} - \delta^\pi_l\kappa_{\pi\cdot}^{\ 3}\mathbf{a}^l = 0\,. \qquad \xi \in S \qquad (2.18)_2$$

As regards the left hand side of the second equation definition $(2.14)_2$ has also been taken into account. It follows from the fulfillment of condition $(2.17)_1$ that

$$\kappa_{\eta\cdot}^{\ b}\mathbf{a}^\eta\mathbf{a}_b = \mathbf{a}^\eta\frac{\partial}{\partial\xi^\eta}(\varphi^b\mathbf{a}_b)\,. \qquad \xi \in S \qquad (2.19)$$

Substituting the above equation into $(2.18)_1$ and utilizing then the definition

$$\frac{\partial\mathbf{a}^\eta}{\partial\xi^\pi} = \Gamma^\eta_{\pi m}\mathbf{a}^m$$

for the Christoffel symbol $\Gamma^\eta_{\pi m}$ we arrive at

$$\begin{aligned} e^{3b}\mathbf{a}_b &= \mathbf{a}_\nu \cdot \epsilon^{3\pi\nu}\frac{\partial}{\partial\xi^\pi}\left[\mathbf{a}^\eta\frac{\partial}{\partial\xi^\eta}(\varphi^b\mathbf{a}_b)\right] \\ &= \epsilon^{3\pi\eta}\frac{\partial^2}{\partial\xi^\pi\partial\xi^\eta}(\varphi^b\mathbf{a}_b) + \epsilon^{3\pi\nu}\Gamma^\eta_{\pi\nu}\frac{\partial}{\partial\xi^\eta}(\varphi^b\mathbf{a}_b) \equiv 0 \end{aligned}$$

which is nothing but the identical fulfillment of boundary condition of compatibility $(2.16)_1$.

Fulfillment of boundary condition of compatibility $(2.16)_2$ can be proved in an analogous way. For this reason a brief outline of the proof will only be presented herein. To begin with, substitute the following equation, which is equivalent to $(2.17)_2$, into $(2.18)_2$:

$$\gamma_{\chi l}\mathbf{a}^\chi\mathbf{a}^l = \mathbf{a}^\chi\frac{\partial}{\partial\xi^\chi}(u_l\mathbf{a}^l) + \epsilon_{l\chi b}\varphi^b\mathbf{a}^\chi\mathbf{a}^l. \qquad \xi \in S \qquad (2.20)$$

Then, by making use of the equation

$$\begin{aligned} \mathbf{a}_\nu\epsilon^{3\pi\nu}\cdot\frac{\partial}{\partial\xi^\pi}\left[\epsilon_{l\chi b}\varphi^b\mathbf{a}^\chi\mathbf{a}^l\right] &= \epsilon^{3\pi\chi}\epsilon_{l\chi b}\varphi^b_{\cdot;\pi}\mathbf{a}_l = \\ &= \left(-\delta^3_l\varphi^\pi_{\cdot;\pi} + \delta^\pi_l\varphi^3_{\cdot;\pi}\right)\mathbf{a}^l \quad \xi \in S \end{aligned}$$

and repeating the steps of the formal transformations which follow equation (2.10) we can readily show the validity of $(2.18)_2$.

2.20. On the basis of *Fig.3.* it follows from equation $(2.17)_1$ that

$$\varphi^b(P)\mathbf{a}_b = \varphi^b(P_o)\mathbf{a}_b + \int_{P_o}^{P} \tau^\eta \kappa_{\eta\cdot}^{\ b}\mathbf{a}_b\, ds \qquad (2.21)_1$$

is the rotation at the point P of the surface S. From equation $(2.17)_2$ — referring again to *Fig.3* — we obtain for the displacement at P:

$$\begin{aligned} u_l(P)\mathbf{a}^l &= u_l(P_o)\mathbf{a}^l + \int_{P_o}^{P} \tau^\chi(\gamma_{\chi l} + \epsilon_{l\chi b}\varphi^b)\mathbf{a}^l\, ds = \\ &= u_l(P_o)\mathbf{a}^l + \varphi^b(P_o)\mathbf{a}_b \times (\mathbf{r}_P - \mathbf{r}_{P_o}) \\ &\quad + \int_{P_o}^{P} \frac{d\xi^\chi}{ds}\left[\gamma_{\chi l} + \epsilon_{blk}\mathbf{a}^k \cdot (\mathbf{r} - \mathbf{r}_P)\kappa_{\chi\cdot}^{\ b}\right]\mathbf{a}^l\, ds. \end{aligned} \qquad (2.21)_2$$

2.21. All that has been said in paragraphs *2.19.* and *2.20.* proves the assertion given in paragraph *2.18.* Returning to the general primal form of principle of virtual work we should notice that equations $(2.15)_{1,2}$ and $(2.17)_{1,2}$ are the missing subsidiary con-

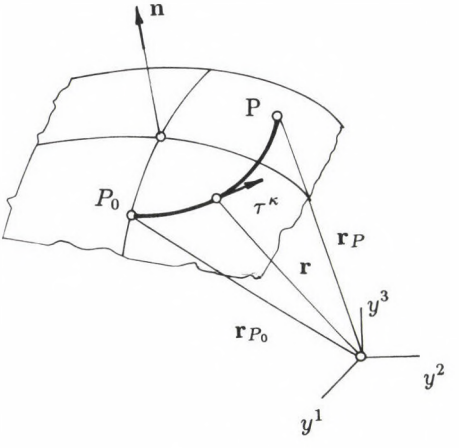

Fig. 3.

ditions. Since they cannot be substituted directly into the form (2.12) of principle of virtual work *Lagrange's* method of undetermined multipliers should be employed. Let

$$\begin{aligned} &H_S^{\ T}, && F_{XY} && x \in V \\ &\tilde{H}_\eta^{\ l}, && \tilde{F}_{\eta l} && \xi \in S \end{aligned}$$

be the undetermined *Lagrange's* multipliers. Suppose that the side conditions $(2.15)_{1,2}$ and $(2.17)_{1,2}$ hold. Then both the volume integral I_1^V and the surface integral I_1^S are identically vanishing:

$$I_1^V = \int_V \left[\epsilon^{Spq}(\gamma_{qT;p} + \epsilon_{qTb}\kappa_{q\cdot}^{\ b})H_S^{\ T} + \epsilon^{Xpk}\kappa_{k\ ;\pi}^{\ Y} F_{XY}\right] dV \equiv 0\,, \qquad (2.22)_1$$

$$I_1^S = \int_S [(\gamma_{\chi l} - u_{l;\chi} - \epsilon_{l\chi b}\varphi^b)\epsilon^{3\chi\eta}\tilde{H}_{\eta.}^{\ l} + (\kappa_{\pi.}^{\ b} - \varphi^b_{.;\pi})\epsilon^{3\pi\eta}\tilde{F}_{\eta b}]dA \equiv 0 \qquad (2.22)_2$$

and moreover a form with no side conditions of principle of virtual work can be established by subtracting I_1^V and I_1^S from the left and right hand side of (2.12). To attain a more suitable form it is expedient to transform both I_1^V and I_1^S by performing partial integrations before the subtraction. When transforming I_1^V

- we replace $H_{S.}^{\ L}$ and F_{XY} by $H_{p.}^{\ l}$ and F_{yb} bearing in mind, however, that $H_{K.}^{\ L}$ and F_{AB} are obviously zero and moreover
- we shall assume, in conformity with paragraph *2.6.* — see $(2.12)_{1,2}$ —, that there exists a one-to-one relationship between *Lagrange* multipliers

$$H_{\eta.}^{\ l}(\xi), \qquad F_{\eta b}(\xi) \qquad \xi \in S$$

and

$$H_{S.}^{\ T}(x), \qquad F_{XY}(x). \qquad x \in V$$

Without detailing the transformation by partial integrations and suitable renaming dummy indices we obtain:

$$I_1^V = \int_V [\epsilon^{kyp}H_{p.;y}^{\ \ l}\gamma_{kl} + \epsilon^{kpy}(F_{yb;p} + \epsilon_{bpl}H_{y.}^{\ l})\kappa_{a.}^{\ b}]dV$$
$$+ \int_S (H_{\eta.}^{\ l}\epsilon^{3\chi\eta}\gamma_{\chi l} + F_{\eta b}\epsilon^{3\pi\eta}\kappa_{\pi.}^{\ b})dA\,. \qquad (2.23)_1$$

Surface integral I_1^S can be transformed with the aid of *Stokes'* theorem employed here in such a form — see $(A.1)$ in Appendix — which is valid in a coordinate system defined on surface S. If, in addition to that $(A.2)_{1,2}$ is also taken into consideration we find that

$$I_1^S = \int_S (\tilde{H}_{\eta.}^{\ l}\epsilon^{3\chi\eta}\gamma_{\chi l} + \tilde{F}_{\eta b}\epsilon^{3\pi\eta}\kappa_{\pi.}^{\ b})dA$$
$$+ \int_S [\epsilon^{3\chi\eta}\tilde{H}_{\eta.;\chi}^{\ \ l}u_l + \epsilon^{3\pi\eta}(\tilde{F}_{\eta b;\pi} + \epsilon_{b\pi l}\tilde{H}_{\eta.}^{\ l})\varphi^b]dA\,. \qquad (2.23)_2$$

Subtraction of $(2.23)_1$ and $(2.23)_2$ from the left and right hand side of (2.12) and a subsequent rearrangement lead to the result

$$I_2^V + I_2^{S\chi\gamma} + I_2^{Su\varphi} = 0 \qquad (2.24)_1$$

where

$$I_2^V = \int_V (t^{kl} - \epsilon^{kyp}H_{p.;y}^{\ \ l} - g^{ks}B^l_{.;s})\gamma_{ks}dV +$$
$$\int_V [\mu^a_{.b} - \epsilon^{apy}(F_{yb;p} + \epsilon_{bpl}H_{y.}^{\ l}) - g^{al}(\epsilon_{lbs}B^s + C_{b;l})]\kappa_{a.}^{\ b}dV \qquad (2.24)_2$$

$$I_2^{S\kappa\gamma} = \int_S n_3[(\tilde{H}_{\eta.}^{\ l} - H_{\eta.}^{\ l})\epsilon^{3\chi\eta}\gamma_{\chi l} + (\tilde{F}_{\eta b} - F_{\eta b})\epsilon^{3\pi\eta}\kappa_{\pi.}^{\ b}]dA \qquad (2.24)_3$$

and

$$I_2^{Su\varphi} = \int_S n_3(t^{3l} - \epsilon^{3\chi\eta} H_{\eta\ ;\chi}^{\ l} - a^{3s} B^l_{\ ;s}) u_l dA + \int_S n_3 \left[\mu^3_{\ .b} - \epsilon^{3\pi\eta}(\tilde{F}_{\eta b;\pi} + \epsilon_{b\pi l} H_{\eta .}^{\ l}) - a^{3l}(\epsilon_{lbs} B^s + C_{b;l})\right] \varphi^b dA \,. \tag{2.24}_4$$

Since in (2.24) no conditions for

$$\gamma_{kl}(x), \qquad \kappa_{a.}^{\ b}(x) \qquad x \in V$$
$$\gamma_{\kappa l}(\xi), \qquad \kappa_{\pi.}^{\ b}(\xi) \qquad \xi \in S$$

and

$$u_l(\xi), \qquad \varphi^b(\xi) \qquad \xi \in S$$

are set down $\gamma_{kl}, \ldots, \varphi^b$ are arbitrary. Consequently, it follows from the disappearance of (2.24) the fulfillment of the field equations

$$t^{kl} = \epsilon^{kyp} H_{p\ ;y}^{\ l} + g^{ks} B^l_{\ ;s} \qquad x \in V \qquad (2.25)_1$$

$$\mu^a_{\ .b} = \epsilon^{aby}(F_{yb;p} + \epsilon_{bpl} H_{y .}^{\ l}) + g^{al}(\epsilon_{lbs} B^s + C_{b;l}) \qquad x \in V \qquad (2.25)_2$$

and boundary conditions

$$\tilde{H}_{\eta .}^{\ l} - H_{\eta .}^{\ l} = 0\,, \qquad \tilde{F}_{\eta b} - F_{\eta b} = 0\,, \qquad \xi \in S \qquad (2.26)_{1,2}$$

$$n_3 t^{3l} = n_3(\epsilon^{3\eta\pi} H_{\pi\ ;\eta}^{\ l} + a^{3s} B^l_{\ ;s})\,, \qquad \xi \in S \qquad (2.27)_1$$

$$n_3 \mu^a_{\ .3} = n_3 \left[\epsilon^{3\pi\eta}(\tilde{F}_{\eta b;\pi} + \epsilon_{b\pi l} \tilde{H}_{\eta .}^{\ l}) + a^{3l}(\epsilon_{lbs} B^s + C_{b;l})\right]. \qquad \xi \in S \qquad (2.27)_2$$

If we now substitute $(2.26)_{1,2}$ into $(2.27)_{1,2}$ and then compare $(2.27)_{1,2}$ with $(2.25)_{1,2}$ we get the result that the stresses t^{kl} and $\mu^a_{\ .b}$ can be calculated in the same way both in V and on S i.e. by using formulas $(2.25)_{1,2}$.

2.22. Equations $(2.25)_{1,2}$ provide equilibrated stresses as it can readily be shown by substituting them into the equilibrium equations $(2.6)_{1,2}$ and also by taking into account $(2.9)_{1,2}$. In addition to this they coincide with the representation found by *H.Schaeffer* [3]. For this reason multipliers $H_{y.}^{\ l}$ and F_{yb} will be referred to as stress functions.

2.23. It is worthy of special mention – with reference to paragraph 2.17. – that $H_{y.}^{\ l}$ and F_{yb} involve six-six scalar functions since $H_{K.}^{\ L} \equiv F_{AB} \equiv 0$. Inasmuch as $H_{y.}^{\ l}$ and F_{yb} are of nine-nine components fulfillment of the mentioned condition can always be ensured, by a proper choice of the vector components r^l and w_b, essentially, by the solution of the differential equations [1]

$$H_{K.}^{\ L} - r^L_{\ ;L} = 0\,, \qquad x \in V$$
$$F_{AB} - (w_{B:A} + \epsilon_{BAm} r^m) = 0. \qquad x \in V$$

[1] The stresses that are obtained from the stress functions

$$H_{y\ .}^{\ l} = r^l_{\ ;y}, \qquad F_{yb} = w_{b;y} + \epsilon_{bys} r^s$$

are identically zero [8].

These equations serve as a basis for the explanation why a proper choice of indices obey the rules presented in paragraph 2.17. [11].

3. Variational Principles of Lagrange's Type

3.1. In connection with the equation (2.24) obtained from the general primal form of principle of virtual work the question arises whether it is possible or not to establish such free variational problem where

- vanishing of variations with respect to the strain fields γ_{kl}, $\kappa_a{}^b_{.}$ of the corresponding functional ensures the fulfillment of the field equations $(2.25)_{1,2}$ on the volume V of body and that of boundary conditions $(2.26)_{1,2}$ on part S_t of boundary
- furthermore vanishing of variations with respect to the displacements u_k, φ^b yields the fulfillment of the boundary conditions $(2.27)_{1,2}$ consequently the fulfillment of stress boundary conditions on S_t.

The sought functional can be derived from the functional of the total potential energy by applying the method of *Lagrange's* multipliers. The domain of the functional involves the strain fields

$$\gamma_{kl} \qquad \kappa_a{}^b_{.} \qquad x \in V$$

the displacement fields

$$u_l, \qquad \varphi^b \qquad \xi \in S$$

and the stress functions

$$\begin{aligned} &H_S{}^T_{.}, && F_{XY} && x \in V \\ &\tilde{H}_\eta{}^l_{.}, && \tilde{F}_{\eta l}\,. && \xi \in S_t \end{aligned}$$

In the latter case, as we have assumed so far, $H_K{}^L_{.}$ and F_{AB} are regarded to be zero.

3.2. Equations of micropolar elasticity in terms of the above mentioned variables consist of the field equations

$$A^{klpq}\gamma_{pq} = \epsilon^{kpq}H_q{}^l_{.;p} + g^{km}B^l_{.;m}, \qquad x \in V \qquad (3.1)_1$$

$$B^{a\,pq}_{.b\,.}\kappa_{pq} = \epsilon^{aml}(F_{lb;m} + \epsilon_{bmq}H_l{}^q_{.}) + g^{al}(\epsilon_{lbm}B^m + C_{b;l})\,, \qquad x \in V \qquad (3.1)_2$$

$$\epsilon^{Xpk}\kappa_k{}^Y_{.;p} = 0\,, \qquad x \in V \qquad (3.2)_1$$

$$\epsilon^{Spq}(\gamma_{qT;p} + \epsilon_{qTb}\kappa_p{}^b_{.}) = 0\,, \qquad x \in V \qquad (3.2)_2$$

the boundary conditions

$$\tilde{H}_\eta{}^l_{.} - H_\eta{}^l_{.} = 0\,, \qquad \xi \in S_t \qquad (3.3)_1$$

$$\tilde{F}_{\eta b} - F_{\eta b} = 0\,, \qquad \xi \in S_t \qquad (3.3)_2$$

$$\kappa_\eta{}^b_{.} - \varphi^b_{.;\eta} = 0\,, \qquad \xi \in S_t \qquad (3.4)_1$$

$$\gamma_{\chi l} - u_{l;\chi} - \epsilon_{l\chi b}\varphi^b = 0 \qquad \xi \in S_t \qquad (3.4)_2$$

$$\kappa_{\eta\ .}^{\ b} - \hat{\varphi}^b_{\ .;\eta} = 0\,, \qquad \xi \in S_u \qquad (3.5)_1$$

$$\gamma_{\chi l} - u_{l;\chi} - \epsilon_{l\chi b}\hat{\varphi}^b = 0\,, \qquad \xi \in S_u \qquad (3.5)_2$$

$$\hat{t}^l - \epsilon^{3\chi\eta}\tilde{H}_{\eta\ .;\chi}^{\ l} - B^{\ l}_{\ .;3} = 0\,, \qquad \xi \in S_t \qquad (3.6)_1$$

$$\hat{\mu}_b - \epsilon^{3\pi\eta}(\tilde{F}_{\eta b;\pi} + \epsilon_{b\pi l}\tilde{H}_{\eta\ .}^{\ l}) - a^{3l}(\epsilon_{lb\sigma}B^\sigma + C_{b;l}) = 0$$

$$\xi \in S_t \qquad (3.6)_2$$

and the continuity condition

$$u_l = \hat{u}_l\,, \qquad \varphi^b = \hat{\varphi}^b. \qquad \xi \in g \qquad (3.7)_{1,2}$$

Really, simultaneous fulfillment of equations $(3.2)_{1,2}$, $(3.4)_{1,2}$, $(3.5)_{1,2}$ and $(3.7)_{1,2}$ ensures that the strain fields γ_{kl}, $\kappa_{a\ .}^{\ b}$ are kinematically admissible. We note that — in accordance with paragraph *2.20.* and with regard to the continuity conditions $(3.7)_{1,2}$ – integration of equations $(3.4)_{1,2}$ yields the actual displacement fields $u_k(\xi)$, $\varphi^b(\xi)$ $\xi \in S_t$. If furthermore field equations $(3.1)_{1,2}$ are satisfied then the equilibrium on V is maintained while the simultaneous fulfillment of $(3.6)_{1,2}$ is equivalent to that of stress boundary conditions.

3.3. Now let

$$\Pi_2 = \Pi_2(\gamma_{kl}, \kappa_{a\ .}^{\ b}, u_l, \varphi^b, H_{y\ .}^{\ l}, F_{yb}, \tilde{H}_{\eta\ .}^{\ l}, \tilde{F}_{\eta b}) = \Pi_2^{V1} + \Pi_2^{V2} + \Pi_2^{St} + \Pi_2^{Su} + \Pi_2^G + C_2^{Su} \qquad (3.8)_1$$

be the sought functional where

$$\Pi_2^{V1} = \frac{1}{2}\int_V (\gamma_{kl}A^{klpq}\gamma_{pq} + \kappa_{ab}B^{abpq}\kappa_{pq})dV -$$

$$\int_V \left[g^{km}B^{\ m}_{.;m}\gamma_{kl} + g^{al}(\epsilon_{lbm}B^m + C_{b;l})\kappa_{a\ .}^{\ b}\right]dV\,, \qquad (3.8)_2$$

$$\Pi_2^{V2} = -\int_V \left[\epsilon^{Spq}(\gamma_{qT;p} + \epsilon_{qTb}\kappa_{p.}^{\ b})H_{S\ .}^{\ T} + \epsilon^{Xpk}\kappa_{k\ .;p}^{\ Y}F_{XY}\right]dV \qquad (3.8)_3$$

$$\Pi_2^{St} = -\int_{St}\left\{(\hat{t}^l - n_3 a^{3l}B^{\ l}_{.;3})u_l + \left[\hat{\mu}_b - n_3 a^{3l}(\epsilon_{lb\sigma}B^\sigma + C_{b;l})\right]\varphi^b\right\}dA$$

$$+\int_{St}\left[(\gamma_{\chi l} - u_{l;\chi} - \epsilon_{l\chi b}\varphi^b)\epsilon^{3\chi\eta}\tilde{H}_{\eta\ .}^{\ l} + (\kappa_{\eta\ .}^{\ b} - \varphi^b_{\ .;\eta})\epsilon^{3\pi\eta}\tilde{F}_{\eta b}\right]dA\,, \qquad (3.8)_4$$

$$\Pi_2^{Su} = \int_{Su}\left[(\gamma_{\chi l} - \hat{u}_{l;\chi} - \epsilon_{l\chi b}\hat{\varphi}^b)\epsilon^{3\chi\eta}H_{\eta\ .}^{\ l} + (\kappa_{\eta\ .}^{\ b} - \hat{\varphi}^b_{\ .;\eta})\epsilon^{3\pi\eta}F_{\eta b}\right]dA\,, \qquad (3.8)_5$$

$$\Pi_2^G = \oint_g \left[\tau^\eta(u_l - \hat{u}_l)\tilde{H}_{\eta\ .}^{\ l} + \tau^\eta(\varphi^b - \hat{\varphi}^b)F_{\eta b}\right]ds \qquad (3.8)_6$$

and

$$C_2^{Su} = \int_{Su} \left[n_3 a^{3m} B^l_{\cdot;m} \hat{u}_l + n_3 a^{3l} (\epsilon_{lbm} B^m + C_{b;l}) \hat{\varphi}^b \right] dA = const. \tag{3.8}_7$$

3.4. Vanishing of variation

$$\delta \Pi_2 = \delta_{\gamma,\kappa} \Pi_2 + \delta_{u,\varphi} \Pi_2 + \delta_{H,F} \Pi_2 = 0 \tag{3.9}$$

as a variational principle ensures the fulfillment of the field equations (3.1), (3.2), (3.3) and (3.4), the boundary conditions (3.5) and (3.6) furthermore the continuity condition (3.7).

In the following we briefly outline the proof of the above assertion. Because of the independence of variations with respect to the distinct variables of functional (3.8) stationary condition (3.9) is equivalent to the equations

$$\delta_{\gamma,\kappa} \Pi_2 = \delta_{\gamma,\kappa} \Pi_2^{V1} + \delta_{\gamma,\kappa} \Pi_2^{V2} + \delta_{\gamma,\kappa} \Pi_2^{St} + \delta_{\gamma,\kappa} \Pi_2^{Su} = 0 \,, \tag{3.10}_1$$

$$\delta_{u,\varphi} \Pi_2 = \delta_{u,\varphi} \Pi_2^{St} + \delta_{u,\varphi} \Pi_2^{G} = 0 \tag{3.10}_2$$

and

$$\delta_{H,F} \Pi_2 = \delta_{H,F} \Pi_2^{V2} + \delta_{H,F} \Pi_2^{St} + \delta_{H,F} \Pi_2^{Su} + \delta_{H,F} \Pi_2^{G} = 0 \,. \tag{3.10}_3$$

Equation $(3.10)_1$ can be transformed by substituting $(2.22)_1$ and $(2.23)_1$ provided that in the latter equations strain fields are replaced by their variations. From the resulting equation, taking into account that the variations are arbitrary, we obtain the field equations $(3.1)_{1,2}$ and $(3.3)_{1,2}$.

Using transformation rules $(A.2)_{1,2}$ from equation (3.10) we can readily derive the boundary conditions $(3.6)_{1,2}$.

Fulfillment of equation $(3.10)_3$ is equivalent to all the conditions i.e. to equations $(3.2)_{1,2}$, $(3.4)_{1,2}$, $(3.5)_{1,2}$ and $(3.7)_{1,2}$ kinematically admissible strain fields should meet.

3.5. If the strain fields are kinematically admissible and stress functions $\tilde{H}_{\eta\cdot}^{\ l}$, $\tilde{F}_{\eta b}$ satisfying the conditions $(3.6)_{1,2}$ are known then functional (3.8) reduces to functional

$$\Pi_1 = \Pi(\gamma_{k,l}, \kappa_{a\cdot}^{\ b}) = \Pi_1^V + \Pi_1^{St} + C_1^{Su} + C_1^G \tag{3.11}_1$$

where

$$\Pi_1^V = \Pi_2^{V1} \,, \tag{3.11}_2$$

$$\Pi_1^{St} = \int_{St} (n_3 \epsilon^{3\chi\eta} \gamma_{\chi l} \tilde{H}_{\eta\cdot}^{\ l} + n_3 \epsilon^{3\chi\eta} \kappa_{\pi\cdot}^{\ b} \tilde{F}_{\eta b}) dS \,, \tag{3.11}_3$$

$$C_1^{Su} = C_2^{Su} = const \tag{3.11}_4$$

and

$$C_1^G = -\oint_g \tau^\eta \tilde{H}_{\eta\cdot}^{\ l} \hat{u}_l ds - \oint_g \tau^\eta \tilde{F}_{\eta b} \hat{\varphi}^b ds \,. \tag{3.11}_5$$

During the transformations leading to (3.11) it had to be taken into account that due to their definition the kinematically admissible strain fields meet the preconditions

(3.2), (3.4), (3.5) and (3.7). In addition to this integral ($A.3$) should also be substituted by a suitable renaming of dummy indices and performing simultaneously some rearrangements.

3.6. Functional (3.11) is subjected to subsidiary conditions which should ensure that the strain fields are kinematically admissible. In contrast to the foregoing it is worthwhile to choose such subsidiary conditions on S_t which do not contain the displacement fields.

In accordance with all that has been said about the requirements the subsidiary conditions should meet when seeking the equations which follow from the stationarity of functional $\Pi_1(\gamma_{kl}, \kappa_{a.}^{\ b})$ one should supplement Π_1 by a sum of integrals

$$\Pi_S = \Pi_S^V + \Pi_S^{St} + \Pi_S^{Su} + \Pi_S^G \tag{3.12}_1$$

which vanishes if the subsidiary conditions are satisfied. Here

$$\Pi_S^V = I_1^V(H_{S.}^{\ T}, F_{XY}), \tag{3.12}_2$$

$$\Pi_S^{St} = \int_{St} \left[n_3 \epsilon^{3\pi\eta} \kappa_{\eta.;\pi}^{\ b} w_b + n_3 \epsilon^{3\pi\chi}(\gamma_{\chi l;\pi} + \epsilon_{\chi lb} \kappa_{\pi.}^{\ b}) r^l\right] dA \tag{3.12}_3$$

$$\Pi_S^{Su} = \Pi_2^{Su}(\overset{*}{H}_{\eta.}^{\ l}, \overset{*}{F}_{\eta b}) \tag{3.12}_4$$

and

$$\Pi_S^G = \oint_g \tau^\eta (\kappa_{\eta.}^{\ b} - \hat{\varphi}_{;\eta}^{\ b}) \overset{*}{w}_{\ b} \, ds + \oint_g \tau^\chi \left[\gamma_{\chi l} - (u_{l;k} + \epsilon_{l\chi b} \hat{\varphi}^b)\right] \overset{*}{r}^{\ l} ds \,. \tag{3.12}_5$$

Lagrange's multipliers in the above integrals are denoted by

$H_{S.}^{\ T}$,	F_{XY}	$x \in V$
w_b ,	r^l	$\xi \in S_t$
$\overset{*}{w}_{\ b}$,	$\overset{*}{r}^{\ l}$	$\xi \in g$
$\overset{*}{H}_{\eta.}^{\ T}$,	$\overset{*}{F}_{\eta b}$.	$x \in V$

Because of the same meaning the letters we used earlier are deliberately utilized again to designate unknown *Lagrange's* multipliers.

3.7. By varying the sum $\Pi_1 + \Pi_2$ with respect to the strain fields and utilizing appropriately the relations ($A.1$) and $(A.4)_{1,2}$ we obtain

$$\delta_{\kappa,\gamma}\Pi_1 + \delta_{\kappa,\gamma}\Pi_S = I_S^V + I_S^{St} + I_S^{Su} + I_S^G \tag{3.13}_1$$

where

$$I_S^V = \int_V \left[A^{klpq}\gamma_{pq} - (\epsilon^{kyp} H_{p.;y}^{\ \ l} + g^{ks} B_{.;s}^{\ l})\right] \delta\gamma_{kl} \, dV + \int_V \left[B_{.b..}^{\ apq} \kappa_{pq} - \epsilon^{ami}(F_{ib;m} + \epsilon_{bmq} H_{i.}^{\ q}) - g^{al}(\epsilon_{lbm} B^m + C_{b;l})\right] \delta\kappa_{a.}^{\ b} \, dV, \tag{3.13}_2$$

$$I_S^{St} = \int_{St} n_3 \epsilon^{3\pi\eta} \left[\tilde{F}_{\eta b} - F_{\eta b} - (w_{b;\eta} + \epsilon_{b\eta m} r^m)\right] \delta\kappa_{a.}^{\ b} \, dV + \int_{St} n_3 \epsilon^{3\chi\eta}(\tilde{H}_{\eta.}^{\ \ l} - H_{\eta.}^{\ \ l} - r_{.;\eta}^{\ l}) \delta\gamma_{\chi l} \, dA, \tag{3.13}_3$$

$$I_S^{Su} = \int_{Su} [n_3 \epsilon^{3\pi\eta} (\overset{*}{F}_{\eta b} - F_{\eta b}) \delta\kappa_{\pi.}^{\ b} + n_3 \epsilon^{3\pi\eta} (\overset{*}{H}_{\eta.}^{\ l} - H_{\eta.}^{\ l}) \delta\gamma_{\chi l}] \, dA \qquad (3.13)_4$$

and

$$I_S^G = \oint_g [\tau^\eta (\overset{*}{w}_b - w_b) \delta\kappa_{\eta.}^{\ b} + \tau^\chi (\overset{*}{r}^l - r^l) \delta\gamma_{\chi l}] \, ds. \qquad (3.13)_5$$

3.8. Equation

$$\delta_{\kappa,\gamma} \Pi_1 + \delta_{\kappa,\gamma} \Pi_S = 0 \qquad (3.14)$$

as a variational principle ensures that the stress fields obtained from (2.7) are statically admissible. Really, if we compare the above equation and equation (3.13) we get the followings:

1. Vanishing of integral I_S^V yields the equilibrated representation $(3.1)_{1,2}$ for strain fields in V.
2. Vanishing of integral I_S^{Su} leads to the validity of the representation on S_u.
3. From the vanishing of I_S^{St} – taking into account, that the stress functions

$$\check{H}_{\eta.}^{\ l} = r^l_{.;\eta} \qquad \xi \in S_t \qquad (3.15)_1$$

$$\check{F}_{\eta b} = w_{b;\eta} + \epsilon_{b\eta m} r^m \qquad \xi \in S_t \qquad (3.15)_2$$

result in identically zero stresses and utilizing furthermore that the stress functions $\tilde{F}_{\eta b}$ and $\tilde{H}_{\eta.}^{\ l}$ satisfy $(3.6)_{1,2}$ – it follows the fulfillment of the stress boundary conditions imposed on S_t.
4. Vanishing of integral I_S^G yields the fulfillment of continuity condition concerning *Lagrange's* multipliers.

3.9. It is worthy of special mention that to the fulfillment of stress boundary conditions there is no need to satisfy the boundary conditions

$$\tilde{H}_{\eta.}^{\ l} - H_{\eta.}^{\ l} = 0\,, \qquad \tilde{F}_{\eta b} - F_{\eta b} = 0\,. \qquad \xi \in S_t$$

Instead fulfillment of the weaker forms

$$\tilde{H}_{\eta.}^{\ l} - H_{\eta.}^{\ l} = \check{H}_{\eta.}^{\ l}\,, \qquad \tilde{F}_{\eta b} - F_{\eta b} = \check{F}_{\eta b} \qquad \xi \in S_t$$

is also sufficient. Although this result has been known [8], it appears here as a consequence of a variational principle.

4. Concluding Remarks

4.1. The main result of the present work has been the proof of the possibility, that for micropolar bodies the general and complete solution of equilibrium equations in terms of stress functions – valid therefore not only for a self-equilibrated case – can be derived from the general primal form of principle of virtual work. The proof is grounded on two circumstances. As well known, the general primal form of principle of virtual work ensures the fulfillment of equilibrium equations provided that the strain fields are kinematically admissible. Therefore an appropriate choice of the side conditions – and this is the second circumstance – leads to the desired final result as it has turned out. Since the side conditions involve six-six field equations any state

of stress can be given in terms of six-six stress functions. Consequently three-three components of the corresponding stress function tensors $H_{y.}^{\ l}$ and F_{yb} can be set to zero. In addition to this special care should be taken to the calculations carried out on the boundary surface S. We note that the line of thought presented herein is of methodological significance and can be applied to other cases including the classical one. This work is now in progress.

4.2. A further question arises concerning the formulation of the corresponding variational principles. The most important functionals of *Lagrange's* type have also been presented assuming that the micropolar body under consideration is linearly elastic. The vanishing of variations with respect to the strain fields of the functionals as a variational principle ensures, through stress functions, the fulfillment of equilibrium equations and stress boundary conditions. Representation of stresses obtained in terms of stress functions from the stationarity condition coincide with the general and complete solution of equilibrium equations.

5. Appendix

5.1. Let $d_q(\xi)$ be sufficiently smooth vector field defined on S_t. According to *Stokes'* theorem

$$\int_{St} n_3 \epsilon^{3\chi\eta} d_{\eta;\chi}\, dA = \oint_g \tau^\eta d_\eta\, ds. \tag{A.1}$$

If S_t is closed then the integral in the right hand side is vanishing.

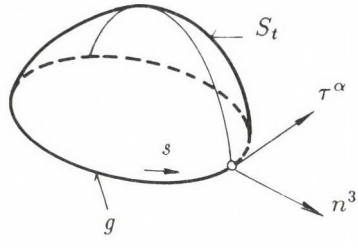

Fig. 4.

5.2. Integral appearing in equation (2.22) can be transformed with the aid of (*A*.1):

$$\int_{St} n_3 \epsilon^{3\chi\eta} u_{l;\chi} \tilde{H}_{\eta.}^{\ l}\, dA = \oint_g \tau^\eta u_l \tilde{H}_{\eta.}^{\ l}\, ds - \int_{St} n_3 \epsilon^{3\chi\eta} \tilde{H}_{\eta.;\chi}^{\ l} u_l\, dA, \tag{A.2}_1$$

$$\int_{St} n_3 \epsilon^{3\pi\eta} \varphi^{\ b}_{.;\pi} \tilde{F}_{\eta b}\, dA = \oint_g \tau^\eta \varphi^b \tilde{F}_{\eta b}\, ds - \int_{St} n_3 \epsilon^{3\pi\eta} \tilde{F}_{\eta b;\pi} \varphi^b\, dA. \tag{A.2}_2$$

If S_t is again closed i.e. $S_t \equiv S$ then the line integrals in the right hand side can be omitted.

5.3. Transformation of integral

$$I' = \int_{St} (\hat{t}^l u_l + \hat{\mu}_b \varphi^b)\, dA$$

appearing in $(3.8)_{1,2}$ requires the application of *Stokes'* theorem, the kinematic equations $(3.4)_{1,2}$ and the continuity condition $(3.7)_{1,2}$:

$$I' = \int_{St} \left[n^3 B^l_{.;3} + n^3(\epsilon_{3b\sigma} B^\sigma + C_{b;3})\varphi^b\right] dA + \oint_g \tau^\eta \tilde{H}_{\eta.}^{\ l} \hat{u}_l\, ds + \oint_g \tau^\eta \tilde{F}_{\eta l} \hat{\varphi}^b\, ds + \int_{St} (n_3 \epsilon^{3\chi\eta} \gamma_{\chi l} \tilde{H}_{\eta.}^{\ l} + n_3 \epsilon^{3\pi\eta} \kappa_{\pi.}^{\ b} \tilde{F}_{\eta b})\, dA\,. \qquad (A.3)$$

5.4. Transformation of variation of integral $(3.12)_3$ can be carried out by the substitution of integrals

$$\int_{St} n_3 \epsilon^{3\pi\eta} \delta\kappa_{\eta;\pi}^{\ b} w_b\, dA = \oint_g \tau^\eta w_b \delta\kappa_{\eta.}^{\ b}\, ds + \int_{St} n_3 \epsilon^{3\pi\eta} w_{b;\eta} \delta\kappa_{\eta.}^{\ b}\, dA \qquad (A.4)_1$$

and

$$\int_{St} n_3 \epsilon^{3\pi\chi} \delta\gamma_{\chi l;\pi} r^l\, dA = \oint_g \tau^\chi r^l \delta\gamma_{\chi l}\, ds + \int_{St} n_3 \epsilon^{3\chi\eta} r^l_{.;\eta} \delta\gamma_{\chi l}\, dA \qquad (A.4)_2$$

obtained by partial integrations and a renaming of dummy indices.

Acknowledgment. I am grateful to Prof.Dr.Imre Kozák – University of Miskolc, Department of Mechanics – for valuable comments and helpful suggestions concerning this article.

References

1. Abovski,N.P.-Andreev,N.P.-Deruga,A.P.: Variational Principles of the Theory of Elasticity and Theory of Shells (in Russian), Nauka Publishers, Moscow 1978
2. Carlson,D.E.: On Günther's Stress Functions for Couple-Stresses, *Quart. Appl. Math.*, **25** (1967), 139-146
3. Gurtin,M.E.: The linear Theory of Elasticity in Handbuch der Physik, Festkörpermechanik II., Springer-Verlag, 1972 p.17
4. Günther,M.: Zur Statik und Kinematik des Cosseratschen Kontinuums, *Abh. Braunschweig.Wiss. Ges.*, **10** (1958), 195-213
5. Kozák, I.: Determination of Compatibility Boundary Conditions in Linear Elastostatics with the Aid of the Principle of Minimum Complementary Energy, *Publ. Techn. Univ. Heavy Industry, Miskolc, Ser.D. Natural Sciences*, **34**(2) (1980), 83-98
6. Kozák,I.: Notes on the Field Equations with Stresses and on the Boundary Conditions in the Linearized Theory of Elasticity, *Acta Techn. Hung.* **90**(3-4) (1980), 221-225
7. Kozák,I.: Principle of Virtual Work in Terms of Stress Functions, *Publ. Techn. Univ. Heavy Industry, Miskolc, Ser.D. Natural Sciences*, **34**(2) (1980), 147-163

8. Kozák,I.-Szeidl,Gy.: The Field Equations and the Boundary Conditions with Force-Stresses and Couple-Stresses in the Linearized Theory of Micropolar Elastostatics, *Acta Techn. Hung.* **91**(1-2) (1980), 57-80
9. Schaefer, H.: Die Spannungsfunktionen eines Kontinuums mit Momentenspannungen I.-II. *Bulletin de l'Academie Polonaise des Sciences*, Serie des sciences techniques, **15**(1) (1967), 63-67, 69-73
10. Szeidl,Gy.: Principle of Virtual Work in Terms of Stress Functions for Micropolar Body, *Publ. Techn. Univ. Heavy Industry, Miskolc, Ser.D. Natural Sciences*, **34**(2) (1981) 221-238
11. Stippes,M.: On Stress Functions in Classical Elasticity, *Quart. Appl. Math.*, **24**(1966), 119-120
12. Tonti,E.: A Mathematical Model for Physical Theories I.II., *Rendiconti Accademia Nazionale dei Lincei*, **52** (1972), 175-181, 351-356

Acta Technica Acad.Sci.Hung., 104(1-3), pp. 297-299 (1991/92)

BOOK REVIEWS

Krasnosel'skij, M.A.-Lifshits, Je.A.-Sobolev, A.V.: Positive linear systems. The method of positive operators. (Sigma Series in Applied Mathematics 5). Heldermann Verlag, Berlin, 1989, 354 p.

In system theory, an important subcase is characterized by the monotonicity of the inputs and outputs, by the positiveness of some mappings. Let us consider for example a system where increase of the output follows from the increase of the input. Such systems can be described in certain cases by operator equations defined in spaces partially ordered by some cone.

This book collects facts, notions, theorems from monographs which cannot be found easily. Proofs are complete or almost complete. The problems dealt with are mainly linear. Experts in system theory, mechanics, electromechanics, electrical circuit theory will find this book useful and interesting. Among the four chapters, the first one studies the basic notions, such as cones, orderings, positive linear functionals and operators, smoothness points of cones, normal cones, regular cones, suprema and infima, cones of rank k.(Note that the theory of cones and partially ordered spaces goes back among others to F. Riesz,too.)

The second chapter concerns applications to spectral properties (spectral radius, eigenvectors, focussing operators, the spectral margin, etc.). The third chapter gives applications to iteration procedures (e.g. estimates for the spectral radius, iteration with proportional corrections, a posteriori error estimates for positive eigenvectors, etc.). Especially interesting can be for practicants the fourth chapter; in this we find studies on absolutely positive system, the impulse - frequency characteristic of a linear link, frequency-positive linear links, general theorems on positive invertibility, forced periodic oscillations in nonlinear systems, the harmonic balance method, positive solutions of nonlinear problems, problems with parameters, criteria for stability and absolute stability.

A large number of exercises of various grades of difficulty can be found in numerous sections. Some exercises are in themselves interesting.

The book can be highly recommended for systems theorists.

Bosznay, Á.

Akadémiai Kiadó, Budapest

Góschy, B.: Design of buildings to withstand abnormal loading, Butterworth and Co. Ltd., London, 1990

The book is designed and shaped very well, and contains 197 pages, 98 figures, 37 tables and 179 references altogether.

As far as its content is concerned, the book is an amplified and revised edition of author's former work "Építmények tervezése rendkívüli terhekre és hatásokra" (Design of buildings for abnormal loads and effect, Műszaki Könyvkiadó Budapest, 1984), which was brought up-to-date with respect to the principles and recommendations of the foreign technical literature, guide-lines,etc. published in the meantime. There are two basic conditions of taking into consideration even the effect of the abnormal random loads by the design engineer already in the state of design. On the one hand,he has to obtain reliable data on the character of the physically available abnormal loads (effects), on their expected magnitude, the probability of their occurrence, and the measure of the safety requirements. On the other hand, since these loads generally are of dynamic character, he designer is required to have such computing methods used in dynamics the labour-intensity of which is still acceptable for a practising designer. The author, Béla Góschy was going to provide a reliable theoretical basis for meeting those requirements.

In this book, similarly to the method of manuals, author recapitulizes all the problems emerging in the course of dimensioning and developing the structural layout of the buildings subject to all kinds of abnormal loads and effects, and provides the possible ways to their solution. All the effects which are brought about by inner or outer explosion, impact caused by either the inner or outside environment, earthquake, wind load, unexpected ground flow and other unusual phenomena of natural origin or due to human activity acting on the building and structures are discussed in details by the author.

In Chapter 1, the problems on interaction between the environmental events like abnormal random loads and the system of supporting structures are dealt with briefly. It is theoretically confirmed it is possible to extend the applicability of the dimensioning methods based on probability or semi-probability considerations used presently for the design of supporting structures to the abnormal loads (effects) of rarely occurrence provided that the characteristics of the change of state are considered as random variables.

In Chapter 2, from among the abnormal loads, the following are dealt with in detail: inner explosion (gas, powder, explosives, etc.), the burst effect of outer explosion (on-surface or underground explosions, air explosion), the impact (of a vehicle, an object falling down, a bomb or a rocket), and the seismic effects (earthquake, earth-fall). Each of those are characterized by random occurrence, their effect shows a relatively short-time duration, rapid change and a dynamic character. In the book, the possible ways of model simulation of the effects mentioned above are dealt with in detail.

In Chapter 3, the sphere of problems concerning the dynamic model simulation of supporting structures are described. The structural materials behave differently under static and dynamic loads. With structural models, which are dynamic ones, in addition to the usual characteristics of structural materials, their energy-consumption property should also be taken into consideration, as well as the character of the state of stress in the structure, and the chronology of load (effect). This latter one can be single, or an impulsive load, or impact load, respectively, or perhaps a rarely repeated, low cycle-number load, and an often repeated, high cycle-number one.

In Chapter 4, the dynamic characteristics of supporting structures are discussed. In it, a good description and clear recapitulation is provided about the differential equations and their solutions describing the state of undamped vibrations of the bars and beams, plates, cantilever-like beams, plane multiple-storey frames and composite structures containing wall-beams and frames. There are formulae in it for the approximate determination of the free vibration period of multi-storey buildings, as well as the computation method of the reduced mass of different beams and girders is given in it for the use in dynamic calculations. There can be found numerous tables providing assistance to the designer so as he can apply the information contained in this valuable chapter in finding solutions to his problems in practice.

The subject of Chapter 5 concerns the expected dynamic behaviour of the structures under abnormal impulsive load. The problems discussed here can also be worded as the problems of "what answer is given" by the supporting structure to the dynamic effects acting upon it. Author discusses the general examination of systems of one and more degree of freedom, then he gives full particulars of the effect of earthquake, the latter being considered both as a deterministic and a stochastic effect.

In the first part of Chapter 6, the system of differential equations describing the stable state of equilibrium of spatial structures and the general way of its solution are described, and later on, the detailed analysis of the dynamic stability conditions of plane supporting structures is given on the basis of physical or geometric non-linearity, respectively. In this chapter, it is also discussed what is the criterion for the stability of structures in case of earthquake.

In the relatively brief Chapter 7, recommendations are offered for the general aspects and the detail solutions of the structural layout with the buildings of expectedly dynamic load. These recommendations should be taken into consideration, first of all, in case of imminent earthquake.

As it can be seen, the content of the book covers a wide range of special lines and it shows a theoretical character. With proper mathematical knowledge in their possession, both the practising designers, structural engineers and the students of continuing professional training can make a good use of this book in their work. However, the presentation of some properly chosen particular numerical examples could have contributed to the easier application of the calculation methods described above.

Csellár, Ö.

PRINTED IN HUNGARY

Akadémiai Kiadó és Nyomda Vállalat, Budapest

NOTICE TO CONTRIBUTORS

Papers in English* are accepted on condition that they have not been previously published or accepted for publication.

Manuscripts in two copies (the original type-written copy plus a clear duplicate one) complete with figures, tables, and references should be sent to

Acta Technica
Nádor u. 7. I. 118
Budapest, Hungary
H-1051

Although every effort will be made to guard against loss, it is advised that authors retain copies of all material which they submit. The editorial board reserves the right to make editorial changes.

Manuscripts should be typed double-spaced on one side of good quality paper with proper margins and bear the title of the paper and the name(s) of the author(s). The full postal address(es) of the author(s) should be given in a footnote on the first page. An abstract of 50 to 100 words should precede the text of the paper. The approximate locations of the tables and figures should be indicated on the margin. An additional copy of the abstract is needed. Russian words and names should be transliterated into English.

References. Only papers closely related to the author's work should be referred to. The citations should include the name of the author and/or the reference number in brackets. A list of numbered references should follow the end of the manuscript.

References to periodicals should mention: (1) name(s) and initials of the author(s); (2) title of the paper; (3) name of the periodical; (4) volume; (5) year of publication in parentheses; (6) numbers of the first and last pages. Thus: 5. Winokur, A.—Gluck, J.: Ultimate strength analysis of coupled shear walls. American Concrete Institute Journal 65 (1968) 1029-1035

References to books should include: (1) author(s)' name; (2) title; (3) publisher; (4) place and year of publication. Thus: Timoshenko, S.—Gere, J.: Theory of Elastic Stability. McGraw-Hill Company. New York, London 1961

Illustrations should be selected carefully and only up to the necessary quantity. Black-and-white photographs should be in the form of glossy prints. The author's name and the title of the paper together with the serial number of the figure should be written on the back of each print. Legends should be brief and attached on a separate sheet. Tables, each bearing a title, should be self-explanatory and numbered consecutively.

Authors will receive proofs which must be sent back by return mail.

Authors will receive 50 reprints free of charge.

*Hungarian authors can submit their papers also in Hungarian.

HU ISSN 0864-8085